The Pennsylvania State University

The Graduate School

Department of Materials Science and Engineering

DYNAMICS OF HYDROGEN BONDING POLYMER BLENDS EXHIBITING MINIMIZED SELF ASSOCIATIONS AND LIQUID CRYSTALLINE POLYMERS OF UNIQUE CHEMISTRY

A Dissertation in

Materials Science and Engineering

by

Kevin Allen Masser

Submitted in Partial Fulfillment
of the Requirements
for the Degree of

Doctor of Philosophy

December 2010

The dissertation of Kevin Allen Masser was reviewed and approved[i] by the following:

James Runt
Professor of Materials Science and Engineering
Dissertation Adviser
Chair of Committee

Paul C. Painter
Professor of Materials Science and Engineering

Michael Hickner
Associate Professor of Materials Science and Engineering

Qiming Zhang
Professor of Materials Science and Engineering
Professor of Electrical Engineering

Gary Messing
Distinguished Professor of Ceramic Science and Engineering
Head of the Department of Materials Science and Engineering

[i]Signatures on file in the Graduate School.

Abstract

The dynamics and states of hydrogen bonding in miscible polymer blends which preferentially form intermolecular associations are investigated. A homopolymer and a copolymer based on poly(*p*-(hexafluoro-2-hydroxyl-2-propyl)styrene) (PolyHFS) form strong intermolecular associations, while the two-CF3 groups provide steric shielding around the hydroxyl group, reducing the ability to form hydrogen bonds with other PolyHFS molecules, while maintaining the ability to form intermolecular associations with another polymer. As well as the HFS homopolymer, a copolymer of the HFS monomer with 2,3-dimethylbutadiene (DMB) was synthesized (HFS[14]:DMB[86]). Purified PolyHFS was blended with a variety of proton accepting polymers, including poly(vinyl methyl ether) (PVME), poly(2-vinyl pyridine) (P2VPy), poly(vinyl acetate) (PVAc), poly(ethylene[30]-ran-vinyl acetate[70]) (EVA70), and poly(ethylene[55]-ran-vinyl acetate[45]) (EVA45). The purified HFS[14]:DMB[86] was blended with PVME. The selection of proton accepting polymers allows for a systematic variation of the hydrogen bonding strength: P2VPy>>PVME>vinyl acetate, as well as a systematic variation of the numbers of interacting sites: PVAc>EVA70>EVA45, and PolyHFS > HFS[14]:DMB[86]. Broadband dielectric relaxation spectroscopy was used to evaluate the relaxation behavior of the blends. Fourier transform infrared spectroscopy was used to quantify the hydrogen bonding types and concentrations. HFS[14]:DMB[86] blends with PVME exhibit a single glass transition temperature, but two dynamic glass transitions (α relaxations) at certain compositions due to concentration fluctuations. The glassy state motion of PVME in the copolymer blends is not suppressed, since a relatively small number of HFS segments are present at any composition. In contrast, the local motion of the HFS:DMB copolymer, related to motions of the HFS segment, is completely suppressed by hydrogen bonding in all blends. Glassy state motions are suppressed in the PVME and P2VPy blends with the HFS homopolymer, and the suppression is dependent on the functional group accessibility. Due to the reduced hydrogen bond strength between HFS and the vinyl acetate functionality, local relaxations are not suppressed in these blends. A local relaxation for free functional groups as well as hydrogen bonded functional groups is present, and the relative magnitudes of these processes can be quantified by the predictions of the Painter-Coleman association model. Based on these results, it is likely the glassy state behavior can be well described in any hydrogen bonding blend where the hydrogen bonding behavior can be quantified. The HFS homopolymer blends all exhibit a single glass transition, and a single α relaxation. The dynamic fragility is dependent upon the fraction of intermolecularly associated segments, and the compositions with the highest fragilities are the compositions with the greatest degree of intermolecular coupling. The blends with the highest fragility can be predicted based upon quantification of the infrared and dielectric results. A relaxation related to the breaking and reforming of hydrogen bonds is present in all HFS homopolymer blends, and its relaxation behavior is dependent on the numbers and strengths of intermolecular associations. Finally, the dynamics of main chain liquid crystalline polymers

consisting of rigid mesogens and siloxane spacer segments are investigated. These immiscible segments are covalently bound, and the immiscibility gives rise to their unique structures.

Table of Contents

List of Tables

List of Figures

Acknowledgments

Many thanks are owed to my advisor, Professor James Runt. His guidance and support throughout the past several years have been of critical importance to my degree. His keen eye and his depth of knowledge have helped me immensely.

My family has also been incredibly supportive of me during this time. My mother Amy, my father Rick, and in particular Hanqing provided much encouragement and support. Without them, this would not have been possible.

I am eternally indebted to Daniel Fragiadakis. His constant patience, kindness and textbook understanding of all things scientific are truly impressive. His willingness to assist others provided me, on occasions too numerous to recall, the key bit of information needed to solve a problem. In addition to Daniel, I have met many friends at Penn State who have assisted me in one way or another, including but not limited to: Charles Hogshead, Brian Erwin, Ronald Hedden, Rebeca Hernandez, Harshad Patil, Kun Li, Justin Langston, Yuichi Matsuyama, Shihai Zhang, Noi Atorngitjawat and Rob Klein. I would also like to thank my co-researchers, the members of Professor Runt's group: Taeyi Choi, Amanda McDermott, Alicia Castagna and Hanqing Zhao for many fruitful discussions.

I appreciate the National Science Foundation's financial support of my research through DMR-0907139.

Finally I would like to thank the remainder of my committee for providing helpful discussions and guidance, but most importantly, taking the time to be on my committee. Professors Michael Hickner, Qiming Zhang, and particularly Paul Painter, have each provided me with useful insight into the fundamentals of my research.

You do not really understand something unless you can explain it to your grandmother.

-Albert Einstein

Chapter 1

Introduction

1.1 Polymer Blends

Although an attractive solution to the problem of designing new materials, finding a pair of miscible polymers is relatively rare. The difficulty in finding two miscible polymers lies in the effect of low entropy of mixing and the lack of specific intermolecular interactions. Miscibility in binary polymer blends without strong intermolecular associations is dictated by the solubility parameters (δ) of the component polymers, with miscibility requiring $\Delta\delta$ of ≤ 0.1 $(cal.\ cm^{-3})^{0.5}$, a difficult criteria for most high molecular weight polymers[1,2].

Considering a binary polymer mixture, miscibility occurs only if the free energy of mixing ($\Delta G_m = \Delta H_m - T\Delta S_m$) is negative (equation 1.1), and the second derivative of the free energy of mixing with respect to composition (ϕ) is positive (equation 1.2). This typically requires a small value of the Flory-Huggins interaction parameter, χ.

$$\frac{\Delta G_m}{RT} = \left[\frac{\phi_1}{M_1}\ln\phi_1 + \frac{\phi_2}{M_2}\ln\phi_2\right] + \phi_1\phi_2\chi < 0 \tag{1.1}$$

$$\frac{\partial^2 \Delta G_m}{\partial \phi^2} > 0 \tag{1.2}$$

R is the universal gas constant and M is essentially the degree of polymerization of the component (1 or 2). The bracketed terms of equation 1.1 correspond to the very small, but favorable entropic contribution. The last term ($\phi_1\phi_2\chi$) accounts for the presence of physical forces which are typically unfavorable to mixing. The Flory-Huggins interaction parameter χ is related to the solubility parameters of the components by equation 1.3.

$$\chi = \frac{V_r}{RT}\left(\delta_A - \delta_B\right)^2 \tag{1.3}$$

V_r is a reference volume, and δ_A and δ_B are the solubility parameters of components A and B, which are related to the vaporization energy (E_A^v) and the cohesive energy density (C_{AA}) by equation 1.4.

$$\delta_A = C_{AA}^{0.5} = \left(\frac{\Delta E_A^v}{V_A}\right)^{0.5} \tag{1.4}$$

For high molecular weight polymers lacking specific interactions (hydrogen bonds, ionic interactions, dipole-dipole interactions), the critical value of the χ parameter is approximately $2\text{x}10^{-3}$ (equation 1.5)[3].

$$\chi_{Crit} = \frac{1}{2}\left[\frac{1}{M_1^{1/2}} + \frac{1}{M_2^{1/2}}\right]^2 \tag{1.5}$$

Failing these requirements, a binary polymer mixture will form a heterogeneous system. In reality, no single characteristic defines a miscible polymer blend, other than the thermodynamic conditions mentioned above. A single T_g determined via differential scanning calorimetry is often used as a criteria for miscibility, but exceptions to this exist: thermodynamically miscible polymer blends exhibiting two T_g's[4]. Miscible blends lacking specific interactions often exhibit a single, yet extremely broadened T_g. As will be shown below, a binary polymer mixture may exhibit a single broadened T_g, yet two distinct dynamic T_g's in dielectric spectroscopy, owing to the enhanced sensitivity of broadband dielectric spectroscopy. So it is not clear from calorimetric or dielectric measurements whether a polymer mixture is immiscible, but a single dynamic T_g measured by dielectric spectroscopy does indicate that a blend is thermodynamically miscible, since coupling on the segmental level is necessary for the appearance of a single dynamic T_g.

Perhaps the most widely studied miscible polymer blend is that of polystyrene (PS) and poly(vinyl methyl ether) (PVME). Blends of PVME and PS exhibit a χ parameter favorable for mixing at certain temperatures and compositions[5], and have been studied extensively with broadband dielectric relaxation spectroscopy (DRS)[6–9].

A single T_g is observed via differential scanning calorimetry (DSC)[10,11], a broadened dynamic T_g (segmental, or α relaxation) is observed[7,12], and time-temperature superposition (t-TS) fails[9]. It is likely that two distinct segmental relaxations occur in these blends, but the negligible dipole moment of PS renders it essentially undetectable by dielectric relaxation spectroscopy (DRS). Although mixing on the repeat unit level does occur in these systems, the local relaxation of PVME, associated with rotation of the methoxy group, is unaffected by blending, and maintains its temperature dependence at all compositions.

A similar miscible polymer blend, poly(2-chlorostyrene) (P2CS) with PVME, was investigated by Urakawa et al.[13] (see Figure 1.1). Although miscible and exhibiting a single (albeit broadened) calorimetric T_g between those of the neat components, the blends exhibit two distinctly different segmental relaxations. This is a result of concentration fluctuations[14] (or self contacts[15]), and the large mobility difference between the two components. This dynamic heterogeneity, or the appearance of two α relaxations or calorimetric T_g's in blends lacking specific interactions, is the norm for blends with differences in T_g's greater than approximately 50 °C[16–20], due to an incomplete coupling of the segmental relaxations. As with blends of PVME and PS, the local relaxations in these blends are unaffected by blending.

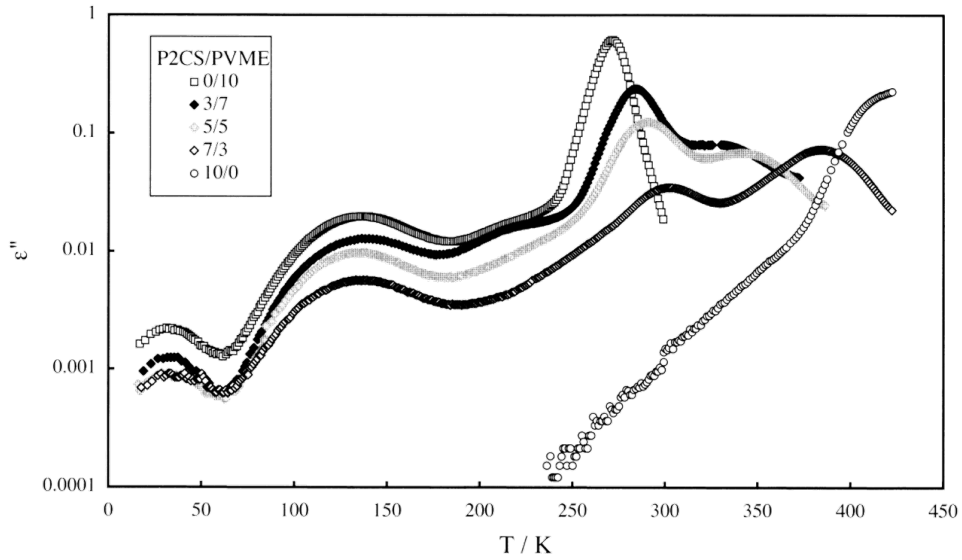

Fig. 1.1: Dielectric loss (ε'') as a function of temperature for miscible blends of P2CS and PVME at 1 kHz. Figure taken from reference 13.

Due to the effects of chain connectivity, segments of one polymer chain interact with similar segments more than they do with segments of the other component of the mixture. This self concentration, or screening, within a miscible polymer blend is the reason for the occurrence of two T_g's (see Figure 1.2). On segment-level length scales, regions of the blend contain higher concentrations of one component than the overall blend composition would suggest.

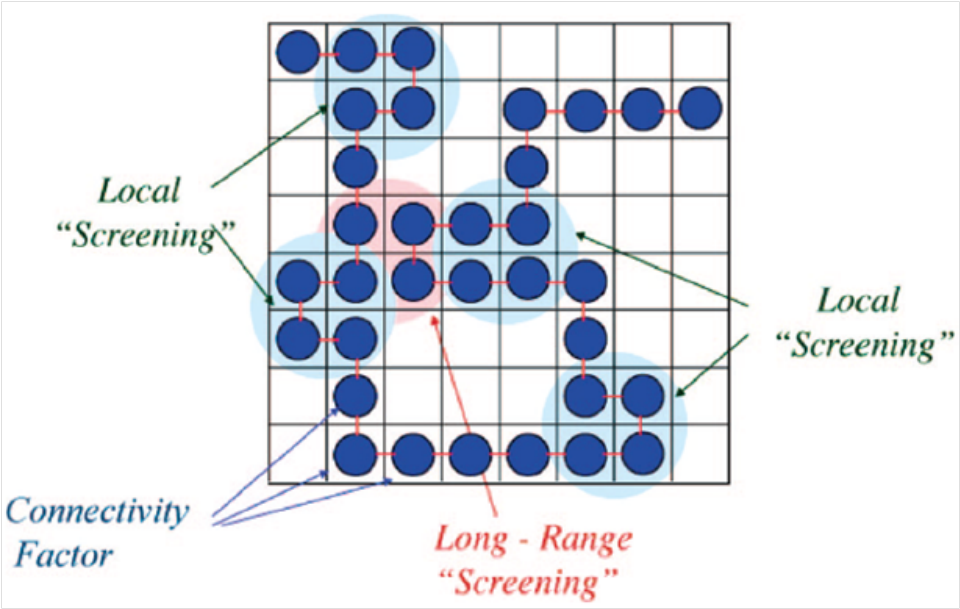

Fig. 1.2: Schematic representation of self contacts and concentration fluctuations in polymer blends. Figure taken from reference 15.

For most polymer mixtures, the compositional dependence of the blend T_g typically cannot be described by simple mixing rules such as the Fox equation (equation 1.6), which was originally used to predict the T_g of random copolymers and has subsequently been adopted for mixtures of two components [21,22].

$$\frac{1}{T_{g_{mix}}} = \frac{W_1}{T_{g_1}} + \frac{W_2}{T_{g_2}} \tag{1.6}$$

W_1 and W_2 are the weight fractions of components 1 and 2, respectively. Other equations, such as the Couchman and Karasz equation [23] and the Kwei equation [24,25] (which describes the compositional dependence of T_g in hydrogen bonding blends) can be used to approximate blend T_g's.

When the effects of chain connectivity or self concentration become relevant, and the miscible blend exhibits a broadened T_g (or even two T_g's), the Lodge-McLeish model [14] defines an effective local concentration ϕ_{eff} as follows:

$$\phi_{eff} = \phi_{self} + \left(1 - \phi_{self}\right) \langle \phi \rangle \tag{1.7}$$

ϕ is the global composition, and ϕ_{self} is the self concentration, given by:

$$\phi_{self} = \frac{C_\infty M_\circ}{k \rho N_{av} V} \tag{1.8}$$

$M_\circ$ is the molar mass of the repeat unit, k is the number of backbone bonds per repeat unit, N_{av} is Avogadro's number, ρ is the density, V is the volume, and C_∞ is the characteristic ratio, related to the polymer Kuhn length (l_K) and the length of a backbone bond (l) by:

$$l_K = C_\infty l \tag{1.9}$$

The compositional dependence of the glass transition can then be modeled by a modified Fox equation which describes the effective $\mathrm{T_g}$ ($\mathrm{T_g}^{eff}$) of each component by:

$$\frac{1}{\mathrm{T_g}^{eff}(\phi)} = \frac{\phi_{eff}}{\mathrm{T_g}_A} + \frac{1 - \phi_{eff}}{\mathrm{T_g}_B} \tag{1.10}$$

The theoretical basis for the compositional dependence of the glass transition in athermal polymer blends, and a much more thorough explanation of the effects of self contacts and self concentrations, is given in reference 15.

1.2 Hydrogen Bonding in Polymer Blends

When a proton donating group such as an alcohol shares its proton with an acceptor group, such as a carbonyl oxygen atom, hydrogen bonding occurs[26,27]. This proton sharing is the basis for a number of fundamental phenomena, ranging from interactions in DNA and its folding, to the quite unusual physical properties of water. Hydrogen bonding in polymer blends is, and has been, a topic of great interest in polymer science[1,2]. Unlike blends lacking specific interactions, miscibility in intermolecularly hydrogen bonded blends is dictated by the number of hydrogen bonds, their strength (1-10

kcal mol^{-1} versus covalent bonds with an energy of ∼50 kcal mol^{-1})[1] and functional group accessibility[28–31].

Painter and Coleman introduced a modification to the Flory-Huggins equation (equation 1.1) which accounts for the presence of specific interactions such as hydrogen bonds.

$$\frac{\Delta G_m}{RT} = \left[\frac{\phi_1}{M_1}\ln\phi_1 + \frac{\phi_2}{M_2}\ln\phi_2\right] + \phi_1\phi_2\chi + \frac{\Delta G_H}{RT} \tag{1.11}$$

The free energy of mixing equation (equation 1.11) now contains three parts. The first is the entropic part given by the terms in the brackets, which is generally favorable to mixing. The second part is a physical forces term ($\phi_1\phi_2\chi$) accounting for the non hydrogen bonding solubility parameters, and is generally unfavorable to mixing. The third part of equation 1.11 accounts for the free energy change due to the formation of hydrogen bonds, and is generally favorable to mixing. The contribution of this term to the overall free energy of mixing can be calculated from infrared spectroscopy measurements[1].

A minimum of three equilibrium constants are necessary for describing the formation of hydrogen bonds in polymer blends. Here, molecules of A and B are considered: A is a proton acceptor such as a carbonyl functionality and B a proton donor such as an OH group which is capable of forming self associations as well as associations with an A unit. The equilibrium constant K_A describes the formation of an intermolecular association; between an A and B molecule, or between an A molecule and a chain of B-mers:

$$B_n + A \rightleftharpoons B_hA \tag{1.12}$$

Since many intermolecularly hydrogen bonded polymers also readily form self associations, an equilibrium constant describing the formation of dimers (K_2) is necessary, given by equation 1.13.

$$B_1 + B_1 \rightleftharpoons B_2 \tag{1.13}$$

One additional equilibrium constant is necessary, used to describe the formation of OH 'chainlike' structures, given in equation 1.14. An individual equilibrium constant can be determined for hydrogen bonded chains for a given length (e.g. K_3, K_4, etc.), but it was found that a single equilibrium constant was sufficient to describe all chainlike structures[1], as shown in equation 1.14. A schematic of the different types of hydrogen bonds formed in these systems is given in Figure 1.3.

$$B_n + B_1 \rightleftharpoons B_{n+1} \tag{1.14}$$

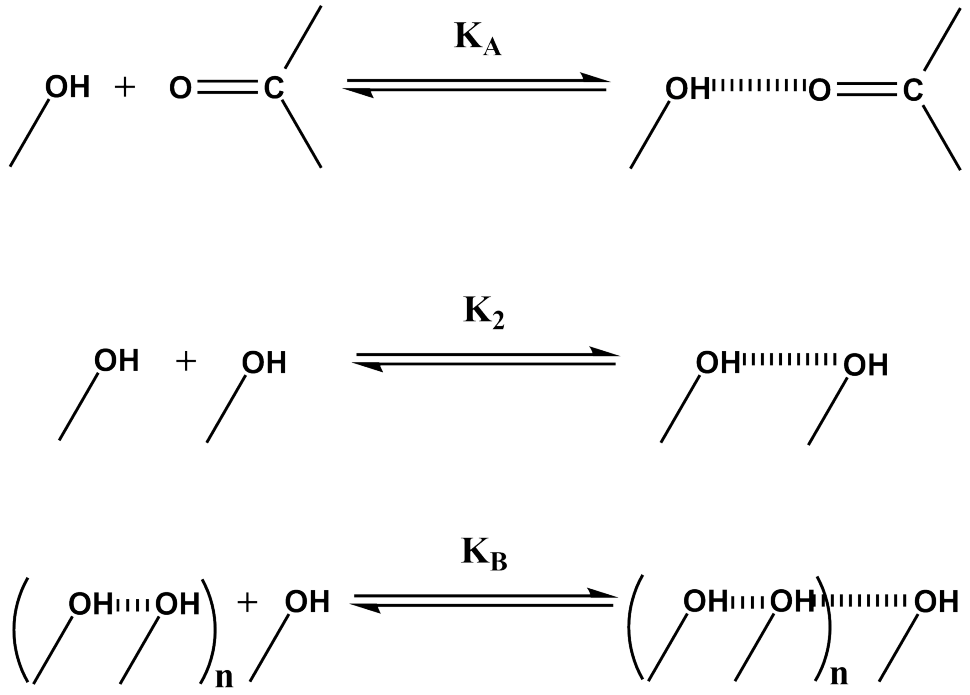

Fig. 1.3: Schematic of the three different equilibrium constants.

In the determination of the self-association equilibrium constants, K_2 and K_B, dilute solutions of the self associating species in a non-interacting solvent are evaluated spectroscopically[2]. Hydrogen bonded blends consisting of the self associating polymer

and a proton accepting polymer can then be evaluated. Values of the equilibrium constants (scaled to a common reference volume) can be determined for carbonyl-containing blends through Fourier Transform Infrared (FTIR) spectroscopy. The carbonyl region of the FTIR spectrum is sensitive to hydrogen bonding, and can be modeled with equation 1.15, which is a combination of Gaussian and Lorentzian bands[32].

$$I(\nu) = fA_\circ \exp\left[-\ln 2\left[\frac{\nu-\nu_\circ}{\Delta\nu_{1/2}}\right]^2\right] + (1-f)\frac{A_\circ}{1+\left[\frac{\nu-\nu_\circ}{\Delta\nu_{1/2}}\right]^2} \tag{1.15}$$

f is the Gaussian fraction, ν is the frequency, $\Delta\nu_{1/2}$ is the half width at half height, and $A_\circ$ is the peak height. Fitting FTIR data with equation 1.15 yields the fractions of free and hydrogen bonded segments. This data can then be fit with the stoichiometric equations developed by Painter, Coleman, and coworkers[1,2], yielding the other equilibrium constants shown schematically in equations 1.12 to 1.14. Once the various equilibrium constants are known, the stoichiometric equations can be used to determine the relative amounts of the different types of hydrogen bonding species present at any blend composition. If the equilibrium constants are evaluated as a function of temperature, the enthalpy of hydrogen bond formation can be determined using a Van't Hoff plot[1].

When polymers capable of forming intermolecular associations are mixed, hydrogen bonds form on the segmental level, and coupling of segmental motions is expected. Several studies[33–40] have examined the influence of hydrogen bonding on the dynamics of polymer blends. Since one of the components of the mixture often forms strong self associations, complete coupling of segmental motions (dynamic homogeneity) is often only observed when the molar ratio of the components approaches unity, as shown in Figure 1.4[33]. Comparing these blends to their non-hydrogen bonding counterparts such as P2CS with PVME, which has a difference in T_g's of approximately 154 °C and exhibits two segmental relaxations (see Figure 1.1), blends of PVME with poly(4-vinyl phenol) (PVPh) (Figure 1.4) exhibit a single segmental relaxation, yet have a greater difference in T_g's (nearly 200 °C). When sufficient numbers of strong intermolecular hydrogen bonds are present, complete coupling of segmental relaxations is observed.

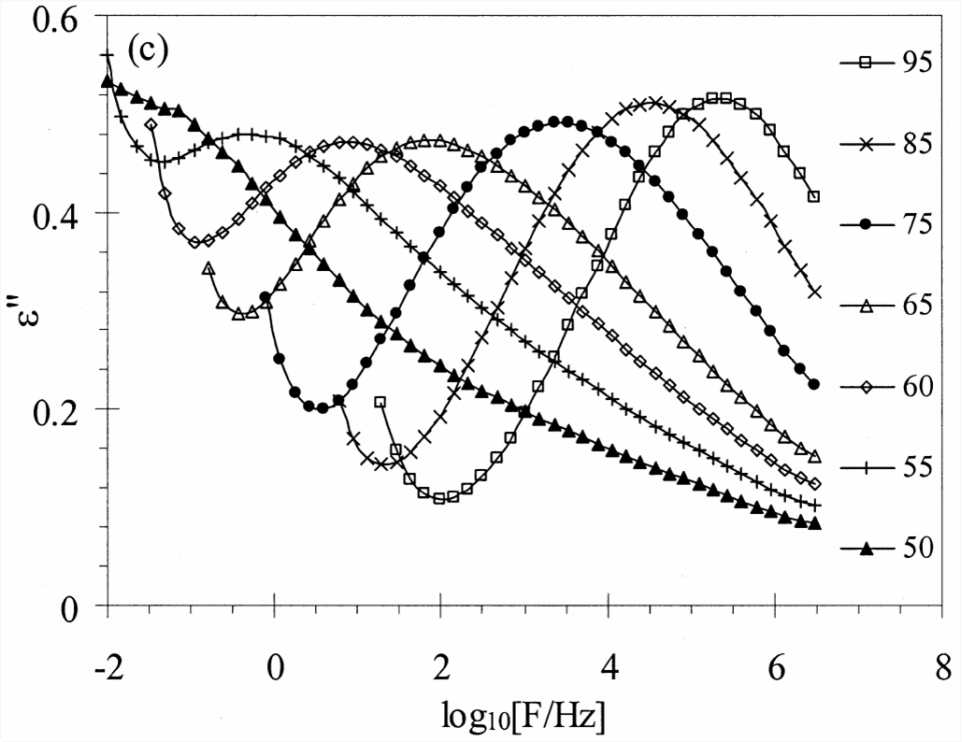

Fig. 1.4: Dynamic homogeneity in a 50:50 blend of PVME with PVPh. Temperatures listed on the right. Figure taken from reference 33.

Even in the presence of strong intermolecular interactions, dynamic heterogeneity may persist if a sufficient amount of *intra*molecular hydrogen bonding is present. In blends of PVPh and PVME, dynamic heterogeneity was observed in blends with high PVPh content (see Figure 1.5)[41]. This was attributed to the strong *intra*molecular hydrogen bonds formed within PVPh, and results in the observation of two segmental (α) relaxations[41]. Coupling of the α relaxations can be achieved in blends containing PVPh at selected compositions[35,42], but the relaxations are always broadened in these systems compared to the neat components, indicating some degree of heterogeneity.

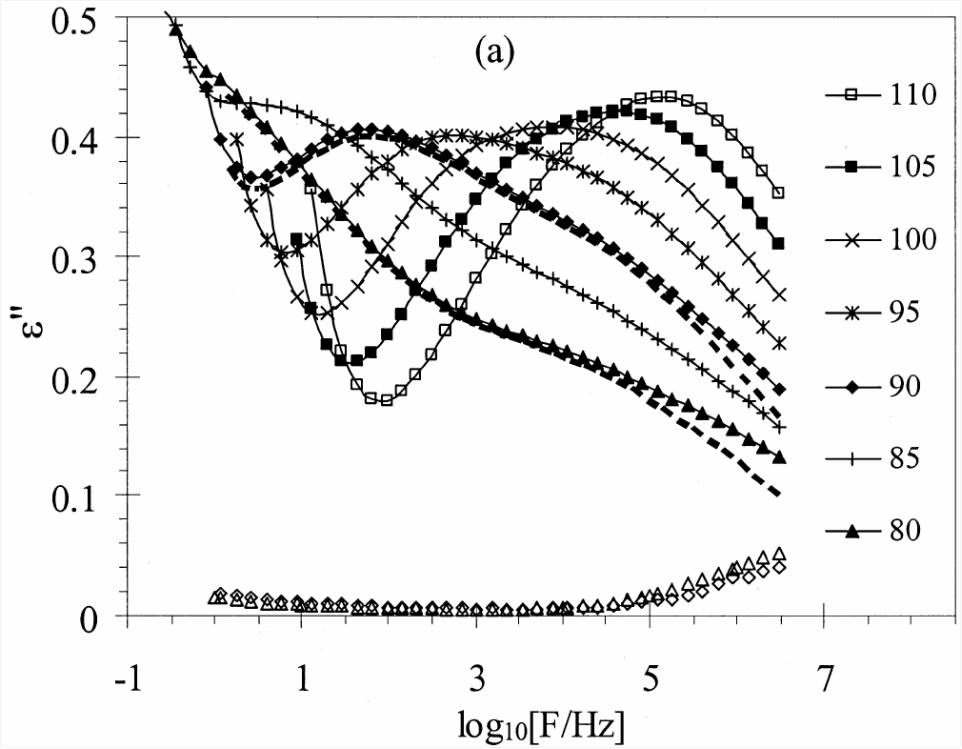

Fig. 1.5: Dynamic heterogeneity in blends of PVME with PVPh. Temperatures listed on the right. The empty diamonds and empty upward triangles are neat PVPh at 90 and 80 °C, respectively. Figure taken from reference 33.

The effects of intermolecular hydrogen bonding in polymer mixtures are not only relegated to segmental relaxations, but can influence the local glassy-state motions as well. Local relaxations often involve motions of the very functional groups which participate in hydrogen bonding, so a change in the relaxation behavior is expected as these functional groups form intermolecular associations. In non-hydrogen bonded polymer mixtures, such as polystyrene with PVME, the β relaxation of PVME is unaffected by blending, beyond simple segment dilution with the addition of polystyrene, since the PVME ether groups do not form specific interactions with polystyrene[7]. The presence of strong intermolecular hydrogen bonds (6-8 kcal/mol[1]) were found to suppress the β relaxations in blends of PVPh and P2VPy[43], as well as blends of PVME with PVPh[33]. The intermolecular associations in blends of PVPh and P2VPy were sufficiently strong

(see Chapter 4 for further details) that a complex was formed which exhibited a T_g higher than either component [43].

In blends exhibiting somewhat weaker intermolecular hydrogen bonds (less than 5 kcal/mol), such as those in blends of PVPh and poly(ethyl methacrylate) (PEMA) [42], the relaxation time of the local relaxation of PEMA is increased due to the formation of these weaker hydrogen bonds, which are insufficient for complete suppression of the local relaxation. A similar increase in relaxation time of the PVME β process was observed for mixtures of PVME with small-molecules which form weaker associations [44]. In mixtures of PVME [44] or P2VPy [45] with small molecules, it was found that as the strength of the associations decreases, the blends transition from exhibiting complete suppression of local relaxations, to broadened or slower relaxations, to relaxations which are unaffected because the interactions are too weak ($\sim$1 kcal/mol). It was proposed that the greater the extent of intermolecular hydrogen bonding, the greater the suppression of the secondary relaxation of P2VPy [43,45] and similar systems.

Functional group accessibility plays an important role in determining miscibility of blends containing specific interactions. It has been established that appropriate functionalization can dramatically reduce the fraction of *intra*molecular hydrogen bonds (or self associations), without an appreciable loss of *inter*molecular interactions [2,28–30,46–48]. Coleman, Painter and coworkers studied a series of PVPh derivatives, where the functionality at the meta positions of the phenyl ring in PVPh was systematically varied [28]. As the size of the functionality increased (proton-PVPh < methyl-PDMVPh < isopropyl-PDIPVPh), the fraction of free (non-bonded) OH groups systematically increased, as shown in Figure 1.6. Additionally, the infrared bands due to the formation of self associations shifted to higher wavenumber. The equilibrium constants describing the formation of OH-OH dimers (K_2) and OH-OH multimers (K_B) for PVPh are 21 and 66.8, respectively. For the methyl-functionalized system, PDMVPh, K_2 and K_B are 4.8 and 17.4, respectively. The isopropyl-functionalized system, PDIPVPh has equilibrium constants K_2 and K_B of 1.1 and 2.7, respectively.

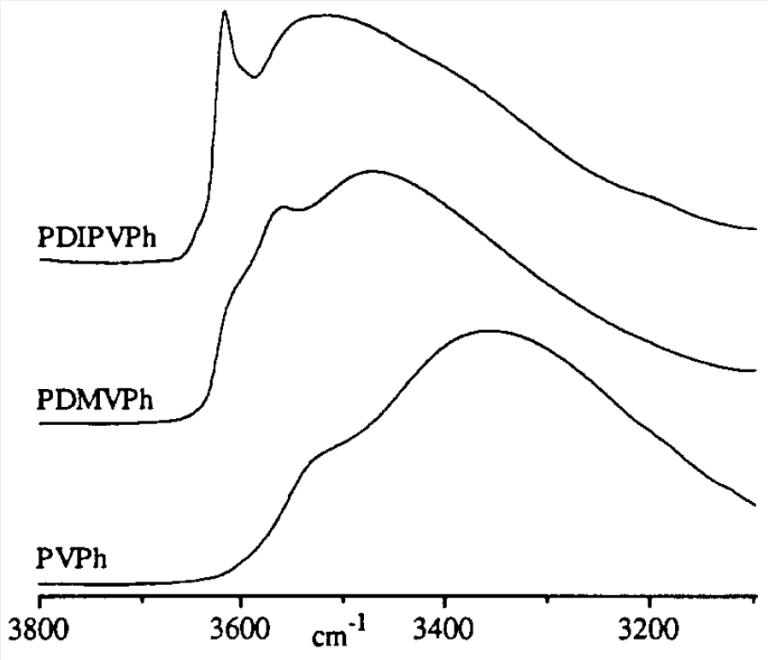

Fig. 1.6: FTIR spectra of the OH stretching region as a function of functional group size. Functionalized PVPh derivatives are shown: isopropyl (top, PDIPVPh), methyl (middle, PDMVPh), along with neat PVPh (bottom). Figure taken from reference 28.

In a similar vein, polymers based on the monomer 1,1,1,3,3,3-hexafluoro-2-(4-vinylphenyl)propan-2-ol (HFS) have been shown to form relatively few self associations[48], while readily forming strong intermolecular associations with proton accepting groups[49–51]. The equilibrium constants describing HFS self associations (K_2 and K_B) are 2.53 and 3.41, respectively, an order of magnitude lower than for PVPh. The increase in free OH groups with increasing size of the functionality providing steric shielding occurs because the diisopropyl groups (or the CF_3 groups), compared to protons, physically inhibit intramolecular hydrogen bond formation. Put simply, these groups block another similarly functionalized group from forming a hydrogen bond with its OH group, while not being too bulky to prevent the formation of desirable intermolecular associations. This strongly reduced intramolecular hydrogen bonding provides an ideal system where the effects of self associations can be largely ignored.

Although previous studies have examined the effects of intermolecular hydrogen bonding on the dynamics of polymer blends, the role of reduced intramolecular interactions on blend dynamics is not completely understood. Experiments in which the amounts and strengths of hydrogen bonding are controlled are necessary to understand how strong intermolecular coupling, when intramolecular interactions are minimized, influences blend dynamics.

1.3 Motivation and Dissertation Outline

The main focus of this work is to understand the dynamics of hydrogen bonded blends composed of polymers which exhibit minimized intramolecular interactions, and varying the number of interacting sites through carefully controlled chemistry. Systems based on the HFS monomer, shown to form relatively few intramolecular hydrogen bonds (compared to PVPh)[48], including a copolymer with dimethylbutadiene (DMB) and an HFS homopolymer, were evaluated. Copolymerizing the HFS unit with DMB, a low-T_g comonomer, allows for the direct control of the number of preferentially interassociating sites in the copolymer. The second component of the blend was chosen such that the hydrogen bonding strength is varied (P2VPy >> PVME > vinyl acetate). Additionally, ethylene-vinyl acetate copolymers provide another means by which the number of interacting sites can be controlled, by controlling the amount of ethylene in the ethylene-vinyl acetate copolymers.

Along with the ability of FTIR to detect the types and strengths of hydrogen bonding[1], DRS is an integral tool in this study. DRS is able to access an extremely broad temperature and frequency range, making it especially suitable for the study of the dynamics of hydrogen bonded blends[52,53]. It has been shown that DRS has the ability to detect dynamic heterogeneity in blends, even in the presence of a single calorimetric T_g[13,36,41,54].

The dissertation is organized as follows: Chapter 2 will provide an introduction to the basic principles and operation of broadband dielectric relaxation spectroscopy, as well as techniques used for data analysis. Chapter 3 outlines the general experimental techniques used for sample preparation, instrument operation, and general blend information.

Chapter 4 is adapted from a publication in Macromolecules (see reference 55), and deals with blends of PolyHFS with PVME and P2VPy, and how not only the strength of the hydrogen bond (P2VPy >> PVME), but also functional group accessability (PVME > P2VPy) is important. Chapter 5 is adapted from a publication in Macromolecules (submitted for publication September 2010), and examines blends of PolyHFS with ethylene vinyl-acetate copolymers, and how quantifying the carbonyl region of the FTIR allows for careful analysis of not only the glassy state relaxations, but also the dynamic fragility. Chapter 6 is adapted from a publication in Macromolecular Symposia (see reference 54), and examines blends of PVME with an HFS copolymer with dimethylbutadiene (HFS:DMB). Although possessing relatively few interacting sites, the HFS:DMB copolymer is miscible over the entire compositional range. Chapter 7, is adapted from a publication in the Journal of Non Crystalline Solids (see reference 56), and is a study on the dynamics of novel main chain liquid crystalline polysiloxanes, which are essentially blends of rigid segments and soft segments covalently bound to each other. Chapter 8 contains concluding remarks and suggestions for future work. Appendix A outlines the experimental details and results of a functionalization routine by which truly random copolymers of the HFS homopolymer and its redox product can be synthesized. Finally, Appendix B through D list C code written in Origin 8 for processing dielectric data.

Chapter 2

Broadband Dielectric Relaxation Spectroscopy

Broadband dielectric relaxation spectroscopy (BDRS or DRS) is, at its core, a method of measuring the electrical response of a sample to an applied electric field. Due to the ultrabroad frequency range probed by DRS (μHz to THz), a variety of analyzers and measurement setups are required, each with its own frequency range [52,53].

The most common technique for evaluating electrical properties in the range of μHz to MHz is impedance analysis. This method, as will be described below in section 2.1, evaluates the impedance by measuring the current passed through a sample of known geometry. Modern impedance analyzers (e.g. Novocontrol Alpha) readily measure extremely broad impedance ranges, with high resolution in phase angle.

At frequencies above approximately 30 MHz, the impedance of the cables used to carry the signal becomes significant, and a standing wave pattern can develop, obscuring any signal from the sample. At these higher frequencies, precision lines are required with known transmission coefficients. At intermediate frequencies (MHz to 10 GHz), RF Reflectometry is often used. Unlike impedance analysis, the sample is loaded at the terminus of a precision coaxial line with known propagation constant. The incident and reflected electromagnetic waves are measured in amplitude and phase. In contrast to network analysis (see below), the transmitted electromagnetic wave is not measured, since the sample is loaded at the cable terminus. From this information, the complex impedance can be calculated. In practice, these measurements are somewhat difficult, as complicated calibration procedures are necessary.

For frequencies from tens of MHz to 100 GHz, network analysis is often used. In contrast to measurements at lower frequencies, samples for network analysis are not necessarily prepared in thin film form, but loaded as part of a coaxial line. Network analysis examines the properties of both the reflected and transmitted electromagnetic waves. The intensity and phase of the reflected and transmitted waves are used in the

so-called 'S' parameter calculations, from which the complex dielectric constant can be determined[57–59]. The resolution in tan δ for this measurement setup is quite a bit lower (by 2-3 orders of magnitude) than frequency response analysis. This method also requires several calibrations to compensate for potential air gaps, and for the impedance of the transmission line. At still higher frequencies, quasi-optical setups are required, and will not be discussed here. The interested reader is referred to reference 53.

In addition to the above-mentioned methods, measurements of the complex dielectric function can also be conducted in the time domain via time domain spectroscopy. This method measures the time dependent impedance of a sample under a dc polarization. It has the benefit of being able to measure a very broad frequency range: 10 GHz to 1 μHz, albeit at an accuracy less than that of a frequency response analyzer. It also benefits from the lack of a conductivity contribution to the loss, since there is no driving electric field. An additional advantage is the measurement time at low frequencies. The amount of time required for each time sweep is the amount of time needed for the longest time (lowest frequency) measured. In contrast, a frequency response analyzer applies each measured frequency to the sample, so measurement length depends not only on the frequency range, but also on the number of frequencies being measured.

2.1 Principle of Operation

In the frequency range of the Novocontrol Alpha analyzer mentioned earlier (μHz to MHz), a frequency response analyzer is the most useful technique, which is shown schematically in 2.1. This method is perhaps the simplest of the above-mentioned methods, and it measures directly the phase and magnitude of the sample current and voltage. A bank of reference capacitors are used to accurately measure a very broad range of impedance values (0.01 to 10^{14} Ω) with high precision (Tan $\delta > 10^{-4}$).

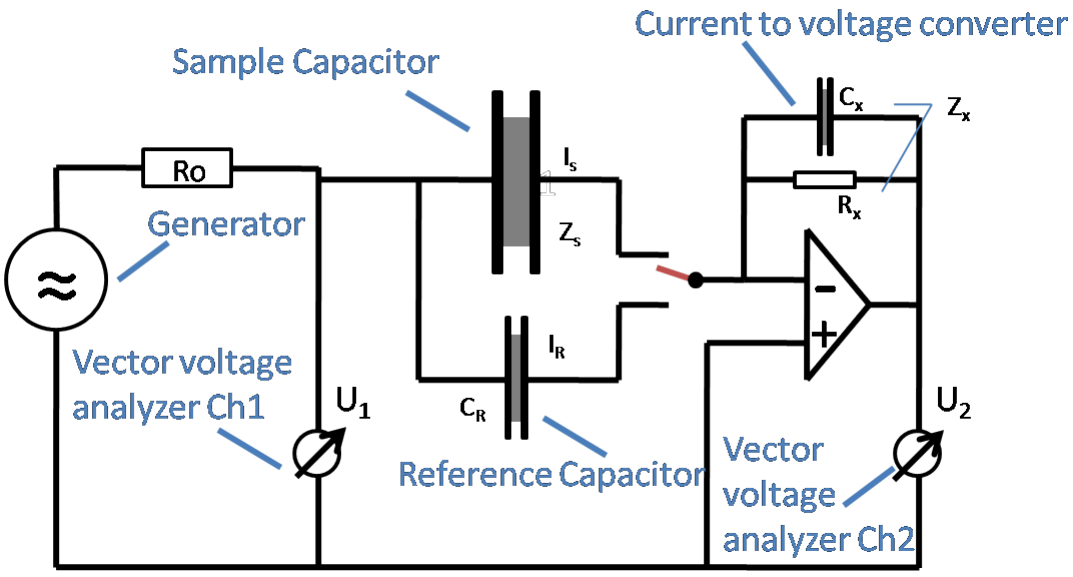

Fig. 2.1: Schematic of the Novocontrol Alpha analyzer. Figure redrawn from Novocontrol Alpha Analyzer manual.

A sine wave generator creates a voltage which is measured in amplitude and phase as U_1 ($\omega = 2\pi * \text{frequency}$). The resistor $R_\circ$ protects the machine amplifier if the sample impedance becomes too low. The sample current, I_s (see Figure 2.1) is fed to the current to voltage converter, and the resulting amplitude and phase are measured as U_2. I_s is related to the impedance by:

$$I_s = -\frac{U_2}{Z_x} \tag{2.1}$$

where the impedance (Z_x) for the sample s is given by:

$$Z_{xs} = \left({R_x}^{-1} + i\omega C_x\right)^{-1} \tag{2.2}$$

In addition to the sample measurement, a reference measurement (C_R, I_R) is performed.

$$Z_{xR} = \frac{U_{2R}}{U_{1R}} \frac{i}{\omega C_R} \tag{2.3}$$

From the reference and sample measurements, the sample impedance is calculated from

$$Z_s = -\frac{U_{1S}}{U_{2S}} Z_{xR} \tag{2.4}$$

From the sample impedance ($Z^* = Z' + iZ''$) the complex dielectric constant can be calculated.

$$\varepsilon^*(\omega) = \varepsilon' - i\varepsilon'' = -\frac{i}{\omega Z^*(\omega) C_\circ} \tag{2.5}$$

where $C_\circ$ is the capacity of an empty sample capacitor. It is the dielectric constant ($\varepsilon'(\omega)$) and loss ($\varepsilon''(\omega)$) which are most useful in understanding the dynamics of polymers, and are derived from the complex impedance, which contains the same information.

2.2 Polymers Under An Alternating Electric Field

2.2.1 Dipolar Response to an Applied Field

A dipole moment exists if a permanent (or induced) charge disparity is present, meaning the center of positive and negative charge ($\pm q$) are separated by some distance d. The dipole moment μ, having units of Debye (D), is given by:

$$\mu = qd \tag{2.6}$$

Following Kremer and Schönhals[53], and Riande and Diaz-Calleja[60], the polarization P is related to dipole moments μ_i within a particular volume V by:

$$P = \frac{1}{V} \sum \mu_i + P_\infty = \frac{N}{V} \langle \mu \rangle + P_\infty \tag{2.7}$$

where P_∞ is an induced or distortion polarization, $\langle \mu \rangle$ is the mean dipole moment, and N/V is a dipole density. If the linear response regime is considered, a time-dependent external electric field $E(t)$ will have polarization (response):

$$P = P_{\infty} + \varepsilon_{\circ} \int_{-\infty}^{t} \varepsilon \left(t - t'\right) \frac{dE(t')}{dt'} dt' \tag{2.8}$$

$\varepsilon(t)$ is the time dependent electric function, and $\varepsilon_{\circ}$ is the vacuum permittivity. If a periodic disturbance (an ac field) $E(t)(\omega) = E_{\circ} \exp\left(-i\omega t\right)$ with angular frequency ω is applied, equation 2.8 becomes:

$$P(\omega) = \varepsilon_{\circ} \left(\varepsilon^{*}(\omega) - 1\right) E(\omega) \tag{2.9}$$

ε^{*} is the complex dielectric function, and is related to the time domain by a one sided Fourier transform.

$$\varepsilon^{*}(\omega) = \varepsilon^{'}(\omega) - i\varepsilon^{''}(\omega) = \varepsilon_{\infty} - \int_{0}^{\infty} \frac{d\varepsilon(t)}{dt} \exp(-i\omega t) dt \tag{2.10}$$

ε' is related to the energy stored per cycle, or the in-phase component (analogous to the storage modulus, G'), and ε'' is the energy dissipated per cycle, or the out-of-phase component (analogous to the loss modulus, G''). ε_{∞} is the infinite frequency dielectric constant, and is defined as the square of the refractive index.

If a hypothetical frequency sweep is performed at a temperature where one type of dipole can respond to the electric field with a single relaxation time, the dielectric response (ε'' and ε') would resemble Figure 2.2.

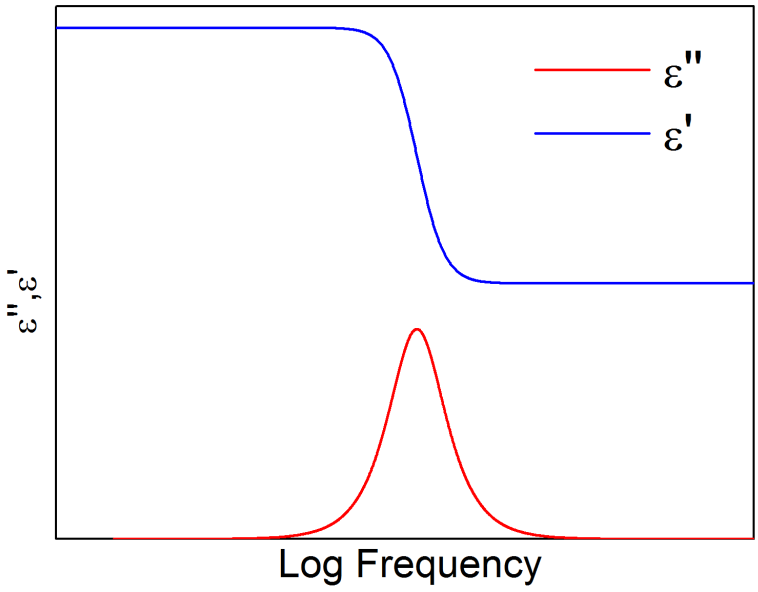

Fig. 2.2: Simulated dielectric constant and dielectric loss for a single relaxation time. The simulated dielectric constant has been offset for clarity.

The dielectric constant (ε', blue line in Figure 2.2) undergoes a stepwise increase, the magnitude of which is given by $\Delta\varepsilon = \varepsilon_s - \varepsilon_\infty$, which is the dielectric strength. ε_s is the value of ε' at low frequency, and ε_∞ is as defined above. $\Delta\varepsilon$ is given by[61,62]:

$$\Delta\varepsilon = \varepsilon_s - \varepsilon_\infty = \frac{Fg}{3\varepsilon_\circ}\frac{\mu^2 N}{k_B T V} \tag{2.11}$$

or, from the dielectric loss (ε'', red line in Figure 2.2):

$$\Delta\varepsilon = \frac{2}{\pi}\int_0^\infty \varepsilon''(\omega) d\ln\omega \tag{2.12}$$

k_B in equation 2.11 is the Boltzmann constant, F from equation 2.11 is given by:

$$F = \frac{\varepsilon_s(\varepsilon_\infty + 2)^2}{3(2\varepsilon_s + \varepsilon_\infty)} \tag{2.13}$$

and the Kirkwood-Frölich correlation factor g[53,62]

$$g = \frac{\mu^2_{\text{Interact}}}{\mu^2} \tag{2.14}$$

μ^2 is the mean square dipole moment of isolated dipoles which are not interacting (gas phase). The Kirkwood-Frölich correlation factor was introduced because calculated dipole moments are often determined in the gas phase, and are not representative of dipoles in, for example, a polymer melt where dipole correlations become relevant. This g factor can be smaller or greater than 1, and quantification of dipole moments in the condensed phase from dielectric spectroscopy is difficult at best.

2.2.2 Classification of Dipoles and Relaxations

Here only molecular dipoles which can be oriented by an electric field on the timescale of our measurements ($\sim 10^{-7}$ seconds to hours) are considered, since atomic and electronic polarization occur at frequencies well outside the range of this study (THz and above).

2.2.2.1 Type A Dipoles

Polymers possess one or more types of molecular dipoles. Stockmayer[63] classified polymeric dipoles into one of three types: A, B and C, shown schematically in Figure 2.3. Note that the schematic representation of polymeric dipoles in Figure 2.3 is an idealized case. Dipoles are oriented randomly in a polymer, and the effects of this orientation need to be considered[53,60]. Type A dipoles are dipoles which point parallel to the contour of the chain, or along the polymer backbone. The relaxation time of type A dipoles, or normal mode, is related to the terminal relaxation time (tube disengagement) of the polymer, as measured by mechanical spectroscopy[64], and its dynamics are highly dependent on molecular weight[53,65,66]. This normal mode has been observed in a small number of polymers such as polyisoprene[64,67,68], poly(oxybutylene)[69], and polyalanine[63].

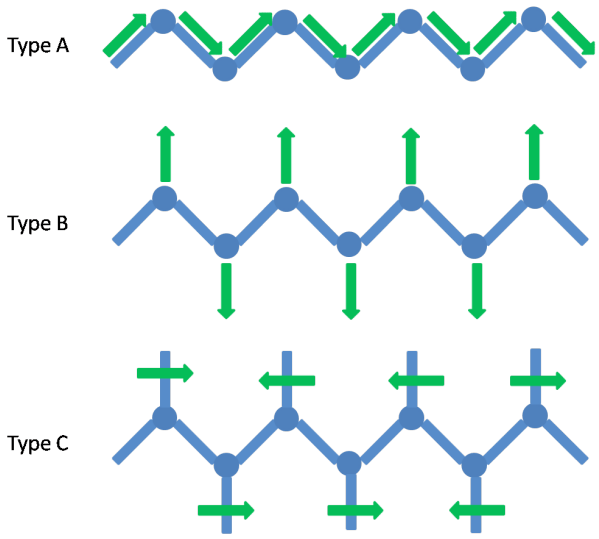

Fig. 2.3: Schematic representation of the different types of dipoles present in polymers.

2.2.2.2 Type B Dipoles

Perhaps the most important in polymer physics, type B dipoles point perpendicular to the chain contour, and are present in nearly every polymer, and is related to the dynamic glass transition, or segmental (α) relaxation. Corresponding to segmental level (micro Brownian) motion, the ability to determine the timescale of this process as a function of temperature is a task for which DRS is particularly well-suited. Type B dipoles begin to respond to the applied electric field as the experimental temperature is increased above T_g. Being a cooperative process, the α relaxation involves the motion of several repeat units, and the change in cooperativity can be quantified as a function of temperature with DRS[60,70]. DRS has been shown to be far more sensitive to inhomogeneous systems than differential scanning calorimetry and mechanical spectroscopy, often revealing the presence of multiple dynamic T_g's when only a single calorimetric T_g is observed[33,53,54].

2.2.2.3 Type C Dipoles

Type C dipoles are classified as being in the side chain of a polymer. These relaxations usually occur in the glassy state, typically termed β relaxations (or γ or δ), and involve a rotation of a dipole-containing functional group. Examples include poly(n-alkyl methacrylates)[63,71–75], poly(vinyl methyl ether)[44,54,76,77], and poly(vinyl acetate)[78–80]. Shown in Figure 2.4 is a representative three-dimensional loss spectra, containing a variety of dipolar motions. At low temperatures and high frequencies (purple arrow, or the γ relaxation), a glassy state relaxation related to type C dipoles is present.

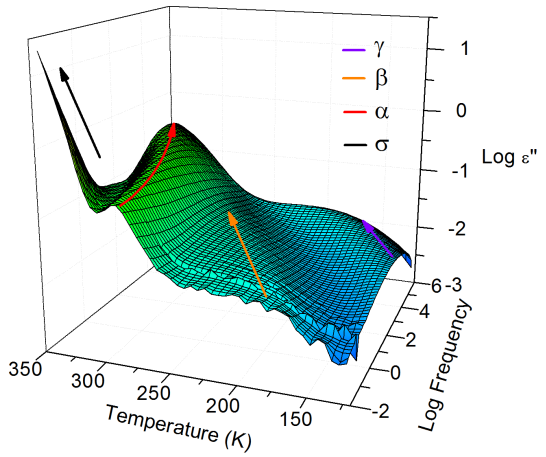

Fig. 2.4: Representative dielectric loss as a function of temperature and frequency. The purple, orange and red arrows note the approximate locations of the γ, β and α relaxations respectively. The black line is the contribution from conductivity ($\sigma_\circ$).

2.2.2.4 Water

Although containing a molecular dipole, water can be treated here as a type of relaxation. The dielectric response of water in the gigahertz frequency range has been studied extensively[57,59,81,82], and is of particular interest in proton transport in fuel cell membranes[58,83–87], biopolymers[88–91], and is the basis of microwave oven operation. In addition to the gigahertz response of water, an additional response (or responses) from

water has been found in a wide array of materials on the timescales mentioned above (100 ns to hours)[77,78,88,92–94], as shown in Figure 2.5, taken from reference 88.

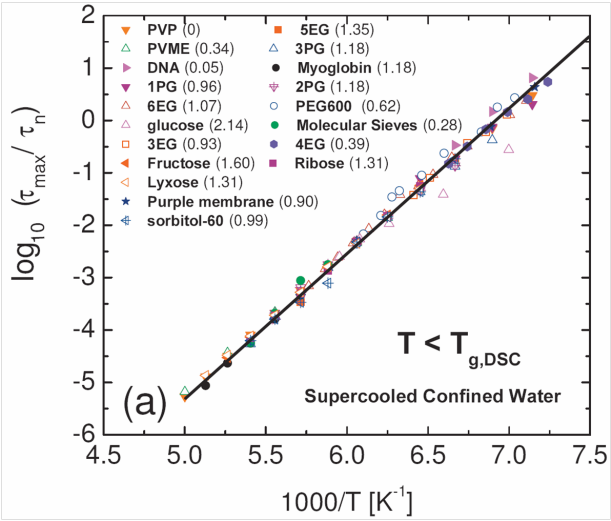

Fig. 2.5: The universal water dynamics observed in a variety of systems. Figure 3a taken from reference 88.

It is likely the 'water relaxation' in the glassy state is a ubiquitous feature of hydrated systems, and has often been mistaken as an additional polymeric relaxation[13,95]. Returning to Figure 2.4, the orange arrow, or β relaxation appears as an additional dipolar response from the polymer, but it is actually the water relaxation seen in so many systems. Water's effects on dielectric relaxations have been observed since at least the early 1990's[96]. The water relaxation does not necessarily alter the relaxation behavior of other dipoles at low water contents (see Figure 8 of reference 78), but an effect can be seen at high water contents, since water solvates many systems. Cerveny et al. observed nearly universal features of this local process, having an activation energy of approximately 50 kJ/mol, and relaxation times scaled to a universal curve (Figure 2.5). Due to the seemingly universal behavior of this process, its strength (see equation 2.11 on page 21) provides an estimate of the amount of water in the system, and it may be possible to quantify the water content if the dipole moment of the confined water can

be determined. An example of the water relaxation is shown in Figure 2.6, which is the dielectric response of PVME at -60 °C under a variety of conditions.

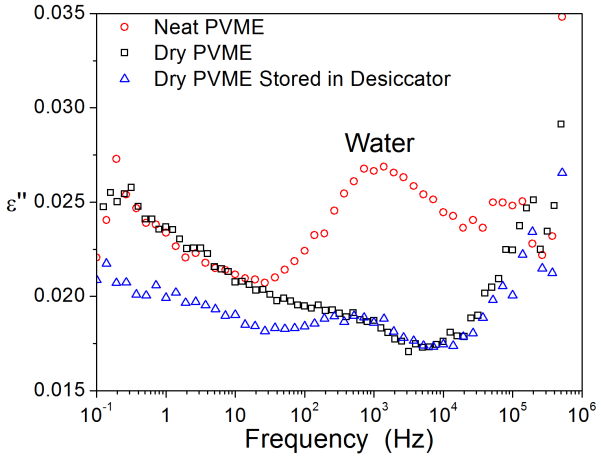

Fig. 2.6: Poly(vinyl methyl ether) at -60°C under three different conditions: neat, dried, and stored in a vacuum desiccator after drying.

The peak at approximately 1000 Hz in Figure 2.6 corresponds to water in the sample. The 'neat' polymer (red circles) was run as-received without drying. The dried polymer (black squares) was dried at 60 °C (T_g + 85 °C) under vacuum ($2-5$ μbar) for several days. The dried polymer was then placed in a vacuum desiccator with a drying agent for several days (blue triangles). Although the intensity of the water process is low for the blue triangles, its presence is a clear indication of the presence of water. The blue triangles in Figure 2.6 illustrate not only the sensitivity of DRS to the presence of water, but also waters' ubiquity. Even in a seemingly dry environment, hydroscopic samples such as PVME and those listed in the legend of Figure 2.5 will still absorb water.

2.2.2.5 Ion Motion

Conductivity is related to the motion of charged species under an applied field (ac or dc) and can be represented by

$$\sigma_{\circ} = qn_{\circ}\mu_{\circ} \tag{2.15}$$

q is the charge of the species with mobility $\mu_{\circ}$, and $n_{\circ}$ is the number density of mobile ions. The real part of the complex conductivity (from which the dc conductivity is determined) can also be calculated from the dielectric loss using equation 2.16.

$$\sigma'(\omega) = \omega\varepsilon_{\circ}\varepsilon''(\omega) \tag{2.16}$$

Conductivity is not a dipolar response, but charged species will move in response to an applied field. Conductivity often contributes significantly to the dielectric loss in the form of a power law at low frequencies, shown by the black arrow in Figure 2.4, and is a feature of nearly every system, no matter how extensive the purification. The lossy contribution from charge motion often obscures molecular (dipolar) relaxations of interest, so numerous methods have been developed to remove the contribution of charge carriers, which will be explained in detail in later sections.

Maxwell-Wagner-Sillars (MWS) interfacial polarization appears as a relaxation in the dielectric loss, and is related to the buildup of charges at the interface(s) of inhomogeneous systems, not from molecular dipole motion[53,97]. If a system such as a nanocomposite is considered, shown schematically in Figure 2.7, mobile charges in one phase will migrate under the applied field (equation 2.15) and accumulate at the interface between the inclusion and matrix.

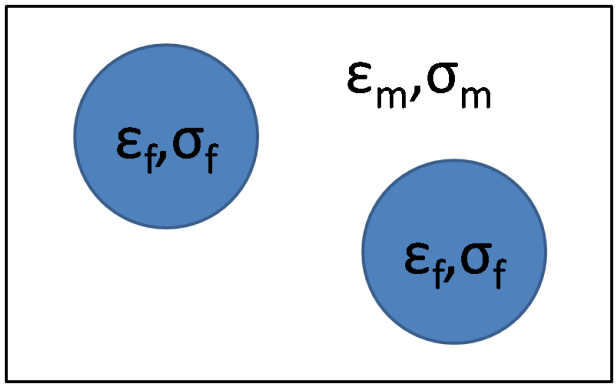

Fig. 2.7: Schematic of an inhomogeneous system.

This charge accumulation results in a dipole which can respond to the applied electric field in the same way as molecular dipoles. This relaxation may or may not occur above the bulk T_g of the system, since MWS requires charge conduction in only one phase. If, for example, an inhomogeneous mixture of two polymers is evaluated, and the T_g of one component is higher than the other, a lossy response from interfacial polarization may occur once the temperature is sufficiently above the T_g of the low-T_g component, even if the temperature is below the T_g of the high-T_g component. Charges will begin to accumulate at the interface between the two polymers, since mobile charges are present in one phase, which will create a large dipole moment.

2.2.2.6 Electrode Polarization

Electrode polarization (EP) is a specific subset of MWS interfacial polarization, and is the buildup of charged species at a blocking electrode under an applied field. In polymeric systems, this occurs at temperatures above and frequencies below the dynamic glass transition. This buildup of charged species at the electrodes causes the formation of a double layer at each electrode, screening the electric field, and causes a substantial increase (by as much as a factor of 10^6 or more) in the dielectric constant, and a correspondingly large relaxation peak in the dielectric loss, which can completely obscure dipolar relaxations of interest. This is shown more clearly in Figure 2.8. Comparing the

magnitude of the dielectric loss and constant in Figure 2.8 with those of Figure 2.6, it is clear that the effects of EP dominate the dielectric spectra when present.

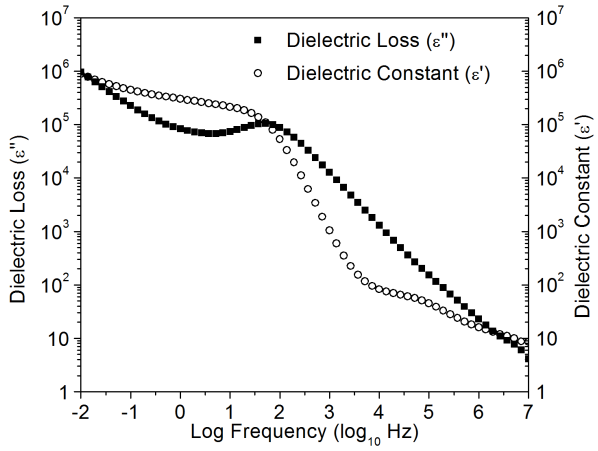

Fig. 2.8: Electrode polarization for an ion conducting polymer.

Being related to the motions of charged species, a model has been proposed to determine the numbers and mobilities of the mobile species under these conditions. Previous studies have focused on the dynamics of an idealized system consisting of blocking *uncharged* electrodes in contact with a charged species[98–104]. Fitting the EP peak with a Debye function (equation 2.24), the timescale for electrode polarization is given by[98,101]

$$\tau_{EP} = M\tau = \frac{L}{2\mu_\circ}\left(\frac{\varepsilon_R\varepsilon_\circ}{n_\circ kT}\right)^{1/2} \tag{2.17}$$

where L is the electrode separation, ε_R is the dielectric constant of the material before the onset of EP, k is Boltzmann's constant, $n_\circ$ is the free ion content, $\mu_\circ$ is the ion mobility given by

$$\mu_\circ = \frac{qL^2}{4M\tau_{EP}kT} \tag{2.18}$$

M is equivalent to 1/2 the electrode spacing multiplied by the inverse Debye length, and q is the charge of the ionic species. From equations 2.17 and 2.18, it is clear that the timescale of electrode polarization can be increased by increasing sample thickness, providing a useful method of reducing the overlap of EP with dipolar relaxations which may be of interest. Rearranging equation 2.15, the free ion content ($n_\circ$) is given by:

$$n_\circ = \frac{\sigma_\circ}{q\mu_\circ} \tag{2.19}$$

The free ion content and the mobility obtained from these calculations can be described with an Arrhenius (see equation 2.30 below) and a VFT function (see equation 2.31 below) respectively.

These models are restrictive in that the electrodes must not only be blocking, but must also be uncharged, a difficult criteria at best. In 1954, Macdonald published a series of papers dealing with the motions of ions under an applied field, specifically taking into account the presence of charged electrodes[105–109]. His work was further investigated by the colloids community, who have made much progress in describing the motions of charged species under an applied field[110–114], and was largely missed in the polymers community. A recent paper by Sangoro et al.[115] highlighted the limitations of the original model proposed by Macdonald[98]. In their study, they found the choice of electrode material (all assumed flat and blocking) *changed the relaxation time of electrode polarization by more than an order of magnitude* (see Figures 3 and 4b of reference 115), suggesting something is missing in the current treatment of electrode polarization, and native charge on the surfaces of electrodes somehow alters charge buildup at the electrode surfaces, or the timescale of EP (equation 2.17). This phenomenon means analysis based on Macdonald and Coelho's original works is valid *only* in the idealized case of a zero surface charge. Shown in Figure 2.9 is the EP relaxation for neat poly(ethylene glycol) with molecular weight 300. The relaxation time of EP is changed by more than an order of magnitude depending on the choice of electrode material. Note the differences between polished (orange diamonds) and unpolished (green circles) aluminum.

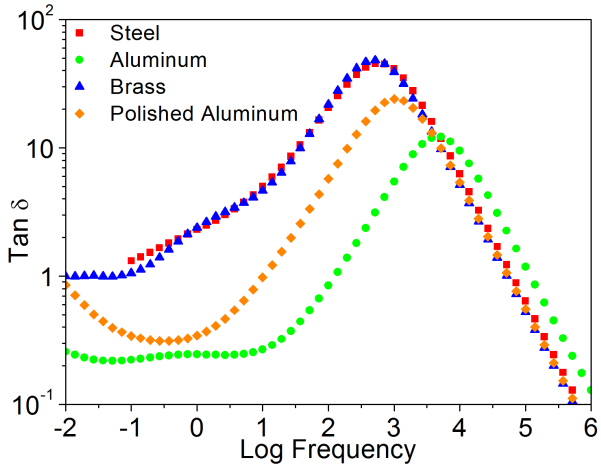

Fig. 2.9: Tan δ ($\varepsilon''/\varepsilon'$) for neat poly(ethylene glycol), molecular weight 300 at 20 °C for a variety of electrode types.

In the more realistic situation where electrodes possess some nonzero surface charge[116,117], we begin with the assumptions that the electrodes are planar, atomically smooth, non-injecting and are unreactive with the species with which they are in contact. The condition of smooth electrodes, although often imposed, seems to only be important in the limit of small electrode separations, being unimportant in the usual case where the surface roughness is far less than the electrode separation. The charged layer on the surface of the electrodes under an applied ac field has been fully described by Stern, Helmholtz and others[118]. Zhou et al., recently calculated the impedance of the double layer from the Gouy-Chapman-Grahame theory[119]. In their calculations, the resting surface charge (or ζ potential) is considered for the calculations of the total impedance of the cell. They show, albeit through the equations they define, how the voltage drop across the double layer is dependant on the ζ potential. They predict several phenomena which can be seen in impedance measurements. For instance, they predict that a change in ζ potential will change the relaxation time of the system, as well as the apparent *conductivity*. Scott et al. independently derived the solutions for the impedance of the entire cell, finding the impedance is simply the double layer impedance plus the electrode separation divided by the conductivity, where the double layer impedance is given by[112].

$$Z_{\mathrm{DL}}(\zeta,\omega) = \frac{L}{K(\omega)}\left[\frac{1}{C(\zeta,\omega)} - 1\right] \tag{2.20}$$

L is the electrode separation, $K(\omega)$ is the conductivity and $C(\zeta,\omega)$ is the capacitance of the double layer.

Scott et al.[111,112] further suggest that the relaxation time seen under an applied ac field with a nonzero ζ potential is really a weighted average, since charged species will move against a different force at each half cycle, due to the native charge on the electrodes.

We will consider here the situation defined in an excellent review by Bazant et al[120]. Under an applied potential, mobile ions migrate to the appropriately charged electrode with mobility $\mu_\circ = D/kT$ (with diffusivity D as determined by Einstein in 1905). Note that the dynamics are assumed to be in the linear regime, so a low field strength is assumed. As with other treatments of this situation, blocking electrodes are considered, and no surface reactions are assumed to occur. As noted by Bazant et al.[120] (from which the solution is obtained), the Debye length is given by

$$\lambda_D = \sqrt{\frac{\varepsilon kT}{2z^2e^2C_{\mathrm{b}}}} \tag{2.21}$$

where ε is the dielectric constant, C_{b} is the solute concentration, k is Boltzmann's constant, T is the temperature, e is the electronic charge, and z is the charge number ($z^+ = z^-$). Note that the Debye length defined in equation 2.21 is equivalent to that defined by Coelho[99]. The charging time for the double layer buildup is defined as

$$\tau_{\mathrm{c}} = R_{\mathrm{b}}C_{\mathrm{D}} = \frac{\lambda_D L}{D} = \frac{C_{\mathrm{D}}L}{\sigma_{\mathrm{b}}} \tag{2.22}$$

where R_{b} is the resistance, 2L is the electrode separation (versus L in references 101 and 104) and σ_{b} is the conductivity. This charging (or "RC") time has been part of circuit models for more than one hundred years[120]. C_{D} is the diffuse layer capacitance as defined by Chapman

$$C_{\mathrm{D}}(\zeta) = \frac{\varepsilon}{\lambda_{\mathrm{D}}} \cosh\left(\frac{ze\zeta}{2kT}\right) \tag{2.23}$$

where ζ is the steady state potential or the voltage across the diffuse layer in thermal equilibrium[118]. If the resting surface charge is neglected ($\zeta = 0$), the hyperbolic cosine of equation 2.23 is unity, and we return to the definition of τ_{EP} given by Macdonald[98] and Coelho[99]. This is shown indirectly by Scott et al.[112] in the case of a zero ζ potential. Since most experiments concerning EP are carried out using electrodes of finite (nonzero) surface charge, neglecting the ζ potential of the system will likely introduce the artifacts shown by Sangoro[115], and predicted by the model of Zhou et al[119], as shown in Figure 2.9.

Bazant considers several physical situations, including high voltages and the 'strongly nonlinear regime', but the timescales in each case are on the order of τ_{c} as defined above, as long as the thickness of the sample is large compared to the Debye length, and the Debye length is large compared to the Stern layer[120]. If the Debye-Hückel limit of small potentials is exceeded, the effect of the ζ potential is to '*slow down the final stages of double-layer charging*'[120], which will alter the timescale of EP (see Figure 2.9).

In the absence of direct measurements of the ζ potential, the model proposed by Macdonald[98] can still be used if the magnitude of the ζ potential is sufficiently low. For example, considering a ζ potential of 25 mV at 300 K, typical for oxidized aluminum, equation 2.23 is simply $(\varepsilon/\lambda_{\mathrm{D}}) * 1.005$.

An alternative approach for the determination of the fundamental quantities related to charge motion has been proposed by Kremer and coworkers[115,121–123], and will not be discussed here. The interested reader is referred to the citations listed.

One factor which should become immediately clear from the above discussion is the screened electric field is confined entirely to the charged double-layers, which are on the order of the Debye length. This has been shown theoretically by Bazant et al[120]. Shown in Figure 2.10 are the theoretical charge densities and potential distributions for a variety of voltages and timescales.

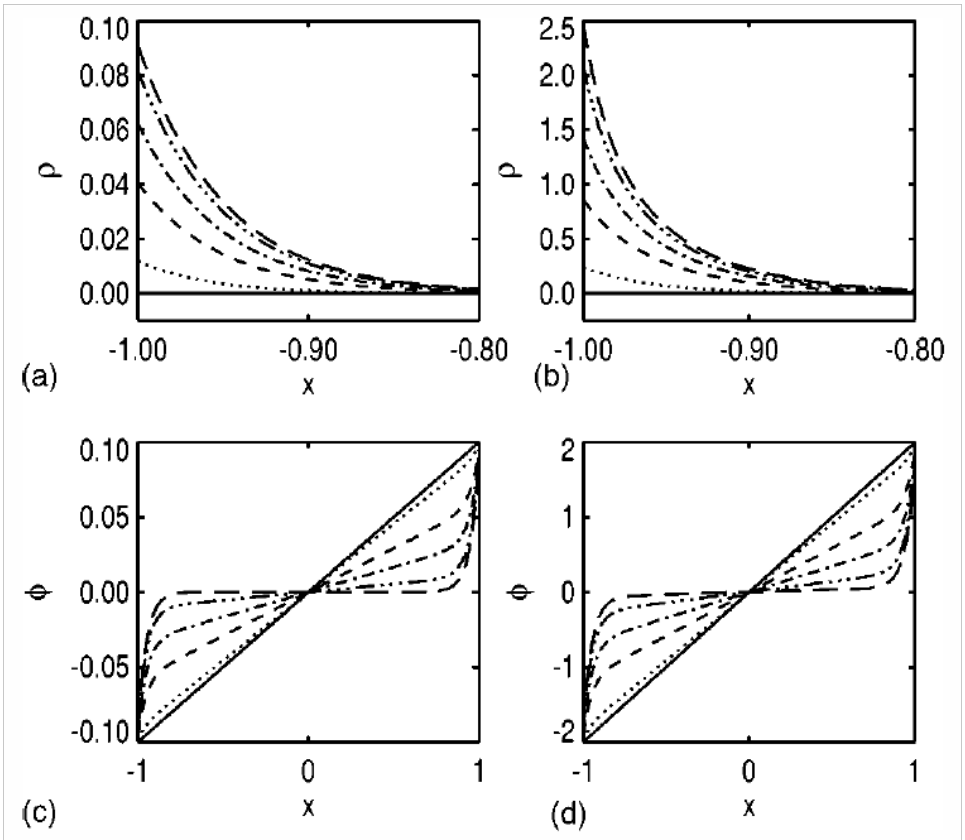

FIG. 3. Profiles for t=0 (solid), 0.1 (dot), 0.5 (dash), 1 (dot-dash), 2 (dot-dot-dot-dash), ∞ (long dash) of the dimensionless charge density $\rho(x,t)$ for dimensionless voltage (a) v=0.1 and (b) v=2, and of the dimensionless potential ϕ for (c) v=0.1 and (d)v =2(ϵ=0.05, δ=0.1).

Fig. 2.10: The charge density and potential distribution for a variety of timescales and voltages. Figure taken from reference 120.

For timescales corresponding to $\tau \geq \tau_{EP}$, the field is confined entirely within the Debye length. Assuming timescales sufficiently below τ_{EP} and an applied voltage of 0.1 Volts, the resulting field strength over a sample 50 μm thick is 2 kV/m. For the same sample at $\tau \geq \tau_{EP}$, the field is confined within the double layers, and assuming a Debye length of 5 nanometers, the field strength is 20 MV/m, well beyond the non-linear

regime. Any experiments where electrode polarization occurs (or is the main focus) must be aware of this situation.

An additional concern when analyzing highly conductive polymeric systems is the problem of reactions at the electrode surfaces. Many conductive systems are doped either with salts or with acids or bases. Under an applied potential (voltage) at elevated temperatures, ions can leach from the electrodes, invalidating any analysis based on a model used to evaluate ion motion, because the stipulation of no charge injection is violated. This problem will be particularly acute on timescales equal to or greater than τ_{EP}, since, as mentioned above, the field strength within the electrical double layers will be particularly strong. Metallic ions leached into a sample will change the free ion content, have a mobility different from the intentionally-added ion, and therefore change the conductivity. Brass electrodes in particular are sensitive to this leaching. Shown in Figure 2.11 is the wide angle X-ray scattering pattern of a polymer with an ionic liquid functionality which has been measured dielectrically.

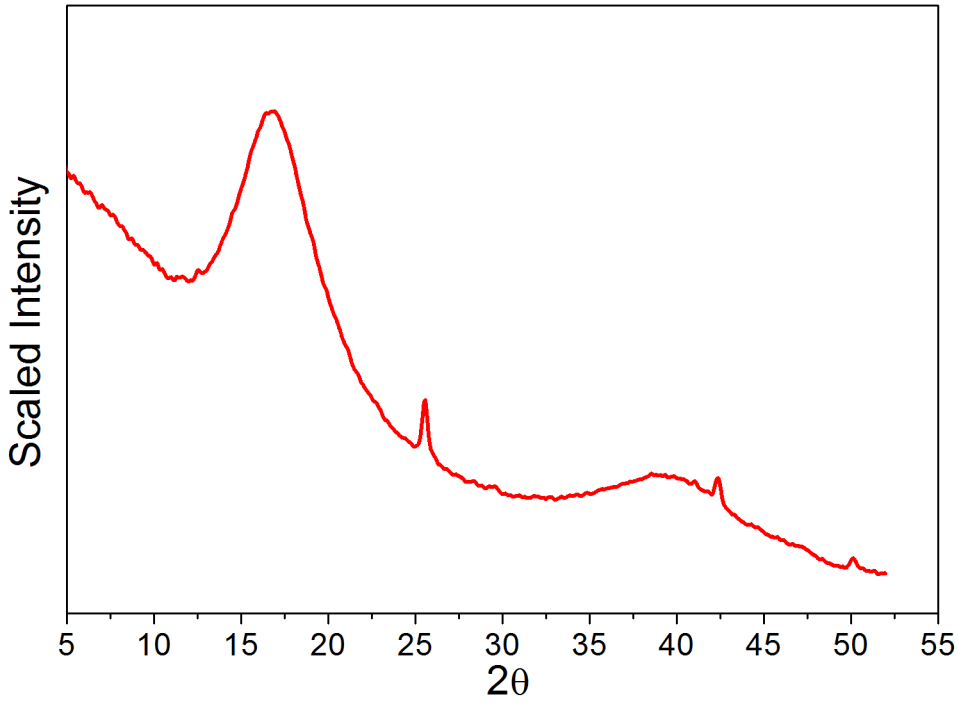

Fig. 2.11: Wide angle X-ray scattering of a polymeric sample with an ionic liquid functionality after a dielectric measurement.

The data in Figure 2.11 are for a sample where the X-ray beam was focused just next to the area covered by the brass electrodes. The sharp peaks at 25.6, 42.4, and 50.2, 2θ are from copper ions which have leached from the brass electrodes into the bulk of the polymer. The assignment of these peaks to copper ions is further supported by the observance of a metallic coating on the surfaces of the film beneath the electrodes, and a distinct discoloration of the electrode surfaces in contact with the sample. It is likely the leaching of metallic ions into the bulk of polymeric samples, in particular ionic samples, is a common occurrence and care must be taken to minimize this.

2.3 Analysis of Complex Dielectric Data

As noted earlier, the dielectric constant and dielectric loss are analogous to the storage and loss modulus measured in mechanical spectroscopy. They relate to the in

phase (ε') and out of phase (ε'') portions of the systems' dipolar response to an applied ac field.

2.3.1 Fitting Functions

In the simplest case of a single relaxation time[53,60,124], the complex dielectric function ($\varepsilon^*(\omega)$) can be described by a Debye function

$$\varepsilon^*(\omega) = \varepsilon_\infty + \frac{\Delta\varepsilon}{1 + i\omega\tau_D} \tag{2.24}$$

Again, ε_∞ is the square of the refractive index, or the permittivity at infinite frequency, $\Delta\varepsilon$ is the dielectric strength, as defined in equation 2.11, i is the imaginary number ($i = \sqrt{-1}$), and ω is angular frequency. The Debye relaxation time, τ_D is related to the maxima in the dielectric loss (ε'') by $\omega = 2\pi f = 1/\tau_D$. In the Debye case, the relaxation maximum is defined as $\omega\tau = 1$.

In the majority of cases, a Debye function fails to accurately model dielectric data. Most polymer relaxations are either broadened, asymmetric, or a combination of both. Symmetric relaxation broadening (a distribution of relaxation times) can be described by a Cole-Cole function, which introduces a broadening parameter, α[125].

$$\varepsilon^*(\omega) = \varepsilon_\infty + \frac{\Delta\varepsilon}{1 + (i\omega\tau_D)^\alpha} \tag{2.25}$$

A relaxation which is asymmetric, or broadened on the high frequency side, such as a segmental (α) relaxation can be described by a Cole-Davidson function, which introduces an asymmetric broadening parameter, γ[126,127].

$$\varepsilon^*(\omega) = \varepsilon_\infty + \frac{\Delta\varepsilon}{(1 + i\omega\tau_D)^\gamma} \tag{2.26}$$

The most commonly used fitting function, however, is the Havriliak-Negami (HN) function which describes any combination of the above-listed equations (2.24, 2.25, 2.26)[128–130].

$$\varepsilon^*(\omega) = \varepsilon_\infty + \frac{\Delta\varepsilon}{(1 + (i\omega\tau_{HN})^\alpha)^\gamma} \tag{2.27}$$

In the above-listed functions, α is the breadth parameter, γ is the high frequency asymmetry parameter, and τ_{HN} is the relaxation time of the HN function. The HN equation empirically describes any type of relaxation. Setting $\gamma = 1$, the Cole-Cole function is returned, setting $\alpha = 1$, the Cole-Davidson function is returned, and setting $\alpha = \gamma = 1$ returns a Debye function. The effect of varying the shape parameters α and γ in the HN function is illustrated in Figures 2.12 and 2.13 respectively.

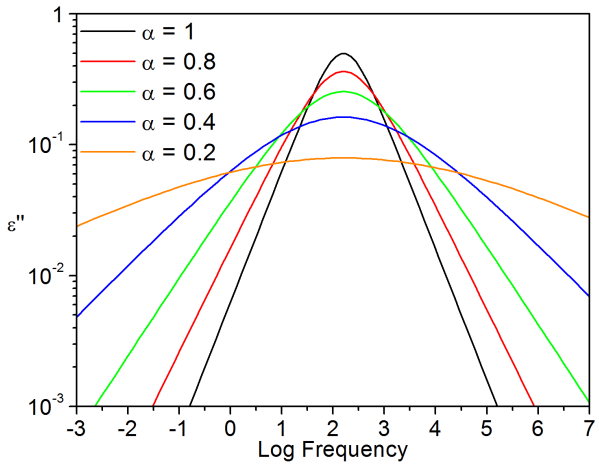

Fig. 2.12: Simulated HN function with varying symmetry parameter α with $\tau_{HN} = 10^{-3}$s, $\gamma = 1$, $\Delta\varepsilon = 1$.

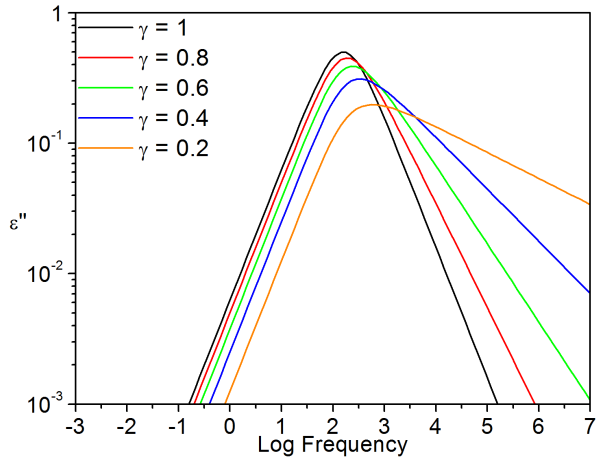

Fig. 2.13: Simulated HN function with varying symmetry parameter γ with $\tau_{HN} = 10^{-3}$s, $\alpha = 1$, $\Delta\varepsilon = 1$.

In Figures 2.12 and 2.13, the black curve is a Debye function (equation 2.24). Figure 2.12, having shape parameter γ equal to 1, is equivalent to a Cole-Cole function (equation 2.25). Figure 2.13 is equivalent to a Cole-Davidson function (equation 2.26), having symmetry parameter α equal to 1.

In the case of a broadened and/or asymmetrically broadened relaxation, the relaxation time is obtained from the shape parameters α and γ by

$$\tau_{Max} = \frac{1}{\tau_{HN}} \left[\sin \frac{\alpha\pi}{2 + 2\gamma} \right]^{\frac{1}{\alpha}} \left[\sin \frac{\alpha\pi\gamma}{2 + 2\gamma} \right]^{-\frac{1}{\alpha}} \tag{2.28}$$

In addition to a peak in the dielectric loss corresponding to a dipolar relaxation, ion motion, as noted above, may contribute to the dielectric loss. In order to describe the conductivity, an additional term is added to the imaginary part of the HN function (see equation 2.27):

$$\left(\frac{\sigma_\circ}{\varepsilon_\circ \omega} \right)^s \tag{2.29}$$

$\sigma_\circ$ is the dc conductivity (see equation 2.15) and s relates to the type of conduction present [53].

The temperature dependence of the relaxation times (or frequencies: $f = 1/2\pi\tau$) can be modeled, depending on the type of relaxation, with an Arrhenius or Vogel-Fulcher-Tamman (VFT) function. An Arrhenius function is typically used in modeling non-cooperative relaxations, such as glassy state, (β) relaxations, which are typically a result of type C dipole motions. The Arrhenius function is given by

$$\tau_{Max} = \tau_\circ \exp\left(\frac{E_a}{RT}\right) \tag{2.30}$$

where $\tau_\circ$ is the infinite temperature relaxation time of the process, R is the universal gas constant, and E_a is the activation energy of the process, usually given in units of kJ/mol or eV (1 eV = 96.5 kJ/mol). The VFT function, which is equivalent to the Williams-Landel-Ferry (WLF) function[131] is given by

$$\tau_{Max} = \tau_\circ \exp\left(\frac{B}{T - T_\circ}\right) \tag{2.31}$$

B, also written as $D * T_\circ$, is a material-specific constant and $T_\circ$ is the Vogel temperature, or the temperature at which the function diverges.

2.3.2 Numerical Methods

While DRS is an extremely powerful tool for determining the electrical properties of polymers, ion motion is mostly a nuisance, and a variety of methods have been introduced to remove its contribution to the dielectric loss.

2.3.2.1 Kramers-Kronig Relationship

The well-known Kramers-Kronig relationships state that the dielectric constant and dielectric loss contain the same information[53,100,132,133].

$$\varepsilon'(\omega_\circ) = \varepsilon_\infty + \frac{2}{\pi}\int_0^\infty \varepsilon''(\omega)\frac{\omega}{\omega^2 - \omega_\circ^2}d\omega \tag{2.32}$$

$$\varepsilon''(\omega_\circ) = \frac{\sigma_\circ}{\varepsilon_\circ \omega_\circ} + \frac{2}{\pi}\int_0^\infty \varepsilon'(\omega)\frac{\omega}{\omega^2 - \omega_\circ^2}d\omega \tag{2.33}$$

Since the motion of charged species does not contribute to the dielectric constant, with the exception of electrode polarization, the conductivity-free dielectric loss can be obtained from the dielectric constant. The relationships listed above cannot be directly applied to dielectric data, since the measured frequency range, although broad, is finite. A numerical approximation can be made, however, to obtain the conductivity-free dielectric loss. Steeman and vanTurnhout developed such a numerical approximation [133]. Steeman and vanTurnhout's approximation, however, must be used with caution because the numerical coefficients were iteratively obtained for a specific frequency spacing (a factor of 2 on a logarithmic scale). If this method is applied to dielectric data with a different frequency spacing, the results will be erroneous. A different frequency spacing requires either the numerical approximation of Steeman and vanTurnhout to be repeated for the frequency spacing of choice, or the data needs to be interpolated to have the correct spacing. Both of these methods are undesirable.

2.3.2.2 Derivative Methods

An attractive alternative to the Kramers-Kronig approximation is the derivative of the dielectric constant, developed by Wübbenhorst and coresearchers [100,134–136], based on the fact that the conductivity-free dielectric loss can be obtained from the dielectric constant.

$$\varepsilon''_D = -\frac{\pi}{2}\frac{\partial\varepsilon'(\omega)}{\partial \ln \omega} \approx \varepsilon'' \tag{2.34}$$

This formalism has been shown to partially resolve overlapping peaks in addition to removing the contribution from ion motion (again, with the exception of EP). It is of critical importance that the correct fitting function be used when modeling either the raw dielectric loss (ε''-equation 2.27) or the derivative loss (ε''_D-equation 2.35). The derivative HN function

$$\frac{\partial\varepsilon'_{HN}}{\partial \ln \omega} = -\frac{\alpha\gamma\Delta\varepsilon(\omega\tau)^{\alpha}\cos\left[\alpha\pi/2 - (1+\gamma)\theta_{HN}\right]}{\left[1 + 2(\omega\tau)^{\alpha}\cos(\pi\alpha/2) + (\omega\tau)^{2\alpha}\right]^{(1+\gamma)/2}} \tag{2.35}$$

with

$$\theta_{HN} = \arctan\left[\frac{\sin(\pi\alpha/2)}{((\omega\tau)^{-\alpha} + \cos(\pi\alpha/2))}\right] \tag{2.36}$$

is equivalent to equation 2.27, but only for the analysis of the derivative loss, since the derivative formalism alters the shape of peaks, as shown in Figure 2.14.

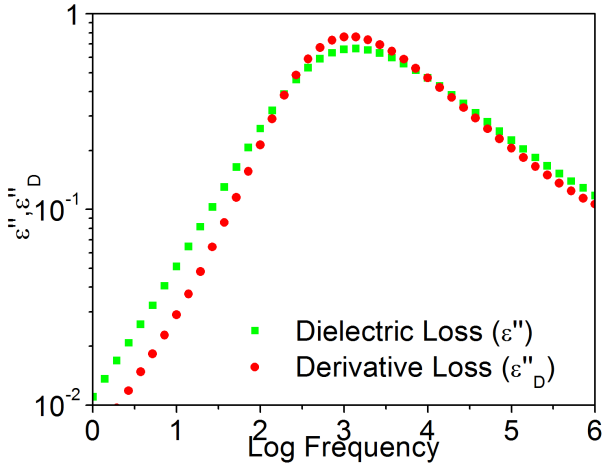

Fig. 2.14: Representative dielectric loss (ε'') and derivative loss (ε''_D) data.

The parameters in equations 2.35 and 2.36 are the same as those from the HN equation (2.27).

In computing (ε''_D), a simple derivative of the dielectric constant can be used. As outlined in Appendix B, however, a SavitzkyGolay smoothing derivative works especially well in preserving peak shapes[100,137]. An example of the application of this formalism is shown in Figure 2.15.

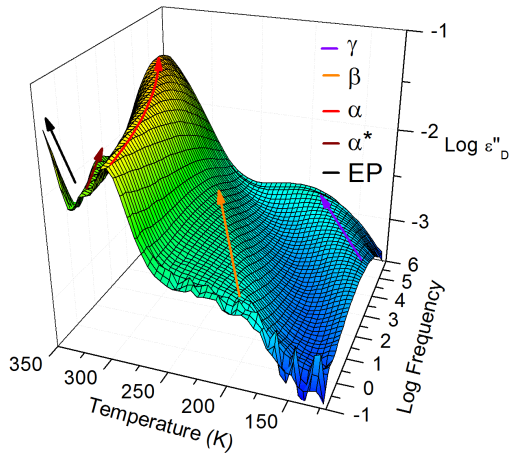

Fig. 2.15: Representative derivative dielectric loss as a function of temperature and frequency. The purple, orange, red and brown arrows note the approximate locations of the γ, β, α and α^* relaxations respectively. The black line is the contribution from electrode polarization.

The data shown in Figure 2.15 are from the same system as the data shown in the raw loss (Figure 2.4). The same features present in the raw loss (Figure 2.4) are present in the derivative loss (Figure 2.15). In addition to the glassy state relaxations and the segmental relaxation, an additional process, obscured by the conductivity in the raw loss, is revealed in the derivative loss.

The derivative formalism is particularly useful in systems where dipolar relaxations occur at temperatures above the segmental (dynamic T_g), such as hydrogen bonded systems[100,138,138–141], liquid crystalline polymers[56,134,142–145], and systems possessing a Maxwell-Wagner-Sillars relaxation such as semi-crystalline polymers[78], ionomers[146], and nanocomposites[147].

As noted above, care must be taken to ensure the appropriate fitting function is used when modeling dielectric data. If the derivative loss (ε''_D) is evaluated, equation 2.35 must be used. If the raw loss is evaluated either equation 2.24, 2.25, 2.26, or 2.27 should be used. When the appropriate fitting function is selected, equivalent results are obtained, as shown in Figures 2.16a and 2.16b. It should also be noted that performing

the Kramers-Kronig transform yields results equivalent to those obtained by derivative methods.

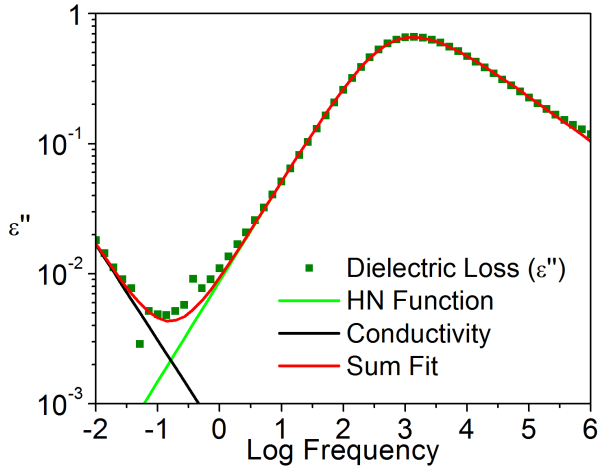

(a) Raw Loss

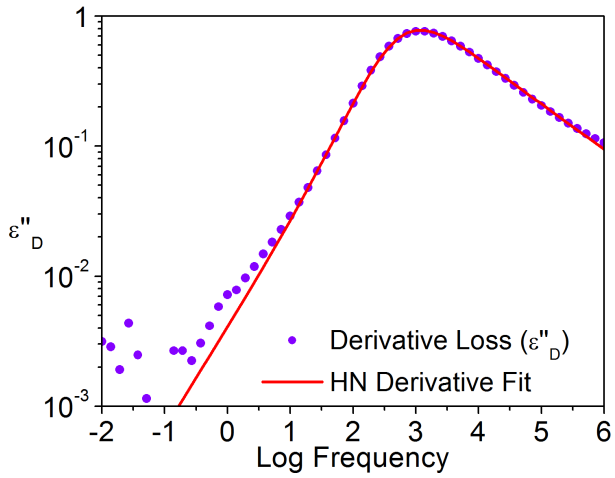

(b) Derivative Loss

Fig. 2.16: A comparison of fitting the raw loss (a) and the derivative loss (b) for the same system at the same temperature.

In Figures 2.16a and 2.16b, the following values were used for each fit: $\alpha = 0.77$, $\gamma = 0.45$, $\tau_{HN} = 10^{-3.54}$ s, $\Delta\varepsilon = 2.74$. Figure 2.16a required an additional power law to describe the contribution from dc conductivity. From equation 2.29, $\sigma_\circ = 10^{-13.7}$

S/m and $s = 0.73$. For further details concerning the application of a Savitzky-Golay derivative, see Appendix B.

As noted above, use of the derivative often reveals additional dipolar relaxations which are otherwise obscured by ion motion. In order to alleviate concerns that these relaxations are not, in fact, errors introduced by the application of a derivative, systematic errors were introduced to real dielectric data to evaluate the resulting derivative spectra. Shown in Figures 2.17a and 2.17b are the dielectric constant and resulting derivative loss when a single error was introduced at 1 Hz.

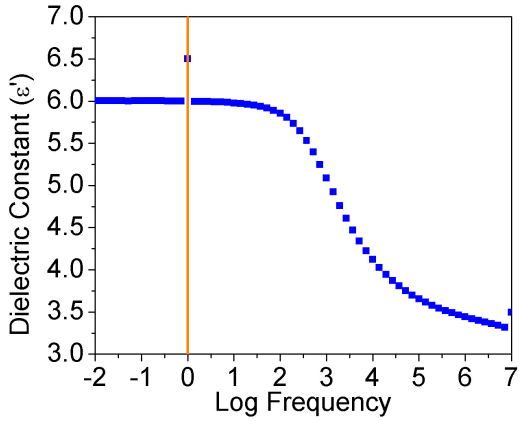

(a) Dielectric Constant

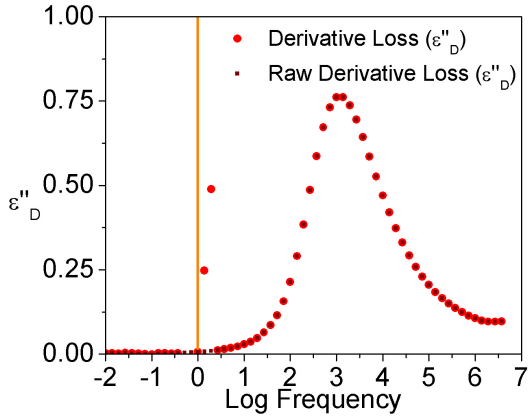

(b) Derivative Loss

Fig. 2.17: The dielectric constant (a) and the derivative dielectric loss (b) with a single error introduced at 1 Hz. The orange line marks the location of the errors. For comparison, the 'raw' derivative loss was added to (b) (brown squares).

Since a Savitzky-Golay derivative with a 5-point 'window' is used in the calculation of the derivative, two points at lower frequencies and two points at higher frequencies are altered by the introduction of this error. Shown in Figures 2.18a and 2.18b are the dielectric constant and resultant derivative dielectric loss when three random errors are introduced about 1 Hz.

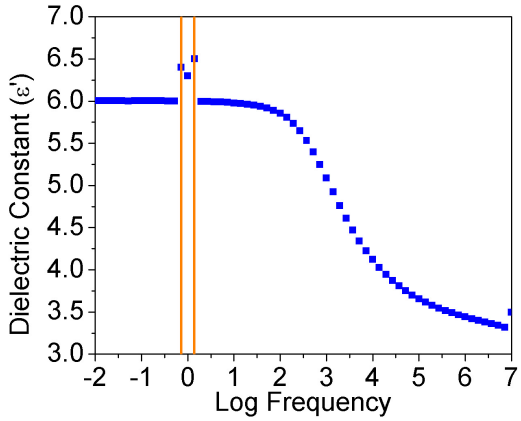

(a) Dielectric Constant

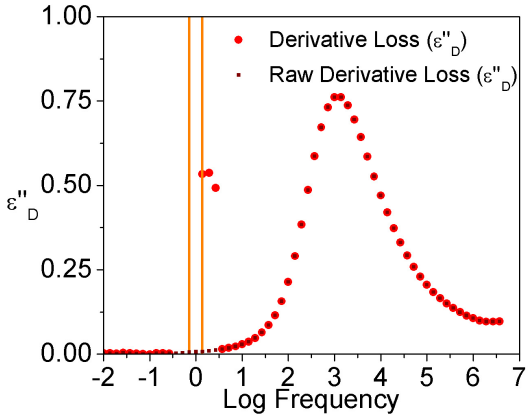

(b) Derivative Loss

Fig. 2.18: The dielectric constant (a) and the derivative dielectric loss (b) with three errors introduced around 1 Hz. The orange lines mark the region of the errors. For comparison, the 'raw' derivative loss was added to (b) (brown squares).

Again, two points above and two points below the three errors are affected, for a total of seven datapoints. Shown in Figures 2.19a and 2.19b are the dielectric constant and resultant derivative dielectric loss when an additional step function is introduced at 1 Hz in the dielectric constant.

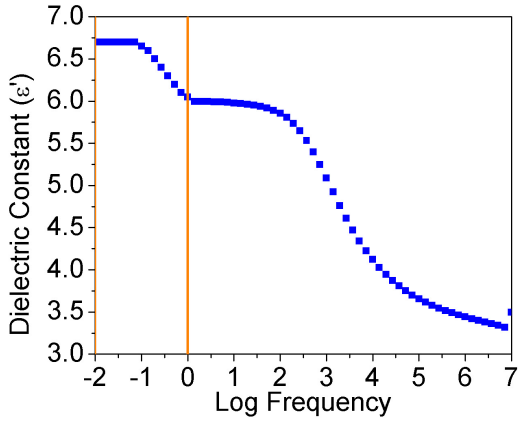

(a) Dielectric Constant

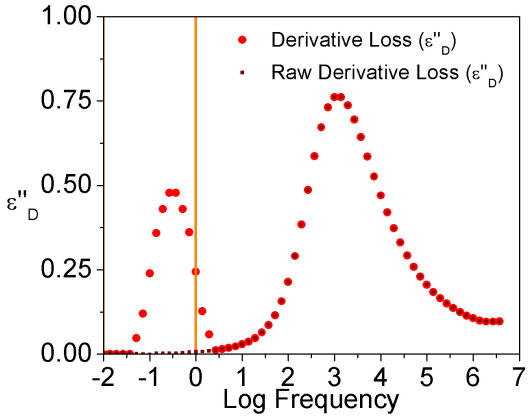

(b) Derivative Loss

Fig. 2.19: The dielectric constant (a) and the derivative dielectric loss (b) with a step introduced in the dielectric constant at 1 Hz. The orange lines mark the region of the errors. For comparison, the 'raw' derivative loss was added to (b) (brown squares).

The resulting curve in Figure 2.19b suggests that random measurement errors are unlikely to produce a non-physical relaxation in the derivative loss spectra, and the only way for an erroneous peak to appear in the derivative dielectric loss is for a corresponding erroneous step to exist in the dielectric constant, an unlikely situation.

A derivative of the dielectric loss ($\partial \ln \varepsilon'' / \partial \ln \omega$) can also be used to determine not only the relaxation frequency of the process ($\partial \ln \varepsilon'' / \partial \ln \omega = 0$) but also the relaxation's shape parameters when viewed isochronally (constant time)[100].

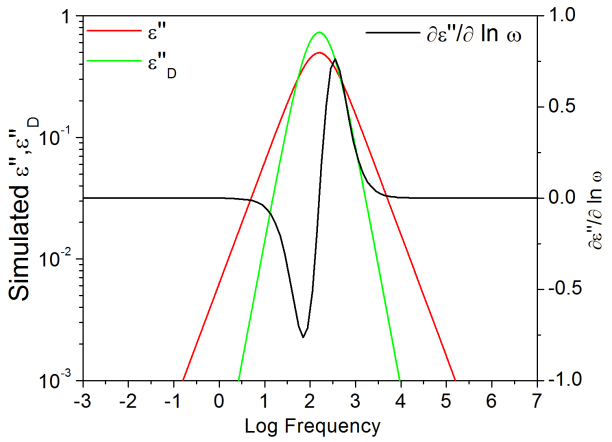

Fig. 2.20: Simulated Debye peak (red), derivative loss (green) and derivative of the loss (black) curves.

The point in Figure 2.20 where the black line crosses the x-axis (y=0) is the relaxation frequency. If several temperatures are converted so one views the loss derivative at a constant frequency as a function of temperature, the local slope ($\alpha * \gamma$ and α from equation 2.27) as a function of temperature can be determined without the need for fitting[100].

2.3.2.3 Isochronal Analysis of Segmental Relaxations

In addition to the more 'traditional' method of modeling the dielectric loss as a function of frequency with the appropriate fitting function, analysis of the dielectric loss as a function of temperature provides useful information. To visualize this using either Figure 2.4 or Figure 2.15, typical isothermal dielectric data correspond to the black lines running approximately in-and-out of the page, or data which resembles Figure 2.6. The isochronal representation of the dielectric loss from Figure 2.4 or Figure 2.15 would be

the black lines running approximately left-to-right on the page. For relaxations such as the dynamic T_g, which are well-pronounced and narrow in the isochronal representation, this is a useful method for determining the relaxation time of the process. As illustrated in Figure 2.21, isochronal analysis and Havriliak-Negami fitting yield identical relaxation times (see Appendix C for further details). Disagreement of the two datasets at high and low frequencies is expected, since a reasonable fit of the isothermal data requires one to make assumptions about the HN shape parameters at those extremes. As long as the temperature range is somewhat above and below the temperature range at which the α process is in the measurable frequency window, the isochronal method will always be more accurate.

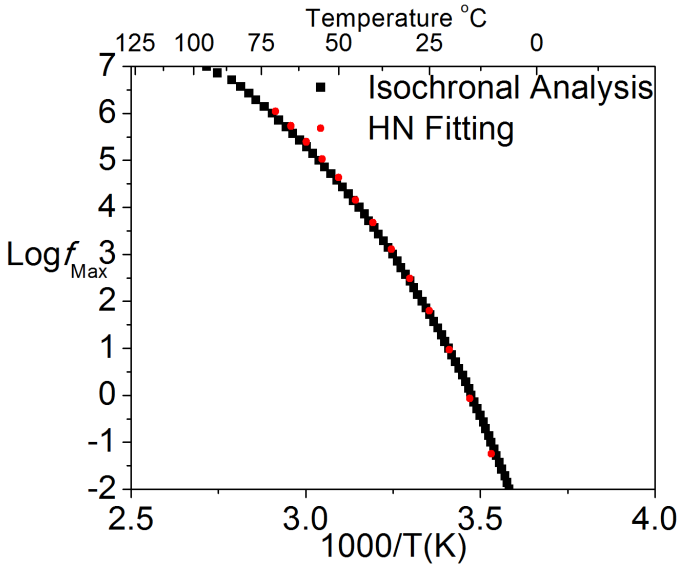

Fig. 2.21: A comparison of Isochronal analysis and Havriliak-Negami fitting for a typical segmental relaxation.

Due to the reduced intensity and increased breadth of local (glassy-state) relaxations, the isochronal method of determining relaxation times often differs from times determined by HN fitting by an order of magnitude or more, and should therefore not be employed in these cases.

Chapter 3

Experimental

3.1 Synthesis

3.1.1 HFS:DMB Copolymer

A copolymer of 1,1,1,3,3,3-hexafluoro-2-(4-vinylphenyl)propan-2-ol (HFS) and dimethylbutadiene (DMB) was synthesized via free radical polymerization. Prior to copolymerization, both the DMB and the HFS monomers were distilled. A flask of either DMB or HFS, partially submerged in room temperature water, was connected to a cold trap which was submerged in liquid nitrogen. Vacuum was slowly drawn on the system to evaporate the monomer and condense it in the solvent trap. After the majority of the monomer was distilled, the distilled monomer was slowly heated to room temperature under an argon purge.

A three neck flask, one neck containing a valve for freeze-drying was flame dried and purged with argon gas. To the three neck flask was added 2.4 mg of azobisisobutyronitrile (AIBN), along with 68.3 g of distilled DMB and 25 g of distilled HFS and a stirring bar. The flask containing the polymerization mixture was then partially submerged in liquid nitrogen to remove dissolved oxygen, a free radical scavenger. When the system had equilibrated, a vacuum line was connected, and vacuum was pulled on the now frozen mixture. After approximately 15 minutes, the vacuum valve was closed, and the system warmed to room temperature. As the mixture thawed (under vacuum), dissolved oxygen evaporated, appearing as bubbles in the mixture[i]. After equilibrating at room temperature, the freeze-thawing process was repeated three times until no bubbles were observed on warming to room temperature. To the evacuated flask was added an argon purge, which was maintained throughout the polymerization. The reaction mixture was

[i]Surely some of the observed bubbles were the DMB and/or HFS monomer evaporating, but this step is critical for the removal of oxygen in free radical polymerizations.

placed in an oil bath which was preheated to 55 °C. The mixture was stirred for 48 hours. This reaction time was chosen based upon several small-scale copolymerizations, which were performed to determine the optimal reaction time, temperature, and concentrations.

After 48 hours, chilled methanol was added to terminate the polymerization. A small sample of the polymerization mixture was taken so NMR could be used to approximate the conversion. The copolymer-containing solution was then dumped into chilled methanol and placed in the freezer. After several hours, the viscosity of the copolymer was such that it could be easily removed from the methanol/monomer solution. The copolymer was placed in a teflon jar, and an air purge was added to remove as much monomer/solvent as possible. After drying, the copolymer was placed in a vacuum oven connected to a solvent trap which was immersed in liquid nitrogen. After the copolymer was completely dried, it was dissolved in THF and precipitated into methanol. The precipitated copolymer was then redissolved in THF and passed through a 0.2 μm teflon syringe filter. After all solvent had evaporated, the copolymer was dried under vacuum at 60 °C for 24 hours.

A few milligrams of the copolymer were added to an NMR tube, and proton NMR was performed in order to determine the copolymer composition. Figure 3.1 shows the proton NMR results for the copolymer.

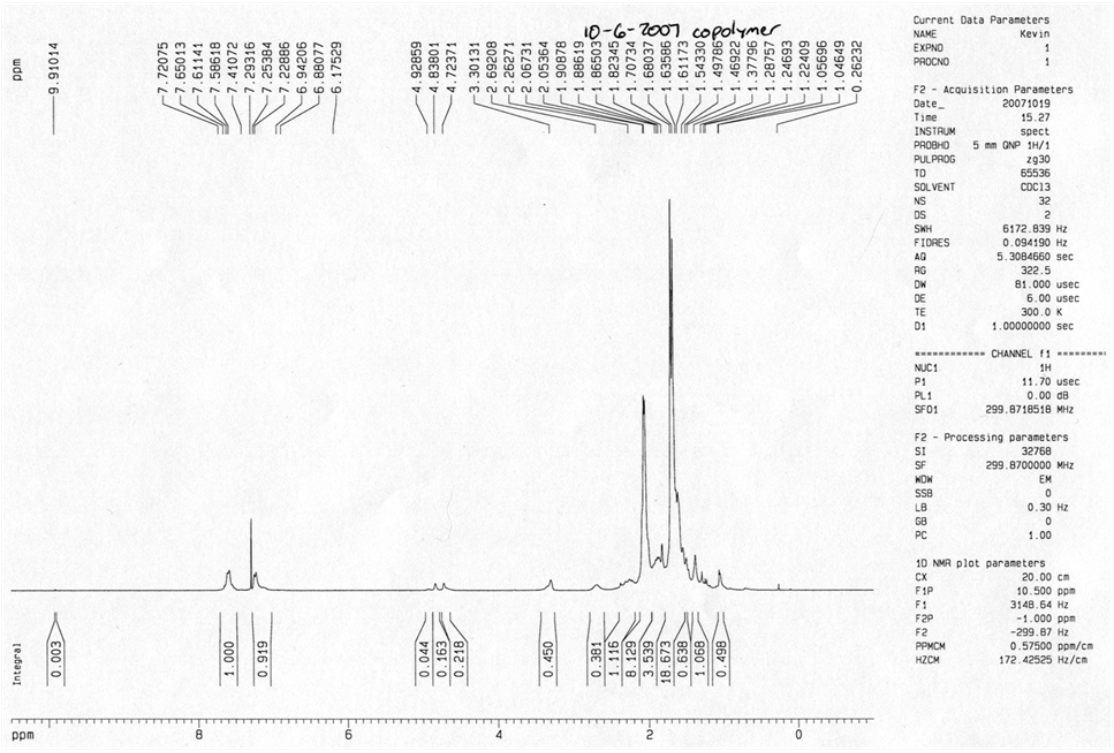

Fig. 3.1: Proton NMR of the purified HFS(14):DMB(86) copolymer.

Based on the peak intensities, the composition of the copolymer was calculated to be approximately 14 mol% HFS, 86 mol% DMB. Based on the proton NMR results of the reaction mixture (not shown), the conversion was approximated to be 12%.

3.1.2 HFS Homopolymer

An HFS homopolymer was also synthesized. Following the procedure outlined for the HFS:DMB copolymer, the HFS monomer was distilled prior to polymerization. 25 g of HFS monomer, 50 ml of toluene, 296.2 mg of AIBN and a stirrer bar were added to a 200 ml airfree flask. Again, following the procedure outlined for the HFS:DMB copolymer, the reaction mixture was freeze-thawed three times. The freeze-dried reaction mixture was placed in an oil bath preheated to 60 °C. An argon purge was added to maintain an inert atmosphere. After 15 hours, chilled methanol was added to terminate the reaction. The reaction mixture was dumped into an excess (∼3 L) of hexanes to

precipitate it from solution. After collecting the precipitate, it was dried under vacuum with a solvent trap. After drying it was redissolved in toluene, passed through a 0.2 μm teflon filter, and precipitated into hexanes. The precipitate was then collected and dried under vacuum with a solvent trap. The resulting ^{1}H-NMR for the HFS homopolymer is shown in Figure 3.2.

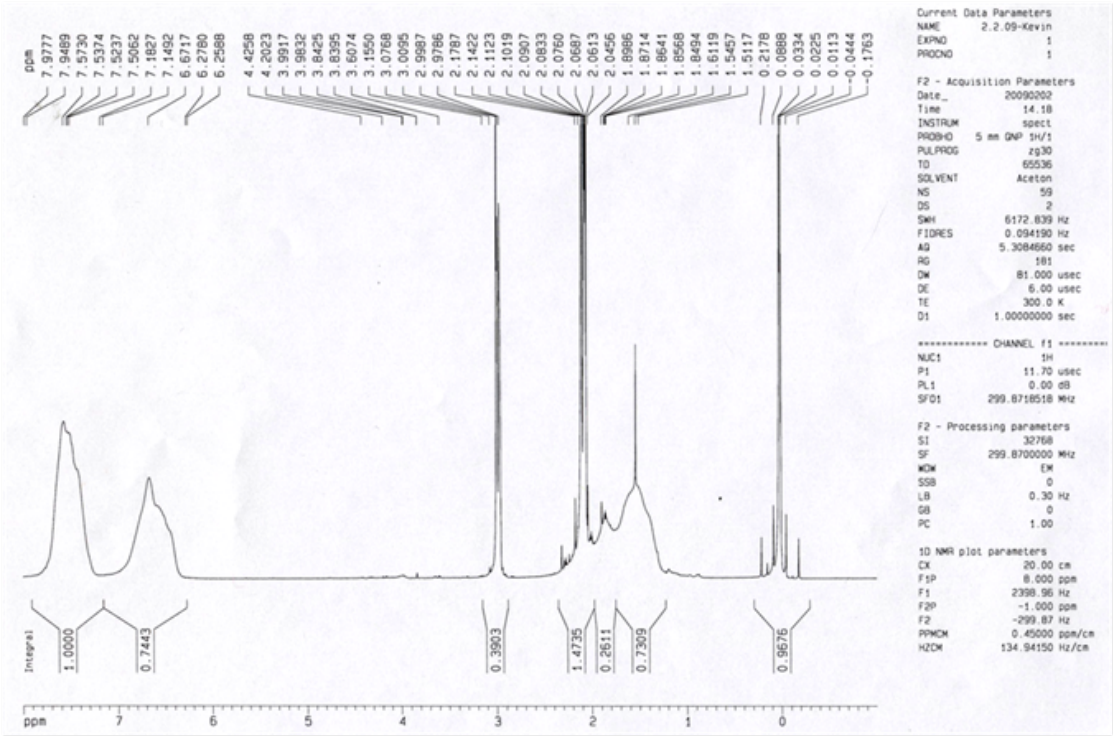

Fig. 3.2: Proton NMR of the purified HFS homopolymer.

3.1.3 Polymer Purification

Prior to any characterization, all systems studied were carefully purified to remove any impurities. After polymerization was complete, both the HFS:DMB copolymer as well as the HFS homopolymer and the commercially purchased (co)polymers were reprecipitated from good solvent. A 14% (weight/volume) solution of each system was created in a good solvent, either tetrahydrofuran or toluene. A 14% solution was found to be the optimal concentration, higher concentrations of polymer result in a larger precipitate,

the center of which is still partially dissolved in good solvent. Lower concentrations of polymer result in a precipitate which is extremely fine and difficult to recover. After the polymers were completely dissolved, the solution was slowly added to an excess of poor solvent (hexanes or water). A precipitate formed which was collected, then redissolved in good solvent. Each (co)polymer was then passed through a 0.2 μm pore size teflon syringe filter to remove any particles. An air purge was used to remove the bulk of the solvent, after which each system was dried under vacuum at least 30 $^{\circ}$C above T_g with a solvent trap for several hours. If any characterization technique suggested impurities still remained, the process was repeated until the impurity was removed.

3.2 Sample Preparation and Instrumentation

3.2.1 Blend Preparation

After sufficient purification, blends were prepared by dissolving appropriate amounts of each component in a good solvent, stirring for 24 hours, filtering the blend solution, removal of the solvent and finally drying the sample under vacuum. Each blend studied is given in either Table 3.1 for the HFS homopolymer blends, or Table 3.2 for the HFS:DMB copolymer blends.

Table 3.1: HFS homopolymer blends studied.

Blend	Weight % HFS (±1%)	Mole % HFS (±1%)	Volume % HFS (±1%)	Good Solvent
P2VPy	25	12	21	THF
	50	28	56	
	75	54	70	
	90	78	88	
PVME	25	7	18	THF
	50	18	40	
	75	38	67	
	90	69	86	
PVAc	25	10	22	Acetone
	50	24	45	
	75	49	71	
	90	74	88	
EVA70	25	13	19	90% Toluene
	50	31	42	
	75	58	68	10% THF
	90	80	87	
EVA45	25	19	17	70% Toluene
	50	41	39	
	75	68	66	30% THF
	90	86	85	

Table 3.2: HFS:DMB copolymer blends studied.

Blend	Weight % HFS:DMB (±1%)	Mole % HFS:DMB (±1%)	Volume % HFS:DMB (±1%)	Good Solvent
PVME	21	2	20	THF
	43	5	43	
	70	15	69	
	90	39	89	

3.2.2 Broadband Dielectric Relaxation Spectroscopy

Broadband dielectric relaxation spectroscopy (BDRS or DRS) measurements were performed on a Novocontrol GmbH Concept 40. The Concept 40 uses a high precision (Alpha-S) analyzer and an attached liquid nitrogen dewar for precise temperature control.

The analyzer, with its attached active sample cell, is capable of impedance measurements of samples having impedances ranging from 0.01 Ω to 10^{14} Ω over the frequency range 3 μHz to 10 MHz. Note that the practical upper limit of this setup is approximately 3 MHz, since the impedance of the lines needs to be accounted for at higher frequencies. The results for lower impedance samples are often unaffected in the 3-10 MHz region, but an observable upturn in the loss above 3 MHz is normal for higher impedance samples. The resolution in phase angle ϕ of this setup is approximately 0.001°, or a resolution in $\tan\delta$ of approximately 10^{-5}.

The temperature control system utilizes an attached liquid nitrogen dewar and a high vacuum insulation system for precise temperature control. The high vacuum system (3-5 μbar) is achieved with an attached Edwards RV5 vacuum pump. A heater in the liquid nitrogen dewar evaporates liquid nitrogen to maintain a gas pressure of 30 mbar. This gas is then heated and passed over the sample. A platinum RTD situated just below the sample provides feedback for corrections to the gas heater temperature. A precision

of 0.05 degrees is possible with this system over the temperature range of -150 °C to 250 °C.

Samples for dielectric measurements were typically cast from solution. The mass of polymer needed for a 60 μm thick film was calculated (usually $\sim$ 70-80 mg for a 30 mm diameter electrode), then dissolved in good solvent to make a 10-14% solution.

A polished brass electrode was placed on a hot plate preheated to 35 °C, and a slow argon purge was maintained over the sample to prevent moisture from dissolving into the sample. The solution was added dropwise to the brass electrode, care being taken to ensure complete coverage of the electrode surface. The argon purge was maintained at all times to remove solvent vapor and prevent the absorption of moisture.

After all solvent evaporated at 35 °C, the hot plate was slowly heated above the T_g of the blend and above the boiling point of the solvent. A five degree interval was used, and the sample was allowed to equilibrate at each temperature for $\sim$5 minutes before the temperature was increased again. After the sample had reached the appropriate temperature, it was slowly cooled to room temperature.

A vacuum oven, connected to a solvent trap, was preheated to at least $T_g + 30$ °C, and/or above the boiling point of the solvent. The now room temperature sample was placed on a glass petri dish and placed into the preheated oven. The room temperature petri dish is used to ensure the sample heats from the outside, so bubbles do not form on the electrode surface beneath the blend/polymer film. After allowing the sample to equilibrate in the oven (at atmospheric pressure), vacuum was slowly increased over the course of approximately one hour to 3-5 μbar. The sample was then kept under vacuum at elevated temperatures with a solvent trap for at least 24 hours, after which it was slowly cooled to room temperature.

An electrode smaller than the lower electrode was polished for use as the upper electrode of the system. Two, 50 μm silica fibers were used to maintain the gap between the upper and lower electrodes. The sample was briefly removed from the oven, and the upper electrode was gently clamped in place with the two silica spacers even spaced beneath the upper electrode. The assembly was then returned to the oven, and reheated to the previously used temperature to allow the sample to flow and make good contact

with the upper electrode. Care was taken when clamping the upper electrode in place to not use too much clamping force, as the silica spacers can cut into the brass electrode, thereby changing the sample thickness and potentially causing a short-circuit.

3.2.3 Fourier Transform Infrared Spectroscopy

Fourier Transform Infrared Spectroscopy (FTIR) was performed on a Nicolet 6700. An attached air purification system provided a constant purge of purified, dry air to the instrument. A background consisting of 200 averaged scans was collected before measuring each sample. 100-200 scans were averaged for each sample, using a 2 cm^{-1} or 1 cm^{-1} resolution, depending on the system. For temperature dependent measurements, a heating cell controlled the temperature of the sample. Sample thickness was adjusted to ensure the absorbance obeyed the Beer-Lambert law.

All FTIR measurements were carried out on thin films solution cast onto potassium bromide (KBr) windows. In a manner similar to dielectric samples, a polished KBr window was placed on a hot plate preheated to 35 °C, along with an enclosure (usually an inverted funnel) and an argon purge. A dilute solution of the blend under study (see Table 3.2 and Table 3.1 for solvents used), usually 2% was used. Approximately ten drops of the solution was added to the KBr window, and the argon purge was maintained to prevent water absorption. After all of the solvent had evaporated, the sample was slowly heated to at least T_g + 30 °C, or above the boiling point of the solvent. After cooling to room temperature, the sample was placed in a vacuum oven equipped with a solvent trap and dried for several hours at T_g + 30 °C, or above the boiling point of the solvent.

3.2.4 Differential Scanning Calorimetry

Differential Scanning Calorimetry (DSC) was performed on a Seiko DSC220CU. An attached liquid nitrogen dewar, as well as a high purity nitrogen gas tank controlled the sample temperature. Indium and sapphire were used to calibrate the temperature and heat capacity of the cell, respectively.

For each blend (as well as the blend components), 5-10 mg were added to an aluminum TA Instruments DSC pan and crimped to ensure no sample leaked out during the experiment. Each sample was run in the following manner:

- Heat to T_g + 50 °C at 10 °C/minute.
- Hold for 5 minutes.
- Cool to T_g - 50 °C at 10 °C/minute.
- Hold for 5 minutes.
- Heat to T_g + 50 °C at 10 °C/minute.

T_g was taken as the midpoint of the heat capacity step from the second heating run. Universal Analysis was used in the determination of T_g as well as the breadth of the transition.

Table 3.3: Molecular weight characteristics of the synthesized systems.

System	$\overline{M_W}$ ($\pm 1\ kg/mol$)	$\overline{M_N}$ ($\pm 1\ kg/mol$)	PDI
HFS:DMB	95	48	2
PolyHFS	161	95	1.7
PolyHFS	149	106	1.4

3.2.5 Gel Permeation Chromatography

Gel Permeation Chromatography (GPC) was performed on a Shimadzu system which used THF as the mobile phase and was calibrated with a series of 10 polystyrene standards. A 10 % solution was created and filtered with a 0.2 μm teflon syringe filter. Typically, 20 μL of solution was injected, and the molecular weight characteristics were determined by the instrument. The molecular weight characteristics of the synthesized HFS:DMB copolymer and the HFS homopolymers are given in Table 3.3. The

other blend components (PVAc, PVME, P2VPy, EVA70, EVA45) were purchased from scientific polymer products who reported approximate molecular weights of 100 kg/mol.

3.2.6 X-Ray Scattering

Wide angle X-ray scattering (WAXS or WAXD) was performed on a Rigaku, using copper K_α radiation ($\lambda = 1.5418$ Angstrom). Small angle X-ray scattering (SAXS) was performed on a Molecular Metrology, also using copper K_α radiation, with a 2D detector. For both WAXS and SAXS, samples approximately 0.5 mm thick were exposed for 20 minutes (WAXS) to 3 hours (SAXS), depending on the scattering intensity of the sample. Background intensity was subtracted for SAXS experiments by examining an empty sample holder for several hours. Silver behenate was used in SAXS experiments to calibrate the q range, and a Matlab routine was used in the analysis of the data.

Chapter 4

Blends of PolyHFS with Poly(vinyl methyl ether) and Poly(2-vinyl pyridine)

4.1 Introduction

Hydrogen bonds have long been known to improve polymer miscibility [1]. Miscible polymer blends which do not possess specific interactions are relatively rare, miscibility being governed by Van der Waals forces, or the so-called χ parameter. In systems where intermolecular hydrogen bonds are formed, however, the strength of these interactions (1-10 kcal/mol) often override the usual driving force for phase separation, even when the non hydrogen bonding solubility parameters of the components suggest immiscibility. For example, copolymerizing polystyrene with just a few mole percent of poly(4-vinyl phenol) (P4VPh) improves miscibility dramatically [1].

Painter and Coleman have shown that controlled steric shielding of the OH functionality reduces the ability of a homopolymer to form self associations [28,48]. Specifically, the equilibrium constants describing the formation of dimers (OH-OH bonds), and multimers (OH 'chainlike' structures) have been found to be more than an order of magnitude lower for poly(*p*-(hexafluoro-2-hydroxyl-2-propyl)styrene) (PolyHFS, see Figure 4.1) than for P4VPh, while not reducing PolyHFS's ability to form intermolecular associations [48]. In fact, as we will show, the FTIR wavenumber difference between the free OH band and the intermolecularly associated OH band(s), an indication of hydrogen bonding strength [48,148–150], is greater for PolyHFS than P4VPh, although this is not strictly due to steric shielding.

Previous studies of the dynamics of miscible polymer blends exhibiting intermolecular hydrogen bonds have found that both local [43,151] and segmental [33,35,36] relaxations are strongly influenced by the presence of these bonds. Strong intermolecular

hydrogen bonding between proton donor and acceptor groups couple the dynamics of the component polymers, even when the dynamic asymmetry (difference in T_g between the components) is as large as 150 °C. In these systems, however, many relatively strong self (intramolecular) hydrogen bonds exist in one of the component polymers, P4VPh[33,35,36,42,43,151]. At the composition extremes, this dearth of intermolecular associations can result in two segmental relaxations, even though the blend is thermodynamically miscible[33]. This is in contrast to polymer blends lacking specific interactions, where large differences in component T_g's ($> 50°C$) results in two easily discernable dynamic T_g's.[13,152]

The aim of the present study is to investigate the dynamics of miscible hydrogen bonding polymer blends with minimized self associations due to steric shielding. The proton donating species, PolyHFS, forms relatively strong intermolecular hydrogen bonds to the second component, either poly(vinyl methyl ether) (PVME) or poly(2-vinyl pyridine) (P2VPy).

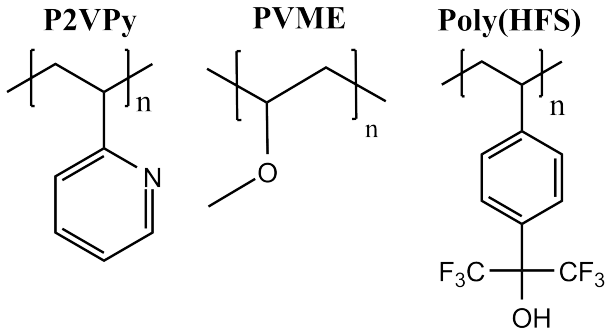

Fig. 4.1: Repeat units of the polymers examined here.

4.2 Experimental

4.2.1 Synthesis

As outlined in section 3.1, the HFS copolymer was synthesized via free radical solution polymerization. The monomer, [1,1,1,3,3,3-hexafluoro-2-(4-vinylphenyl)propan-2-ol] (HFS), was purchased from SynQuest Laboratories. Prior to use, the HFS monomer

was distilled to remove the stabilizing agent. A 50% solution (by volume) of 25 grams of HFS in toluene was added to an airfree flask, along with 140 mg of azobisisobutyronitrile, a free radical initiator. The mixture was freeze dried four times to remove dissolved oxygen. An argon purge was added, and the mixture was stirred at 60 °C for five hours, after which the reaction was terminated by the addition of chilled methanol. The polymer was reprecipitated from tetrahydrofuran (THF) into hexanes multiple times to remove impurities. Proton NMR was used to confirm the structure of the resulting polymer. Gel permeation chromatography, calibrated with polystyrene standards and using THF as the mobile phase, estimated the weight average molecular weight of this polymer as 145 kg/mol with a polydispersity of 1.6.

PVME and P2VPy were purchased from Scientific Polymer Products, both having an approximate molecular weight of 100 kg/mol, and were purified prior to use. Each was first reprecipitated from THF into hexanes for P2VPy and warm water for PVME, then redissolved in THF and passed through a 0.2 μm Teflon syringe filter. The homopolymers were then dried above T_g under vacuum for several days after the solvent had been removed. The structures of the polymers used in this study are shown in Figure 4.1.

4.2.2 Blend Preparation

As noted in Chapter 3, all blends were prepared by mixing the appropriate amounts of each component with THF to form dilute solutions (2-5%). After filtering with a 0.2 μm Teflon syringe filter, the blends were dried above T_g under vacuum with a cold trap for several days to remove solvent and moisture. Unlike P4VPh blends [43,153], PolyHFS does not readily form a complex with P2VPy in THF. No precipitate was formed during mixing or subsequent drying of the P2VPy blends.

The procedures and equipment used to evaluate the thermal characteristics as well as the infrared response of these blends are outlined in Chapter 3, but repeated here for convenience.

4.2.3 Differential Scanning Calorimetry (DSC)

As noted in Chapter 3, thermal characteristics were measured using a Seiko DSC220CU DSC. Each sample was run using the following procedure: Heat at 10 degrees per minute to T_g + 50 °C, cool at 10 degrees per minute to T_g - 50 °C, heat to T_g + 50 °C at 10 degrees per minute. The temperature was held for 5 minutes at each extreme (T_g ± 50 °C) for five minutes before continuing. T_g was taken as the midpoint of the heat capacity step from the second heating scan.

4.2.4 Fourier Transform Infrared Spectroscopy (FTIR)

As outlined in Chapter 3, FTIR was conducted on a Nicolet 6700 with an attached dry air purge. A minimum of 100 scans were averaged with a wavenumber resolution of 2. To verify the stability of the blends at elevated temperatures, temperature-dependent FTIR was conducted with an attached heating cell from room temperature to temperatures above those used in dielectric measurements. Heating and cooling scans were performed to ensure phase separation and degradation did not occur.

4.2.5 Broadband Dielectric Relaxation Spectroscopy (DRS)

As noted in Chapter 3, samples were prepared for DRS measurements by solution casting thin films from THF; 50 - 200 μm (± 3%) thick, and 30 mm in diameter. Brass electrodes were placed onto the surfaces of the film to ensure good electrical contact, usually 25 and 30 mm for the upper and lower surfaces, respectively. Silica fibers, 50 μm in diameter, were pressed into the film with the electrodes to maintain the sample thickness. DRS measurements were performed on a Concept 40 system from Novocontrol GmbH, over the frequency range of 10 mHz to 10 MHz. Temperature was controlled by a Quatro temperature control system which heats evaporated liquid nitrogen with a precision of greater than ±0.1 °C. All blends were measured over the temperature range of -140 °C to well above the calorimetric T_g. After DRS measurements, films were redissolved in good solvent to ensure crosslinking did not occur at elevated temperatures.

The imaginary part (loss) of the complex dielectric function ($\varepsilon^*(\omega) = \varepsilon'(\omega) - i\varepsilon''(\omega)$) was fit using one or more empirical Havriliak-Negami equations (see equation

2.27)[128]. $\Delta\varepsilon$ is the strength of the relaxation, and is related to the number of dipoles contributing to the dispersion[53,61,62]. ω and τ_{HN} are the angular frequency and relaxation time, respectively. α and γ are the broadening and high frequency asymmetry parameters, respectively. The second term of equation 2.27 describes the dc conductivity, a result of motions of impurity ions. $\sigma_\circ$ is the frequency-independent (dc) conductivity, $\varepsilon_\circ$ is the permittivity of free space, and the parameter s relates to the type of conduction present[53].

At temperatures above T_g, the motions of impurity ions begin to dominate the dielectric loss, often obscuring dipolar relaxations. With the exception of the phenomenon of electrode polarization, motions of ionic impurities do not manifest themselves in the dielectric constant (ε')[53]. The fundamental Kramers-Kronig relationship states the dielectric loss and the dielectric constant contain the same information, so one can be calculated from the other. Since a cumbersome numerical approximation is necessary for the Kramers-Kronig relationship to be applied (equations 2.32 and 2.33)[133], the derivative of the dielectric constant was used. Wübenhorst et al. have shown that the derivative of the real part of the complex permittivity (equation 2.34), or the dielectric constant, is a good approximation of the conductivity-free dielectric loss (see equation 2.35)[134,135]. The usefulness of this formalism is its ability to not only remove dc conductivity from the dielectric loss, but it has also been shown to partially resolve overlapping peaks[100]. As long as the appropriate fitting function is used (see equation 2.35[100]) in the analysis of the data, the derivative formalism yields results identical to the raw dielectric loss, with the added benefit of being able to deconvolute dipolar response from ion motion[100,104].

From the relaxation time (τ_{HN}) determined by fitting equation 2.27 to the dielectric loss data, or the appropriate function for the derivative loss, the frequency maxima can be calculated from equation 2.28.

4.3 Results and Discussion

4.3.1 DSC

All blends were found to exhibit a single calorimetric glass transition (see Table 4.1). At select compositions, the T_g of some P2VPy blends is between 12 and 24 degrees *higher* than the high T_g component, a result of the strong intermolecular coupling. Figure 4.2 displays the T_g's of the blends as a function of composition.

Table 4.1: Thermal characteristics of the blends studied. ΔT_g is the breadth of the transition.

Blend	Mole % HFS (±1%)	Weight % HFS (±1%)	T_g (±3°C)	ΔT_g (±5°C)
P2VPy	0	0	100	10
	12	25	110	20
	28	50	137	21
	54	75	149	15
	78	90	138	14
PVME	0	0	-26	5
	7	25	-11	24
	18	50	9	22
	38	75	61	27
	69	90	80	13
	100	100	125	11

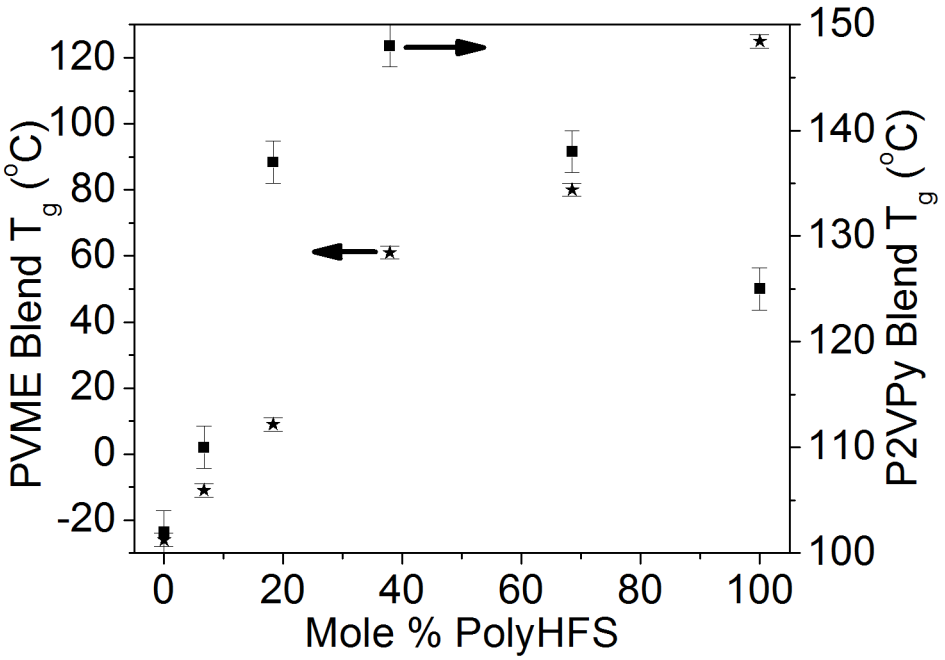

Fig. 4.2: Glass transition temperatures of the blends examined here. PVME (⋆) blend T_g's are plotted on the left axis, P2VPy (■) blend T_g's on the right.

4.3.2 FTIR

FTIR spectroscopy has been shown to be sensitive to the various states of the OH functionality (nonbonded and various types of bonded), exhibiting a variety of absorption bands in the spectral region from 3000 cm^{-1} to 3650 cm^{-1} [1]. For the HFS functionality, bands at 3602 cm^{-1} and 3520 cm^{-1} have been assigned as nonbonded or 'free' OH groups, and dimers and multimers, respectively [48]. It has been shown that as a second hydrogen bonding species is blended with the HFS functionality, an additional band (or bands) appeared, indicating the presence of intermolecular hydrogen bonds. More importantly, it was found that the wavenumber difference between the free OH band and the intermolecular association band is indicative of the strength of the hydrogen bond [48,148,149]. If the absorptivity coefficient of the band in question is unknown, however, as is the case here, only a qualitative assessment of the hydrogen bonding strength is possible [1,48].

Shown in Figures 4.3 and 4.4 is the phenolic stretching region of the blends. Both PVME and P2VPy blends exhibit strong intermolecular associations, evidenced by the appearance of new absorption bands at ∼3200 cm^{-1} and ∼2900 cm^{-1} for the PVME and P2VPy blends with PolyHFS, respectively. The relative wavenumber shifts of both the PVME and P2VPy blends suggests the HFS functionality forms slightly stronger intermolecular associations in these systems compared to poly(4-vinyl phenol) (P4VPh) [1]. In blends of PVME with P4VPh [150,154], bands associated with intermolecular associations were found to shift by no more than 350 cm^{-1}, whereas the wavenumber shift in the PVME blends examined here ranges from 350 to 450 cm^{-1}. For P2VPy blends with P4VPh, a complex was formed, and the wavenumber shift arising from the resulting associations was found to be approximately 600 cm^{-1} [153]. As shown in Figure 4.4, the band associated with intermolecular associations in the P2VPy blends is centered at approximately 700 cm^{-1} below the 'free' OH band at 3602 cm^{-1}, 100 cm^{-1} more than in analogous P4VPh blends. An exact value of the wavenumber shift in these blends is difficult to determine, however, due to the occurrence of the aliphatic and aromatic C-H stretching vibrations in the region from 2800 to 3100 cm^{-1} [153].

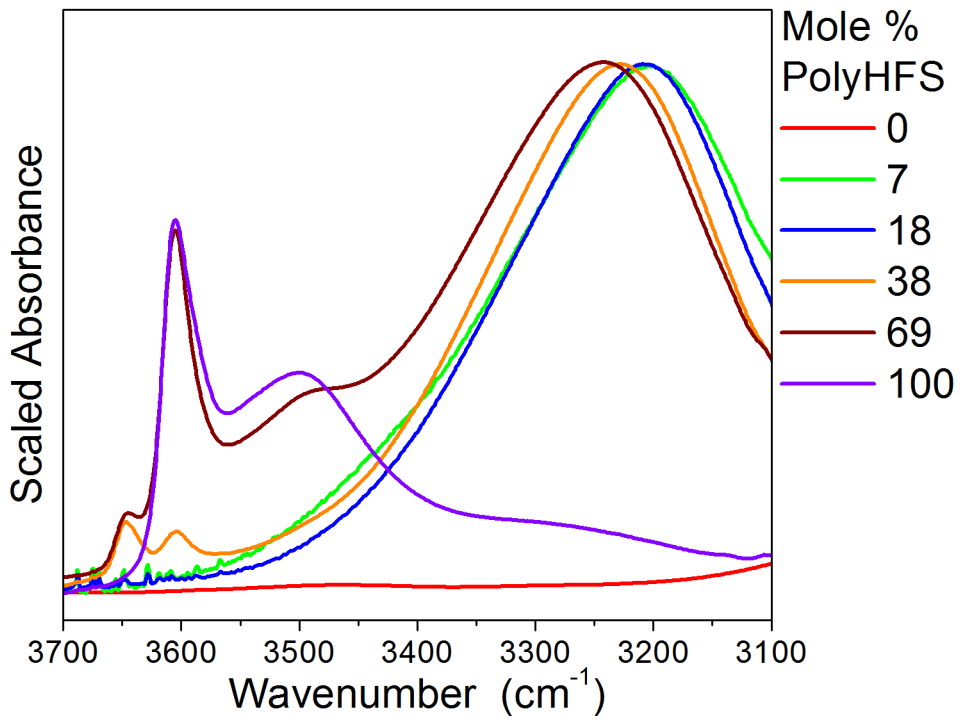

Fig. 4.3: The OH stretching region for blends of the HFS homopolymer with PVME.

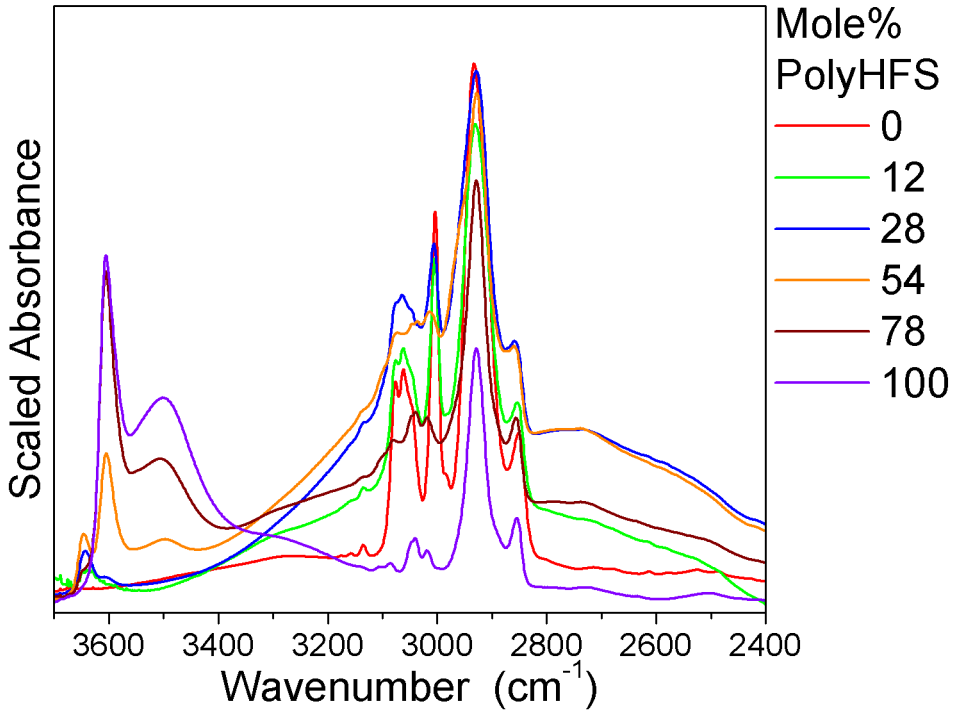

Fig. 4.4: The OH stretching region for blends of the HFS homopolymer with P2VPy.

4.3.3 Broadband Dielectric Relaxation Spectroscopy

4.3.3.1 Local Relaxations

The well-known β relaxation of PVME has been attributed to rotations of PVME's pendant methoxy group[13], and the temperature dependence of this and similar glassy state processes can be modeled with an Arrhenius equation (2.30). It is expected that formation of hydrogen bonds between the PVME methoxy group and the HFS OH group should suppress this relaxation, assuming sufficient numbers of hydrogen bonds are present, as seen in a previous study of intermolecularly hydrogen bonding blends[43]. As shown in Figures 4.5 and 4.8, the temperature dependence of this relaxation is unaffected in the blends, maintaining the same relaxation time as a function of temperature, and an activation energy of 25±2 kJ/mol. The dielectric strength, however, as shown in Figure 4.8 is strongly reduced, beyond what is expected from simply diluting the number of segments. This is shown more clearly in Figure 4.9, where the dielectric loss is scaled by the mole fraction of PVME in the system, and Figure 4.7, where the dielectric strength ($\Delta\varepsilon$ from equation 2.27) for the blend compositions where this process is present is shown. A reduction in the number of dipoles contributing to the relaxation process is expected, since a fraction of the remaining PVME methoxy functional groups will be rotationally restricted due to hydrogen bonds formed with the HFS OH groups. At the highest concentration of the HFS homopolymer (69 mol%), the local relaxation of PVME is completely suppressed. This reduction in strength is in contrast to a previous study of blends of PVME and a strongly interassociating copolymer[54]. It was shown that the relaxation time and strength of the PVME β process was unaffected by blending, beyond the effects of simply diluting the number of PVME segments, which was attributed to the relatively low number of HFS segments (14 mol%) present in the copolymer.

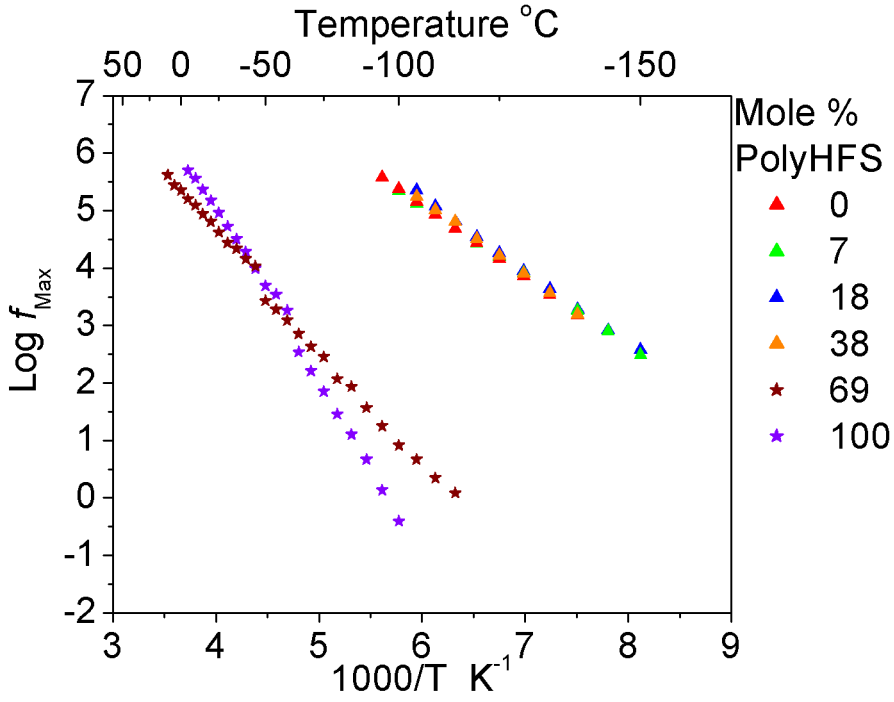

Fig. 4.5: Arrhenius representation of the β relaxations of the blends of PVME. The relaxation times of the local process of PVME [▲] and of PolyHFS [★] are shown.

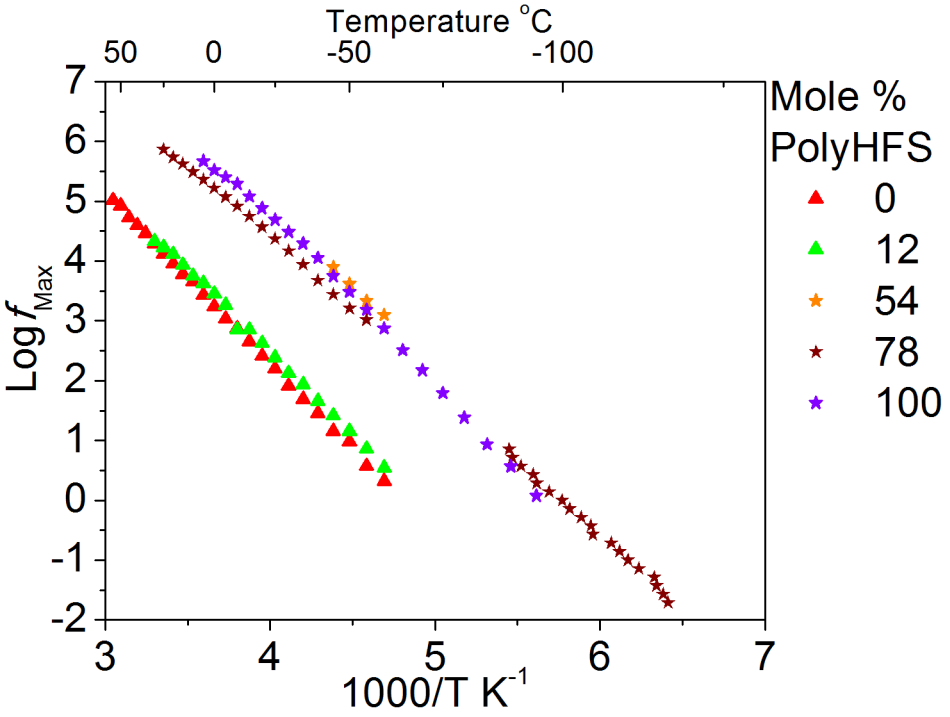

Fig. 4.6: Arrhenius representation of the β relaxations of the blends of P2VPy). The relaxation times of the local process P2VPy [▲] and of PolyHFS [★] are shown.

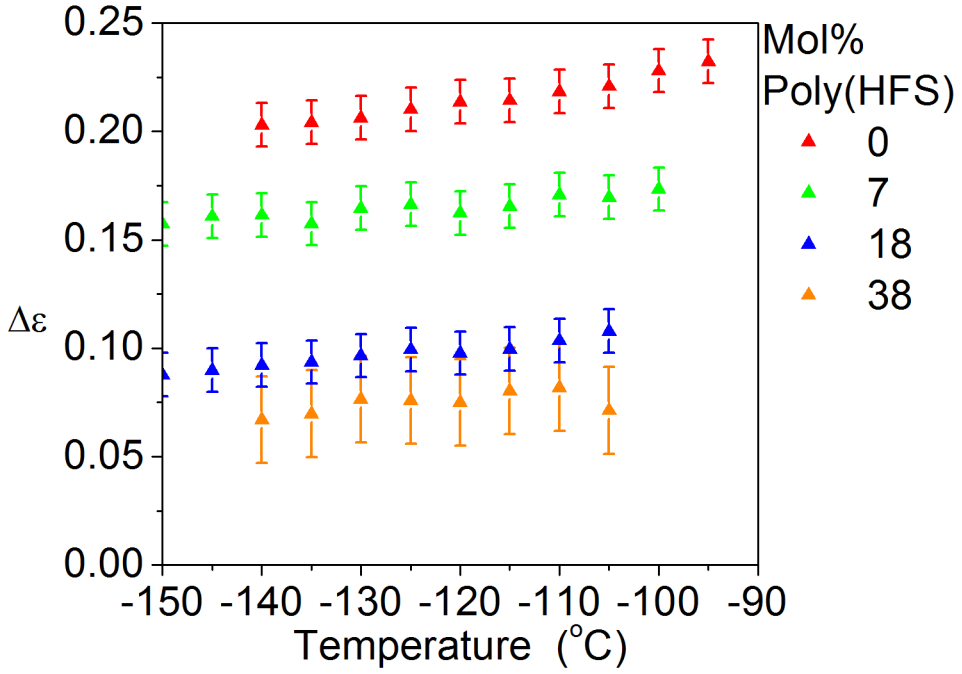

Fig. 4.7: Dielectric strength of the PVME β process in blends of PVME with PolyHFS.

In contrast to the local motions of PVME, the local process of the HFS homopolymer does exhibit a change in activation energy (from 54 to 37 ($\pm$2) kJ/mol) upon blending with PVME. The lowering of the activation energy of the PolyHFS local process in the 69 mol % blend is most likely due to the change in local environment from the neat HFS homopolymer, similar to what is observed in some plasticized systems[45,155]. It is unclear, however, why the PVME local process does not exhibit a change in activation energy in the blends, as seen in antiplasticized blends[156], or why the temperature dependence of the PolyHFS β process is unaffected in the P2VPy blends. The 69 mol% blend is the only PVME blend exhibiting a strong, free OH peak at 3602 cm^{-1} (see Figure 4.3). The 38 mol% blend exhibits a small free OH peak, but it is unlikely the sensitivity of DRS is sufficient to adequately resolve a relaxation resulting from such a small number of free functional groups. As shown in Figure 4.5, the local relaxation of PolyHFS is detectable only when it is the majority component of the blend. In a similar study of blends of

PVME and an HFS-dimethylbutadiene copolymer[54], the copolymer β process is only present in the neat copolymer, and has a temperature dependence similar to that of the PolyHFS homopolymer, suggesting this relaxation is associated with the motion of the HFS functional group.

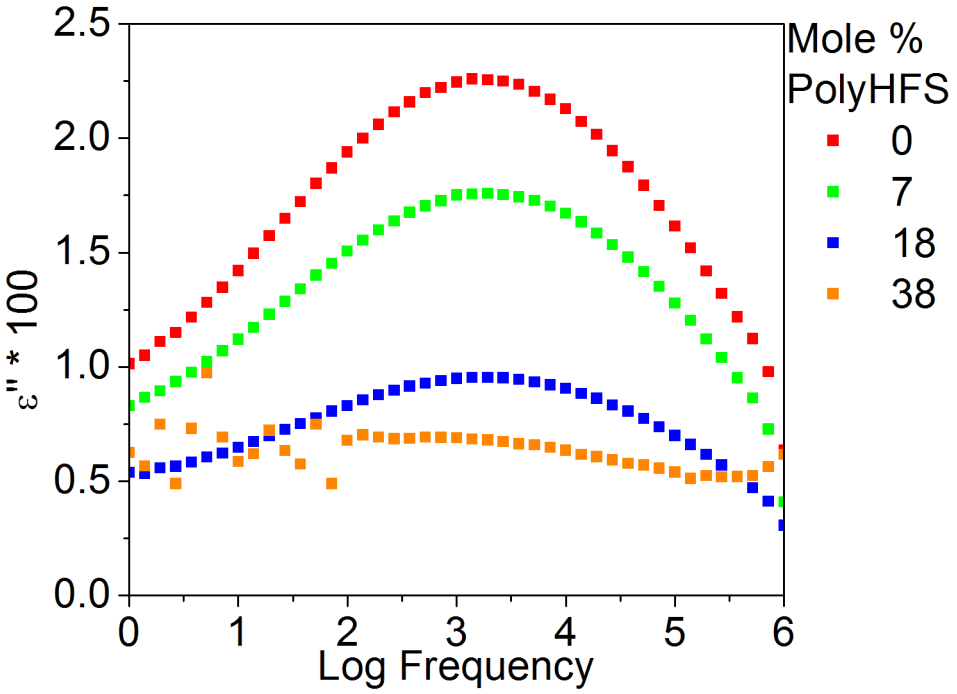

Fig. 4.8: Dielectric loss for the PVME-PolyHFS blends at -140 °C.

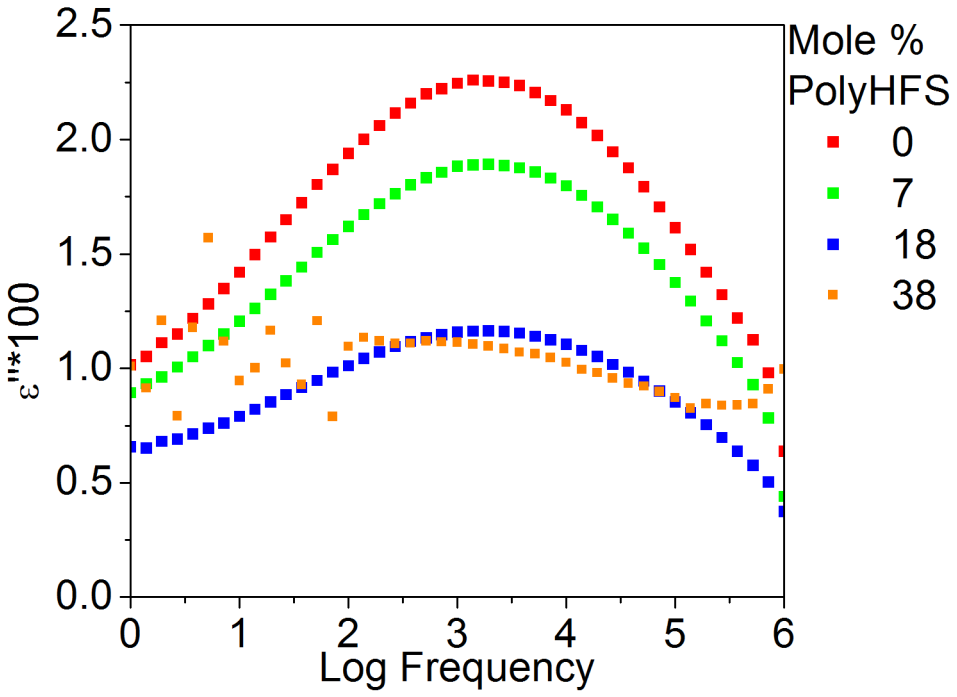

Fig. 4.9: Dielectric loss for the PVME-PolyHFS blends at -140 °C scaled by the mole % PVME.

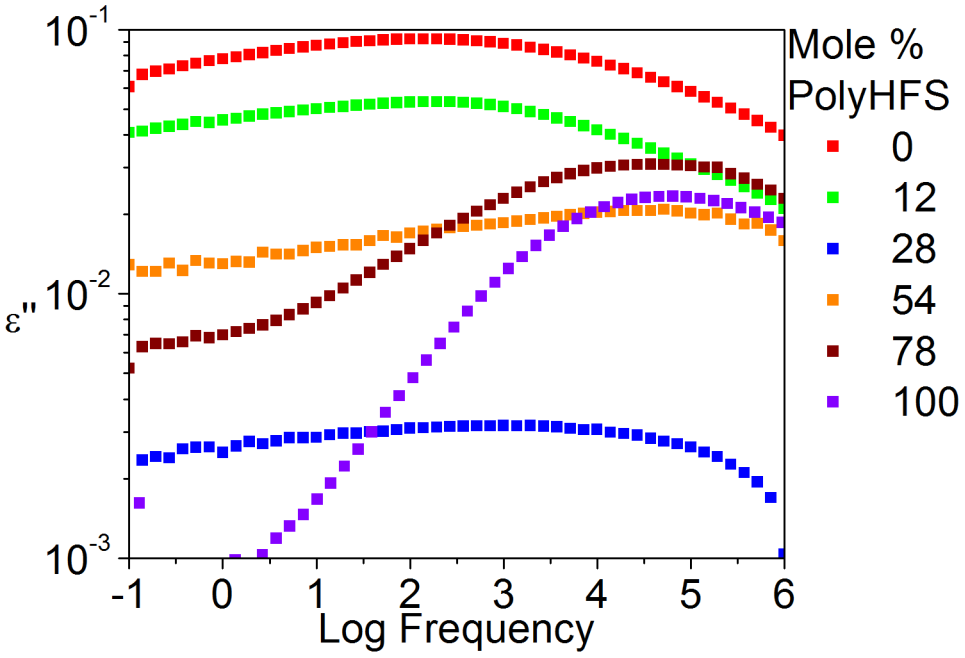

Fig. 4.10: Dielectric loss at -30 °C for the P2VPy blends.

Scaling the loss in the P2VPy blends (Figure 4.10) is not as straightforward as the PVME blends (Figures 4.8 and 4.9), since the local process of P2VPy and PolyHFS overlap. It is, however, clear that local motions are suppressed due to the strong hydrogen bonds formed. Of interest are the 28 and 78 mol% PolyHFS blends (blue and brown squares, respectively in Figure 4.10). There is a molar excess of P2VPy in the 28 mol% blend, yet the local relaxations are suppressed more strongly than at any other blend composition. This can be attributed to the fraction of segments which are hydrogen bonded to each other, and the fact that the volume fractions of P2VPy and PolyHFS are approximately equal at this composition. The P2VPy β process is present in the 78 mol% PolyHFS blend with P2VPy, even though there is a large molar excess of PolyHFS. It is clear from these results that the reduced functional group accessability in these blends plays an important role.

Various studies, including theoretical calculations and measurements, have shown that at nearly any composition, some fraction of functional groups capable of participating in a hydrogen bond will be free[1,41,48]. Examination of Figure 4.4 reveals that the 28 mol% blend is nearly devoid of free OH groups, while the 54 mol% blend exhibits not only free OH groups, but also self associations, evidenced by a small band at 3520 cm^{-1}. This underlines the effect of functional group accessability on the ability of two polymers to form associations. Since both PolyHFS and P2VPy have 'free' functional groups in the 54 mol% blend, the local relaxation of both polymers should be present. Note that in Figure 4.10, a very small peak in the 28 mol% blend related to the local relaxation of P2VPy does appear to be present, but its intensity is too low for its relaxation behavior to be accurately modeled. As noted earlier, since the absorptivity coefficients of the self association bands at $\sim$ 3520 cm^{-1} are unknown, quantitative values of the fraction of hydrogen bonded segments can not be obtained.

4.3.3.2 Segmental Relaxations

The segmental (α) relaxation, or dynamic T_g, is observable in the experimental window at temperatures above the DSC-determined T_g, and involves micro-brownian motion of several repeat units[53,65]. The temperature dependence of the α relaxation time can be modeled with a Vogel-Fulcher-Tamman (VFT) equation[53]. The resulting VFT fit parameters obtained from fitting the segmental relaxation frequencies (see Figures 4.11 and 4.12) are listed in Table 4.2.

All blends exhibited a single segmental relaxation, indicative of dynamic homogeneity, or complete miscibility. In blends containing relatively low concentrations of PVME, the segmental relaxation was broadened, expected due to the large dynamic asymmetry of the components. The 69 mol% PolyHFS blend with PVME could not be accurately modeled with a VFT function. Although exhibiting a single α relaxation and an α^* relaxation (*vide infra*), the blend is likely undergoing phase separation, since the experimental temperatures are near the degradation temperature of PVME.

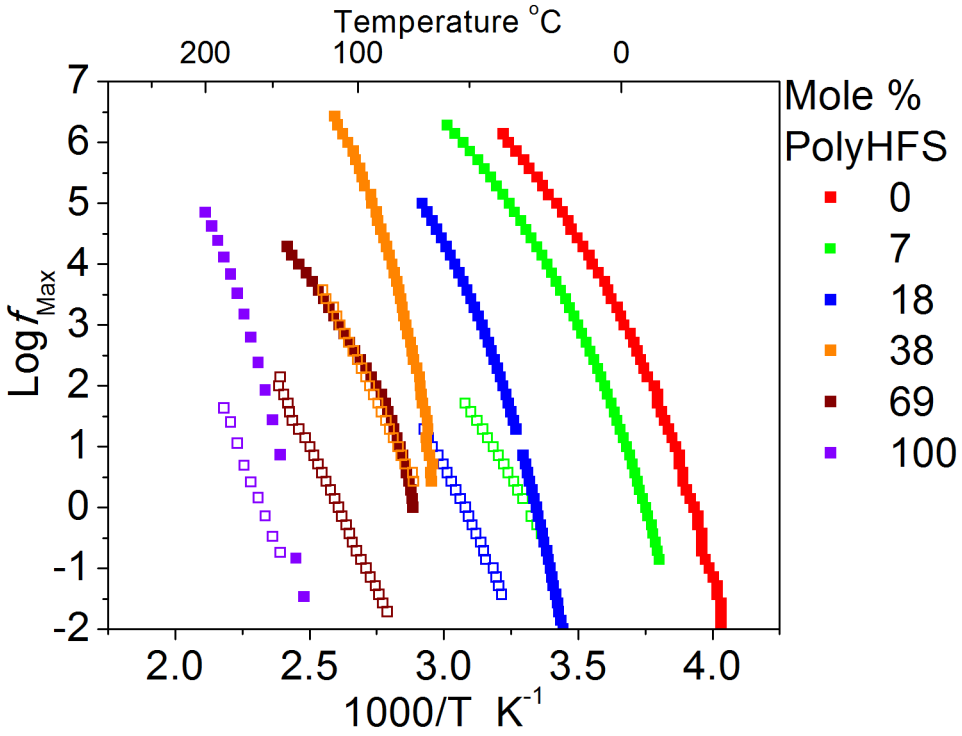

Fig. 4.11: Frequency maxima of the segmental [■] and α^* [□] relaxations for the PVME blends.

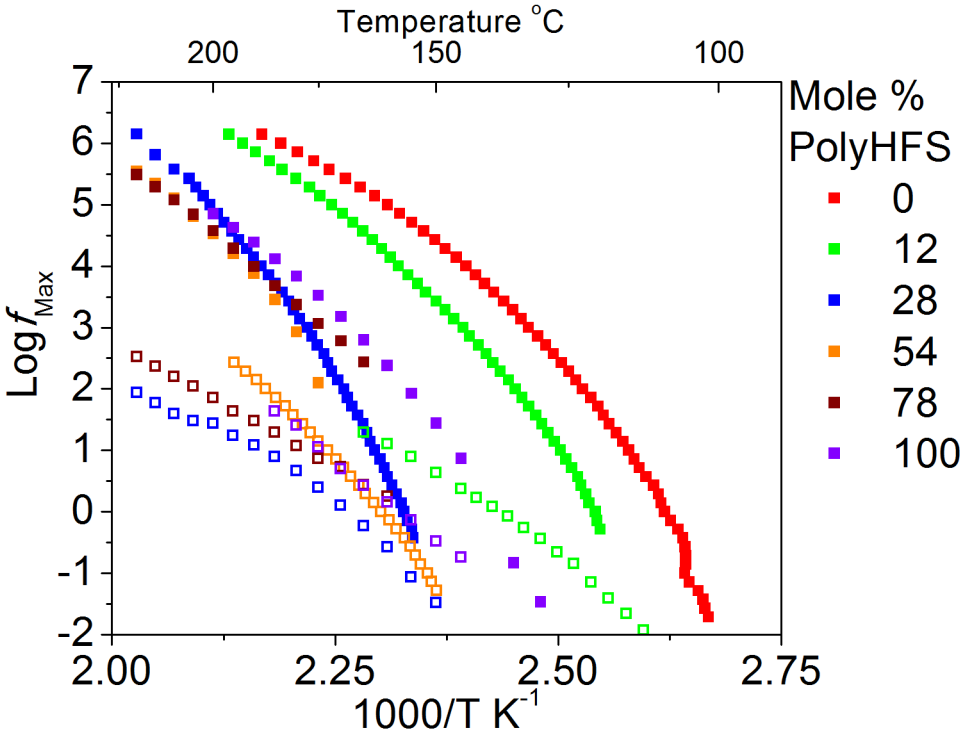

Fig. 4.12: Frequency maxima of the segmental [■] and α^* [□] relaxations for the P2VPy blends.

Table 4.2: VFT fitting parameters for the segmental relaxation. VFT-T_g is defined as the temperature where the relaxation time of the segmental process is 100 seconds. Fragility values calculated using the VFT-T_g.

Blend	Mole % PolyHFS ±1%	$Log_{10}[f_\circ$ (Hz)] ±1	B ±10 (K)	$T_\circ$ ±3 (°C)	VFT-T_g ±3 (°C)	Fragility ±10
P2VPy	0	11	1660	44	95	102
	12	11	1590	58	107	109
	28	11	1370	103	146	135
	54	11	1430	104	149	130
	78	11	1860	74	133	94
PVME	0	12	1310	-68	-28	87
	7	11	1380	-59	-17	87
	18	11	1310	-28	12	101
	38	11	880	28	56	160
	69	–	–	–	–	–
	100	11	1920	63	124	89

The steepness (or fragility) index of a glass former is defined as

$$m = \left.\frac{\partial \log_{10} x}{\partial \left(T_g/T\right)}\right|_{T=T_g} = \frac{B\, T_g}{\ln(10)\left(T_g - T_\circ\right)^2} \tag{4.1}$$

x is a dynamic variable such as viscosity or relaxation time ($\tau = 1/2\pi f$) as in the case of this study, B and $T_\circ$ are the same as equation 2.31 [90]. A 'fragile' glass former (higher value of m) is one with a greater deviation from Arrhenius behavior, or one whose slope of the segmental relaxation time/frequency at $T=T_g$ is higher. Note that fragility was calculated with the VFT-determined T_g ($\tau_{max} = 100\, s$), not the calorimetric T_g.

Although not explicitly stated by Adam and Gibbs, the fragility can be related to the configurational entropy available to the system [157]. It was shown that the height

of the potential energy barrier per monomer unit ($\Delta\mu$) was higher for hydrogen bonding systems, owing to the increased intermolecular coupling. This increase in $\Delta\mu$ implies an increase in the steepness index (see equations 28 and 29′ of Ref. 157), or fragility.

A correlation between the fragility and the size of a cooperatively rearranging region (CRR) has been proposed[158]. As the degree of intermolecular coupling is increased, the configurational entropy available to the system decreases, $\Delta\mu$ and the CRR increase, and the fragility of the system increases. As temperature increases, the hydrogen bonding strength, as well as the number of intermolecular associations decreases[1], and the system's entropy increases. Since hydrogen bonding strength decreases with increasing temperature, the higher the blend T_g, the weaker the intermolecular associations of that blend at T_g. Assuming two blends have a similar number of intermolecular hydrogen bonds, one would expect the system with the higher T_g to have a stronger temperature dependence of the segmental relaxation; the CRR size decreases rapidly and the number of configurations available to the system (entropy) increases rapidly with temperature. Examination of the blend FTIR spectra (Figures 4.3 and 4.4), shows that the 28 mol% PolyHFS blend with P2VPy and the 38 mol% PolyHFS blend with PVME possess the highest fraction (qualitatively) of *intermolecularly* associated segments. This is evidenced by a small free-OH peak at 3602 cm^{-1} in both systems, meaning nearly every HFS segment in both blends is intermolecularly associated, and supported by the behavior of the local processes of these blends (orange and blue points in Figures 4.8 and 4.10, respectively), being the most strongly suppressed. These blends exhibit the highest fragilities, over 70 higher than the neat components in the case of PVME blends, and 33 in P2VPy blends. It should be noted that due to the strong overlap of the α^* and the α processes in the P2VPy blends, the relaxation behavior of the α relaxation of the 54 and 78 mol% PolyHFS blends with P2VPy could not be modeled accurately near T_g. The fragilities of these two blends should therefore be treated with caution, and may in fact be much larger in the 54 mol% blend, but the observed trends in the calculated fragility values agree well with the observed behavior of the local relaxations and the FTIR results.

Interestingly, the 38 mol% PolyHFS blend with PVME exhibits a fragility which is 25 *higher* than the most fragile P2VPy blend. This appears to be at odds with the strength of the hydrogen bonding in both blend systems (P2VPy≫PVME) and the expected intermolecular coupling. Inspection of the blend FTIR (Figures 4.3 and 4.4) and the local relaxations (Figures 4.8 and 4.10) suggests that the fraction of hydrogen bonded segments (degree of intermolecular coupling) is greater in the 38 mol% PolyHFS blend with PVME than in any other blend (P2VPy or PVME). A small free OH band (see Figure 4.3), and an almost complete suppression of the PVME local process (Figure 4.8) supports the assertion that the fraction of hydrogen bonded segments is highest in this blend, and should therefore have the highest fragility (see Figure 4.13) of the systems studied. The fragilities of the blends reported here suggest that, at least in the case of intermolecularly hydrogen bonded polymer blends, the fragility is dictated not by T_g[159], but by the degree of intermolecular coupling.

The trends in fragilities exhibited by these systems are in qualitative agreement with crosslinked systems, which exhibit increased fragility as the degree of crosslinking is increased[160–162], and with recent studies on the effects of plasticization[163,164]. In a previous study of PVME blends with P4VPh, similar trends were observed in the calculated fragilities; the fragility increased with the fraction of intermolecularly associated segments[33]. The fragility values were somewhat lower than those reported here, due to the relatively strong self associations which exist in P4VPh, which result in a lower degree of intermolecular coupling than in the blends examined here, and the stronger hydrogen bonds formed by PolyHFS versus P4VPh.

It is generally accepted that the dynamic asymmetry ($T_{g,A} - T_{g,B}$) plays a major role in the resulting blend dynamics[12,13,33]. A greater difference in the component T_g's results in a broadened blend T_g. In the systems examined here, however, the calorimetric transition breadth and the segmental relaxation breadth of the PVME blends ($T_{g,PolyHFS} - T_{g,PVME} = 151$) are roughly the same as the P2VPy blends ($T_{g,PolyHFS} - T_{g,P2VPy} = 25$), which have a much smaller difference in component T_g's. This suggests that in the case of hydrogen bonded polymer blends, the degree

of intermolecular associations and the functional group accessability are the important factors in determining the relaxation behavior, not the dynamic asymmetry.

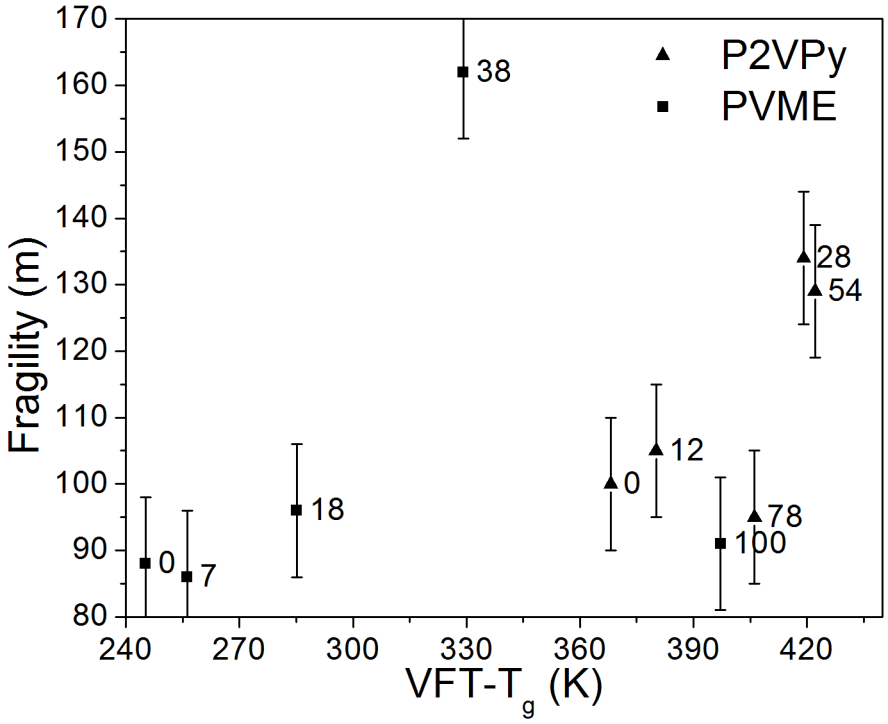

Fig. 4.13: Fragility parameter (m) as a function of T_g for the P2VPy blends (▲) and the PVME blends (■). The PolyHFS mol% of each blend is listed beside the corresponding data point.

4.3.3.3 High Temperature Relaxations

At temperatures above and frequencies below the segmental relaxations of the blends, each blend exhibited an additional relaxation (Figures 4.18 and 4.19) [135,138–140,165] which was nearly Debye (from the derivative HN equation: $\alpha = 0.8 - 0.9$, $\gamma = 1$). This process is not related to the phenomenon of electrode polarization, which is observed at still higher temperatures, and whose magnitude in the derivative dielectric loss is significantly greater than this relaxation. In previous studies of functionalized polybutadienes, [138,139] a similar process was observed with an activation energy [E_a from Equation

2.30] of $\sim$ 110 kJ/mol and an Arrhenius prefactor [$f_\circ$ from Equation 2.30] of 10^{27} Hz were found for this α^* process, significantly higher than for a local relaxation. Fitting equation 2.30 to the PVME α^* data yields an activation energy of 206$\pm$20 kJ/mol, higher than that of Muller et al., and an Arrhenius prefactor of $10^{27\pm1}$ Hz, in agreement with the findings of Muller et al.[138], suggesting this process is of similar origin: the breaking and reforming of hydrogen bonds as segmental relaxation occurs. See Figure 4.14 for a representative fit to this high temperature process. The differences in activation energies between the findings of Muller et al. and this study are likely due to the differences in the numbers and types of hydrogen bonds present in the systems. The increased scatter, and somewhat VFT-like behavior of the α^* process in the P2VPy blends is due to the much stronger overlap of this process with the α relaxation.

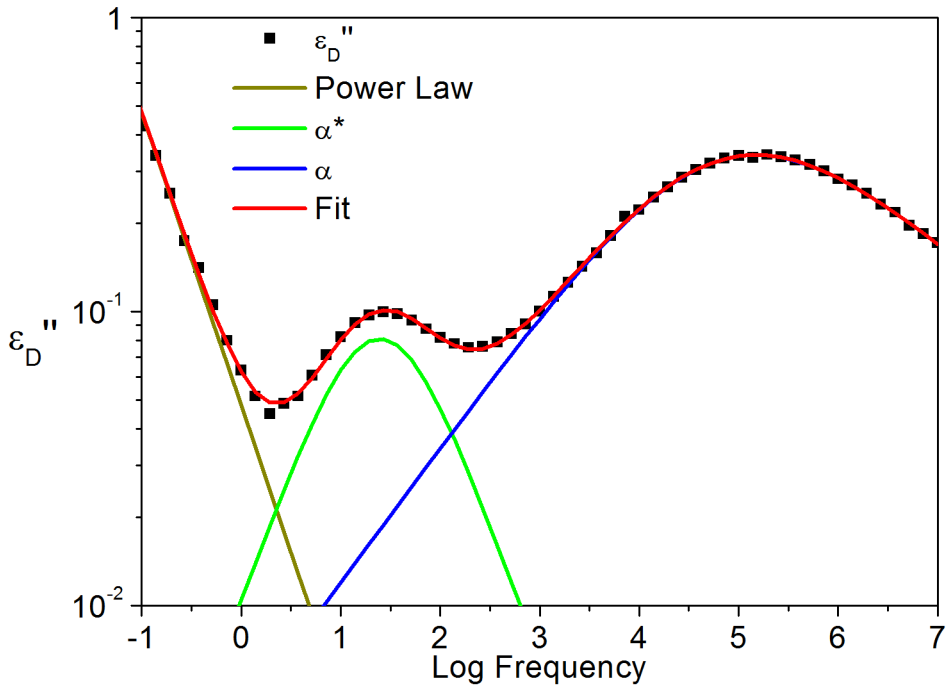

Fig. 4.14: Representative fit of the relaxations above T_g.

In addition to hydrogen bonded systems, relaxations due to the breaking and reforming of associations at elevated temperatures have been seen in ionomers, both in mechanical[166] and dielectric spectroscopy[167], suggesting this relaxation may be an inherent feature of systems possessing strong associations. Its strength ($\Delta\varepsilon$, see equation 2.11 on page 21) is proportional not only to the number of intermolecular associations (see Figure 4.15), but also the strength of the associations (see Figure 4.15).

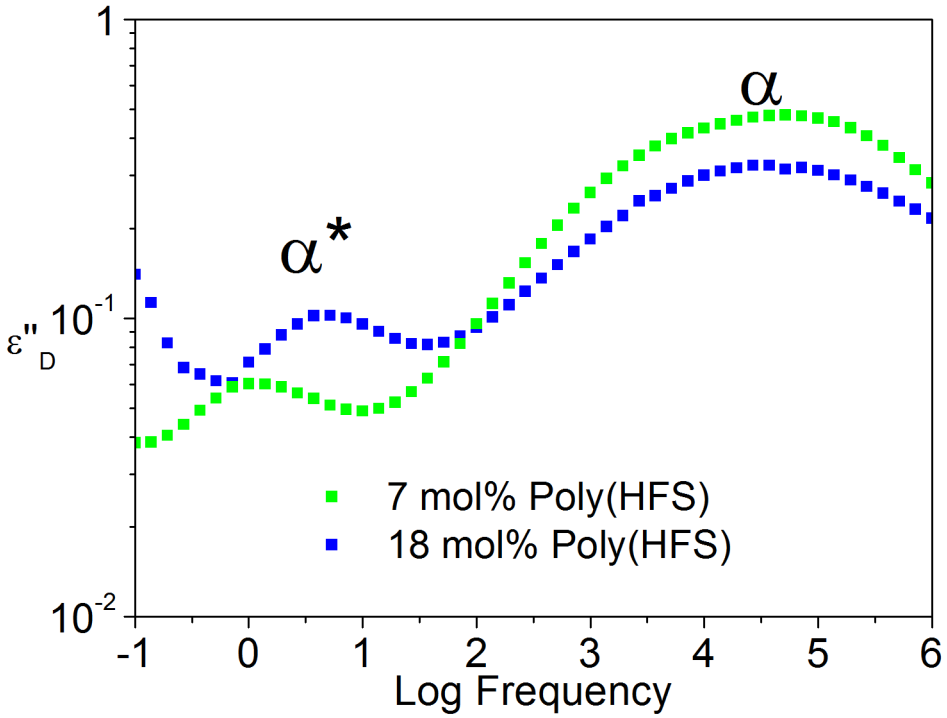

Fig. 4.15: The α^* relaxation in the 7 (green) and 18 (blue) mole % PolyHFS blends with PVME. The approximate locations of the α and α^* relaxations are indicated on the plot.

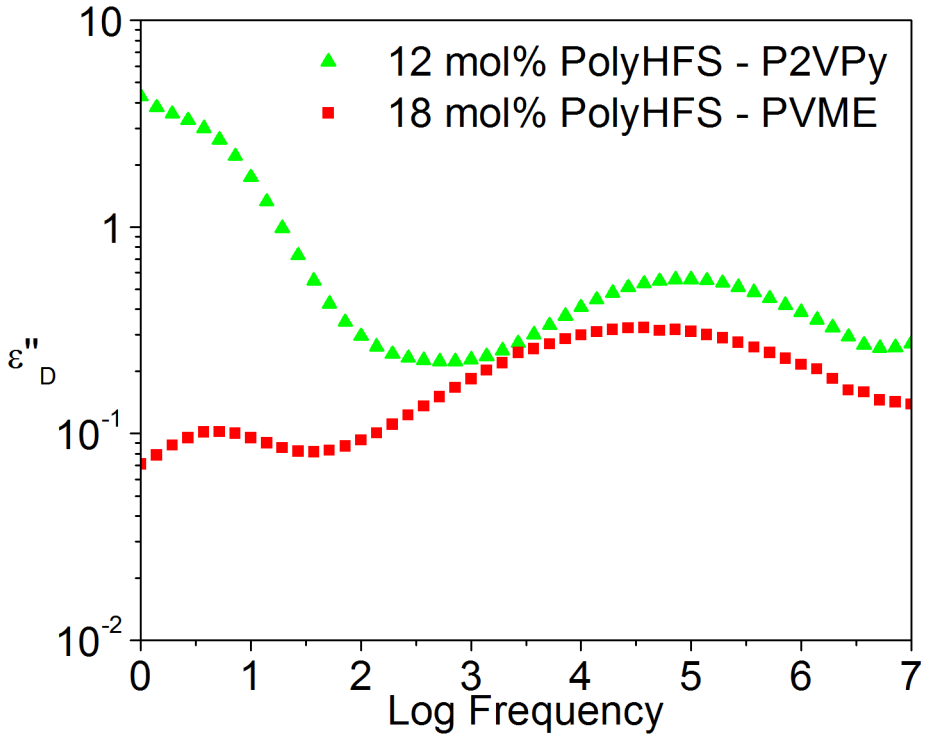

Fig. 4.16: The α^* relaxation in the 12 (green) and 18 (red) mole % PolyHFS blends with P2VPy and PVME, respectively. The α^* relaxations are centered at approximately 5 Hz, and the α relaxations are at higher frequencies.

It is clear that as the number of intermolecular associations increases, the magnitude of the α^* relaxation increases relative to the α relaxation, as shown in Figure 4.15. It is also clear from Figure 4.15 that the α and α^* relaxations are closer in frequency with increasing PolyHFS content. This is expected, since lower fractions of hydrogen bonded segments will reptate more readily without the need to break hydrogen bonds than in blends with more intermolecular associations. From Figure 4.16 it is clear that as the hydrogen bond strength increases (P2VPy >> PVME) the magnitude of the α^*, relative to the α process increases.

Small angle X-ray scattering (Figure 4.17) does not indicate the presence of a second phase, so it is unlikely this relaxation is due to interfacial polarization, the buildup of charge at the interface of inhomogeneous systems (Maxwell-Wagner-Sillars interfacial

polarization, see chapter 13 of reference 53 or Chapter 2 above). At low temperatures ($T_{g,DSC} - 5 < T < T_{g,DSC} + 10$) in the P2VPy blends, the α^* relaxation occurs at higher frequencies than the α relaxation. Since the interfacial polarization phenomena requires mobile charges ($T > T_g$), the α^* process would not be present at these temperatures if this relaxation were related to interfacial polarization. Note that interfacial polarization requires mobile charges in only one phase[53]. If these systems were phase separated, the relative magnitudes of the α and α^* relaxations suggest the α^* process would be from the hydrogen bonded segments, and should have a higher T_g. The α^* process is Arrhenius, and extrapolates to temperatures below the α, strongly suggesting this process is not a result of interfacial polarization.

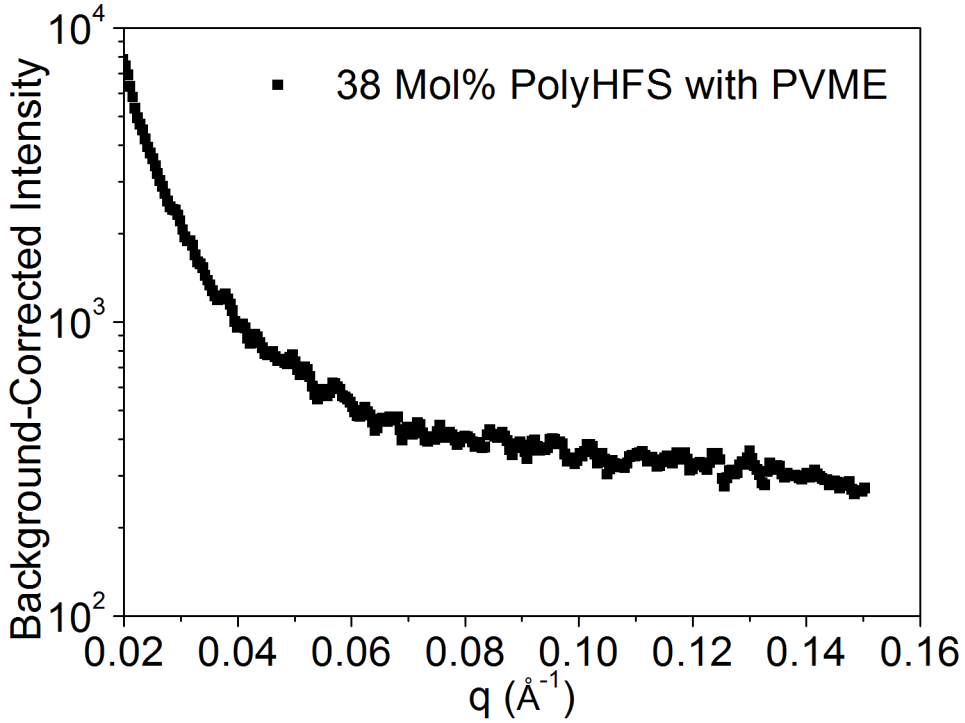

Fig. 4.17: Background-corrected small angle X-ray scattering results for the 38 mol% PolyHFS blend with PVME.

The occurrence of the α^* relaxation at frequencies above (and temperatures below) the α relaxation near T_g suggests that this relaxation, the breaking and reforming of hydrogen bonds, must occur before segmental level relaxation can occur in some of the blends. This observation is in line with the observed trends in the blends' T_g's and the number and strengths of the hydrogen bonds. The 7 and 18 mol% PolyHFS blends with PVME possess relatively few intermolecular associations, so segmental level motion can occur without the breaking of these associations. As the fraction of intermolecularly associated segments approaches 1, segmental level motion cannot occur without breaking intermolecular associations (the α^* relaxation). In the case of the P2VPy blends, the hydrogen bonds are far stronger than the PVME blends (Figures 4.3 and 4.4), so higher temperatures, in some cases greater than the T_g of the blend components, would be required to break enough hydrogen bonds for segmental level relaxation to occur.

This also explains the presence of the α^* relaxation in the HFS homopolymer. Although possessing few self associations[48], some self associations are present. In Figures 4.11 and 4.12, the relaxation time of the PolyHFS α^* extrapolates to timescales shorter than that defined for T_g (100 seconds), again suggesting that hydrogen bonds dictate the T_g of this homopolymer.

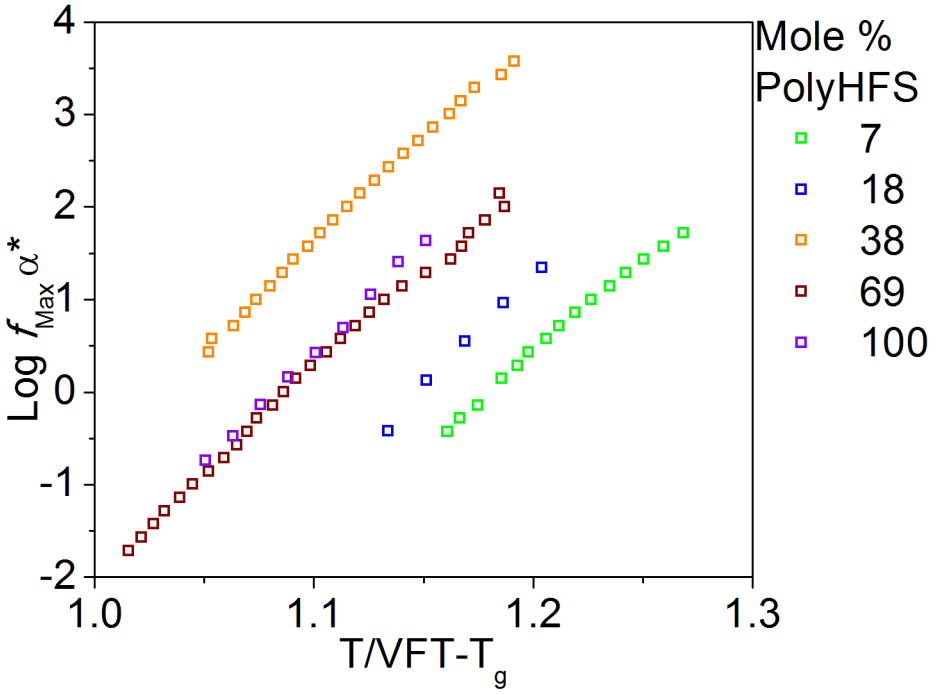

Fig. 4.18: Frequency maxima of the α^* process for the PVME (a) blends versus temperature scaled by the temperature at which $\tau_{\mathrm{Max}} = 100$ seconds (VFT-T_g).

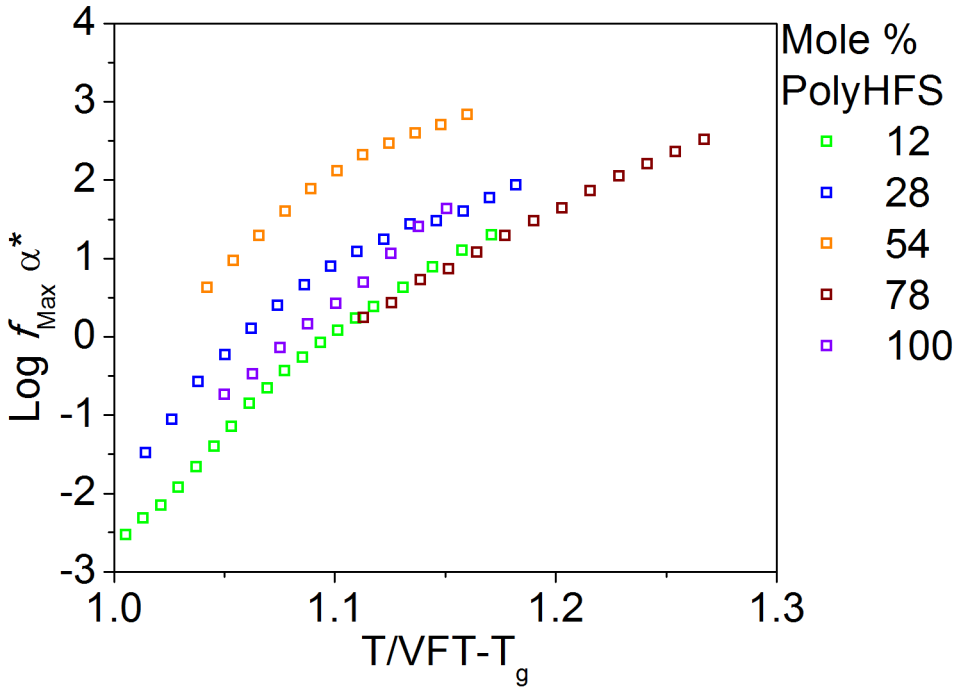

Fig. 4.19: Frequency maxima of the α^* process for the P2VPy blends versus temperature scaled by the temperature at which $\tau_{\mathrm{Max}} = 100$ seconds (VFT-T_g).

4.4 Summary

The effects of strong intermolecular associations on the dynamics of miscible hydrogen bonding polymer blends of PolyHFS with PVME and P2VPy have been explored. Minimized self associations in PolyHFS result in blends with a greater degree of intermolecular coupling compared to analogous P4VPh blends.

Intermolecular coupling was found to strongly influence local relaxations. Strong suppression of the local relaxation of each component was observed, and correlated well with the hydrogen bonding behavior observed in FTIR spectroscopy. In PVME blends, the suppression of local motions scaled well with the blend composition. In P2VPy blends, however, the suppression of the local motions was governed not simply by the ratio of functional groups, but by functional group accessability.

A single calorimetric and dynamic T_g was observed for each blend. The temperature dependence of the segmental relaxation times strongly depends on the numbers and strengths of hydrogen bonds in the system. As the molar ratio of P2VPy to PolyHFS approaches 1, the T_g (and the segmental relaxation) occurs at temperatures above those of the component polymers. The fragility of each system is strongly correlated to the intermolecular hydrogen bonding. The 38 mol% PolyHFS blend with PVME exhibited the highest fragility because it possessed the largest fraction of intermolecularly associated segments (for the PVME blends).

The α^* relaxation was present in the DRS spectra of all blends, and only observable in the conductivity free loss (ε''_{der}), and its temperature dependence follows the strength and number of hydrogen bonds. Future studies will investigate these effects in systems where the fraction of intermolecular associations can be quantified.

Chapter 5

Blends of PolyHFS with Ethylene-Vinyl Acetate Copolymers

5.1 Introduction

With the exception of blends of oligomers with high molecular weight polymers[168], miscible polymer blends in which the components do not form specific intermolecular interactions are now well known to exhibit two segmental (α) relaxations or glass transition temperatures (T_g) when the difference in component T_g's (ΔT_g) is greater than ~50 °C. Chain connectivity effects[169] result in concentration fluctuations and the compositional dependence of the two T_g's or α processes can generally be described by the Lodge-McLeish model[4,14,15]. Painter and Coleman introduced an additional "chemical forces" term ($\Delta G_H/RT$) to the Flory Huggins equation (equation 1.11 on page 7) to account for the free energy change due to hydrogen bonding (typically having energies of 1-10 kcal/mol)[1]. The presence of sufficient intermolecular hydrogen bonding between component polymers in a binary mixture leads to coupling of motions on the molecular level, and typically result in a single T_g and a single segmental (α) relaxation, even when ΔT_g is 100 °C or larger, as seen in Chapter 4, and in blends of PVPh and PVME, shown in Chapter 1.

In earlier studies of miscible PVPh blends, despite the presence of strong hydrogen bonding between the component polymers, two α relaxations are observed at the compositional extremes[33,43,151]. This arises due to a stoichiometric effect, exacerbated by the strong self-associations (OH-OH hydrogen bonds) formed between PVPh segments. To reduce self associations, Painter, Coleman and coworkers used selective steric shielding around the OH functionality[28,30,48]. The steric shielding serves to limit the ability of two such functional groups forming a hydrogen bond, while not appreciably reducing the OH-containing species' ability to form a hydrogen bond with a proton

acceptor such as PVME. Shown in Figure 5.1 are the repeat unit structures of the (co)polymers used in this study. The two-CF_3 groups of poly(1,1,1,3,3,3-hexafluoro-2-(4-vinylphenyl)propan-2-ol) (PolyHFS) provide steric shielding which reduces the ability to form self associations.

The wavenumber shift of the OH band in FTIR spectroscopy has been shown to be an indicator of hydrogen bonding strength[1,48]. In blends of PVPh with PVME, for example, the wavenumber difference between PVPh self associations and intermolecular associations with PVME is less than ~ 50 cm^{-1} greater than the PVPh self associations, meaning that intermolecular associations are only slightly more thermodynamically favorable. In analogous PolyHFS blends with PVME[55], the wavenumber difference between HFS self associations and PVME intermolecular associations is approximately 320 cm^{-1}, underlying the importance of reduced self associations.

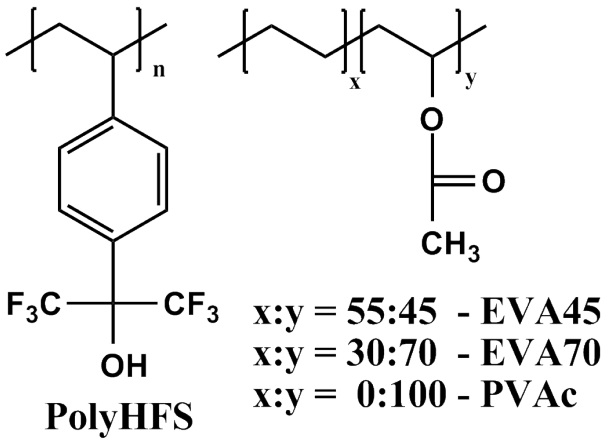

Fig. 5.1: Repeat units of PolyHFS and the EVA copolymers.

The association model has been found to accurately predict phase behavior rather well[1,29]. Knowledge of the equilibrium constants for forming OH-OH bonds (K_2), OH multimers (K_B), OH-carbonyl intermolecular bonds in the present case (K_A) and molar volumes of the blend components, allows for the calculation of the phase behavior and the fractions of hydrogen bonded species present as a function of composition. Knowledge

of the hydrogen bonding enthalpies is necessary to calculate the phase behavior at any temperature.

The carbonyl region of the FTIR spectrum ($\sim 1650 - 1800$ cm^{-1}) is sensitive to hydrogen bonding. An additional band, shifted to lower wavenumber relative to the nonbonded carbonyl absorbance, appears when carbonyl groups participate in a hydrogen bond. This region of the FTIR spectrum is readily modeled compared to the OH region[46,170], yielding quantitative information on the fraction of hydrogen bonded segments. The obtained fraction of free carbonyl groups from a series of blend compositions can be fit to the stoichiometric equations of the association model, yielding the various equilibrium constants[1,48].

In the current investigation, these stoichiometric equations are used to predict the number and types of hydrogen bonding species present in a series of blends of PolyHFS with ethylene-vinyl acetate copolymers. Using information determined by curve-resolving the carbonyl region of FTIR spectra, the glassy state relaxations of these systems can be described, and predictions of which compositions should have the highest fragility can be made. This methodology should be applicable to any miscible blend in which the hydrogen bonding behavior can be quantified.

5.2 Experimental

The experimental procedures used in this study are outlined in Chapter 3, but are repeated here for convenience and because some experimental details differ from other systems studied. The (co)polymers poly(vinyl acetate) (PVAc), poly(ethylene[30]-co-vinyl acetate[70]) (EVA70), and poly (ethylene[55]-co-vinyl acetate[45]) (EVA45) were purchased from Scientific Polymer Products, and have molecular weights of approximately 100 kg/mol. Note that the numbers in brackets refer to the weight % of each component. Each was dissolved in a good solvent, passed through a 0.2 μm Teflon syringe filter, then reprecipitated into hexanes. The precipitate was collected and dried well above T_g prior to use. Synthesis of PolyHFS ($\overline{M_W}$ = 140 kg/mol, PDI = 1.4) is outlined in Chapter 3[55]. As with the other polymers, it was filtered and reprecipitated prior to use.

5.2.1 Blend Preparation

Appropriate amounts (see Table 5.1) of each component were added to a Teflon jar along with an appropriate good solvent. For the PVAc blends, acetone was used. For the EVA70 blends, a mixture of 70 vol% tetrahydrofuran (45 vol% for the EVA45 blends) with toluene was used. After dissolving each component, the solution was passed through a 0.2 μm Teflon syringe filter. Each solution was stirred for approximately 20 hours, after which an air purge was added to remove the solvent. All blends were then dried at approximately 150 °C for at least 12 hours with a liquid nitrogen trap under vacuum (2-3 μbar) to remove solvent and moisture.

5.2.2 Differential Scanning Calorimetry (DSC)

Thermal characteristics were measured using a Seiko DSC220CU DSC. Samples for DSC measurements were cut from the dried blend film and crimped in aluminum pans. Each sample was scanned using the following procedure: Heat at 10 °/min to T_g + 50 °C, cool at 10 °/min to T_g - 50 °C, heat to T_g + 50 °C at 10 °/min. The temperature was held for 5 minutes at each extreme ($T_g \pm 50$ °C) before continuing. T_g was taken from the second heating as the midpoint of the heat capacity change.

5.2.3 Fourier Transform Infrared Spectroscopy (FTIR)

Spectra were collected on a Nicolet 6700 with an attached dry air purge. A minimum of 100 scans were averaged with a wavenumber resolution of 1 cm^{-1}. Note that the wavenumber resolution is different from that used in PVME and P2VPy blends with PolyHFS (see page 65 of Chapter 4). The increased wavenumber resolution was used to increase the accuracy of subsequent calculations. Samples were cast from a good solvent (see above) onto potassium bromide windows, then dried at 150 °C overnight under vacuum (2-3 μbar). Film thickness was controlled such that the absorbance was within the range of the Beer-Lambert Law.

Curve resolving was performed on the carbonyl region of the spectra (1700-1750 cm^{-1}) using a fitting program developed at Penn State in the Painter and Coleman laboratories[1]. Peaks were modeled with two Gaussian functions[32]:

$$I(\nu) = A_\circ \exp\left[-\ln 2\left[\frac{\nu - \nu_\circ}{\Delta\nu_{1/2}}\right]^2\right] \tag{5.1}$$

$\Delta\nu_{1/2}$ is the half width at half height, $\nu_\circ$ is the wavenumber coordinate of the band maximum, and ν is the frequency.

5.2.3.1 Calculations of Hydrogen Bond Types

The hydrogen bond stoichiometry in the blends was calculated using the Painter-Coleman association model[1,171]. The volume fractions (ϕ) of the two polymers can be described by:

$$\phi_A = \phi_{A_1} + K_A\phi_{A_1}\phi_{B_1}\Gamma_1 \tag{5.2}$$

$$\phi_B = \phi_{B_1}\Gamma_2\left[1 + \frac{K_A\phi_{A_1}}{r}\right] \tag{5.3}$$

ϕ_{A_1} and ϕ_{B_1} are the volume fractions of free (non-bonded) A and B segments, respectively, and r is the ratio of the molar volumes of A and B. Γ_1 and Γ_2 are given by:

$$\Gamma_1 = \left[1 - \frac{K_2}{K_B}\right] + \frac{K_2}{K_B}\left[1 - K_B\phi_{B_1}\right]^{-1} \tag{5.4}$$

$$\Gamma_2 = \left[1 - \frac{K_2}{K_B}\right] + \frac{K_2}{K_B}\left[1 - K_B\phi_{B_1}\right]^{-2} \tag{5.5}$$

K_2, K_A and K_B were determined for the systems under investigation here by Yang, et al[48]. The fraction of hydrogen bonded A (vinyl acetate) and B (HFS) groups can then be calculated using equations 5.6 and 5.7, respectively.

$$f_{HA} = 1 - \frac{\phi_{A_1}}{\phi_A} \tag{5.6}$$

$$f_{HB} = 1 - \frac{\Gamma_1}{\Gamma_2}\left[1 + \frac{K_A\phi_{A_1}}{r}\right]^{-1} \tag{5.7}$$

The fraction of free HFS groups, (f_F^{OH}) is simply $1 - f_{HB}$. The fraction of free carbonyl groups ($f_F^{C=O}$) is $(1 - f_{HA})$ or:

$$f_F^{C=O} = \frac{\phi_{A_1}}{\phi_A} = \left\{1 + K_A\phi_{B_1}\left[\left(1 - \frac{K_2}{K_B}\right) + \frac{K_2}{K_B}\left(1 - K_B\phi_{B_1}\right)^{-1}\right]\right\}^{-1} \tag{5.8}$$

Since PolyHFS forms self associations as well as intermolecular associations, an additional term to account for the fraction of these self associations is necessary. The fraction of self associated HFS segments (f_B^{OH-OH}) is related to the volume fraction of self-associated B groups (ϕ_{B_n}) by:

$$f_B^{OH-OH} = \frac{\sum_{n=2}^{\infty}\phi_{B_n}}{\phi_B} = \frac{\frac{K_2}{K_B}\left[\left(1 - K_B\phi_{B_1}\right)^{-2} - 1\right]}{\Gamma_2} \tag{5.9}$$

Note that these calculations are for the state of hydrogen bonding at room temperature (25 °C), and the hydrogen bonding behavior depends on temperature. The enthalpies of hydrogen bond formation, which are currently unknown for these systems, would be required to evaluate the hydrogen bonding behavior at temperatures other than 25 °C.

5.2.4 Broadband Dielectric Relaxation Spectroscopy (DRS)

Samples were prepared for DRS measurements by solution casting thin films, typically 60-70 μm thick, from a good solvent (see above) directly onto brass electrodes, 20-30 mm in diameter. A smaller diameter upper electrode was pressed into the film along with two 50 μm diameter silica spacers to maintain sample thickness. Each sample was dried under vacuum (2-3 μbar) at high temperatures prior to measurement, and samples were transferred from the oven after cooling to room temperature to the spectrometer as quickly as possible. The effects of water on glassy state dynamics are well known[88,172]. Water is known to alter the relaxation behavior of not only the local relaxation of PVAc[96], but also the segmental relaxation[173], so great care was taken to minimize the sample exposure to moisture.

DRS measurements were performed on a Concept 40 system from Novocontrol GmbH, and measured over the frequency range 10 mHz to 10 MHz. Temperature was controlled by a Quatro temperature control system with a precision of greater than ±0.1 °C. All blends were measured over the temperature range from -140 °C to well above the calorimetric T_g. After DRS measurements, films were redissolved in good solvent to ensure that crosslinking did not occur at elevated temperatures.

The imaginary part (loss) of the complex dielectric function ($\varepsilon^*(\omega) = \varepsilon'(\omega) - i\varepsilon''(\omega)$) was fit using one or more empirical Havriliak-Negami (HN) equations (see equation 2.27 on page 37)[128].

At temperatures above T_g, the motions of impurity ions begin to dominate the dielectric loss, often obscuring dipolar relaxations. With the exception of the phenomenon of electrode polarization, motions of ionic impurities are not manifested in the dielectric constant (ε')[53]. The fundamental Kramers-Kronig relationship states the dielectric loss and the dielectric constant contain the same information, so one can be calculated from the other. Since a cumbersome numerical approximation is necessary for the Kramers-Kronig relationship to be applied[133], the derivative of the dielectric constant was used. Wübbenhorst et al. have shown that the derivative of the dielectric constant is a good approximation of the 'conductivity-free' dielectric loss[134,135]. The usefulness of this formalism is its ability to not only remove dc conductivity from the dielectric loss, but it has also been shown to partially resolve overlapping peaks[100]. As long as the appropriate fitting function is used in the analysis of the data, the derivative formalism yields results identical to the raw dielectric loss, with the added benefit of being able to deconvolute dipolar response from ion motion[100,104]. See page 41 of Chapter 2 for further details.

5.3 Results and Discussion

5.3.1 DSC

A single calorimetric T_g was observed for each blend, and these are listed in Table 5.1 along with the blend compositions.

Table 5.1: Thermal characteristics of the blends studied.

Blend	Mole % HFS (±1%)	Weight % HFS (±1%)	T_g (±3°C)
PVAc	0	0	41
	10	25	49
	24	50	65
	49	75	109
	74	90	122
	100	100	125
EVA70	0	0	-10
	13	25	2
	31	50	24
	58	75	86
	80	90	100
EVA45	0	0	-24
	19	25	-12
	41	50	17
	68	75	72
	86	90	75

5.3.2 FTIR

Shown in Figures 5.2a, 5.2b, 5.3a, 5.3b, 5.4a and 5.4b are the FTIR spectra (scaled by each spectra's maximum) illustrating the state of hydrogen bonding present in these blends at room temperature. The spectra in the hydrogen bonding region has been offset vertically for clarity. As noted earlier, careful analysis of the carbonyl region of the FTIR spectra (1700-1750 cm^{-1}) allows one to obtain the fractions of free and hydrogen bonded segments. Shown in Figure 5.5 is an example curve-resolved spectrum.

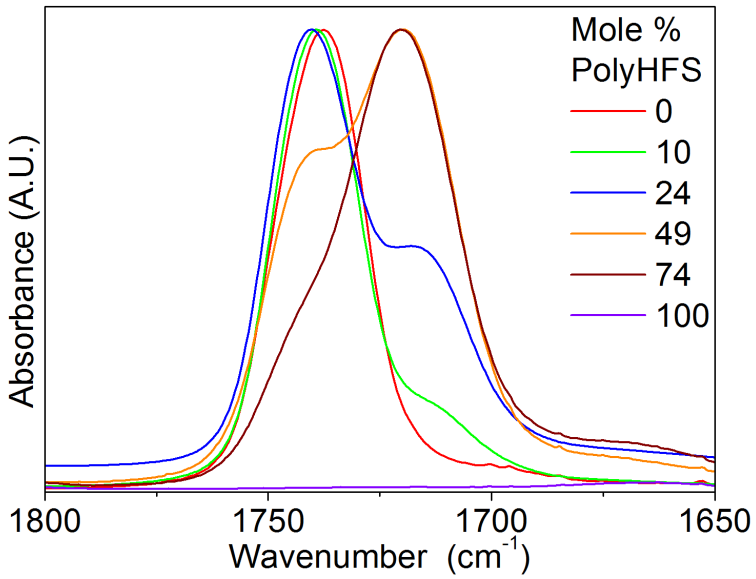

(a) Carbonyl Region

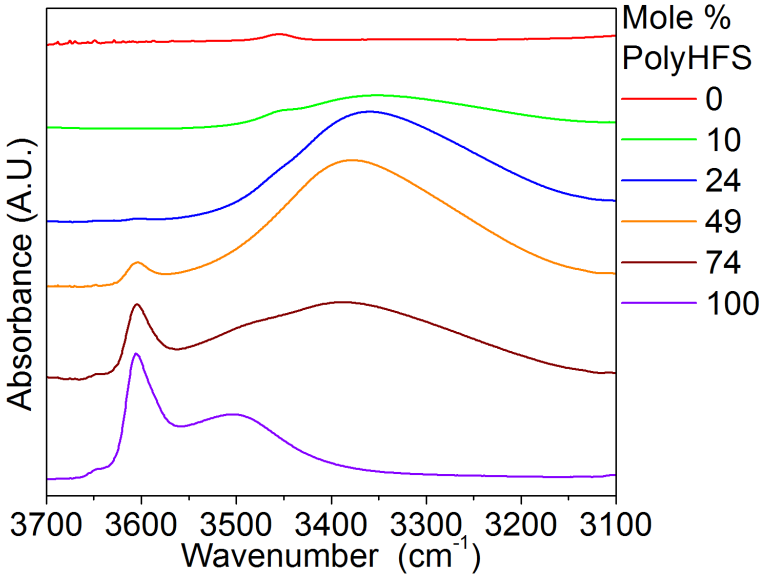

(b) OH Region

Fig. 5.2: Scaled FTIR results for the PVAc blends with PolyHFS. The carbonyl (a) and OH regions (b) are shown. Data in (b) are vertically offset for clarity.

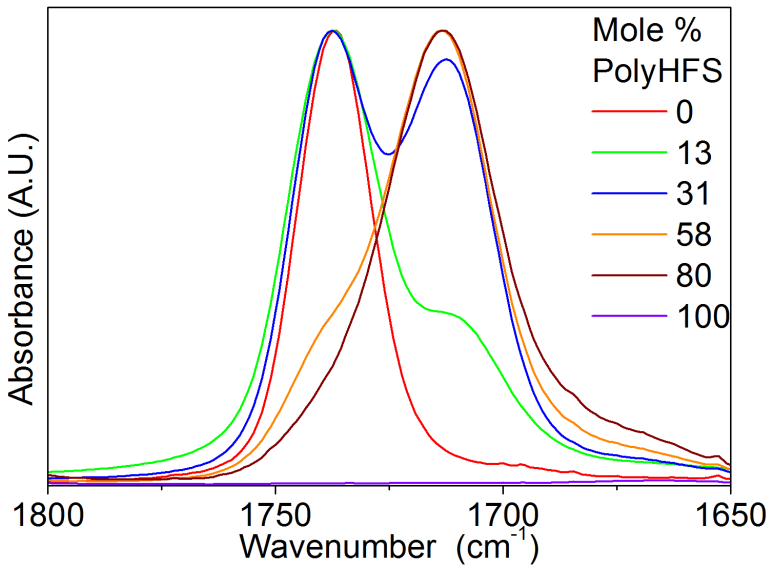

(a) Carbonyl Region

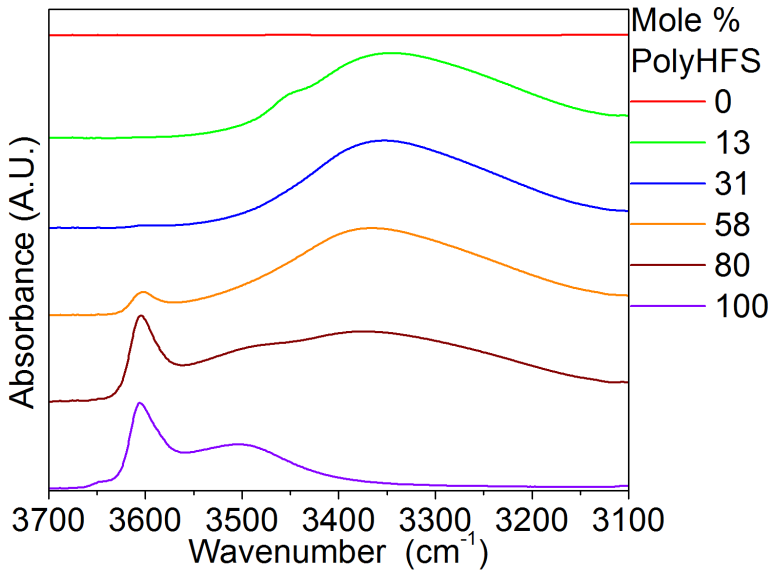

(b) OH Region

Fig. 5.3: Scaled FTIR results for the EVA70 blends with PolyHFS. The carbonyl (a) and OH regions (b) are shown. Data in (b) are vertically offset for clarity.

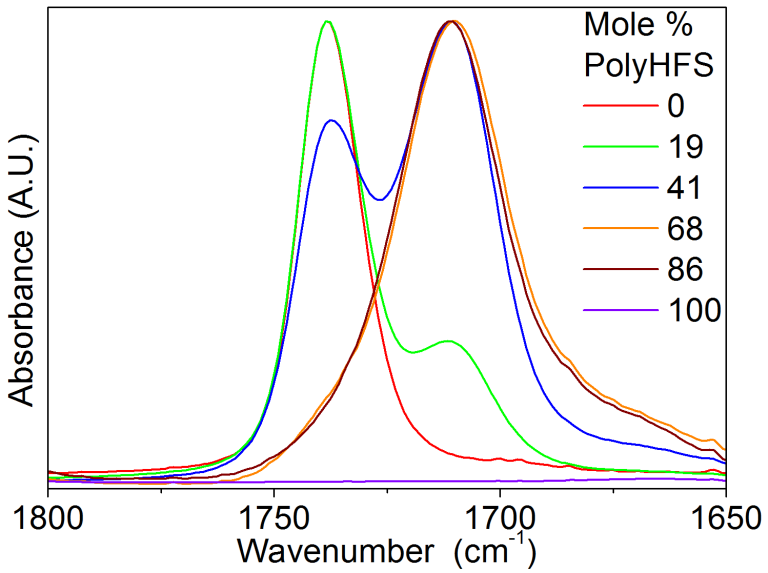

(a) Carbonyl Region

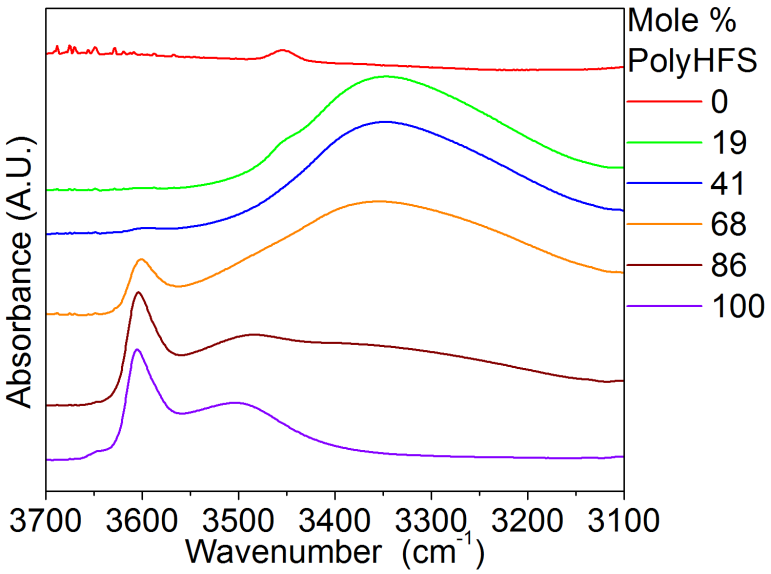

(b) OH Region

Fig. 5.4: Scaled FTIR results for the EVA45 blends with PolyHFS. The carbonyl (a) and OH regions (b) are shown. Data in (b) are vertically offset for clarity.

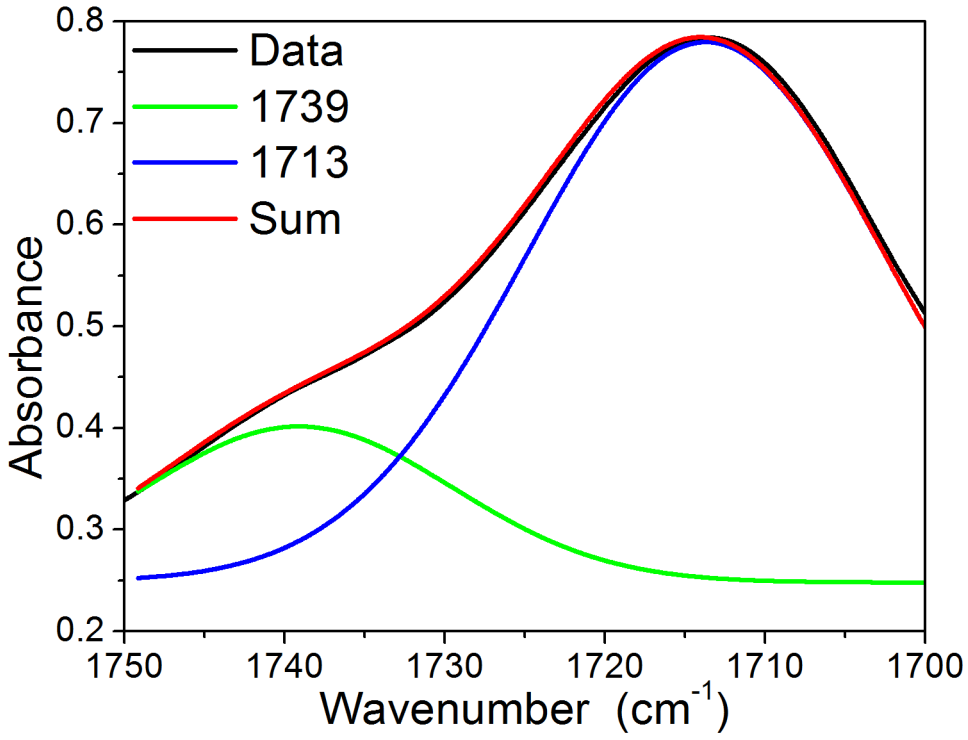

Fig. 5.5: Representative curve-resolved FTIR spectra in the carbonyl region for the 58 mol% PolyHFS blend with EVA70.

The carbonyl region consists of two main peaks, a 'free' (non-hydrogen bonded) band located at 1739 ± 3 cm^{-1}, and a hydrogen bonded carbonyl band centered at approximately 1713 ± 3 cm^{-1}. Two Gaussian functions were used (Figure 5.1) in the curve-resolving, one for the 1739 cm^{-1} band, another for the 1713 cm^{-1} band, along with a linear baseline. From knowledge of the ratio of the absorptivity coefficients (free/interassociated = 1.5)[48], one can obtain the fraction of free carbonyl groups as a function of composition.

In a previous study, the room temperature (25 °C) equilibrium association constants for the formation of an intramolecular hydrogen bond between the HFS and acetoxy functionalities ($K_A = 34.5$), as well as the self-association constants for Poly-HFS (dimers $K_2 = 2.53$, and multimers $K_B = 3.41$) were determined[48]. These values, combined with knowledge of the molar volume of each segment (HFS = 170 cm^3/mol,

VAc = 69.8 cm^3/mol, CH_2 = 16.5 cm^3/mol), and equations 5.2, 5.3, 5.4, 5.5, 5.6, 5.7, 5.8 and 5.9[1], allow for the prediction of the amount and types of hydrogen bonding species present as a function of composition. Shown in Figures 5.6, 5.7 and 5.8 are the fractions of free carbonyl groups determined experimentally, as well as the predicted fractions of free carbonyl groups, *inter*molecularly associated HFS segments, and *intra*molecularly associated HFS segments. At all compositions, good agreement is found between the model predictions for the fraction of free carbonyl groups and the experimental results.

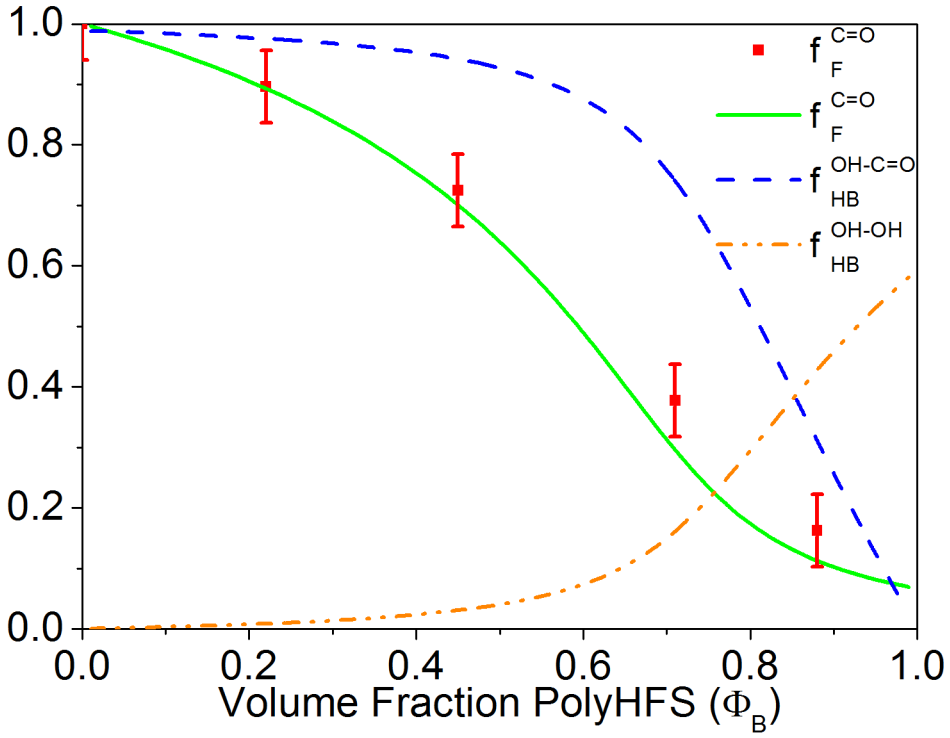

Fig. 5.6: Composition dependence of the fraction of free carbonyl groups from the association model (solid green line), fraction of intermolecularly associated HFS segments from the model (dashed blue line), fraction of self-associated HFS segments from the model (dash-dot orange line) and the experimentally-determined fraction of free carbonyl groups (red squares) for the PVAc blends at 25 °C.

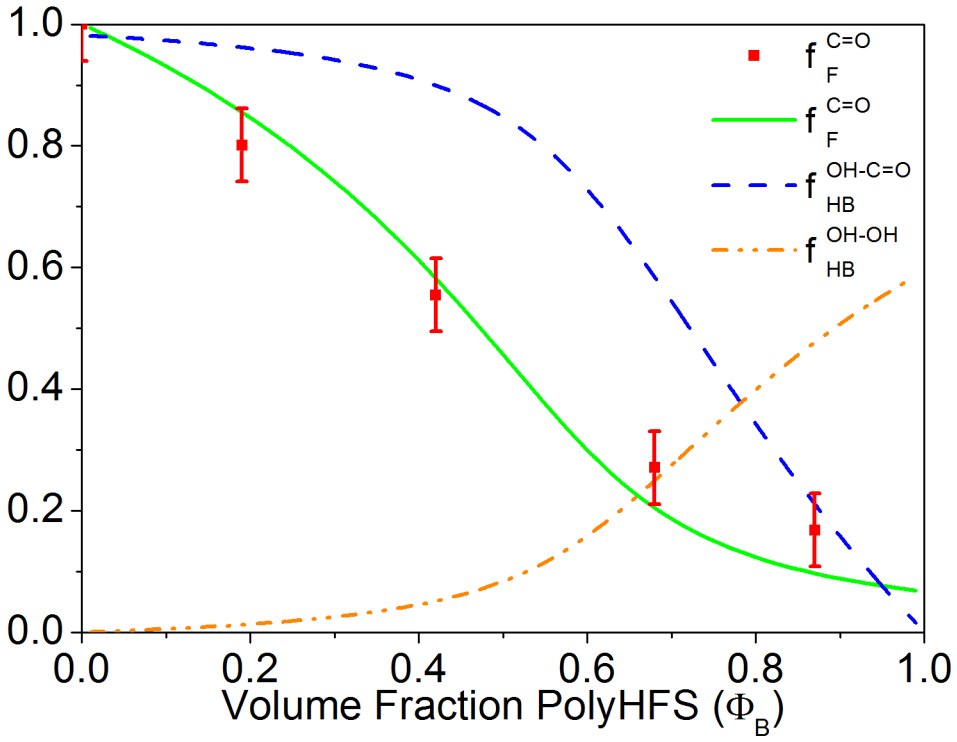

Fig. 5.7: Composition dependence of the fraction of free carbonyl groups from the association model (solid green line), fraction of intermolecularly associated HFS segments from the model (dashed blue line), fraction of self-associated HFS segments from the model (dash-dot orange line) and the experimentally-determined fraction of free carbonyl groups (red squares) for the EVA70 blends at 25 °C.

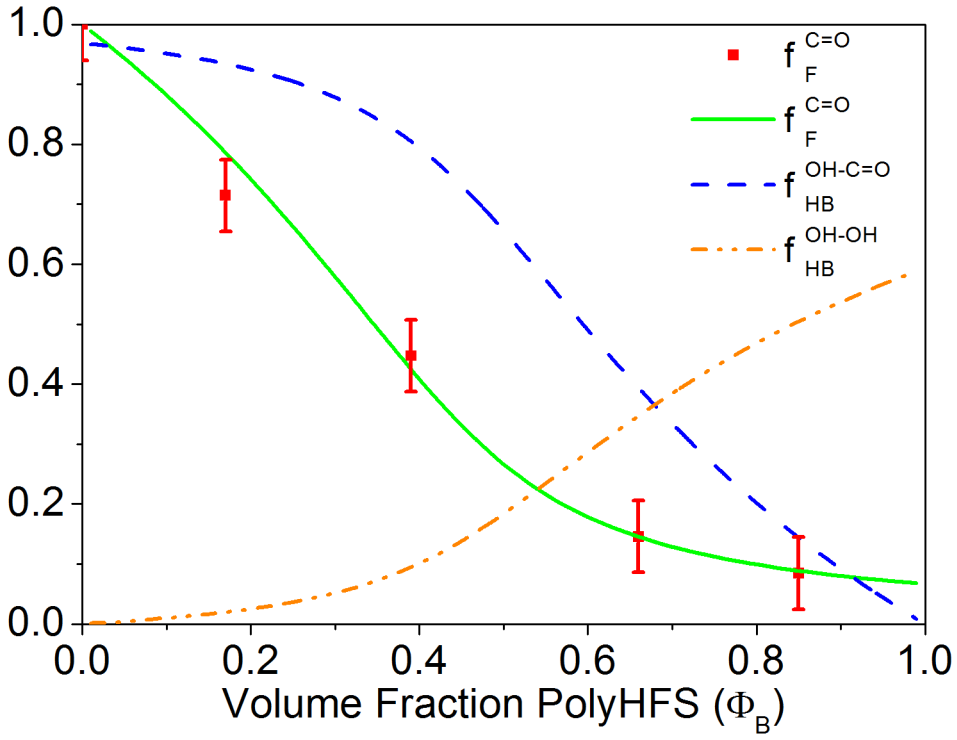

Fig. 5.8: Composition dependence of the fraction of free carbonyl groups from the association model (solid green line), fraction of intermolecularly associated HFS segments from the model (dashed blue line), fraction of self-associated HFS segments from the model (dash-dot orange line) and the experimentally-determined fraction of free carbonyl groups (red squares) for the EVA45 blends at 25 °C.

5.3.3 Broadband Dielectric Relaxation Spectroscopy

5.3.3.1 Local Relaxations

The vinyl acetate functionality exhibits a well-known glassy state motion in PVAc[78,96,174], and the experimental Arrhenius (see equation 2.30) fit parameters for this β relaxation ($f_\circ = 10^{12.5}$ Hz, $E_a = 40$ kJ/mol) agree well with the literature[174]. Shown in Figure 5.9 is an Arrhenius plot containing representative relaxation frequencies of the local relaxations observed, based on the experimentally-determined relaxation times.

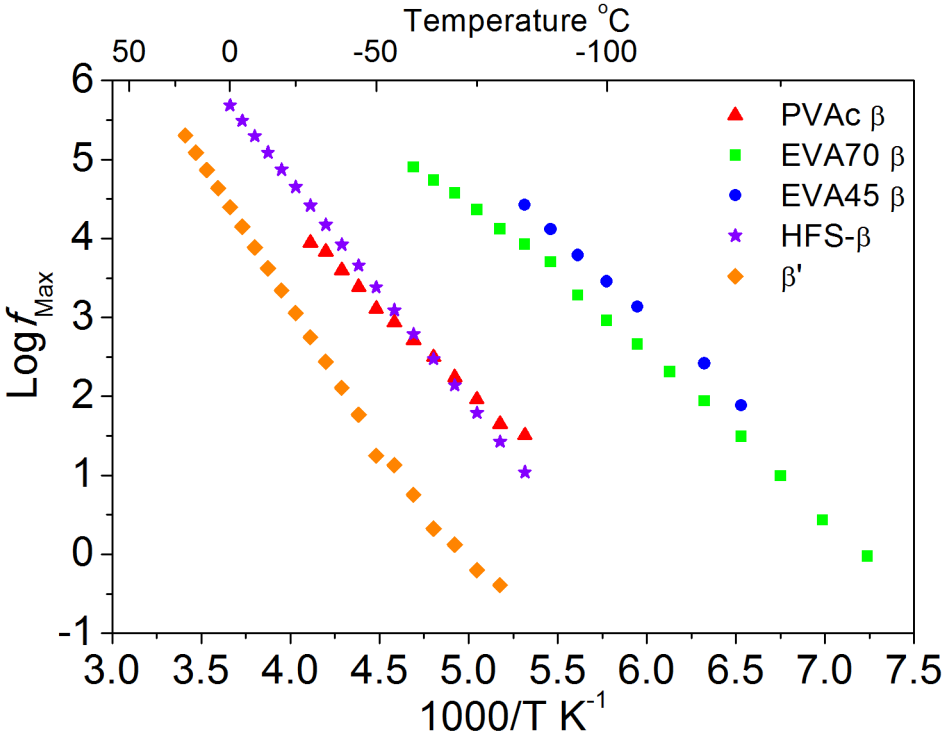

Fig. 5.9: Arrhenius plot of the observed glassy-state relaxations.

Both EVA70 and EVA45 exhibit a local relaxation, which, compared to the PVAc process, is shifted to lower temperatures with increasing ethylene content, in agreement with findings in the literature[96]. The vinyl acetate β relaxation maintains the same activation energy, but the Arrhenius prefactor increases from $f_\circ = 10^{12.5}$ Hz for PVAc to $f_\circ = 10^{15}$ Hz for EVA70 and $f_\circ = 10^{15.3}$ Hz for EVA45 (see Table 5.2). This shift can be ascribed to the coupling of this motion to that of the main chain, as observed in neutron scattering experiments[175], and the degree of coupling decreases with increasing ethylene content. As noted in a previous study[55], PolyHFS exhibits a β relaxation having an activation energy of 54 kJ/mol and an Arrhenius prefactor of 10^{16} Hz.

Table 5.2: Arrhenius fit parameters for the local relaxations present in the blends studied.

Relaxation	$\text{Log}(f_\circ)$ ($\pm$0.1 Log(Hz))	E_a ($\pm$0.5 kJ/mol)
PVAc β	12.5	40
EVA70 β	15	40
EVA45 β	15.3	40
HFS β	16	54
β'	17.2	70

Upon blending PolyHFS with PVAc, EVA70 or EVA45, an additional relaxation appears in the glassy state, shown by the black vertical lines in Figures 5.10a, 5.10b and 5.10c and the orange diamonds in Figure 5.9. The Arrhenius fit parameters for this process, which we refer to as the β' relaxation, are: $f_\circ = 10^{17.2}$ Hz and $E_a = 70$ kJ/mol, both higher than those of the local processes of any of the component polymers (see orange points of Figure 5.9).

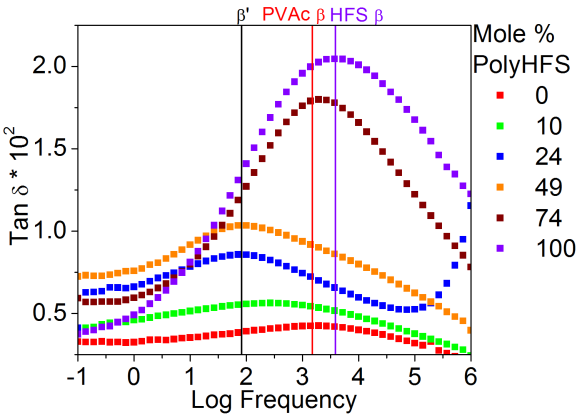

(a) PVAc Blends -50 °C

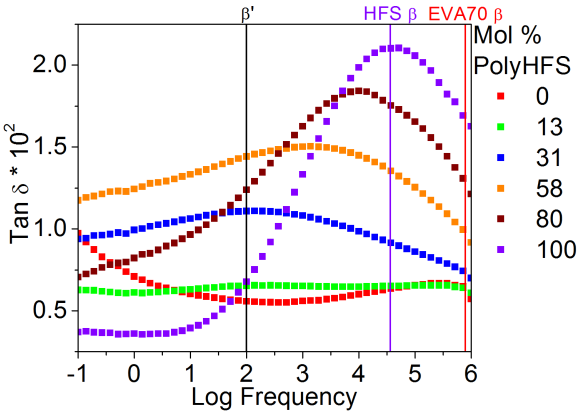

(b) EVA70 Blends -30 °C

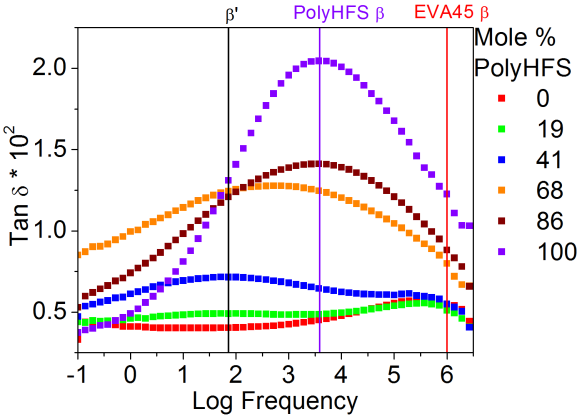

(c) EVA45 Blends -50 °C

Fig. 5.10: Tan δ for the (a) PVAc blends at -50 °C, (b) EVA70 blends at -30 °C, and (c) EVA45 blends at -50 °C. The vertical lines mark the locations of the PolyHFS local relaxation (purple), the vinyl acetate local relaxation (red), and the β' relaxation (black).

Inspection of Figures 5.10a, 5.10b and 5.10c reveals that the magnitude of the β' relaxation changes systematically with composition. The β' process increases in magnitude with increasing PolyHFS content, to a maximum in the 50 PolyHFS mol% blend with PVAc, the 58 PolyHFS mol% blend with EVA70, and the 68 PolyHFS mol% blend with EVA45 (orange points in Figures 5.10a, 5.10b and 5.10c). The strength of this process is reduced at the next highest PolyHFS composition in each blend, suggesting this process is related to the hydrogen bonded HFS segments. Further evidence for this is found in the FTIR OH stretching region of each blend (Figures 5.2b, 5.3b and 5.4b). Each of the blends at higher PolyHFS content (74, 80 and 86 mol% PolyHFS with PVAc, EVA70 and EVA45 respectively) possess not only free HFS segments, demonstrated by the band at 3602 cm^{-1}, but also self associations (HFS-HFS bonds), shown by the broad shoulder at 3500 cm^{-1}, and an absence of free vinyl acetate groups (Figures 5.2a, 5.3a and 5.4a). This demonstrates, beyond the fact that there is a large molar excess of PolyHFS at these compositions, that the majority of the HFS segments are either free or self-associating. The local response for these compositions (brown points in Figures 5.10a, 5.10b and 5.10c), should therefore be dominated by the response of HFS segments which behave as neat PolyHFS.

Using predictions of the fractions of free and hydrogen bonded segments, and assuming the β' process arises from hydrogen bonded HFS segments, it should be possible to fit the local processes with two HN functions (see equation 2.27), keeping a majority of the fit parameters fixed. Specifically, the ratio of dielectric strengths ($\Delta\varepsilon_{Free}$ / $\Delta\varepsilon_{Bonded}$) of the hydrogen bonded functional groups (β') and the free functional groups (HFS-β) can be calculated using the prediction lines in Figures 5.6, 5.7 and 5.8, calculated from equation 5.9. $\Delta\varepsilon$ is related to the number density of dipoles participating in a relaxation[62], so the ratio of the two dielectric strengths should be related to the fraction of segments free and hydrogen bonded. This assumes no difference in dipole moment between the free and hydrogen bonded segments[53]. The temperature dependence of the β' relaxation is constant in all blends (PVAc, EVA70, EVA45), as is the PolyHFS β relaxation. The relaxation times ($\tau_{\beta'}$ and $\tau_{HFS-\beta}$), can therefore also be fixed, since the PolyHFS β relaxation times are determined from the homopolymer results, and

the β' relaxations are determined by iteratively fitting the 12 blend compositions, with particular emphasis placed on the compositions where the β' relaxation is dominant, for instance, the 24 mol% PolyHFS blend with PVAc. Additionally, since these are glassy state relaxations, the high frequency asymmetry parameters ($\gamma_{\beta'}$ and $\gamma_{HFS-\beta}$ from equation 2.27) can be fixed to unity. Since these relaxations occur in the glassy state and no ion motion occurs, the second term in equation 2.27 is omitted. The resulting two HN fit to two relaxations uses three adjustable parameters: the relaxation breadths ($\alpha_{\beta'}$ and $\alpha_{HFS-\beta}$) and the relationship between dielectric strengths determined from the association model prediction ($\Delta\varepsilon_{HFS-\beta} = \Delta\varepsilon_{\beta'}[(1/f_{HB}^{OH-C=O}) - 1]$). Note that the contribution from HFS self-associations is accounted for in the $\Delta\varepsilon_{HFS-\beta}$ term, since they are also present in the HFS homopolymer. Also note that the relaxation breadths ($\alpha_{\beta'}$ and $\alpha_{HFS-\beta}$) were not allowed to change by more than 0.2 ($0 < \alpha < 1$) from the values determined for the relaxations of the 'pure' components.

Blends with high PolyHFS content were chosen to evaluate the validity of the above prediction, since the strength of the vinyl acetate local relaxation is small relative to that of PolyHFS, and its contribution is minimized. Making the assumption that the vinyl acetate local relaxations are negligible, two instead of three fit functions are required. Blends with free HFS segments and relatively few free carbonyl groups were chosen based on the FTIR results. Representative results of this fitting process are shown in Figures 5.11a, 5.11b and 5.11c.

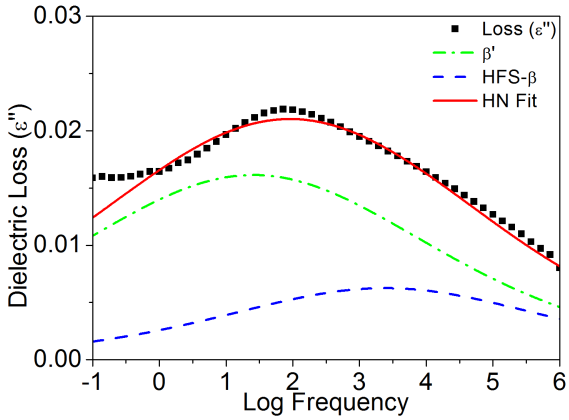

(a) 49 mol% PolyHFS with PVAc

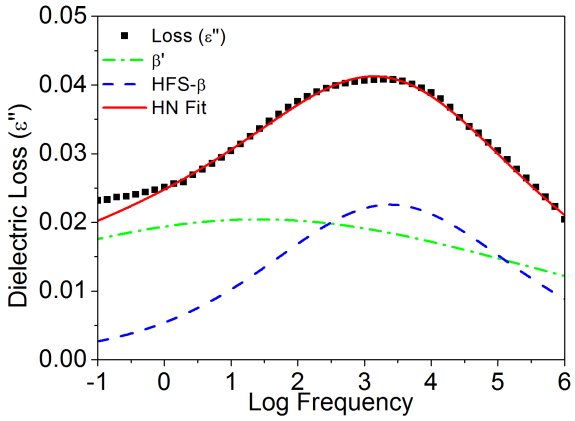

(b) 80 mol% PolyHFS with EVA70

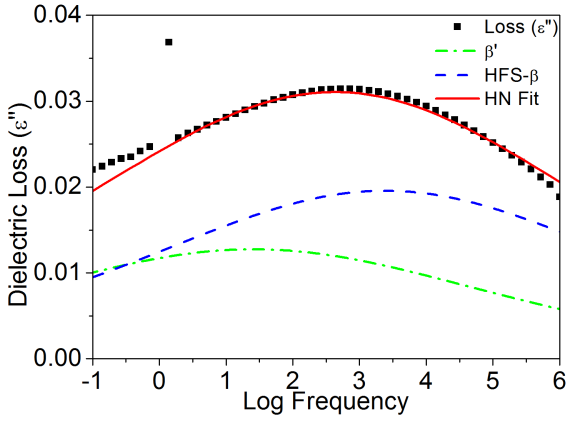

(c) 68 mol% PolyHFS with EVA45

Fig. 5.11: Representative fits to the local relaxations in each blend at -50 °C. The ratio of dielectric strengths were calculated from the Painter-Coleman model.

This method appears to describe the data well, suggesting the β' relaxation does indeed arise from hydrogen bonded HFS segments. As shown in Figure 5.12, the agreement with the data is better at higher temperatures for all blends, but particularly for the PVAc blends. The conclusion that the β' relaxation arises from hydrogen bonded segments is also in agreement with the higher activation energy of this process compared to the other local relaxations (see Table 5.2), since hydrogen bonds must be broken for this relaxation to occur. This fitting routine produced similar fits to all blends with PolyHFS compositions greater than 50 mol%. Fitting low PolyHFS content blends in a similar manner (two HN functions: one for β', one for the vinyl acetate β) is not as straightforward. The low strength of the vinyl acetate β process makes it difficult to accurately model in blends where its intensity is reduced from that of the neat polymer due to hydrogen bonding.

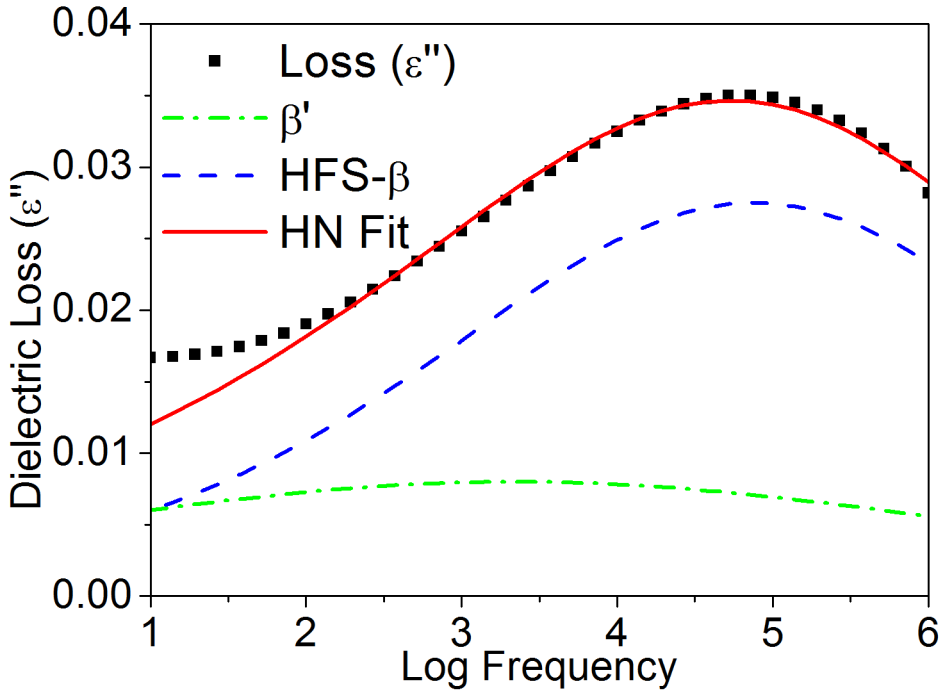

Fig. 5.12: Two HN fit to the PolyHFS local relaxations present in the 74 mol% PolyHFS blend with PVAc at -20 °C.

In contrast to more strongly hydrogen bonded blends such as PVPh with P2VPy [43], PVPh and PVME [33], and PolyHFS blends with P2VPy and PVME [55], the hydrogen bonds formed between the HFS and vinyl acetate functionalities are not sufficiently strong to completely suppress the local relaxations. As mentioned above, the wavenumber difference between the free OH band and the intermolecularly associated OH band provides a relative measure of the hydrogen bonding strength. The blends examined here exhibit an OH wavenumber shift of approximately 250 cm^{-1}, up to several hundred wavenumbers less than equivalent PVME and P2VPy blends [55], suggesting the hydrogen bonds formed in these systems are significantly weaker than in PVME and P2VPy blends.

5.3.3.2 Segmental Relaxations

As shown in Chapter 4 dealing with blends of PolyHFS with PVME and P2VPy, all blends studied here exhibit a single segmental relaxation, indicative of dynamic homogeneity, and in agreement with the miscibility predictions of the Painter-Coleman association model [1,55]. Additionally, small angle X-ray scattering did not reveal any structure. Shown in Figure 5.13 is the background-corrected small angle X-ray scattering for the EVA45 blends. No structure was observed for these blends, despite the relatively high ethylene content.

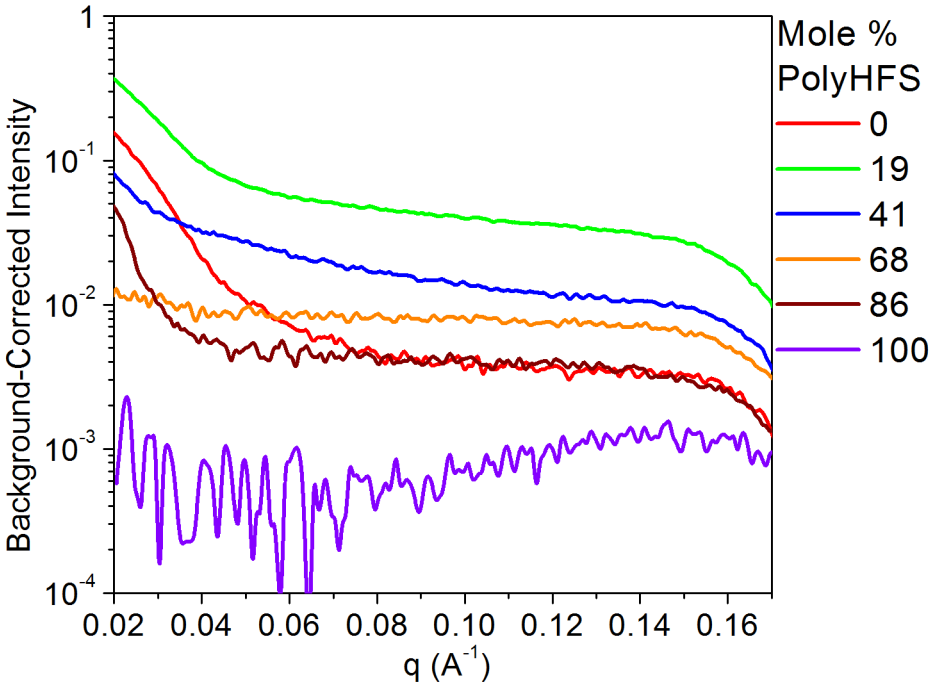

Fig. 5.13: Background corrected small angle X-ray scattering results for the EVA45 blends.

The segmental relaxation frequencies for the blends examined here are shown in Figures 5.14, 5.15 and 5.16.

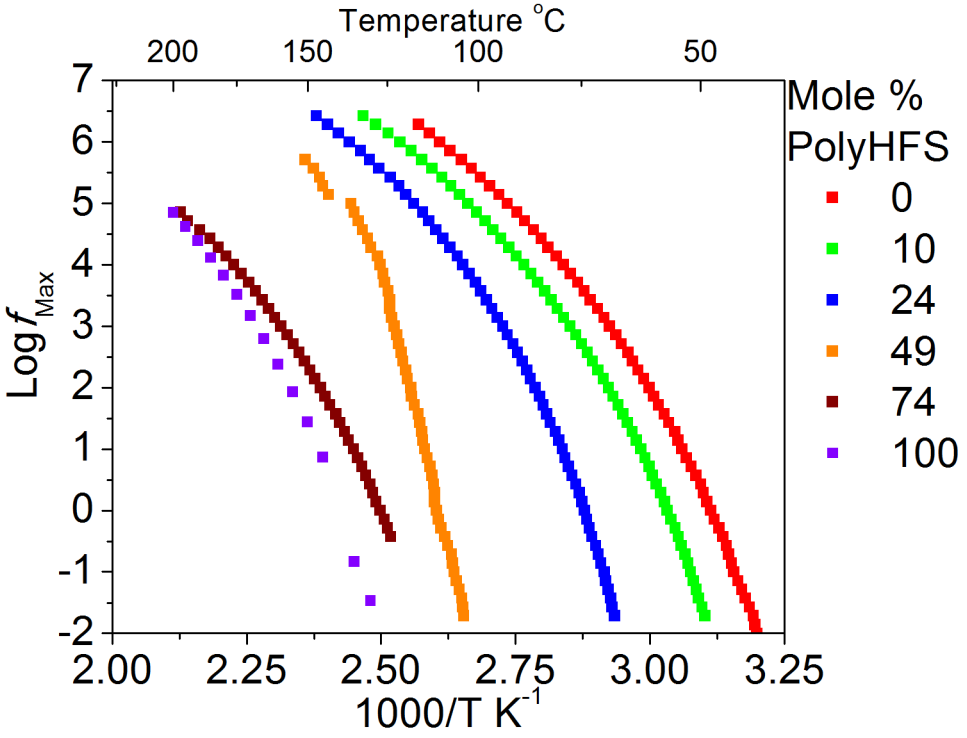

Fig. 5.14: Segmental relaxation frequencies for the PVAc blends.

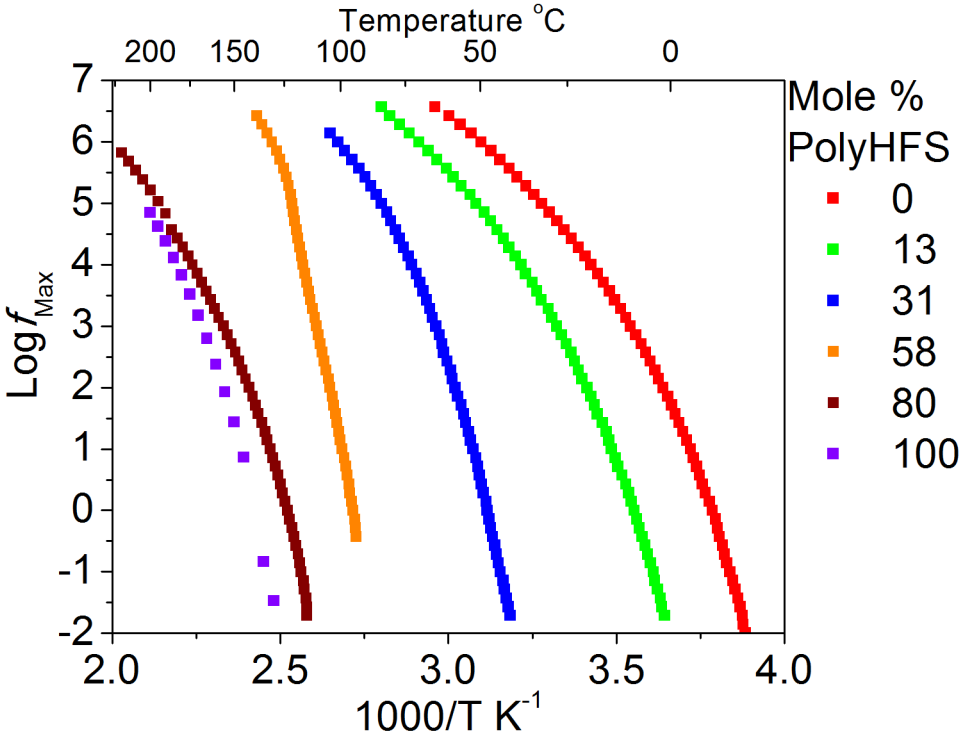

Fig. 5.15: Segmental relaxation frequencies for the EVA70 blends.

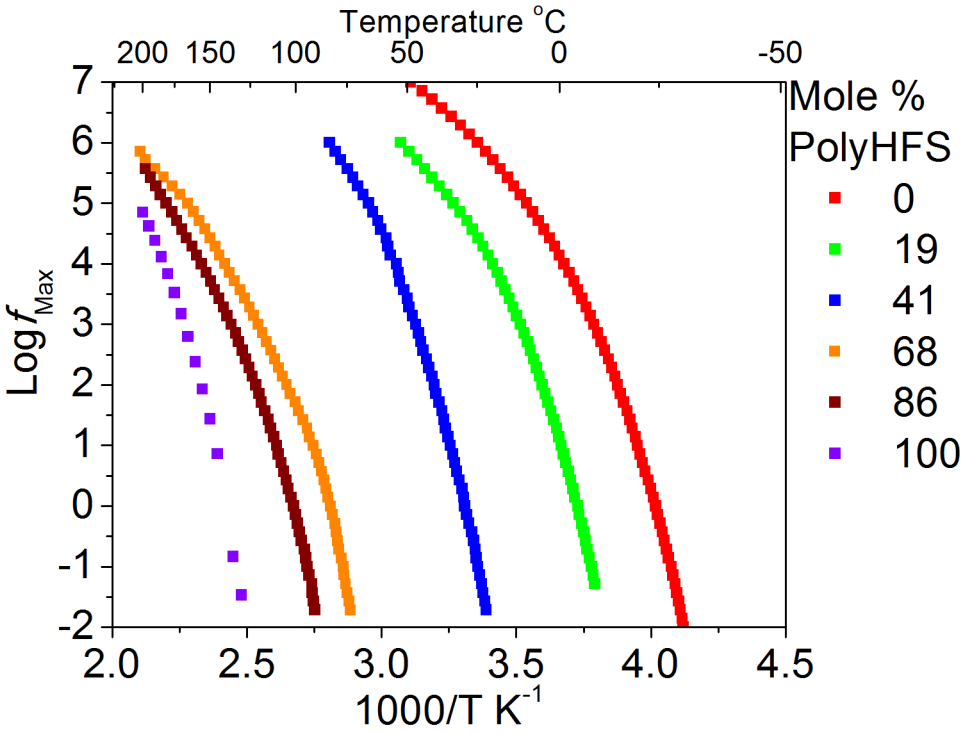

Fig. 5.16: Segmental relaxation frequencies for the EVA45 blends.

The temperature dependence of the segmental relaxation can be described by a Vogel-Fulcher-Tamman (VFT) equation, shown in equation 2.31 [53]. The resulting VFT parameters from the fits to the curves in Figures 5.14, 5.15 and 5.16 are listed in Table 5.3.

Table 5.3: VFT fitting parameters for the segmental relaxations.

Blend	Mole % PolyHFS ±1%	$\mathrm{Log}_{10}[f_\circ$ (Hz)] ±1	B ±10 (K)	$\mathrm{T}_\circ$ ±3 (°C)	$\mathrm{T}_{\mathrm{g,VFT}}$ ±3 (°C)	Fragility ±10
PVAc	0	12	1710	-14	36	91
	10	11	1400	2	45	100
	24	11	1300	23	64	113
	49	11	930	73	102	179
	74	11	2180	41	109	77
	100	11	1920	63	124	89
EVA70	0	11	1080	-53	-18	97
	13	11	1350	-44	-2	90
	31	11	1130	3	39	121
	58	11	860	62	89	185
	80	10	1830	47	108	83
EVA45	0	11	1010	-64	-33	103
	19	10	920	-44	-13	110
	41	10	930	-12	20	119
	68	10	1890	2	66	68
	86	10	1950	19	83	71

As defined in Chapter 4, the steepness (or fragility) index of a glass former is defined as

$$m = \left.\frac{\partial \log_{10} x}{\partial \left(\mathrm{T_g}/\mathrm{T}\right)}\right|_{\mathrm{T=T_g}} = \frac{\mathrm{B\,T_g}}{\ln(10)\left(\mathrm{T_g} - \mathrm{T}_\circ\right)^2} \tag{5.10}$$

x is a dynamic variable such as viscosity (η) or relaxation time ($\tau = 1/2\pi f$) as in the case of this study [90]. A 'fragile' glass former (higher value of m) is one with a greater deviation from Arrhenius behavior: one whose slope of the segmental relaxation

time/frequency at T = T_g is higher. Note that fragility was calculated with the VFT-determined T_g ($\tau_{max} = 100\,s$), and these are also listed in Table 5.3.

Of particular interest is the 49 PolyHFS mol% blend with PVAc (orange points in Figure 5.14), the 58 PolyHFS mol% blend with EVA70 (orange points in Figure 5.15) and the 41 PolyHFS mol% blend with EVA45 (blue points in Figure 5.16). These blends have the highest fragilities (see Table 5.3) in each of their respective blend series. Inspection of the FTIR results reveals these blends have both the fewest free carbonyl groups and fewest free HFS segments in their respective series (demonstrated by the peak at 1737 cm^{-1} in Figures 5.2a, 5.3a and 5.4a and the peak at 3602 cm^{-1} in Figures 5.2b, 5.3b and 5.4b, respectively), demonstrating that they possess the highest fraction of intermolecularly associated segments. Note that the free OH peak in the 41 PolyHFS mol% blend with EVA45 is quite small, but present.

As shown in Chapter 4,[55] the fragility of intermolecularly hydrogen bonded polymer blends seems to depend not on the T_g of the blend, but on the fraction of intermolecularly associated segments. Using the association model, it is possible to calculate the theoretical volume fraction of intermolecularly associated segments as a function of composition. Shown in Figures 5.17a, 5.17b and 5.17c are the blend fragilities and the theoretical volume fraction of intermolecularly associated segments plotted as a function of PolyHFS volume fraction (Φ_B).

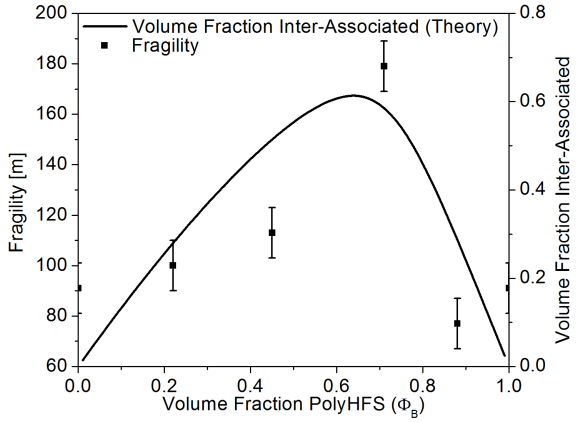

(a) PVAc Blends

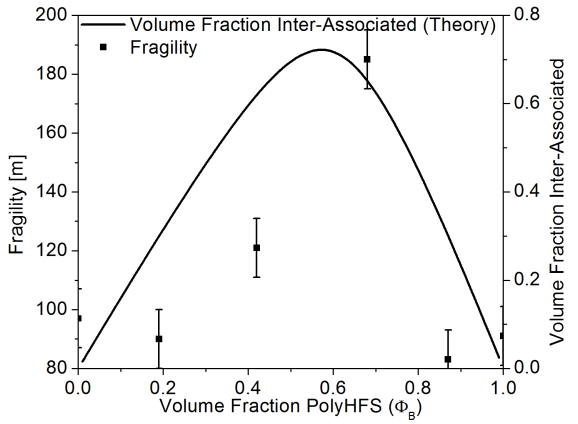

(b) EVA70 Blends

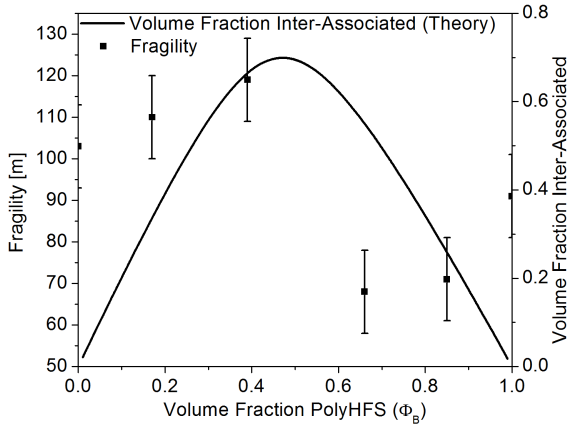

(c) EVA45 Blends

Fig. 5.17: The dynamic fragility (left axes) and the theoretical volume fraction of intermolecularly associated segments (right axes) as a function of PolyHFS composition for (a) PVAc blends, (b) EVA70 blends, and (c) EVA45 blends.

As noted previously, the fractions of free and hydrogen bonded segments determined from the FTIR spectra were calculated at room temperature, and a precise prediction of the volume fraction of intermolecularly associated segments at each blend T_g requires knowledge of the currently-unknown enthalpies of hydrogen bonding. Due to the relatively weak hydrogen bonding present in these blends, the hydrogen bonding behavior at each blend T_g should not substantially differ from that determined here. To evaluate this, dimer and multimer self-association enthalpies of 3 and 1 kcal/mol respectively, were chosen and are slightly less than the self-association enthalpy determined for PVPh self-associations[35]. An intermolecular association enthalpy of 4 kcal/mol was used, and is the same as the enthalpy of intermolecular association determined for blends of PVPh and PVAc[35]. As shown in Figure 5.18, the hydrogen bonding behavior at each PVAc blend T_g does not appreciably differ from that shown in Figure 5.6.

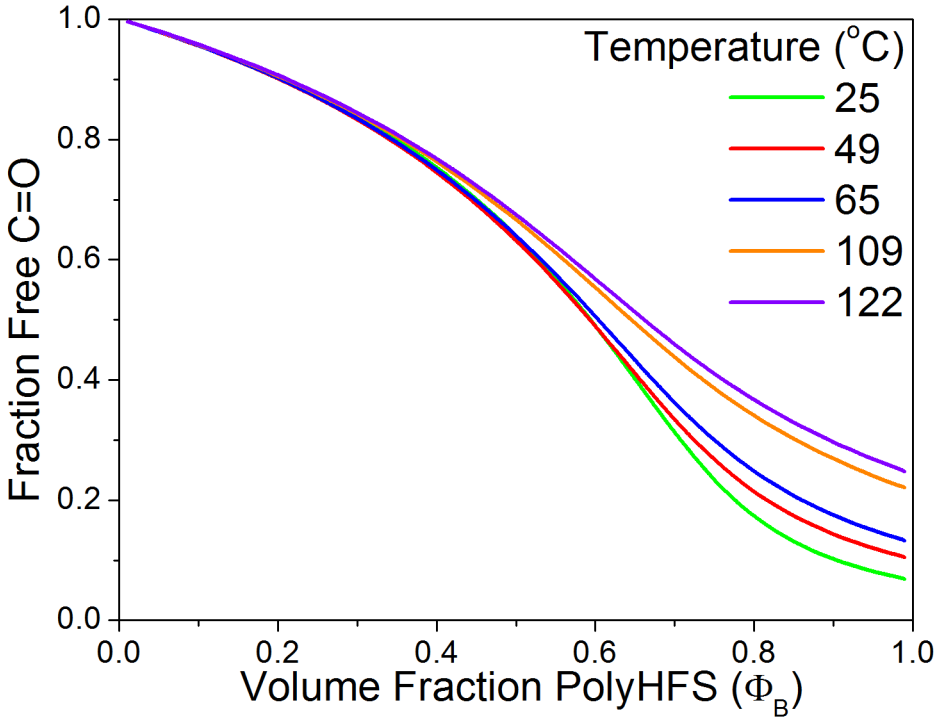

Fig. 5.18: Predicted fraction of free carbonyl groups as a function of composition for PVAc blends at room temperature and the PVAc blend T_g's.

The predicted volume fraction of intermolecularly associated segments (black curve in Figures 5.17a, 5.17b and 5.17c) is not meant as a fit of the compositional dependence of the fragility, but rather an indication of which blend compositions should have the highest fragility. For each blend series, the composition closest to the maxima in the prediction line exhibits the highest fragility. This suggests that not only does the fraction of intermolecularly associated segments dictate the fragility in intermolecular hydrogen bonded polymer blends, but also the Painter-Coleman association model is a useful guide in predicting which compositions should have the highest fragility.

Adam and Gibbs[157], and recently Stukalin et al.[163,164], have shown that the fragility is related to the configurational entropy (s_c) and the number of units involved in collective motion (z). As the degree of intermolecular coupling increases, configurational entropy is reduced and z increases. Segmental motion is hindered by intermolecular associations, requiring the breaking of hydrogen bonds before the motion can occur. As temperature approaches the blend T_g, intermolecular associations begin to break, and segmental motion can occur. As temperature increases, hydrogen bond strength decreases[1], and z will decrease rapidly and the system will gain entropy, s_c, rapidly. It is therefore expected that the compositions with the greatest fraction of intermolecularly coupled segments should have the highest fragility, since the fragility parameter is related to the rate of change of relaxation time with temperature.

As noted in Chapter 4[55], the fragility is not correlated with T_g (see Figure 5.19).

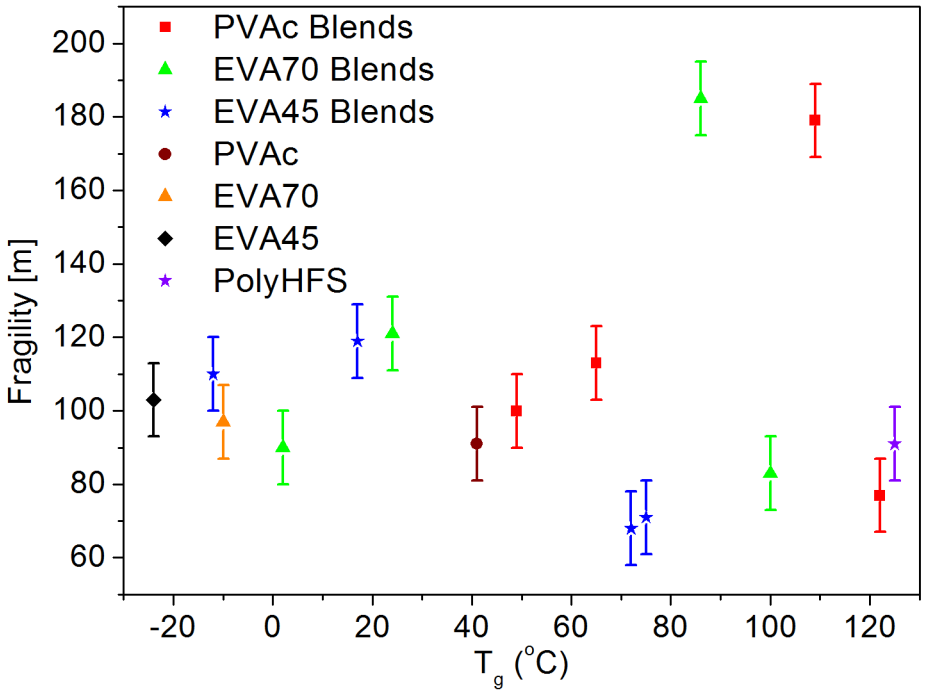

Fig. 5.19: Dynamic fragility as a function of T_g from DSC.

The highest PolyHFS composition of each series (74, 80 and 86 mol% PolyHFS in the PVAc, EVA70 and EVA45 blends, respectively), as well as the 68 mol% PolyHFS blend with EVA45, exhibits fragilies lower than the neat components. This can be attributed to the effects of plasticization. The addition of 20-30 mol% PVAc (or EVA70, EVA45) to PolyHFS will have a plasticization effect, lowering the fragility of the system, similar to what was shown by Stukalin et al[164]. The 68 and 86 mol% PolyHFS blends with EVA45 both exhibit fragilities lower than PolyHFS because EVA45 has relatively few interacting sites, and should have a stronger plasticizing effect than PVAc or EVA70 due to its higher ethylene content.

5.3.3.3 High Temperature Relaxations

At temperatures above and frequencies below the α relaxation, an additional process is present in the dielectric spectrum, α^*. Due to the dc conductivity present,

this relaxation was most easily observed in the 'conductivity-free' (derivative) dielectric loss. An example fit of two derivative HN equations (equation 2.35) and a power law to this additional process, the segmental relaxation and the onset of electrode polarization is shown in Figure 5.20.

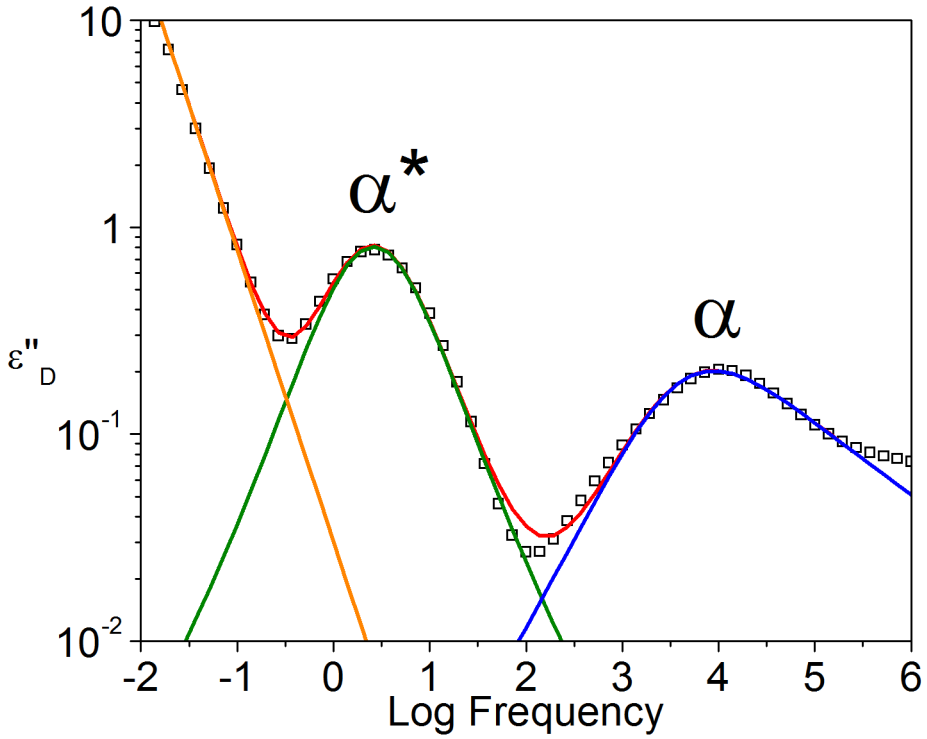

Fig. 5.20: Representative derivative Havriliak-Negami fit to the α^* process (green curve) and α process (blue curve) for the 86 mol% PolyHFS blend with EVA45 at 155 °C. The red curve is the sum of two derivative Havriliak-Negami functions and the orange line is a power law to account for the onset of electrode polarization.

Stadler and Freitas[176], and later Leibler et al.[165], described the high temperature relaxation behavior of systems where temporary thermoreversible crosslinks, or 'stickers', exist. Among the predictions of reference 165 is the existence of an additional relaxation process resulting from the breaking and reforming of hydrogen bonds as chains reptate. As the chain reptates (for low sticker contents), associations must be

broken for the chain to undergo tube disengagement. Broadband dielectric relaxation spectroscopy monitors dipole motion, and therefore only the response of open stickers can be monitored, since a closed sticker would be expected to have a negligible dipole moment [135].

For each blend, the α^* process is nearly Debye ($\alpha = \gamma = 1$), having derivative HN (equation 2.35) shape parameters $\alpha = 0.8 - 0.9$ and $\gamma = 1$. Shown in Figures 5.21a, 5.21b and 5.21c are the relaxation frequencies of the α^* process as a function of temperature normalized by T_g. This process exhibits an Arrhenius (equation 2.30) temperature dependence over the temperature range investigated, having fit parameters: $f_\circ = 10^{27\pm3}$ Hz and $E_a = 150 \pm 60$ kJ/mol. The large uncertainty in activation energies is due to the somewhat VFT-like behavior exhibited by this relaxation in some of the blends, particularly those with EVA70. Wübbenhorst et al. [135] predicted the α^* relaxation should exhibit a VFT temperature dependence over a sufficiently broad temperature range, but Müller et al. [138] modeled this relaxation with an Arrhenius function. The process, does however, appear to exhibit a VFT-like temperature dependence in another study by Müller et al. [139] Due to the relatively small temperature window over which the relaxation time of this process can be determined, a VFT fit would not be reasonable in many cases here.

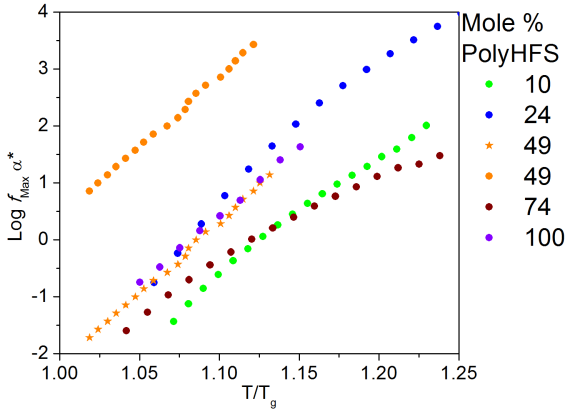

(a) PVAc Blends

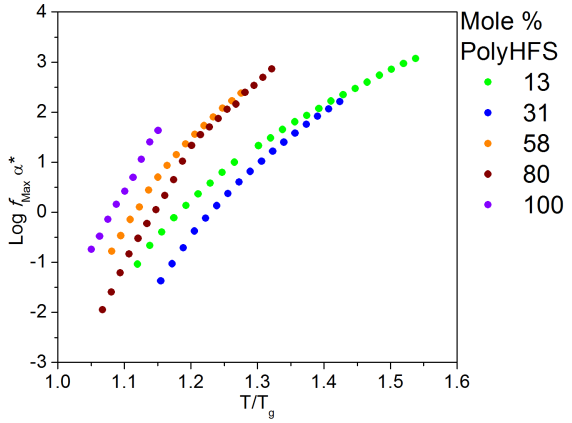

(b) EVA70 Blends

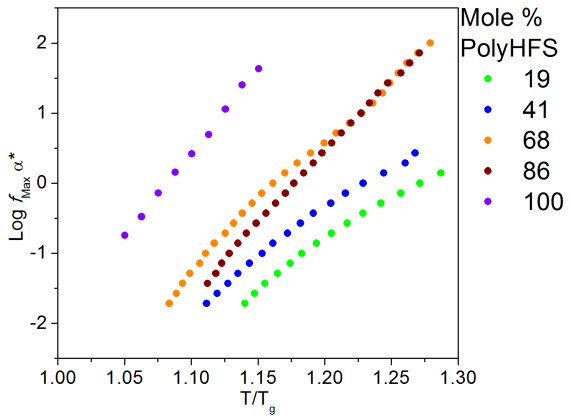

(c) EVA45 Blends

Fig. 5.21: The α^* process in the (a) PVAc blends, (b) EVA70 blends, and (c) EVA45 blends versus temperature normalized by T_g.

Inspection of Figures 5.21a, 5.21b and 5.21c reveals that as the ethylene content in the blend increases (PVAc < EVA70 < EVA45), the α^* relaxation extrapolates to lower frequencies, or higher temperatures, relative to the PolyHFS α^* relxation. This suggests that as ethylene content is increased, the α^* relaxation becomes more disconnected from the segmental process. This trend is expected, since the ethylene portion does not hydrogen bond, so although miscible, a greater fraction of the blend is unassociated as ethylene content is increased. Unassociated segments can reptate without breaking hydrogen bonds, so relative to T_g, segmental-level motion can occur more readily to higher temperatures in the EVA45 blends than in the EVA70 or PVAc blends before hydrogen bonds must be broken. Every segment in the PVAc blends can hydrogen bond, so at blend compositions where the volume fraction of HFS and VAc segments are approximately equal, segmental level motion cannot occur without breaking hydrogen bonds.

The 49 mol% PolyHFS blend with PVAc exhibits two α^* relaxations (orange circles, α^*, and stars, α^{**}, in Figure 5.21a) at temperatures above its segmental process, and is the only blend to do so. One of the relaxations, represented by the stars, occurs at timescales similar to that of PolyHFS when normalized by T_g, and the other process occurs at higher frequencies or lower temperatures. As shown in Figure 5.22, the relaxation represented by the orange stars in Figure 5.21a is of lower magnitude ($\Delta\varepsilon$) than the relaxation represented by the orange circles. This blend likely becomes slightly heterogeneous at elevated temperatures, resulting in a hydrogen bonding relaxation for the HFS homopolymer (orange stars), and a hydrogen bonding relaxation for the PVAc still hydrogen bonded to the HFS homopolymer (orange circles).

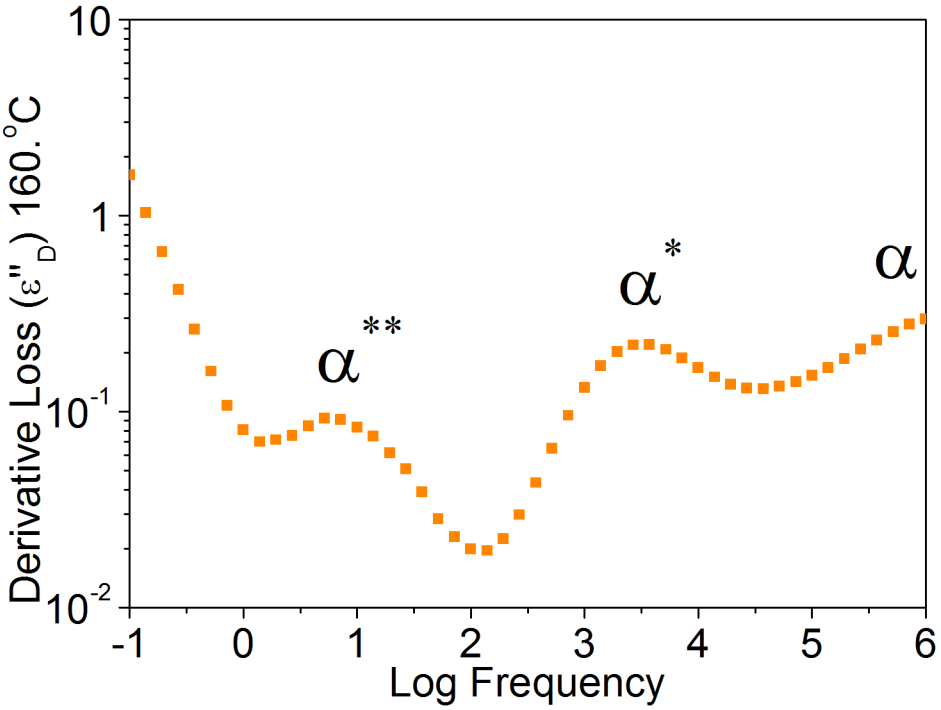

Fig. 5.22: The derivative dielectric loss at 160 °C for the 49 mol% PolyHFS blend with PVAc. The approximate locations of the α, α^* and α^{**} relaxations are shown.

5.4 Summary

The effects of strong intermolecular associations on the dynamics of miscible hydrogen bonded blends of PolyHFS with PVAc, EVA70 and EVA45 have been investigated. The Painter-Coleman association model, along with careful analysis of the state of hydrogen bonding in the blends allows for predictions of the relative strengths of glassy state relaxations of these systems. Hydrogen bonding couples the local relaxations, and retards the PolyHFS local process.

The fragility of hydrogen bonded polymer blends is strongly dependent on the fraction of segments that form hydrogen bonds. The association model allows for a

prediction of which blend compositions have the highest fragility, and should be applicable to any system where the infrared response can be quantified, or the enthalpies of hydrogen bond formation are known.

A high temperature relaxation related to the breaking and reforming of hydrogen bonds as the chains reptate is present in the blends. As the ethylene content of the blends increases, the relaxation moves to higher temperatures relative to the segmental process, since reptation can proceed more readily in these systems without breaking the intermolecular associations.

Chapter 6

HFS:DMB Copolymer Blends with PVME

6.1 Introduction

Intermolecular hydrogen bonding in polymer blends, and the effects of hydrogen bonding on blend dynamics, has been a topic of great interest [1]. Although clearly not as strong as chemical crosslinks (which exhibit a bond strength on the order of 50 kcal mol^{-1} versus a hydrogen bond strength of 1-10 kcal mol^{-1}), hydrogen bonds have a profound effect on the physical and chemical properties of polymers. A number of studies [33–36,38–40] have explored the influence of intermolecular hydrogen bonding on miscible blend dynamics. At intermediate compositions, it has been established that such mixtures exhibit a single (albeit broadened) segmental relaxation, even when the intrinsic component mobilities are very different [33,35,36,151]. However, when the composition is relatively asymmetric, these blends exhibit two segmental processes, arising from a simple hydrogen bonding stoichiometric effect. For example, in miscible poly(vinyl methyl ether) [PVME] - poly(p-vinylphenol) [PVPh] blends with a preponderance of PVME, two segmental processes are observed and assigned to intermolecularly hydrogen bonded PVME and PVPh relaxing segments, and to 'free' PVME segments [33].

Functional group accessibility has been demonstrated to have a significant influence on polymer miscibility [28–31]. Specifically, it has been established that controlled steric shielding can increase the propensity for intermolecular hydrogen bond formation (to functional groups on a miscible second polymer) over intramolecular hydrogen bonding [2,48]. For example, poly(1,1,1,3,3,3-hexafluoro-2-(4-vinylphenyl)propan-2-ol) (poly(HFS)) exhibits a much greater degree of intermolecular versus intramolecular hydrogen bonding, having self-association equilibrium constants K_2 and K_B of 2.5 and 3.4, respectively [48], a result of the two CF_3 groups adjacent to the phenolic –OH. A polymer with a similar structure, lacking such steric shielding (PVPh), exhibits a much

greater degree of intramolecular hydrogen bonding: its self-association equilibrium constants K_2 and K_B are 21 and 66.8, respectively[28], an order of magnitude larger than those of poly(HFS). An extensive analysis of the hydrogen bonding characteristics of the HFS homopolymer and copolymers of HFS with styrene is provided in ref 14.

The overall goal of this and ongoing studies is to establish the role of reduced intramolecular hydrogen bonding on blend dynamics. We also control the number of interacting sites by copolymerizing HFS with a non-hydrogen bonding unit, 2,3-dimethylbuta-1,3-diene (DMB). PVME is selected as the second component in the blend to facilitate comparison with the dynamics of similar blends reported in the literature[33,154]. The ether groups in PVME form relatively strong intermolecular hydrogen bonds with the phenolic -OH of polymers such as PVPh and poly(HFS)[33]. The addition of a relatively small number of HFS hydrogen bonding sites (˜14 mole % of the repeat units) renders the otherwise immiscible poly(DMB) and PVME miscible over the entire composition range, as predicted by the Painter and Coleman association model[1].

6.2 Experimental

The synthesis of a copolymer of 1,1,1,3,3,3-hexafluoro-2-(4-vinylphenyl)propan-2-ol and a low T_g comonomer, 2,3 - dimethylbutadiene is outlined in Chapter 3. As noted in Chapter 3, the molecular weight of the copolymer and poly(vinyl methyl ether) (PVME) were measured via GPC using poly(styrene) calibration standards. The copolymer's weight average molecular weight was determined to be 95 $\frac{kg}{mol}$, having a polydispersity index of 2.0. PVME was purchased from Polymer Laboratories, having a weight average molecular weight of 102 $\frac{kg}{mol}$, and a polydispersity index of 3.0. Blends consisting of 26, 50, 76, and 90 weight percent of the copolymer were created by mixing appropriate amounts of each component in THF, then removing the solvent. Each blend was dried under vacuum (2-3 μbar) at approximately 60°C for 2-3 days prior to any measurement to remove all water.

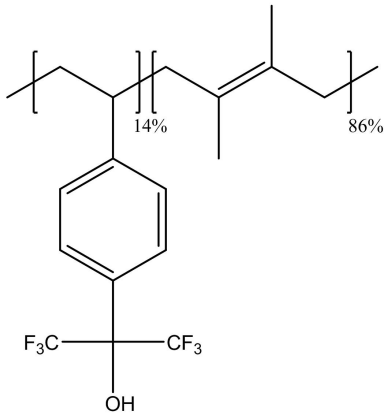

Fig. 6.1: Structure of the HFS:DMB copolymer.

Differential scanning calorimetry (DSC) was carried out on a TA Instruments Q1000 for these blends. Each sample was heated at 10°C/min to 70°C, held for two minutes, cooled at 10°C/min to -70°C, held for an additional two minutes, then reheated at 10°C/min to 70°C. T_g was determined from the midpoint of the heat capacity step on the second heating run.

As noted in Chapter 3, broadband dielectric relaxation spectroscopy (DRS) was carried out on a Novocontrol Concept 40, using an attached liquid nitrogen dewar which uses evaporated nitrogen to control the temperature of the sample within ±0.02°C of the set point. A parallel plate capacitor sample configuration was used, with the sample thickness maintained with two, 50 μm silica spacers. The samples were measured isothermally from -150°C to 60°C in five degree intervals, using a frequency range of 10 MHz to 10 mHz, with seven data points per frequency decade.

The DRS results were analyzed with the traditional HN function with an added conductivity term (see equation 2.27). Although used to fit the data, the conductivity contribution in equation 2.29 was generally ignored, since the derivative of the dielectric constant was used as an estimate of the conductivity-free loss (see equation 2.34).[100,134]

For details on the application of this method, the appropriate derivative HN equation to use in the analysis, and the considerations which need to be made when employing this method, the interested reader is referred to reference 100, or page 41 of Chapter

2. The principle benefit of the derivative formalism is the elimination of the ionic (impurity) conductivity, inherent in any polymeric sample above its T_g. This conductivity contribution does not manifest itself in the dielectric constant, and is effectively removed with the application of equation 2.34.

In addition to the traditional method of fitting the isothermal data with an HN equation (equation 2.27), isochronal data were also examined. The method for determining the relaxation temperature yielded the same relaxation behavior as did traditional fitting, with far more datapoints. Note that the local relaxations were not analyzed in this fashion, due to their greater breadth and lower strength.

A Vogel-Fulcher-Tamman (VFT) equation was used to model the segmental relaxation times as a function of temperature (see equation 2.31). An Arrhenius equation (equation 2.30) was used to model the local processes.

As outlined in Chapter 3, FTIR was conducted on a Nicolet 6700 with an attached dry air purge. A minimum of 100 scans were averaged with a wavenumber resolution of 2.

6.3 Results

6.3.1 DSC

DSC results indicate the blends are miscible, with T_g between those of the components and dependent on blend composition (see Table 6.1). With the exception of the neat copolymer, the VFT-determined T_g (at $\tau = 100$ s) (see Table 6.2) is in excellent agreement with the calorimetric T_g.

6.3.2 FTIR

The FTIR results for the HFS:DMB blends with PVME are shown in Figure 6.2. Unlike the HFS homopolymer blends, the HFS:DMB copolymer exhibits several self-association bands. This is likely due to the increased flexibility provided by the DMB comonomer. This increased flexibility (functional group accessability) makes it easier for two HFS segments to form self associations compared to the relatively rigid

Table 6.1: Glass transition temperatures of the PVME - HFS:DMB blends, determined by DSC.

Weight % HFS:DMB	T_g (°C)±5°C
0	-26
26	-19
50	-6
76	12
90	23
100	23

HFS homopolymer. It is unlikely the additional bands are a result of degradation: the carbonyl region of the HFS:DMB copolymer is devoid of any absorption bands.

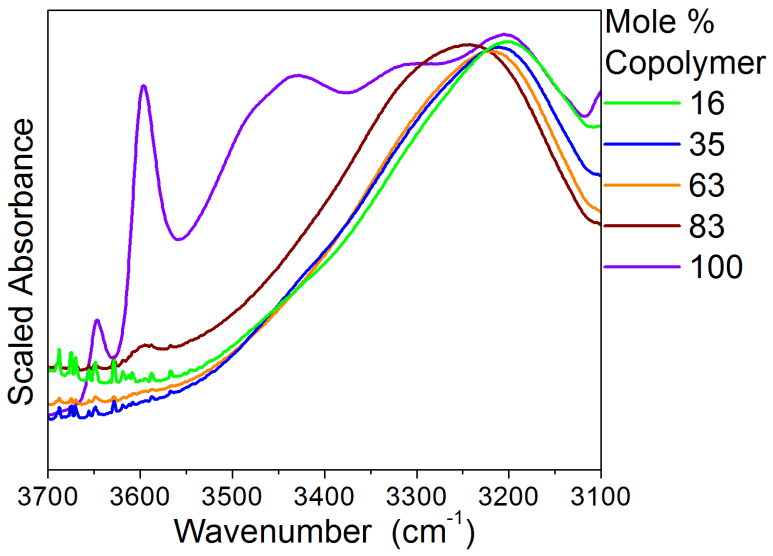

Fig. 6.2: FTIR OH region of the HFS:DMB copolymer and its blends with PVME.

6.3.3 PVME

Our experimental dielectric spectra are in excellent agreement with those reported in the literature.[76,95] A comparison of the VFT and Arrhenius fitting parameters determined here and those from the literature can be seen in Table 6.2, along with those of the relaxations for the HFS:DMB copolymer and the blends.

Table 6.2: VFT and Arrhenius fit parameters for each relaxation for neat polymers and blends under investigation.

Wt% Copolymer	Relaxation	$f_\circ$(Hz)	B (K)	$T_\circ$(K)	$E_a(\frac{kJ}{mol})$	VFT T_g(°C)
0	α	10^{11}	1230	208		-28
	β	10^{13}			24	
0 - Literature	α $^{Gomez\,2001}$	10^{12}	1590	198		-29
	β $^{Casalini\,2003}$	10^{12}			21	
	α_1	10^{11}	2340	182		-19
26	α	10^{11}	1250	213		-21
	β	10^{13}			25	
	α_1	10^{11}	2030	202		-7
50	α	10^{11}	1240	224		-10
	β	10^{12}			23	
76	α	10^{11}	1570	237		11
	β	10^{13}			26	
90	α	10^{12}	1850	242		23
	β	10^{12}			23	
100	α	10^{11}	1457	243		18
	$\beta_{Copolymer}$	10^{13}			40	

6.3.4 HFS:DMB Copolymer

The neat copolymer exhibited two relaxations, a segmental process and a smaller, broad local process in the glassy state, which by analogy to the dielectric relaxation behavior of PVPh, is assigned to motions of the HFS side group. The dielectric loss for the HFS:DMB copolymer as a function of temperature and frequency is displayed in Figure 6.3. The VFT (equation 2.31) and the Arrhenius (equation 2.30) fit parameters characterizing the segmental process and local process of this polymer are located in

Table 6.2. Note in Table 6.2 that the $\beta_{Copolymer}$ and the β process of PVME arise from different molecular motions.

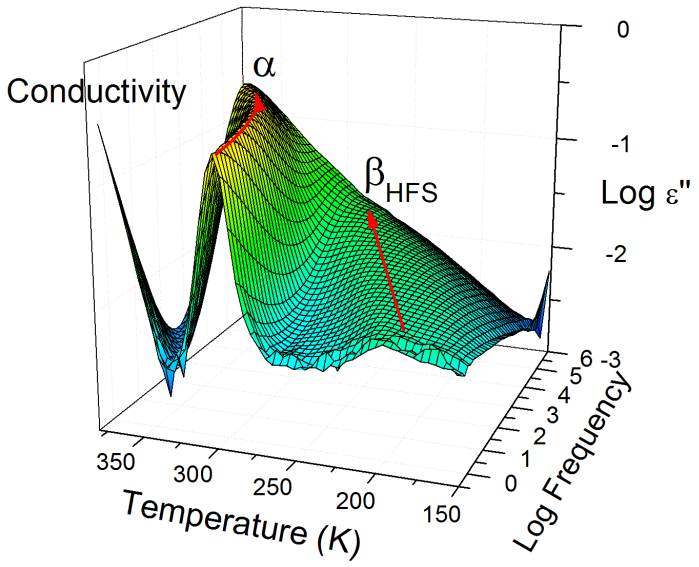

Fig. 6.3: Dielectric loss as a function of temperature and frequency for the 14 mole percent HFS, HFS:DMB copolymer.

6.3.5 The α and α_1 processes

The dielectric loss as a function of temperature and frequency is shown in Figure 6.4 for the 26 wt% copolymer blend. This behavior is typical for the blends studied here. The locations of the relaxations are indicated on the plot with arrows.

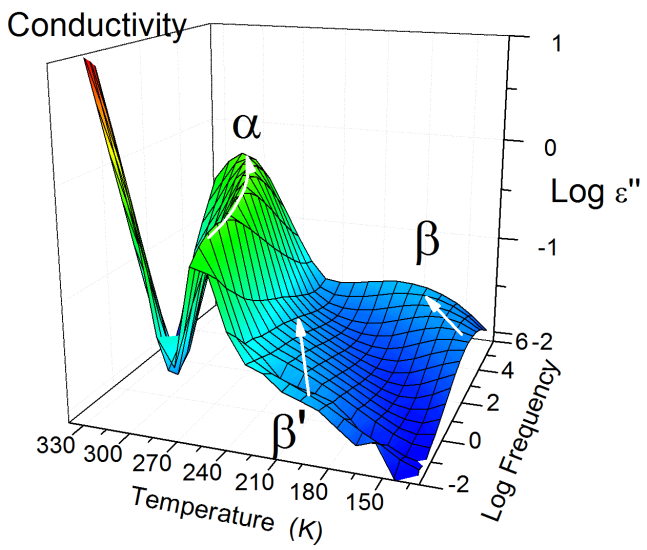

Fig. 6.4: Dielectric loss as a function of frequency and temperature for the 26 wt% copolymer blend.

Two segmental relaxations occur in the 26, 50 and 76 wt% copolymer blends. Due to the proximity of the two relaxations, the relaxation times of the α and α_1 processes could only be determined reliably for the 26 and 50 wt% copolymer blends. Both relaxations appear to be present in the 76 wt% copolymer blend, but only a single relaxation time is reported here, which is likely a combination of those of the two processes. Data typical of the two segmental relaxations in the blends under investigation is shown in Figure 6.5.

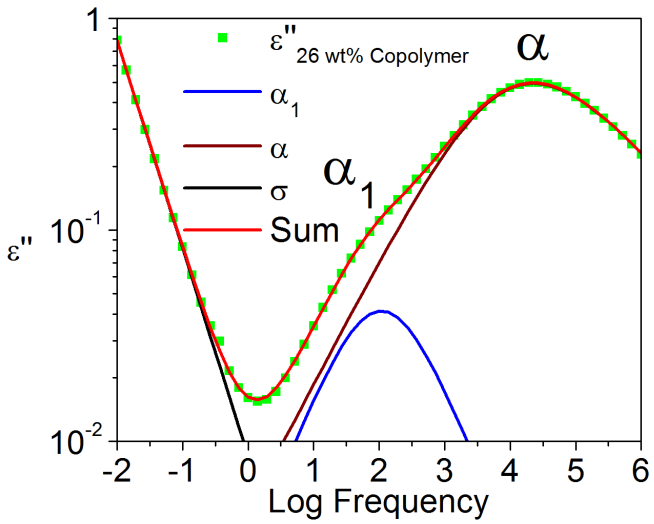

Fig. 6.5: Dielectric loss for the 26 wt% copolymer blend at 20^{o}C.

The existence of two segmental relaxations in miscible binary blends exhibiting weak intermolecular interactions is not an uncommon feature, and arises from chain connectivity and the effective concentration of each component. In hydrogen bonded blends, specific interactions were initially predicted to couple the segmental dynamics of the two components[27], resulting in a single segmental relaxation. However, as noted earlier, it has been demonstrated that even in the case of strong intermolecular hydrogen bonding, simple stoichiometric effects at asymmetric compositions can lead to two segmental processes[33].

It is important to note that the intrinsic mobilities of PVME and the 14 mol% HFS:DMB copolymer are significantly different (ΔT_g ~50 °C). The existence of two segmental relaxations at the 50/50 blend composition is clearly not consistent with a purely hydrogen bonding stoichiometric argument. Inherent in this simple model is that there are sufficient hydrogen bonding stickers to completely couple the segmental relaxations of the components at appropriate compositions. However, the parent copolymer contains only 14 mole% HFS segments and the findings suggest that this is insufficient to completely couple the component segmental processes.

It is proposed, therefore, that the faster segmental processes (α in Figure 6.6) in the 26 and 50 wt% blends arise from motions of the PVME component of the blend modified by the HFS:DMB, at least some of which are hydrogen bonded to HFS units. The slower component (α_1 in Figure 6.6) has a dielectric relaxation strength which is roughly proportional to the concentration of HFS segments in the blend. It is therefore proposed that this is the segmental process of the copolymer, whose dynamics have been modified by the faster PVME segments. The α_1 process exhibits a longer relaxation time in the 50 wt% copolymer blend (and a dielectric strength of ~2X that of the 26 wt% copolymer blend) due to the greater concentration of copolymer in the blend. This can be considered in terms of the Lodge-McLeish model in that the effective concentration of the copolymer is higher in the 50 wt% blend, and experiences an environment richer in itself than it does in the 26 wt% blend. This higher effective concentration should yield a longer relaxation time for the slower segmental process[14].

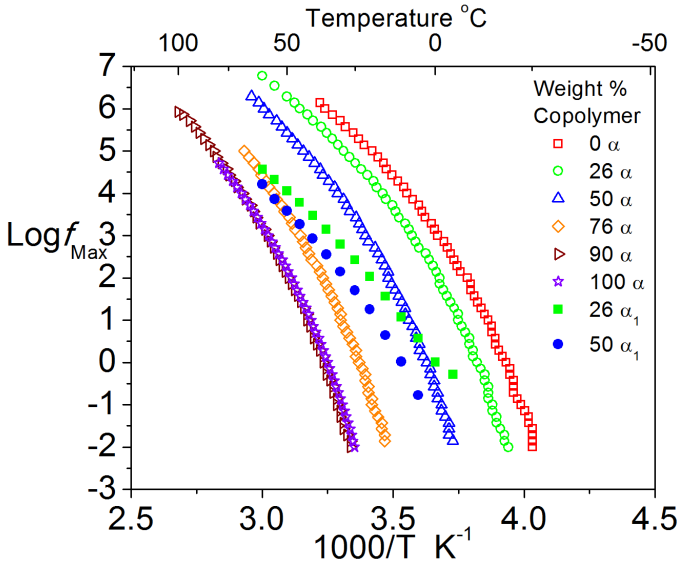

Fig. 6.6: Relaxation times of the α and α_1 processes as a function of inverse temperature.

6.3.6 The β' process

The process designated as β' in the dielectric spectrum of PVME in Figure 6.4 is typically described as a high frequency shoulder on the segmental relaxation [13,95]. It is likely, however, that this is a separate process, associated with the relaxation of residual water in the polymer [94]. It was noted that the strength of this process decreased as the sample was dried and exhibited a small change (increase) in relaxation time. Capaccioli et al. reported a relaxation in the glassy state with an activation energy of $\sim 50\ \frac{kJ}{mol}$ for a series of materials [94]. Cerveny et al. investigated the dynamics of water in several systems, including PVME, also observing a similar activation energy for this glassy state process in each system [77,88]. The fact that the strength of the observed process decreases with decreasing water content, and exhibits an activation energy and relaxation time in the glassy state similar to that seen in the literature [77,88,94], strongly points to water, either on its own or coupled to PVME motions, as the origin of the β' process observed here.

6.3.7 The β process

An Arrhenius plot of the temperature dependence of the relaxation time of the β process is shown in Figure 6.7, with the corresponding Arrhenius fit parameters (equation 2.30) listed in Table 6.2. The PVME β process, assigned to rotation of the methyl ether groups in the side chain of PVME about the O-C bonds [13], maintains the same relaxation time in the blends, independent of composition. Such behavior was also observed in non-interacting blends of PVME and PS [177]. In previous work on analogous PVPh-PVME blends, the findings strongly suggested that the relaxation of some side groups of both polymers were suppressed by blending, and these groups are likely those constrained by intermolecular hydrogen bonding [33]. However, the strength of the PVME β process in the blends simply decreases in proportion with decreasing PVME content and its relaxation time nor peak shape change with blend composition. This likely due to the modest concentration of HFS segments present and hydrogen bonded to the PVME ether pendant groups.

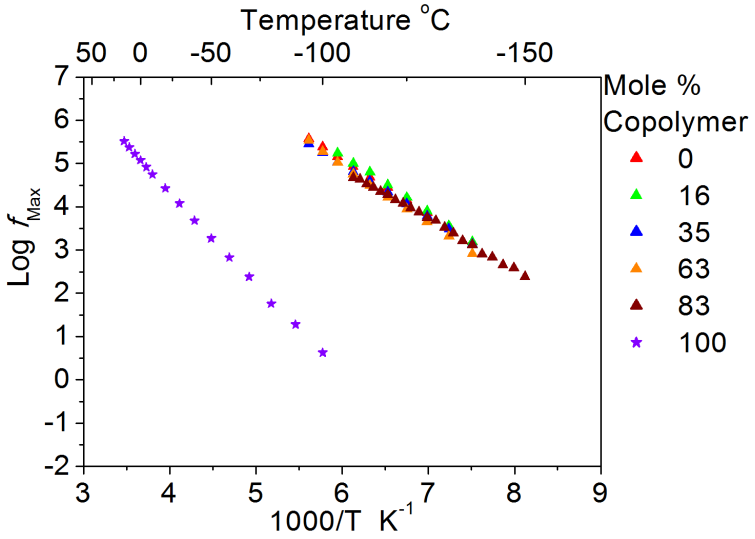

Fig. 6.7: Relaxation times of the PVME β process in neat PVME and the blends as a function of inverse temperature. The relaxation times of the β process of the HFS:DMB copolymer are also displayed for comparison purposes.

A low frequency shoulder appears on the PVME β process in the 90 wt% copolymer blend. This is the β process of the copolymer, and it is present due to the large amount of HFS segments present in the blend.

6.4 Summary

Two segmental relaxations were observed for most of the 14 mol% HFS:DMB copolymer - PVME blends. The α process is attributed to motions of the PVME component of the blend modified by the HFS:DMB copolymer, at least some segments of which are hydrogen bonded to HFS units. We propose that the the slower α_1 process is associated with segmental motions of the copolymer, whose dynamics have been modified by the faster PVME segments.

The β' process of PVME was found to arise from the presence of trace amounts of water within the blends. A similar relaxation is commonly observed not only in polymeric systems, but in many others containing hydrogen bonds, and may provide a quantitative method of determining water content of materials from DRS spectra.

Due at least partly to the low concentration of hydrogen bonding species, the dynamics of the PVME β process are not affected by blending. The strength of the process is found to simply decrease with decreasing PVME content and the relaxation time and shape do not change with blend composition.

Chapter 7

Dynamics of Main-Chain Liquid-Crystalline Polysiloxanes Containing *p*-Phenyleneterephthalate Mesogens

7.1 Introduction

Thermotropic liquid crystalline polymers (LCPs) are semi - flexible macromolecules capable of forming mesophases of one - dimensional or two-dimensional ordering over a characteristic temperature range between their glass transition temperature T_g and their LC to isotropic clearing temperature T_i. Main-chain LCPs (MCLCP) are those having rigid, rod - like or disk - like structural units (mesogens) embedded in the polymer backbone. MCLCP combine the mechanical and rheological properties of polymers with the inherent segment level anisotropy of liquid crystals, representing a class of soft materials with unique physics. Owing to orientational and/or positional couplings between rigid rod-like segments (mesogens) in their semi-flexible backbones, MCLCPs exhibit rich relaxation dynamics and rheological characteristics that distinguish them from all other macromolecules.

This report concerns the relaxation behavior of three novel main-chain liquid crystalline polymers, two of which exhibit a smectic C_A mesophase. The smectic C_A mesophase is a relatively recently described smectic phase in which the mesogens in adjacent layers tilt in an alternating sense with respect to the layer normals. Smectic C_A mesophases have been identified in low molar mass liquid crystals, main-chain thermotropic polyesters[178,179], and main-chain thermotropic polysiloxanes[180,181]. Only a few reports of rheological or dynamic mechanical characterization of smectic C_A polymers exist, so much remains to be learned about the dynamics of their segment-level relaxation processes, especially at high frequencies. As the principles of time-temperature

superposition are generally not applicable to smectic LCP rheology, study of high frequency relaxations in the smectic C_A state requires experimental methods that can probe extremely fast dynamic processes over the relevant temperature range.

Dielectric relaxation spectroscopy (DRS) can investigate a frequency window up to six orders of magnitude greater than that accessible by dynamic mechanical or rheological techniques, making it an ideal tool for studying the dynamics of LCPs. Several studies have examined the dielectric behavior of either MCLCPs or side chain liquid crystalline polymers (SCLCPs)[136,182–189], but few studies have been conducted on smectic C_A MCLCP[188,190,191]. These investigations have demonstrated that LCPs exhibit multiple relaxations in both the glassy and liquid crystalline state(s). Although relaxation processes at temperatures above the dielectric segmental process have been observed previously in LCPs[136,142], determination of their origins is complicated by the presence of conduction losses due to the motion of ionic impurities.

7.2 Experimental

7.2.1 Materials

Main-chain liquid crystalline polysiloxanes F3CH$_3$, F3Cl, and F3H (Figure 7.1) were synthesized via Pt-catalyzed hydrosilylation.[180] F3CH$_3$ and F3H were found to exhibit the smectic C_A mesophase, while the LC structure of F3Cl is still unknown at present. The mesogens in F3CH$_3$ are mixed isomers having variable placement of the methyl groups on the terminal aromatic rings. Fractionated polymer samples having comparatively narrow molar mass distributions were isolated from the raw polycondensation products by fractional precipitation from toluene solution using methanol as a poor solvent. Molar masses of fractionated polymers were determined by size exclusion chromatography (SEC) using a Shimadzu system with a series of three columns (Styragel HR 7.8 x 300 mm columns with 5 μm bead size: 100-10,000, 500-30,000, and 5000-6,000,000 Da) from Polymer Laboratories, Inc., using both refractive index (RI) and ultraviolet absorption (UV, 254 nm) detectors. Measurements were performed in THF at 35°C with a flow rate of 1 mL/min. Molar masses reported were determined by

comparison to polystyrene standards. Characteristics of the LCPs studied in this report are presented in Table 7.1.

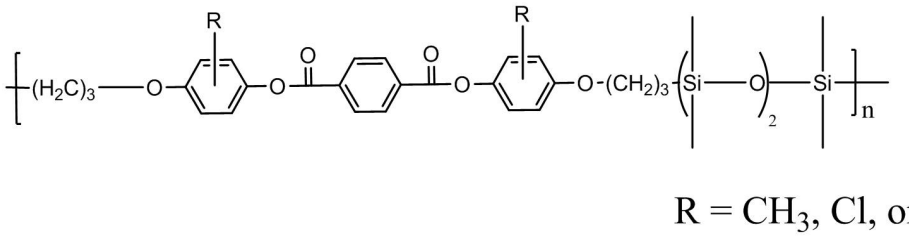

Fig. 7.1: Repeat unit of the LCPs F3CH$_3$, F3Cl and F3H.

7.2.2 Differential Scanning Calorimetry

Thermal transitions were characterized using a Seiko Instruments DSC220CU equipped with a liquid nitrogen dewar. Approximately 5 mg of polymer was crimped into a TA Instruments aluminum pan, which was heated above the clearing temperature T_i and cooled quickly to 22°C, to erase thermal history and improve sample contact with the pan. Samples were then allowed to equilibrate at room temperature for 3 days before DSC characterization. Heating traces were recorded by initially cooling to -30°C and then applying a heating ramp at 10°C/min under a flowing N_2 atmosphere. The glass transition temperature was taken as the midpoint of the inflection response at the chosen heating rate. The temperatures corresponding to a change in liquid crystalline order, T_2, and the transition to the isotropic state, T_i [180], are taken as the temperature at which the peak of the respective endotherm was observed. The uncertainty in reported peak positions was ±5°C or less, based upon multiple runs. Observed values of T_g, T_2, and T_i are reported in Table 7.1, and the DSC trace for each LCP is shown in Figure 7.2.

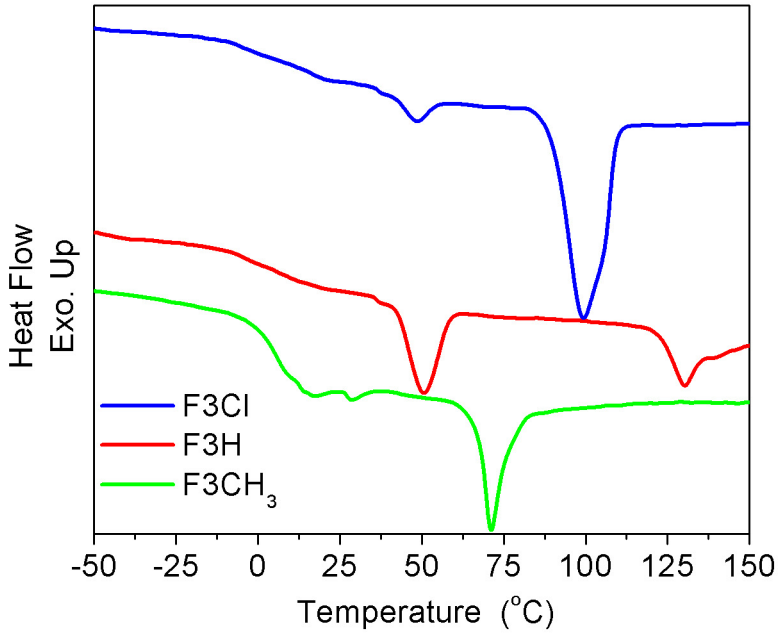

Fig. 7.2: DSC heating traces for the three LCPs.

7.2.3 Dielectric Spectroscopy

Broadband dielectric relaxation spectroscopy (DRS) measurements were collected on a Novocontrol Concept 40 broadband dielectric spectrometer in the frequency range of 0.01Hz to 1MHz. Evaporated nitrogen was heated and passed over the sample, allowing for temperature control within ±0.02°C of the temperature setpoint. The LCPs were studied from -140°C to ∼10°C above their respective clearing temperatures. A ten degree interval was used except within the interval T_g to T_g+30°C, where a three degree interval was used. Samples were allowed to equilibrate at each temperature for five minutes prior to measurement.

Samples were formed between brass electrodes, using a 0.2 mm PTFE spacer by heating the samples above their clearing temperatures on a 30 mm electrode, then pressing a 25 mm upper electrode on top of the sample/spacer. Data analysis accounted for the capacitance of the PTFE spacer.

The Havriliak-Negami (HN) equation was used (see equation 2.27)[128], along with a derivative HN equation (see equation 2.34)[100,134] to model the various relaxations observed in the dielectric spectra of these LCPs. A conductivity term (equation 2.29) can be added to equation 2.27 account for the dc conduction of impurity ions inherent in any polymer.

Under an applied electric field at temperatures above T_g, motions of impurity ions (dc conductivity) dominate the dielectric loss. Conductivity is not directly manifested in the dielectric constant, and an approximation of the conductivity free dielectric loss can be made by taking the derivative of the dielectric constant, as listed in equation 2.34[100,134]. The frequency of the relaxation under consideration can be determined from τ_{HN} via equation 2.28. An Arrhenius relation (see equation 2.30) is often used to describe the temperature dependence of relaxation times of local (β) relaxations. To describe segmental relaxations in polymers, the VFT equation (see equation 2.31) was used[192].

7.3 Results and Discussion

Table 7.1: Characteristics of main-chain polysiloxane LCPs, taken from reference 180. All thermal transitions reported have a standard deviation of 5°C. All molecular weights reported have a standard deviation of 1kg/mol.

LCP	T_g(°C)	T_2 (°C)	T_i(°C)	$\overline{M_W}\left(\frac{kg}{mol}\right)$	$\frac{\overline{M_W}}{\overline{M_N}}$
F3CH_3	8	17	72	69	1.3
F3Cl	8	50	100	16	1.4
F3H	8	51	131	69	1.4

As shown in Figure 7.2 and Table 7.1, three separate transitions are observed in the DSC thermogram of each LCP: T_g, T_2, and T_i. Their assignments are based on optical microscopy observations as well as X-ray diffraction studies[180]. Also shown in Table 7.1 are the molecular weight characteristics measured by GPC.

7.3.1 DRS

A representative plot of dielectric loss as a function of temperature is shown in Figure 7.3. The relaxation times of the processes occurring in each LCP examined here are displayed in Figure 7.4 as a function of inverse temperature, with their corresponding VFT (equation 2.31) and Arrhenius (equation 2.30) fitting parameters listed in Table 7.2.

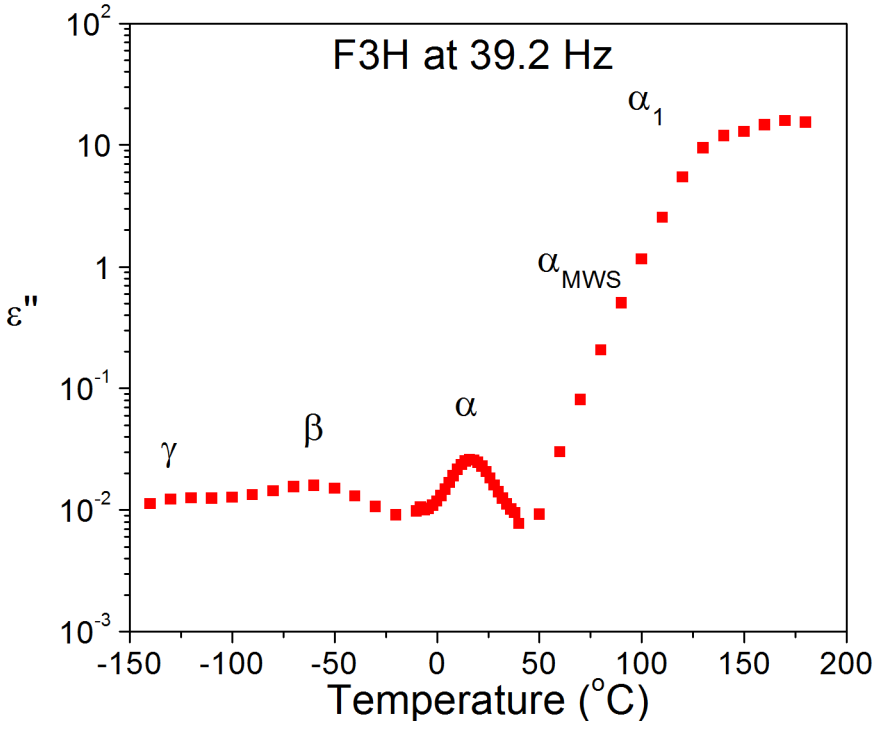

Fig. 7.3: Dielectric loss as a function of temperature for F3H at 39.2 Hz.

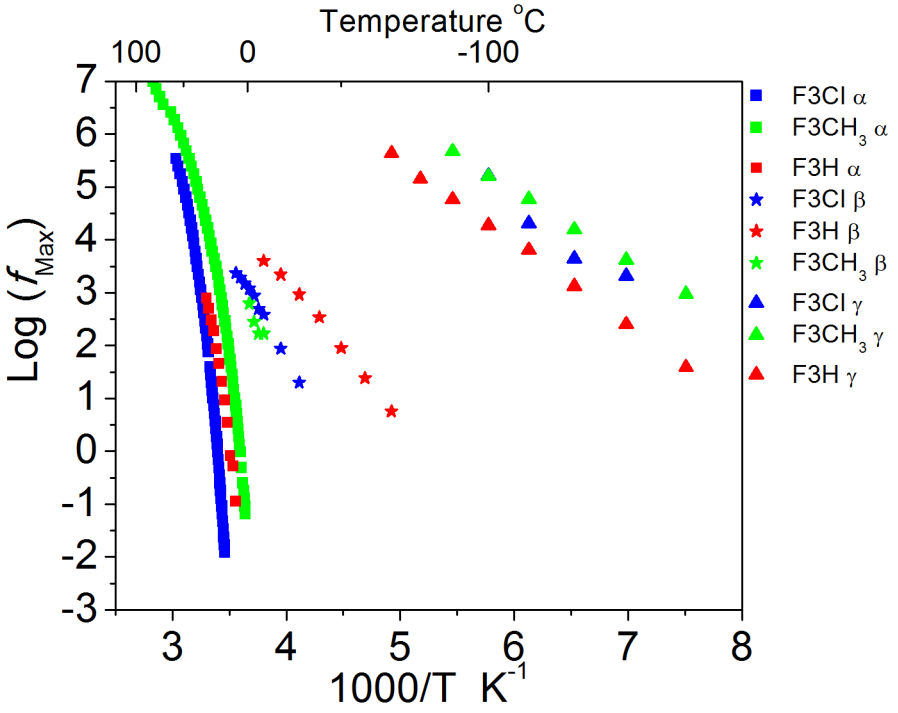

Fig. 7.4: Relaxation times of the α, β, and γ processes for the three LCPs.

7.3.1.1 γ Relaxation

The γ relaxation is observed in the glassy state (Figure 7.3), at temperatures well below that of the dynamic glass transition, and is ascribed to rotations of the alkyl/siloxane segments in the backbone. A relaxation of alkyl segments, having a similar temperature dependence has been observed by dielectric spectroscopy in a number of LCPs[134,136,143,185,193]. The α relaxation of poly(dimethylsiloxane) occurs at temperatures and relaxation times similar to those of the γ relaxation[194]. It is likely the γ process seen here is a relaxation of both the siloxane and alkyl units of the LCPs, both of which are dielectrically active and have been shown to be present at these temperatures.

Table 7.2: VFT and Arrhenius fitting parameters for modeling the relaxations of the LCPs studied here.

LCP	Relaxation	$E_a \pm 1 \left(\frac{kJ}{mol}\right)$	$Log_{10}(f_\circ) \pm 1$ (Hz)	B ±10 (K)	$T_\circ \pm 3$ (°C)
$F3CH_3$	α		11	970	-33
	β	58	14		
	γ	25	13		
F3Cl	α		11	880	-15
	β	58	14		
	γ	29	14		
F3H	α		11	1230	-36
	β	50	14		
	γ	29	14		

7.3.1.2 β Relaxation

The β relaxation also occurs in the glassy state, at temperatures below the dynamic glass transition (α), and above the γ relaxation (see Figure 7.3). This process has a low dielectric relaxation strength, and partially overlaps with the α process, making determination of relaxation times difficult, as illustrated by the relatively few datapoints displayed for this process in Figure 7.4. As the size of the substituent increases (see Figure 7.1), the relaxation time of this process also increases (F3H<F3Cl<$F3CH_3$).

Several studies of liquid crystalline polymers, as well as poly(ethylene terephthalate), have reported a dielectric relaxation in the glassy state arising from motions of phenyl rings in the polymer backbone[143,183,195–199]. All authors report the activation energy for this process to be on the order of 50 ± 10kJ/mol, and $\tau_\circ$ to be on the order of $10^{12\pm1}$Hz. The temperature dependence of this relaxation is nearly identical to the behavior of the β relaxation seen for the LCPs studied here, and we conclude that it arises from the same molecular motion as reported elsewhere.

7.3.1.3 α Relaxation

The relaxation time as a function of inverse temperature for the segmental relaxation for each LCP is shown in Figure 7.4, with the corresponding VFT (equation 2.31) fitting parameters listed in Table 7.2. A constant value of 10^{11} was used for $f_\circ$ in the

VFT fits of the α process, since the range over which the α relaxation time could be accurately determined for F3H was smaller than for the other LCPs. Interestingly, no discernable change in the relaxation behavior of the α process occurs as the LCPs pass through their T_2 transition.

7.3.1.4 α_{MWS} and α_1 Relaxations

A relaxation is present at frequencies below the segmental process (see Figure 7.5), but only at temperatures below the clearing temperature. This suggests that this relaxation is associated in some way with the disappearance of discrete domain walls as the LCP passes through its clearing temperature. A natural explanation, also proposed to explain a similar process in a side chain LCP [53], is that it is associated with Maxwell Wagner Sillars (MWS) interfacial polarization, arising from two regions having different conductivities and dielectric constants. As the LCPs approach their clearing temperatures (see Table 7.1), the dielectric strength begins to decrease. As the LCPs pass through their isotropic transitions, this relaxation disappears.

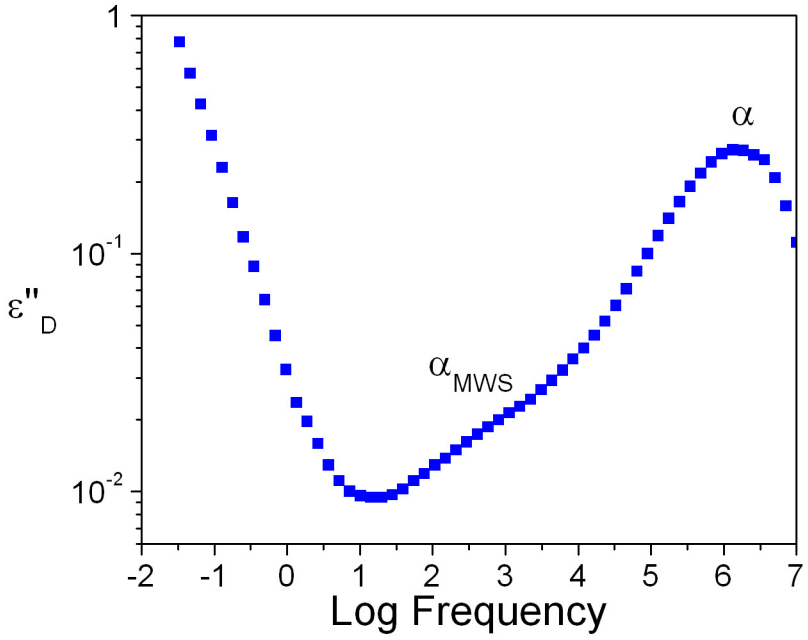

Fig. 7.5: F3Cl ε''_D data at 66°C.

At frequencies below (and temperatures above) α_{MWS}, an additional relaxation is observed (α_1) (see Figure 7.6). This relaxation persists above the isotropic temperature, unlike those observed by Wübbenhorst et. al.[134], which nearly disappear when the LCPs are taken through their clearing temperature. Relaxations occurring at temperatures above the segmental relaxation are not uncommon in LCPs, and are typically attributed to motions of the mesogenic unit about its long and short axes[134,142–144], and are proposed to be present in all liquid crystalline systems[144,145]. This relaxation is likely a rotation of the mesogens corresponding to an increase in rotational freedom, but an assignment of this relaxation to a specific rotational degree of freedom is not possible. This relaxation is overlapped by electrode polarization, associated with the accumulation of charge (impurity ions) at blocking electrodes, and exhibits a much higher relaxation strength than other relaxations[53]. The overlap of electrode polarization, and

the inability to fit this relaxation with a single HN function, prohibited the determination of its temperature dependence.

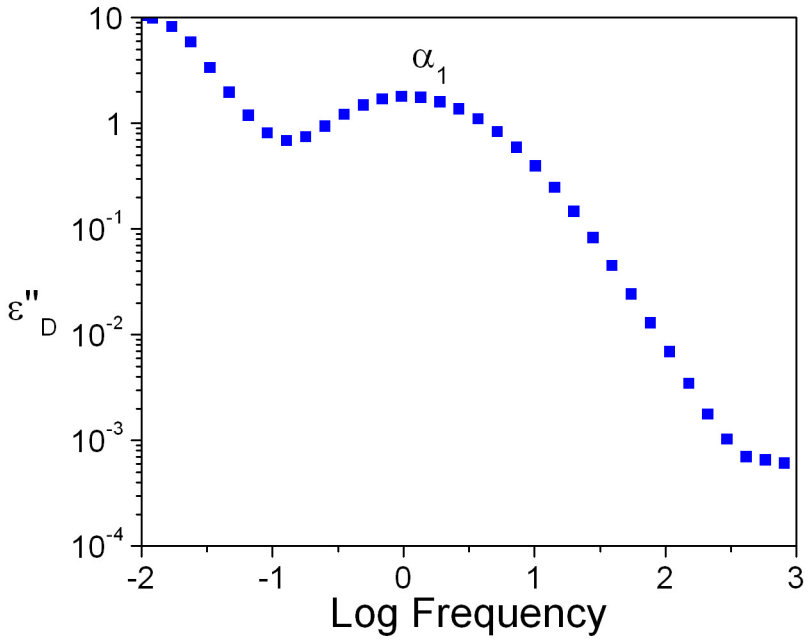

Fig. 7.6: ε''_D for F3CH$_3$ at 114°C (T$_i$+42°C).

7.4 Summary

The dynamics of three main chain liquid crystalline polymers were investigated over a broad frequency and temperature range. Two local processes are observed in the glassy state, γ and β. These relaxations correspond to motions of the spacer segments and the phenyl rings, respectively. A small relaxation at temperatures above the α process arises from Maxwell-Wagner-Sillars interfacial polarization, which disappears as each LCP approaches its isotropic temperature. This process, as well as the α_1 relaxation, were obscured by dc conductivity and were only visible in derivative spectra. At temperatures above the isotropic temperature, a relaxation related to reorientation of the mesogens due to increased degrees of rotational freedom is present.

Chapter 8

Conclusions and Suggestions for Future Work

8.1 Conclusions

The dynamics of hydrogen bonded polymer blends which preferentially form strong intermolecular associations were investigated. Self associations within the HFS functionality are minimized, due to the steric shielding provided by the two CF_3 groups. This minimization of self associations allows for systems where the effects of these associations can largely be ignored. Broadband dielectric relaxation spectroscopy is a powerful tool for the investigation of blend dynamics, and Fourier transform infrared spectroscopy is able to provide quantitative information on the types and strengths of hydrogen bonding present in these blends.

Blends of P2VPy exhibit very strong hydrogen bonding, evidenced by the large wavenumber difference between the free OH and the intermolecular association OH bands. HFS homopolymer blends of PVME exhibit somewhat weaker hydrogen bonds than do P2VPy blends, the wavenumber difference being several hundred wavenumbers less. Finally, blends involving the vinyl acetate functionality exhibit the weakest hydrogen bonds, but the presence of the carbonyl bands allows for quantification of the hydrogen bonding behavior.

In blends where the association constants can be determined spectroscopically, a wealth of information becomes available. The fractions of free as well as hydrogen bonded segments as a function of composition can be predicted. This information can then be used to help quantify the glassy state relaxation behavior of the blends. In the EVA copolymer blends examined in Chapter 5, or similar blends where local relaxations are not suppressed, this method can be applied. Additionally, in blends where local relaxations are suppressed due to the formation of stronger hydrogen bonds, the fraction of hydrogen bonded segments can be quantified, as well as the remaining free units at a

particular blend composition. This methodology may even prove useful in determining not only the number density of dipoles, but may be useful in approximating the dipole magnitude (see equation 2.11 on page 21).

Local relaxations in PVME blends with the HFS homopolymer are strongly suppressed due to the formation of intermolecular associations, but the remaining free PVME segments exhibit a glassy state relaxation whose temperature dependence does not differ from that of bulk PVME. In contrast, PVME blends with the HFS:DMB copolymer do not exhibit any suppression of the PVME local relaxation, reminiscent of blends of polystyrene with PVME, due to the relatively small number of interacting sites in the copolymer. Blends of P2VPy with the HFS homopolymer do not exhibit strong suppression of local relaxations, which appears at odds with the strength of the hydrogen bonding in these blends. This reduced suppression of the local relaxations in these blends can be attributed to reduced functional group accessability, which is supported by the FTIR results. The local relaxation of HFS is present in blends only when it is the majority component, with the exception of the EVA blends described above, and the P2VPy blends, where reduced functional group accessability negatively affects its ability to form intermolecular associations.

At every composition, and in every blend, a single calorimetric T_g is observed. In HFS:DMB copolymer blends, where the number of interacting sites (HFS units) is relatively small (2 and 5 mole %), two dynamic T_g's are observed. The presence of a single T_g is quite remarkable, however, since only 2 mole % of HFS segments copolymerized with dimethylbutadiene renders an otherwise immiscible blend miscible. In all blends with the HFS homopolymer, a single segmental relaxation is observed, even in blends where the difference in T_g between the components is 150 °C. In blends of P2VPy with PolyHFS, the segmental relaxation of intermediate blend compositions occurs at temperatures above the neat components, in agreement with findings from DSC, and is a result of the very strong hydrogen bonds formed in these systems.

The results of this dissertation suggest the fragility in intermolecularly hydrogen bonded polymer blends is correlated to the fraction of intermolecularly associated segments, and not the T_g or even the hydrogen bonding strength. In fact, the results suggest

that fragility is *inversely* proportional to hydrogen bond strength, since the EVA blends have the highest fragilities and the lowest hydrogen bonding strengths. This cannot be stated definitively, however, since the overriding factor here is likely the functional group accessability and hydrogen bonding strength has little to do with the fragility. What is important, however, is the ability of the functional groups to mix on the molecular level. A system with a greater degree of intermolecular coupling possesses more of what can be thought of as temporary crosslinks. The fragility is related to the configurational entropy and the number of units in a cooperatively rearranging region (CRR). As the fraction of intermolecularly hydrogen bonded segments increases, the configurational entropy decreases and the number of units in the CRR at T_g increases. Since the number and strength of hydrogen bonds dictates T_g in the blends, as the T_g is approached, sufficient thermal energy has been added to the system to break hydrogen bonds and the chains begin to reptate. As the intermolecular associations break, the configurational entropy increases, and the CRR size increases.

Hydrogen bonds break and reform rapidly compared to the timescales investigated here, so even when hydrogen bonds break for chain reptation to occur, they reform rapidly. In order for the chains to undergo tube disengagement, this bond breaking/chain reptation with bond reformation cycle continues until the chains relax and disengage from the tube. This hydrogen bond breaking and chain reptation can be observed via DRS as a relaxation separate from the segmental relaxation. The strength of this process (equation 2.11) depends on not only the number of intermolecular associations, but also the strength of the bond. As the number of intermolecular hydrogen bonds increases, this process increases in magnitude relative to the segmental relaxation, and the relaxation time difference between this process and the segmental relaxation decreases. As the strength of the hydrogen bond increases, the magnitude of this relaxation relative to the segmental relaxation increases, as shown in Chapter 4 for blends of P2VPy and PVME with PolyHFS.

Although not a polymer blend, the dynamics of novel main chain liquid crystalline polymers were investigated. These MCLCPs can be thought of as a mixture of rigid mesogens covalently bound to soft segment spacers. The soft segment spacers, oligomeric

poly(dimethyl siloxane) (PDMS), exhibit a glassy state relaxation near that of polymeric PDMS, but modified by the presence of hard segments. The soft segment spacers allow the hard segments to form some two-dimensional ordering (smectic C_A), since the soft and hard segments are immiscible, and gives rise to an interfacial polarization (MWS) relaxation. Above a given temperature, the ordering is lost, the system mixes, and the interfacial polarization relaxation disappears. As with the hydrogen bonded blends, these MCLCPs exhibit an additional relaxation at temperatures above the segmental relaxation, which is related to rotations of the hard segments in the isotropic state, and is believed to be an inherent feature of such systems.

8.2 Suggestions for Future Work

8.2.1 Synthesis

As noted by Coleman, Graf and Painter, an attractive method for quantifying the free OH band in polymers containing this functionality is to create random copolymers of the chosen monomer with an 'inert', i.e. non-hydrogen bonding, monomer[1]. As the number of OH-containing monomers is reduced, the free OH band will increase in magnitude relative to the intramolecular associations. One of the many difficulties in synthesizing copolymers, however, is making a copolymer which is truly random[3]. Finding two monomers whose reactivity ratios satisfy the condition for a random copolymer is nearly impossible. An additional consideration is the composition of a copolymer changes over the course of the polymerization, and the polymerization must be terminated at low conversion to avoid compositional drift. An attractive alternative is randomly functionalizing a homopolymer. As outlined in Appendix A, a truly random copolymer of HFS with its redox product can be synthesized by a procedure adapted from the literature[200]. This synthetic route is a means by which random copolymers can be synthesized from homopolymers which are readily synthesized (see page 53 of Chapter 3). The advantages are not only its simplicity, but the structure of the resulting copolymer does not significantly differ from the initial homopolymer. This provides a system

where changes in functional group accessability (the size/bulkiness of the copolymer) can be ignored.

8.2.2 Functional Group Accessability

As noted in Chapter 4, functional group accessability, or how readily two functional groups form an intermolecular association, plays an important role in the overall blend dynamics. An interesting comparison to the P2VPy blends in examined in Chapter 4 would be blends of PolyHFS with poly(4-vinyl pyridine) (P4VPy). Located at the para position of the ring, P4VPy should more readily form hydrogen bonds with PolyHFS than P2VPy, which has its nitrogen at the ortho position of the ring.

Similarly, blends of PolyHFS with different poly(alkyl acrylates) would provide a series of systems where the steric hinderance can be systematically increased. As the size of the alkyl group increases, the functional group accessability should systematically decrease. Additionally, the carbonyl functionality of these polymers allow for quantitative analysis of the numbers and strength of the hydrogen bonding, similar to what was done in Chapter 5. Although poly(alkyl *meth*acrylates) appear to be similar to poly(alkyl acrylates), methacrylates would be challenging systems, since the dielectric behavior of these polymers is difficult to evaluate[74,201,202].

Quantifying the hydrogen bonding in polymer blends via FTIR measurements is particularly useful, and if the enthalpies of hydrogen bonding can be determined, much greater insight into the dynamics of these blends can be obtained. If the fractions of hydrogen bonded and free segments can be calculated, systematic studies on polymers of varying functionality can be performed (poly(ethylene oxide), poly(methyl methacrylate), etc.). This may provide further insight into what structural/chemical factors are responsible for changes in fragility, and may prove useful in furthering understanding of the glass transition.

8.2.3 Equilibrium Constants From Dielectric Measurements

A useful future study would be the prediction of the fraction of free and hydrogen bonded segments from the dielectric data. A system such as the EVA blends, where local

relaxations are not suppressed would be a good candidate. Similar to the methodology outlined in Chapter 5, the local relaxations could be modeled with a sum of two HN functions, one for the free HFS segments, and one for the hydrogen bonded HFS segments. The HN shape parameters should be kept constant, as well as the relaxation time of the two processes. These parameters would be determined in the same way as in Chapter 5, fitting each blend composition iteratively, and fitting the neat HFS homopolymer, to determine the HN shape parameters. The only adjustable parameter from the two HN fit would be the ratio of the dielectric strengths ($\Delta\varepsilon$). The resulting ratio of dielectric strengths could be used to determine the fraction of hydrogen bonded HFS segments, and from this, the fraction of free carbonyl groups. This information can be used to determine the equilibrium constant K_A as a function of temperature, and perhaps calculate the enthalpy of the hydrogen bonds. This method has the advantage of being able to investigate an extremely broad temperature range, making the determination of the enthalpy of hydrogen bonding possible over a broader temperature range. This method should first be compared to previous studies where the enthalpies of hydrogen bonding have been determined from FTIR measurements, to ensure its validity.

Appendix A

Synthesis of a Novel HFS Copolymer

This appendix outlines the experimental procedure used in a small-scale random functionalization of the HFS homopolymer to create a truly random copolymer. This procedure is an attractive alternative to the copolymer synthesis outlined in the Experimental section (see page 51 of Chapter 3). The copolymer (see Figure A.1 for structure) composition is controlled by the amounts of reactants, and is not so strongly dependent on reaction time.

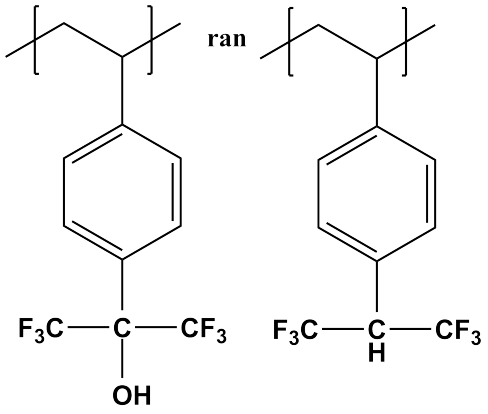

Fig. A.1: Chemical structure of the copolymer of HFS and its redox product.

Nimmagadda and McRae recently described a synthetic route by which, among other functionalities, tertiary alcohols can be converted from an OH functionality to a proton[200]. The generalized reaction mechanism is shown in Figure A.2.

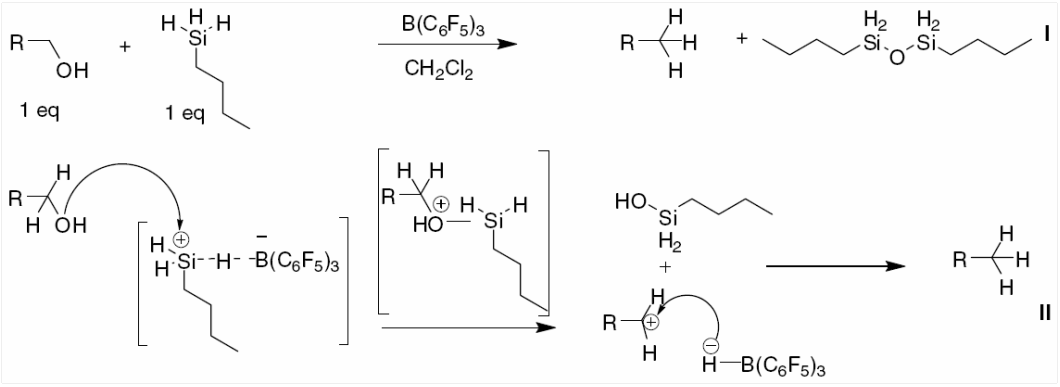

Fig. A.2: Synthetic route by which alcohols are converted to alkanes. Figure taken from reference 200.

This procedure, if carried out on a homopolymer, has the advantage of producing a truly random copolymer, where the chemical structure of the two monomers differs only by the presence (or not) of the OH functionality (see Figure A.1). Following the general reaction scheme shown in Figure A.2, a 52:48 copolymer of HFS with its reduct was synthesized, according to the reactant amounts.

To a flame-dried, nitrogen purged, 25 mL round bottom flask, a stirring bar, 1 gram ($3.7 * 10^{-3}$ mole) of the HFS homopolymer, and 10 mL of dichloromethane were added and heated to 35 °C in an oil bath. 0.133 grams ($2.6 * 10^{-4}$ mole) of the $B(C_6F_5)_3$ catalyst was quickly added to the flask. This step should be performed under moisture-free conditions, since the catalyst is hydroscopic. The solution was returned to the oil bath maintained at 35 °C and stirred for ten minutes. After ten minutes, 0.1563 grams of n-butylsilane was slowly injected into the reaction to prevent excessive foaming. After 5 hours, 1 mL of triethylamine was injected to terminate the reaction.

The reaction product was dumped into silica gel, and the dichloromethane was allowed to evaporate. The gel/copolymer mixture was then washed with hexanes and filtered with a funnel filter fitted with a 1 μm paper filter to remove the silane. The

product was then washed with acetone, collected, and the acetone was allowed to evaporate. The product was then dissolved in a 90% toluene, 10% tetrahydrofuran mixture, and passed through a 0.2 μm Teflon syringe filter and dried again.

Although not performed here, ^{13}C-NMR should easily distinguish between the HFS monomer and its reduced counterpart. Specifically, the carbon on the functional group at the para position of the phenyl ring of HFS should have an ^{13}C-NMR shift of approximately 101 ppm, while the reduced monomer should have a shift of approximately 59 ppm, according to predictions from ChemDraw software.

Suggestions that this procedure has, in fact, succeeded in producing a random copolymer of the HFS monomer and its reduced counterpart are found in the DSC and FTIR results. The T_g of the neat HFS homopolymer is 125 °C. The T_g of the reaction product is 90 °C. It is clear that intramolecular hydrogen bonding increases the T_g of a polymer. For example, PVPh as a T_g of approximately 175 °C, 75 °C higher than polystyrene, and the only difference is the OH functional group at the para position of the phenyl ring which (strongly) self-associates. A reduction in T_g has been observed in copolymers of styrene with hydroxy styrene[154], so a similar decrease in T_g would be expected here. Shown in Figure A.3 is the OH stretching region from FTIR for the random copolymer and the starting material (HFS homopolymer).

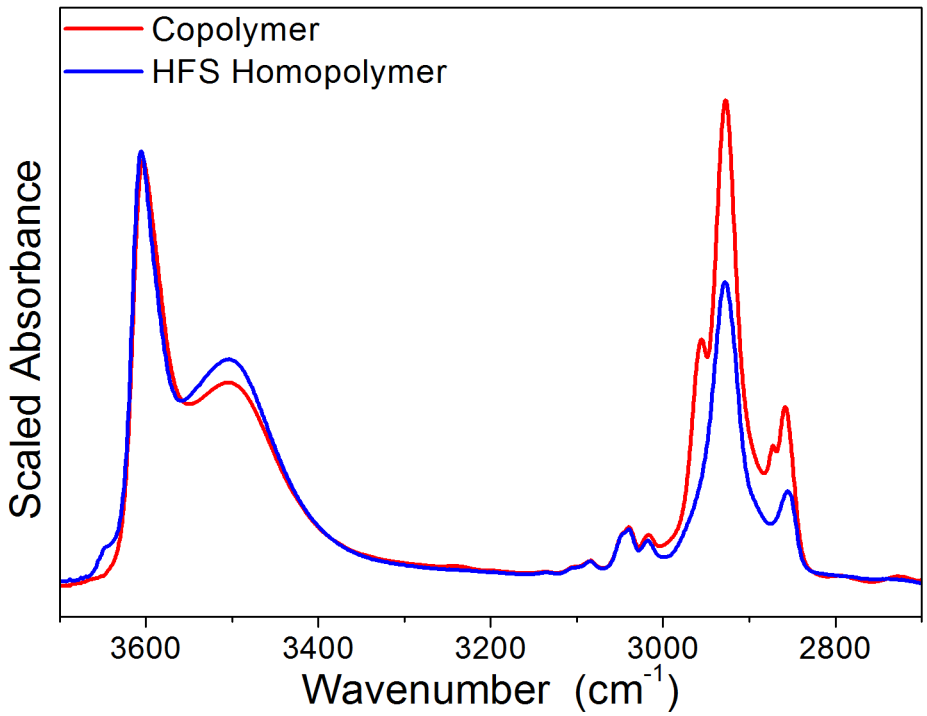

Fig. A.3: FTIR OH stretching region for the random copolymer of HFS and its reduced counterpart. The HFS homopolymer is shown in blue, and the copolymer is shown in red.

A few features of the OH stretching region are worth noting. First, the self association band(s), centered around 3500 cm^{-1} are of lower intensity in the copolymer than in the homopolymer, suggesting fewer self associations relative to free functional groups are present, as seen in the literature for similarly copolymerized systems[48,154,171,203]. Second, the total area under the aliphatic/aromatic CH stretching region (3000-2800 cm^{-1}) compared to the OH region (3650-3300 cm^{-1}) is greater for the copolymer than the HFS homopolymer, suggesting fewer OH groups exist in the copolymer compared to the HFS homopolymer. Finally, an additional band appears in the copolymer at approximately 2950 cm^{-1}, possibly from the C-H stretch from the converted alcohol.

Appendix B

Origin C Import Code for Processing Dielectric Data

The following Appendices list the Origin C code used in the processing of dielectric data. The code can be copied and pasted into Origin's code builder workspace as-is. Many thanks are owed to Dr. Daniel Fragiadakis for his assistance in providing the starting point for these programs.

A typical dielectric measurement produces a vast quantity of data: 20-50 temperatures, each with ~ 60 datapoints. The dielectric software can export a number of variables calculated from the measured impedance, but not the derivative of the dielectric constant. Additionally, the software exports a single text file with all of the results data, or a single text file for each temperature. In an effort to reduce the amount of time spent on simple, repetitive data processing, this program was developed.

The program assumes the user's result file contains the following columns: Frequency, Temperature, Dielectric Constant, Dielectric Loss. All temperatures should be in a single text file. Extra columns will be ignored. From the above-listed values, the program will produce a single Origin workbook for each temperature with the following column structure:

1. Log_{10} Frequency
2. Dielectric Constant (ε')
3. Dielectric Loss (ε'')
4. Derivative Dielectric Loss (ε''_D) [see equation 2.34]
5. tan δ ($\frac{\varepsilon''}{\varepsilon'}$)
6. Real Conductivity (σ')
7. Imaginary Conductivity (σ'')

8. Storage Modulus (M')
9. Loss Modulus (M'')
10. $\frac{\partial \ln \varepsilon''}{\partial \ln f}$
11. Import Comments including the dc conductivity (if present)

The program will rename each workbook to reflect the temperature of the dataset within the workbook, in both Kelvin and Celsius. The code is in its unaltered state, and compiles without errors in Origin 8.0 Pro, service release two, but will not work in previous versions of Origin.

The derivative dielectric loss (ε''_D) utilizes a 5-point moving window, Savitzky-Golay smoothing derivative. Due to the difficulty in determining coefficients for the first and last two points of the array, the first and last two frequencies should be treated with caution.

The program will also determine the dc conductivity at each temperature if frequency-independent conductivity exists at that temperature. It does this by performing a first order derivative on the real part of the complex conductivity and finding the dataset minimum. If the conductivity is truly dc at that temperature, the derivative will be zero over some frequency range at that temperature. In reality, the dc conductivity is never truly constant, so the minimum is used. Since every dataset will contain a minimum, an additional condition is tested: the magnitude of the difference between the conductivity at the minimum and the conductivity at the previous (high frequency) datapoint must be less than a somewhat arbitrarily-chosen value. If the difference is less than a critical value, the conductivity is assumed to be frequency-independent. The value of dc conductivity is then recorded in the last column of the workbook. In addition, a workbook is created which contains all temperatures in the imported file, and if it exists, the dc conductivity at each temperature. Shown in Figure B.1 is a screen shot of an example workbook imported using this program.

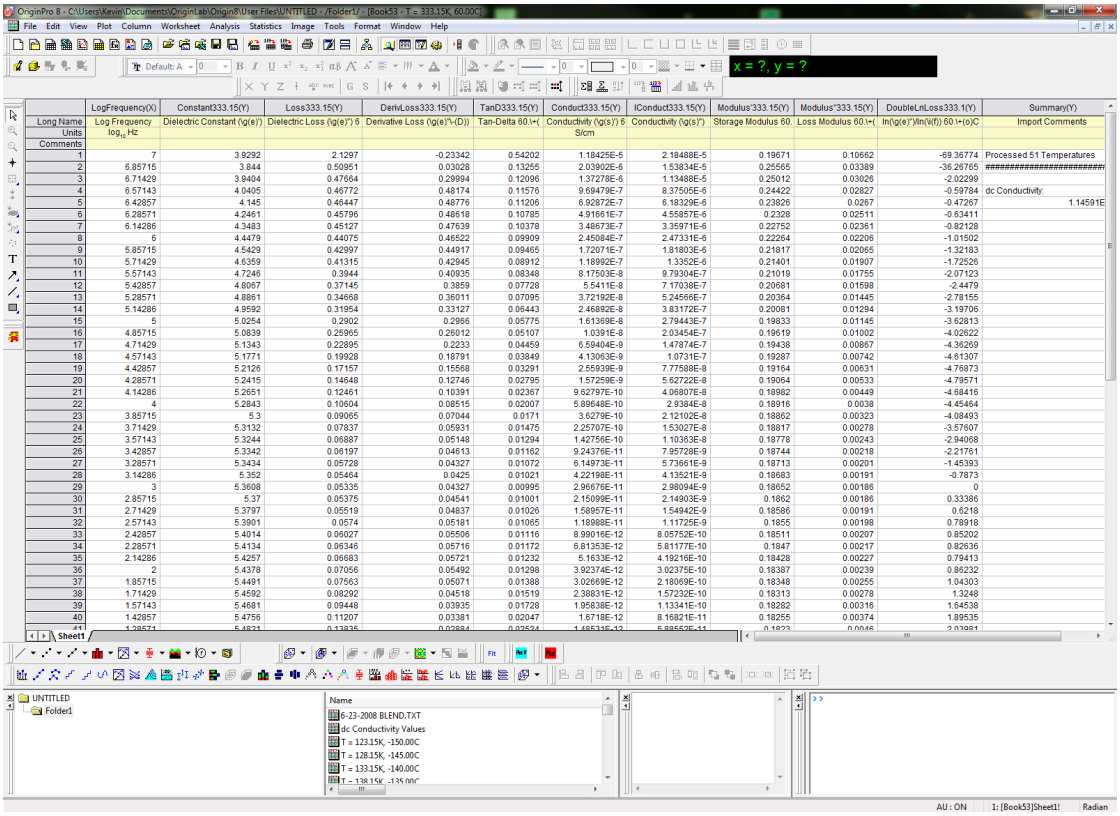

Fig. B.1: Screenshot of the import program.

```
/*-------------------------------------------------------------------------*
 * File Name:NewImportRoutine.c V2 *
 * Creation: 7-4-2008 *
 * Purpose: OriginC Source C file *
 * Copyright (c) ABCD Corp. 2003, 2004, 2005, 2006, 2007, 2008, 2009, 2010 *
 * All Rights Reserved *
 *  *
 * Modification Log: *
 * 4-01-2010: Changed temperature check routine to exit properly if user *
 *  clicks cancel. *
 *  5-10-2010: Added routine to calculate dc conductivity automatically. *
 *-------------------------------------------------------------------------*/

////////////////////////////////////////////////////////////////////////////
// Including the system header file Origin.h should be sufficient for most Origin
// applications and is recommended. Origin.h includes many of the most common system
// header files and is automatically pre-compiled when Origin runs the first time.
// Programs including Origin.h subsequently compile much more quickly as long as
// the size and number of other included header files is minimized. All NAG header
// files are now included in Origin.h and no longer need be separately included.
//
// Right-click on the line below and select 'Open "Origin.h"' to open the Origin.h
// system header file.
#include <Origin.h>
#include <stdio.h>
#include <data.h>
#include <math.h>
#include <utilities.h>
#include <complex.h>
#include <wksheet.h>
#include <OC_nag8.h>
#include <ocmath.h>
#include <Range.h>
#include <XFbase.h>
#include <time.h>
#include <GetNbox.h>
#include <mswin.h>
#include <string.h>
////////////////////////////////////////////////////////////////////////////
void dataimport()//Type 'dataimport' (without quotes) to run the program.
{
// int iStatus;
ASCIMP ascimp;
string strFile = GetOpenBox("*.txt", NULL,"I love grad school","KILL ALL HUMANS!!!");
string fileName = GetFileName(strFile);
Worksheet wks;

//////////////Setup for conductivity worksheet//////////////////
Worksheet wksCond;
wksCond.Create("origin.otw");
WorksheetPage wksCondPage;
```

```
wksCondPage = Project.Pages();
wksCondPage.SetLongName("dc Conductivity Values");
LT_execute("wks.ncols = 4");
wksCond.SetName("Cond");
wksCond.Columns(0).SetName("Temp");
wksCond.Columns(0).SetLongName("Temperature");
wksCond.Columns(0).SetUnits("\+(o)C");
wksCond.Columns(1).SetName("dcCond");
wksCond.Columns(1).SetLongName("dc Conductivity");
wksCond.Columns(1).SetUnits("S/cm");
wksCond.Columns(2).SetName("InvTemp");
wksCond.Columns(2).SetLongName("1000/T");
wksCond.Columns(2).SetUnits("K\+(-1)");
wksCond.Columns(3).SetName("LogCond");
wksCond.Columns(3).SetLongName("Log\-(10) Conductivity");
wksCond.Columns(3).SetUnits("S/cm");
wksCond.Columns(0).SetWidth(8);
wksCond.Columns(1).SetWidth(9);
wksCond.Columns(2).SetWidth(8);
wksCond.Columns(3).SetWidth(13);
wksCond.SetColDesignations("XYXY");
//////////////End Setup for Conductivity Worksheet////////////////

if(AscImpReadFileStruct(strFile,&ascimp) == 0)
{
ascimp.iRenameCols = 0;
wks.Create("test1.otw");
wks.ImportASCII(strFile, ascimp);
WorksheetPage wksPage;//Declare a worksheet page so we can set the
        //long name.
wksPage = Project.Pages();
wksPage.SetLongName(fileName);//Set the long name of the master worksheet
        // to the filename.

Dataset dS0 (wks,0);
Dataset dS1 (wks,1);
Dataset dS2 (wks,2);
Dataset dS3 (wks,3);

//////////////////////////Begin the GetNBox Temperature Check////////////////
GETN_BOX( treeTest )
GETN_CHECK(tempCheck, "Temperatures in Kelvin?",1)
if(GetNBox(treeTest, "Temperature Check"))
{
if( treeTest.tempCheck.nVal == 0 )//If they don't have their temperatures
            //in Kelvin:
{
dS1 += 273.15;//Convert degrees C to K
printf("Thats OK\nI'll do it for you...\n");
}
}
```

```
else
{
printf("Quitter!");
wks.Destroy();
wksCond.Destroy();
return;
}
//////////////////////End the GetNBox Temperature Check////////////////////


int datasetSize=dS0.GetSize();//Get the value of the size of the dataset.
short numTemps = numTemps(1);//Call the program to get the number of temperatures,
        // passing the temperature column to the program.;

double refval = dS1[0];//Declare the reference temperature.  This will change
        // for each temperature.

for (int z = 0; z<numTemps; z++)//For all of the temperatures in the file.
{
Worksheet wksT;
wksT.Create("Origin.otw");//, CREATE_HIDDEN
LT_execute("wks.nCols = 3");

int indexer = 0;//Declare the indexer which will designate the row number
            // for copying matches from the master file to the individual files.
int refindexer = 0;//Declare another indexer to change the reference value
            // (temperature) for each temperature in the file.
double tcrefval = round(refval - 273.15,2);//Declare a double to contain the
            //temperature of the dataset in degrees C.
string strName;//Declare a string to hold the name of the worksheet.
strName.Format("T = %.2fK, %.2fC",refval, tcrefval);//Format the string.

Page pg = Project.Pages();
pg.SetLongName(strName);//Set the long name to the string defined above.

for (int q = 0; q<datasetSize; q++)//Begin looking for temperatures matching
            //the reference temperature.
{
if (dS1[q] == refval)
{
wksT.SetCell(indexer, 0, dS0[q]);
wksT.SetCell(indexer, 1, dS2[q]);
wksT.SetCell(indexer, 2, dS3[q]);
indexer++;
refindexer = q;
}
}
//printf("q is :%d\n",q);//Diagnostic lines
//printf("refval is %f\n",refval);

double nameVal = refval;//Declare a double to hold the value of refval
```

```
            //before we change it.  This was done so the column names don't get
            //indexed to the next temperature before they are created.

if(refindexer<datasetSize-2)//This if statement added because when q is equal
            //to the size of the dataset, we can't declare a value for refval
            //which doesn't exist!
{
refval = dS1[refindexer+1];///Change the reference value for the next temperature.
}

Dataset d0 (wksT,0);//Declare some datasets for the raw data.  This is d-ZERO!
Dataset d1 (wksT,1);
Dataset d2 (wksT,2);
int Size = d0.GetSize();

d0 = log10(d0);//Set d-Zero(!) to the base ten log of d0.

////////////////Add some housekeeping to the first three columns//////////////
wksT.Columns(0).SetName("Log Frequency");
wksT.Columns(0).SetLongName("Log Frequency");
wksT.Columns(0).SetUnits("log\-(10) Hz");

wksT.Columns(1).SetName("Constant"+nameVal);
wksT.Columns(1).SetLongName("Dielectric Constant (\g(e)') "+tcrefval+"\+(o)C");

wksT.Columns(2).SetName("Loss"+nameVal);
wksT.Columns(2).SetLongName("Dielectric Loss (\g(e)'') "+tcrefval+"\+(o)C");
////////////////End housekeeping section for the first three columns////////

////////Now we need to add columns on which the derivative can operate
wksT.AddCol("Deriv Loss"+nameVal);//Natural log of frequency
wksT.Columns(3).SetName("Deriv Loss"+nameVal);//The AddCol command doesn't
            //support putting a period in the name.
wksT.Columns(3).SetLongName("Derivative Loss (\g(e)''\-(D)) "+tcrefval+"\+(o)C");

//////////////////////////////////Begin Derivative////////////////////////////////////
////////////////////////////////////////////////////////////////////////////////////
Dataset derLoss (wksT,3);//Declare a dataset for the derivative loss.

vector vy(d1,TRUE);
vector vOut;
vOut.SetSize(Size);

//////////Section for setting up SG values////////////
double HighF = d0[0];
double HighF1 = d0[1];
double fDiff = HighF-HighF1;
double SGval = log(pow(10.0,fDiff));
//////////Section for setting up SG values////////////

ocmath_savitsky_golay(vy, vOut, Size, 2, 2, 2, 1);//Do the derivative
```

```
derLoss = vOut;
derLoss *= ((PI/2.0)/SGval);//Set the result of the derivative.
////////////////////////////////End Derivative////////////////////////////////////
//////////////////////////////////////////////////////////////////////////////////

wksT.AddCol("TanD"+nameVal);
wksT.Columns(4).SetName("TanD"+nameVal);
wksT.Columns(4).SetLongName("Tan-Delta "+tcrefval+"\+(o)C");
Dataset tanDelta (wksT, 4);
tanDelta.SetSize(Size);
tanDelta = d2/d1;

wksT.AddCol("Conduct"+nameVal);
wksT.Columns(5).SetName("Conduct"+nameVal);
wksT.Columns(5).SetLongName("Conductivity (\g(s)') "+tcrefval+"\+(o)C");
wksT.Columns(5).SetUnits("S/cm");//This is why epsilon_o is e-14.....
            //need to convert from meters to centimeters
Dataset conduct (wksT, 5);
conduct.SetSize(Size);
conduct = 2.0*PI*pow(10.0,d0)*8.85e-14*d2;//Take 10^Frequency because the
            //column is now log10 frequency

wksT.AddCol("IConduct"+nameVal);
wksT.Columns(6).SetName("IConduct"+nameVal);
wksT.Columns(6).SetLongName("Conductivity (\g(s)'') "+tcrefval+"\+(o)C");
Dataset iConduct (wksT,6);
iConduct.SetSize(Size);
iConduct = 2.0*PI*pow(10.0,d0)*8.85e-14*d1;//Take 10^Frequency because the
            \\column is now log10 frequency

wksT.AddCol("Modulus'"+nameVal);
wksT.Columns(7).SetName("Modulus'"+nameVal);
wksT.Columns(7).SetLongName("Storage Modulus "+tcrefval+"\+(o)C");
Dataset storMod (wksT,7);
storMod.SetSize(Size);
storMod = d1/(pow(d1,2.0) + pow(d2,2.0));

wksT.AddCol("Modulus''"+nameVal);
wksT.Columns(8).SetName("Modulus''"+nameVal);
wksT.Columns(8).SetLongName("Loss Modulus "+tcrefval+"\+(o)C");
Dataset lossMod (wksT,8);
lossMod.SetSize(Size);
lossMod = d2/(pow(d1,2.0)+pow(d2,2.0));

wksT.AddCol("DLnLoss" + nameVal);
wksT.Columns(9).SetName("DoubleLnLoss"+nameVal);
wksT.Columns(9).SetLongName("ln(\g(e)'')/ln(\i(f)) "+tcrefval+"\+(o)C");
Dataset dLnLoss (wksT,9);
dLnLoss.SetSize(Size);
vector vLoss;
vLoss = log(d2);
```

```
vector vLnFreq;
vLnFreq = log(d0);
ocmath_derivative(vLnFreq,vLoss,Size,DERV_PEAK_AS_ZERO);
dLnLoss = -vLoss;

wksT.AddCol("Summary");
wksT.Columns(10).SetLongName("Import Comments");
string comStr1;
string comStr2;
comStr1.Format("Processed %d Temperatures", numTemps);
comStr2.Format("From File: %s", strFile);
wksT.SetCell(0,10,comStr1);
wksT.SetCell(1,10,comStr2);

/////*  Section for finding the conductivity */////
vector vX (d0);
vector vCond (conduct);
vCond = log10(vCond);//Take the base 10 log of the conductivity
vector vDerivCond;//Output
vDerivCond.SetSize(Size);
vDerivCond = vCond;

double vMin, vMax;//Both of these are unnessary for me,
            //but GetMinMax needs them.
uint vIMin, vIMax;//Need to get both the min and max, although
            //only minimum is important

ocmath_derivative(vX,vDerivCond,Size);//Do the derivative,
            //set vDerivCond as output

vDerivCond.GetMinMax(vMin,vMax, &vIMin, &vIMax);//Find the Derivative
            //Minimum, Maximum, and Indicies.

//printf("Min:%d\n",vIMin);
//printf("Max:%d\n",vIMax);
try//Not every dataset will have dc conductivity,
               //so need to deal with this.
{
double condAtMin = vCond[vIMin];//Value of conductivity at minimum
double condComparison = vCond[vIMin - 1];//We will compare this value
                //to the minimum

double difference = abs(condAtMin - condComparison);//Find the difference
                //between the value and the preceeding value.
wksCond.SetCell(z,0,tcrefval);
wksCond.SetCell(z,2,(1000/(273.15+tcrefval)));
if(difference < 0.01)//If the slope didn't change within some
                                    //ARBITRARY limit (0.01)
{
wksT.SetCell(3,10,"dc Conductivity:");//Set a cell for a label
wksT.SetCell(4,10,10^condAtMin);//Set the cell with the value.
```

```
wksCond.SetCell(z,1,10^condAtMin);
wksCond.SetCell(z,3,condAtMin);
}

}
catch (int nErr)//I don't care about the error, as long as it continues.
{
//printf("Nothing here\n...Move along.");
}
///////* End Section for finding conductivity *///////

//////////////////////////////////////Time to make stuff pretty/////////////
wksT.Columns(0).SetWidth(12);
wksT.Columns(1).SetWidth(15);
wksT.Columns(2).SetWidth(14);
wksT.Columns(3).SetWidth(16);
wksT.Columns(4).SetWidth(10);
wksT.Columns(5).SetWidth(12);
wksT.Columns(6).SetWidth(12);
wksT.Columns(7).SetWidth(12);
wksT.Columns(8).SetWidth(12);
wksT.Columns(9).SetWidth(15);
wksT.Columns(10).SetWidth(20);
}



}
else
{
printf("Call Kevin.\nSomething bad has happened.\nOr, you clicked cancel.\n");
}
}


//////////////Start the program to get the number of temperatures///////////////
short numTemps(int col)//This program is called by the master program.
{
Worksheet wks = Project.ActiveLayer();
Dataset ds1 (wks,col);
int Size = ds1.GetSize();

int numTemps = 1;

for (int n=1; n<Size;n++)
{
if( ds1[n] != ds1[n-1] )
{
numTemps++;
}
}
```

```
printf("Processing %d temperatures...\n", numTemps);
return numTemps;
}
//////////////End the program to get the number of temperatures////////////////
```

Appendix C

Origin C Code for Isochronal Data Analysis

This appendix contains the Origin C code for the Isochronal program. This program looks at dielectric data as a function of temperature at a constant frequency. This has been shown to very accurately determine the temperature dependence of the segmental relaxation time. It may work for local relaxations, but as always, the data needs to be carefully examined to ensure its validity.

This program contains several options. Typing 'isochronal' into the command window of Origin 8 (without the quotes) will start the program. The user will be prompted to select a result file for analysis. Note that tan δ and the loss modulus do not need to be exported. They will be calculated by the program if needed. The result file should be a single text file exported from WinDETA which has the following file structure: Frequency, Temperature, Dielectric Constant, Dielectric Loss. All temperatures should be exported in a single file, and no duplicate temperatures should exist, and the same frequencies should exist for each temperature.

After selecting the file, a dialog will appear and prompt the user to select from one of several options as shown in Figure C.1. The program will evaluate any of the following: raw dielectric loss, derivative dielectric loss, tan δ, loss modulus. Additionally, a help file can be opened from this dialog. This dialog also contains a checkbox to determine if your temperatures, exported from WinDETA, are in Kelvin or Celsius. The program will convert to Kelvin if the user's temperatures are in Celsius, but the user is required to indicate this by unchecking the box.

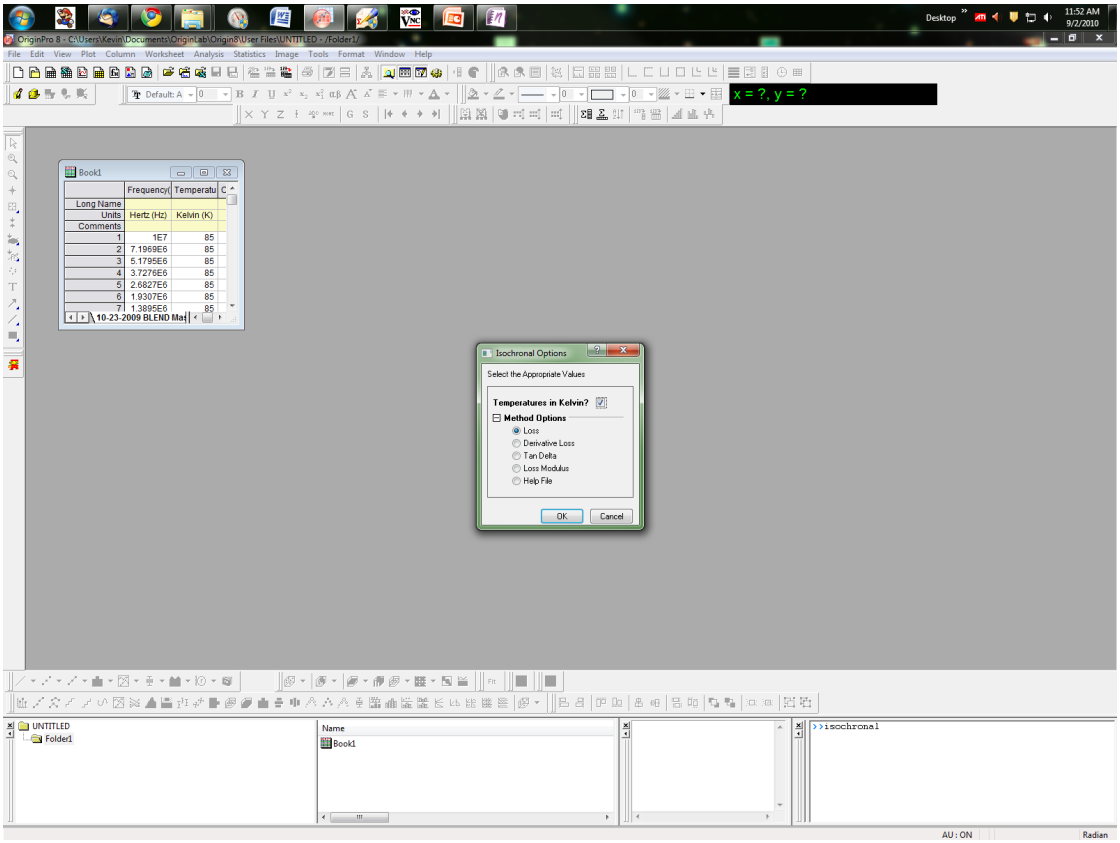

Fig. C.1: Screenshot of the isochronal program.

Once the method is selected the program will start. The program creates a single workbook for each frequency, and renames that workbook in accordance with the frequency. For each frequency, the program will scan the result file and add all data associated with a particular frequency into that workbook.

For each frequency (workbook) the following procedure is performed: The program performs a trace interpolation, making the dataset 500 points in size. A first derivative of this interpolated data is then performed, and the locations of the peaks (the zero's from the derivative) are stored. The workbook now contains the following columns: raw temperature, raw loss (or raw derivative loss, raw tan δ, raw loss modulus), interpolated temperature, interpolated loss, the dataset (array) index of the maxima, the x-value (temperature) of the maxima, the y-value of the maxima. Note that the derivative method produces an additional column, raw derivative, and the workbook will have a slightly different file structure. The program stores the first four maxima found (for each frequency) in a separate workbook. After performing the calculations,

the program then creates a plot of the interpolated data, and also puts the peak maxima determined from the derivative on the plot as green points. This was added to provide a quick visual check of the peak positions.

This procedure is repeated for every frequency in the file, until the last frequency is reached. The program then takes the workbook containing the maxima, and organizes it so it can be plotted in an Arrhenius fashion. Finally the program creates an Arrhenius plot and adds the data from the workbook containing the maxima to this plot.

This program will likely find many maxima at each frequency. It is up to the user, and of critical importance to the validity of this method, that the results be checked thoroughly for errors. Concerns have been raised since interpolated data are used in the determination of peak locations. This program has been applied to a multitude of samples, and in *every* case, it provides relaxation times identical to evaluating the raw data.

This method, as outlined in Chapter 2, is an excellent way to determine the relaxation times of the segmental process. If the temperature range is sufficiently below and above the temperatures where the relaxation is within the frequency window, 60 datapoints for the Arrhenius plot describing the relaxation time of the segmental process is common. To increase the accuracy of this program, the temperature interval should be as small as possible. A five degree or smaller temperature interval is ideal.

```
/*-------------------------------------------------------------------------*
 * File Name: Frequency.c   *
 * Creation:  5-10-2007 *
 * Purpose: OriginC Source C file *
 * Copyright (c) ABCD       2007, 2008, 2009, 2010 *
 * All Rights Reserved *
 *  *
 * Modification Log:                          *
 *-------------------------------------------------------------------------*/

////////////////////////////////////////////////////////////////////////////
#include <Origin.h>
#include <stdio.h>
#include <data.h>
#include <math.h>
#include <utilities.h>
#include <complex.h>
#include <wksheet.h>
#include <XFbase.h>
#include <RangeEx.h>
#include <GetNbox.h>
////////////////////////////////////////////////////////////////////////////
void isochronal()
{
ASCIMP ascimp;
string strFile = GetOpenBox("*.txt", NULL,"I love grad school","Select your
result file");
\\The previous line needs to be moved to the end of the line before it!!!!
Worksheet wksa;
if(AscImpReadFileStruct(strFile,&ascimp) == 0)
{
ascimp.iRenameCols = 0;
wksa.Create("test1.otw");
wksa.ImportASCII(strFile, ascimp);
LT_execute("wks.ncols = 5");
wksa.Columns(0).SetName("Frequency");
wksa.Columns(1).SetName("Temperature");
wksa.Columns(2).SetName("Constant");
wksa.Columns(3).SetName("Loss");
wksa.Columns(4).SetName("Tand");

wksa.Columns(0).SetUnits("Hertz (Hz)");
wksa.Columns(1).SetUnits("Kelvin (K)");
////////////////////////////////////////////////////
//Start the GetNBox Temperature Check...
Dataset Temperatures(wksa,1);
short method;
GETN_BOX( treeTest )
GETN_CHECK(AllCurves,"Temperatures in Kelvin?",1)
GETN_BEGIN_BRANCH(Method, "Method Options")
GETN_RADIO_INDEX(mthd,0,"Loss|Derivative Loss|Tan Delta|Loss Modulus|Help File"
```

```
 )GETN_OPTION_DISPLAY_FORMAT(DISPLAY_EDITOR_LEFT)
 \\The previous line needs to be moved to the end of the line before it!!!!
GETN_END_BRANCH(Method)
     if(GetNBox(treeTest, "Isochronal Options", "Select the Appropriate Values"))
     {
         if(treeTest.AllCurves.nVal == 0)//If the checkbox is unchecked...
         {
         Temperatures += 273.15;//convert to Kelvin.
         printf("RTFM!!\n");//Chide them for not paying attention.
        }
        method = treeTest.Method.mthd.nVal;
        //////printf("Val is:%d\n",method);
     //////0,1,2,3 are the options
     if(method ==0)//If they choose the Loss
     {
     printf("->Running Loss Option...\n");
     loss();
     }
     else if(method==1)//If they choose Derivative Loss
     {
     printf("->Running Derivative Loss Option...\n");
     derivloss();
     }
     else if(method==2)//If they choose Tan Delta
     {
     printf("->Running Tan Delta Option...\n");
     tandelta();
     }
     else if(method==3)//If they choose Loss Modulus
     {
     printf("->Running Loss Modulus Option...\n");
     lossmodulus();
     }
     else if(method==4)//If they choose the Help File
     {
     printf("->Opening Help File");
     freqhelp();
     }
     }
     else//If the user clicks cancel on the GetNBox
     {
     printf("Quitter!\n");
     return;
     }
}
else//If the user clicks cancel on the import dialog.
{
printf("Quitter!\n");
return;
}
}
```

```
////////////////////////////////////////////////////////////////////////////////
void loss()
{
Worksheet wksa = Project.ActiveLayer();
////Get the results worksheet ready!
Worksheet wks1("Results");

if( !wks1 )
{
wks1.Create("IsoChronal.otw");
wks1.LT_execute("wks1.ncols = 5");
}


Dataset ds0  (wksa,0);//Frequency
Dataset ds1  (wksa,1);//Temperature
Dataset ds2  (wksa,2);//Constant
Dataset ds3  (wksa,3);//Loss
ds3 = log10(ds3)+5;//Take the base ten log of the loss and add five so the program
//can find a maxima.
int Size = ds0.GetSize();

printf("->%d datapoints in your file\n",Size);

int numfreqs = 1;
int i = 1;

while (ds0[i] != ds0[0])//While the current frequency (at index i) is not equal to
// the reference frequency.
{
numfreqs++;
i++;
}

printf("->I am assuming you have %d frequencies\nfor each temperature.\n", numfreqs);

for(int k=0; k<numfreqs; k++)
{
double wName = ds0[k];
string stri = wName;
Worksheet wks2;
wks2.Create();
Page wpg = Project.Pages();
wpg.SetLongName(""+wName+"Hz");

LT_execute("wks.nCols = 3");

wks2.Columns(0).SetName("Temperature");
```

```
wks2.Columns(1).SetName("Constant");
wks2.Columns(2).SetName("Loss");

Dataset d0 (wks2,0);
Dataset d1 (wks2,1);
Dataset d2 (wks2,2);

int indexer = 0;//Declare an indexer so matches aren't dumped in the same row.

for(int j = 0; j<Size; j++)//Now lets loop over the main worksheet,
// finding matching frequencies.
{
if( ds0[k] == ds0[j] )//If a match is found in the main file
//(matching frequencies), dump the match into the individual frequency
// worksheet.
{
wks2.SetCell(indexer,0,ds1[j]);//Add the matched temperature
//value to the frequency worksheet
wks2.SetCell(indexer,1,ds2[j]);//Add the matched dielectric constant value
// to the frequency worksheet
wks2.SetCell(indexer,2,ds3[j]);//Add the matched dielectric loss (LOG10!!!!)
// value to the frequency worksheet

indexer++;
}
}

//printf("Indexed %d\n",j);

wks2.LT_execute("wsort descending:=0 bycol:=1");//Sort the worksheet by the
// temperature column in ascending order.

////////////////////////////////////////////////////////////////
/*Begin the peak-find section*/

wks2.AddCol("Xresult");
wks2.AddCol("Yresult");

wks2.LT_execute("interp1trace iy:=Col(3) method:=2 npts:=1000 oy:=(Col(4),Col(5))");

Curve crvData(wks2, 3, 4);

GraphPage gp;

gp.Create("Temperature.otp");

gp.Rename("Graph"+wName);//name Graph after Worksheet

gp.SetLongName(stri);

gp.LT_execute("page.title=1");
```

```
GraphLayer gly = gp.Layers();

gly.AddPlot(crvData, IDM_PLOT_LINESYMB);


string sCmd;

sCmd.Format("\i(f) = %f Hz",wName);

page_insert_label(gly, sCmd, "MyLabel", 20, 90);

GraphLayer gl = Project.ActiveLayer();
if (!gl)
{
return;
}

DataPlot dp = gl.DataPlots(0);
DataRange dr;
vector vxData, vyData;
if(dp.GetDataRange(dr))
{
DWORD dwPlotID;
if(dr.GetData(DRR_GET_DEPENDENT | DRR_NO_FACTORS, 0, &dwPlotID, NULL,
 &vyData, &vxData) < 0)
 \\The previous line needs to be moved to the end of the line before it!!!!
    {
       printf("get_plot_data failed GetData");
        return;
    }
}
gl.Rescale();

uint nDataSize = vxData.GetSize();
int iSize = vxData.GetSize();

vector vxPeaks, vyPeaks;
vector<int> vnIndices;

vxPeaks.SetSize(nDataSize);
vyPeaks.SetSize(nDataSize);
vnIndices.SetSize(nDataSize);

int nRet = ocmath_find_peaks_1st_derivative( &nDataSize, vxData, vyData, vxPeaks,
 vyPeaks, vnIndices, POSITIVE_DIRECTION,0);
 \\The previous line needs to be moved to the end of the line before it!!!!
if( nRet < OE_NOERROR )
{
printf("error code: %d\n", nRet);
return;
```

```
}


vxPeaks.SetSize(nDataSize);
vyPeaks.SetSize(nDataSize);
vnIndices.SetSize(nDataSize);
int nIndCol, nXCol, nYCol;
nIndCol = wks2.AddCol("Indices");
nXCol = wks2.AddCol("X Coordinate");
nYCol = wks2.AddCol("Y Coordinate");
wks2.Columns(nIndCol).SetType(OKDATAOBJ_DESIGNATION_X);
wks2.Columns(nXCol).SetType(OKDATAOBJ_DESIGNATION_X);
wks2.Columns(nYCol).SetType(OKDATAOBJ_DESIGNATION_Y);
DataRange drOut;
drOut.Add("X", wks2, 0, nIndCol, -1, nIndCol);
drOut.Add("Y", wks2, 0, nXCol, -1, nXCol);
drOut.Add("Z", wks2, 0, nYCol, -1, nYCol);
drOut.SetData(&vyPeaks, &vxPeaks, &vnIndices);
XYRange plotRange;
plotRange.Add("X", wks2, 0, nXCol, -1, nXCol);
plotRange.Add("Y", wks2, 0, nYCol, -1, nYCol);
gl.AddPlot(plotRange, IDM_PLOT_SCATTER);

DataPlot dp1 = gl.DataPlots(1);
dp1.SetColor(2,TRUE);

Dataset dd (wks2,6);
int Size1 = dd.GetSize();
if( Size1 > 1 )
{
wks2.LT_execute("wsort descending:=1 bycol:=7 c1:=6 c2:=8");
}

Dataset dz (wks2,7);
dz -= 5;//Subtract 5 from the y-coordinate



/*End the peak-find section*/
////////////////////////////////////////////////////////////

if (!wks1)
{
printf("Origin Sucks!\nAnd Fails at Life.\n");
}
if (wks2)
{
Dataset dsa(wks2,6);
double colsize = dsa.GetSize();
wks1.SetCell(k,0,wName);//Declare the first column as the frequency point
for(int ii = 0; ii<colsize; ii++)
```

```
{
double Val = dsa[ii];
wks1.SetCell(k,ii+1.0,Val);//Cell, Column, Value
}
}

Dataset d3 (wks2,4);
d3 -= 5;//Subtract 5 from the interpolated loss data (to undo the addition above).

Dataset d4 (wks2,2);
int d4Size = d4.GetSize();
//printf("Size is %d\n", d4Size);
for (int p = 0; p<d4Size; p++)
{
d4[p] -= 5;//Subtract 5 from the raw loss data.
}

gly.Rescale();
}

if (wks1)
{
wks1.AddCol("1000T1");
wks1.AddCol("LogF1");
wks1.AddCol("1000T2");
wks1.AddCol("LogF2");
wks1.AddCol("1000T3");
wks1.AddCol("LogF3");
wks1.AddCol("1000T4");
wks1.Columns(5).SetType(OKDATAOBJ_DESIGNATION_X);
wks1.Columns(7).SetType(OKDATAOBJ_DESIGNATION_X);
wks1.Columns(9).SetType(OKDATAOBJ_DESIGNATION_X);
wks1.Columns(11).SetType(OKDATAOBJ_DESIGNATION_X);
wks1.AddCol("LogF4");
Dataset dsFreq(wks1,0);
Dataset temp(wks1,1);
Dataset temp1(wks1,2);
Dataset temp2(wks1,3);
Dataset temp3(wks1,4);
Dataset logfreq(wks1,12);
double FreqSize = dsFreq.GetSize();
logfreq.SetSize(FreqSize);
logfreq = log10(dsFreq);

Dataset temp4(wks1,5);
Dataset LogF1(wks1,6);
Dataset temp5(wks1,7);
Dataset LogF2(wks1,8);
Dataset temp6(wks1,9);
Dataset LogF3(wks1,10);
Dataset temp7(wks1,11);
```

```
temp4.SetSize(FreqSize);
LogF1.SetSize(FreqSize);
temp5.SetSize(FreqSize);
LogF2.SetSize(FreqSize);
temp6.SetSize(FreqSize);
LogF3.SetSize(FreqSize);
temp7.SetSize(FreqSize);
temp4 = 1000.0 / temp;
LogF1 = logfreq;
temp5 = 1000.0 / temp1;
LogF2 = logfreq;
temp6 = 1000.0 / temp2;
LogF3 = logfreq;
temp7 = 1000.0 / temp3;
}

wks1.LT_execute("wsort descending:=0 bycol:=1 c1:=1 c2:=13");


Curve crv(wks1, 5, 6);
GraphPage crvgp;
crvgp.Create("Arrhenius.otp");
GraphLayer gly = crvgp.Layers();
gly.AddPlot(crv, IDM_PLOT_SCATTER);
DataPlot dp = gly.DataPlots(0);
dp.SetColor(2, TRUE);
MessageBox(GetWindow(),"Check Your Data!  This Program Sucks!","IsoHappy",
MB_OK | MB_ICONEXCLAMATION);
\\The previous line needs to be moved to the end of the line before it!!!!

printf("->Operation Completed Successfully\n");

}




/*BREAK TO DERIVATIVE ISOCHRONAL FILE WITH ITS HELP FILE*/

void derivloss()
{
Worksheet wks = Project.ActiveLayer();//Set the imported ASCII file as
// the active worksheet.

Dataset ds0  (wks,0);
Dataset ds1  (wks,1);
Dataset ds2  (wks,2);
Dataset ds3  (wks,3);
Dataset ds4  (wks,4);
int Size = ds0.GetSize();
```

```
ds4.SetSize(Size);
wks.Columns(4).SetName("DerivLoss");//Rename this column to the derivative loss.
//  The import function names it as Tan Delta.

vector vyOut;
vyOut.SetSize(Size);
vector vy(ds2, TRUE);
vector vx(ds0, TRUE);

double HighF = log10(ds0[0]);
double LowF = log10(ds0[1]);
double Fdiff = HighF-LowF;
double SGval = log(pow(10.0, Fdiff));//Natural log [log()], not base
// ten log [log10()].

printf("->Doing calculus...\n\n->REMEMBER, your lowest and highest\n
frequencies will be CRAP!!\n\n");
\\The previous line needs to be moved to the end of the line before it!!!!

ocmath_savitsky_golay(vy, vyOut, Size, 2,2,2,1);

DataRange derOut;
derOut.Add(wks, 0, "X");
derOut.Add(wks, 4, "Y");
derOut.SetData(&vyOut, &vx);

double pye = PI/2.0;

ds4 *= pye;//Multiply the derivative data by 3.14/2

ds4 /= SGval;//Divide by the natural log of the frequency spacing.
//  See Wubbenhorst 2002 for details.

ds4 = abs(ds4);

ds4 = log10(ds4);//Set the derivative loss to the base ten log
// of the derivative loss.  This should improve the accuracy of
// the program slightly.

////Lets set up the results worksheet.
Worksheet wks1("DerivIsoResults");

if( !wks1 )
{
wks1.Create("IsoChronalDer.otw");
WorksheetPage wp = wks1.GetPage();
wks1.LT_execute("wks1.ncols = 5");
wp.Rename("DerIsoResults");
}
```

```
/////Break for the pasted section
//printf("%d datapoints in your file\n",Size);

int numfreqs = 1;
int i = 1;
//int r,n;

while (ds0[i] != ds0[0])//While the current frequency (at index i) is not
// equal to the reference frequency.
{
numfreqs++;
i++;
}

printf("->I am assuming you have %d frequencies\nfor each temperature.\n\n",
 numfreqs);
\\The previous line needs to be moved to the end of the line before it!!!!

for(int k=0; k<numfreqs; k++)
{
double wName = ds0[k];
string stri = wName;
Worksheet wks2;
wks2.Create();
Page wpg = Project.Pages();
wpg.SetLongName(""+wName+" Hz");

LT_execute("wks.nCols = 3");

wks2.Columns(0).SetName("Temperature");
wks2.Columns(1).SetName("Constant");
wks2.Columns(2).SetName("SGDerivLoss");

Dataset d0 (wks2,0);
Dataset d1 (wks2,1);
Dataset d2 (wks2,2);

int indexer = 0;//Declare an indexer so matches aren't dumped in the same row.

for(int j = 0; j<Size; j++)//Now lets loop over the main worksheet,
//finding matching frequencies.
{
if( ds0[k] == ds0[j] )//If a match is found in the main file
//(matching frequencies), dump the match into the individual frequency worksheet.
{
wks2.SetCell(indexer,0,ds1[j]);//Add the matched temperature value to the
// frequency worksheet
wks2.SetCell(indexer,1,ds2[j]);//Add the matched dielectric constant value
// to the frequency worksheet
wks2.SetCell(indexer,2,ds4[j]);//Add the matched SG derivative value to the
// frequency worksheet
```

```
indexer++;
}
}

//int d2Size = d2.GetSize();
//
//for(int p=0; p<d2Size; p++)
//{
//d2[p] = d2[p]+5.0;//Add five to d2.
//}

//printf("Indexed %d\n",j);

wks2.LT_execute("wsort descending:=0 bycol:=1");//Sort the worksheet by the
//temperature column in ascending order.

////////////////////////////////////////////////////////////
/*Begin the peak-find section*/

wks2.AddCol("Xresult");
wks2.AddCol("Yresult");


wks2.LT_execute("interp1trace iy:=Col(3) method:=2 npts:=1000 oy:=(Col(4),Col(5))");


Dataset SGInterp (wks2,4);
int interpsize = SGInterp.GetSize();
for(int p=0; p<interpsize; p++)
{
SGInterp[p] += 5.0;//Add five to the interpolated data.
}

Curve crvData(wks2, 3, 4);

GraphPage gp;

gp.Create("IsoChronalDer.otp");

gp.Rename("Graph"+wName);//name Graph after Worksheet

gp.SetLongName(stri);

gp.LT_execute("page.title=1");

GraphLayer gly = gp.Layers();

gly.AddPlot(crvData, IDM_PLOT_LINESYMB);

string sCmd;
```

```
sCmd.Format("\i(f) = %f Hz",wName);

page_insert_label(gly, sCmd, "MyLabel", 20, 90);

GraphLayer gl = Project.ActiveLayer();
if (!gl)
{
printf("Origin can't find a graph!\n");
return;
}

DataPlot dp = gl.DataPlots(0);
DataRange dr;
vector vxData, vyData;
if(dp.GetDataRange(dr))
{
DWORD dwPlotID;
if(dr.GetData(DRR_GET_DEPENDENT | DRR_NO_FACTORS, 0, &dwPlotID, NULL,
 &vyData, &vxData) < 0)
\\The previous line needs to be moved to the end of the line before it!!!!
    {
       printf("get_plot_data failed GetData");
        return;
    }
}

uint nDataSize = vxData.GetSize();
int iSize = vxData.GetSize();

vector vxPeaks, vyPeaks;
vector<int> vnIndices;

vxPeaks.SetSize(nDataSize);
vyPeaks.SetSize(nDataSize);
vnIndices.SetSize(nDataSize);

int nRet = ocmath_find_peaks_1st_derivative( &nDataSize, vxData, vyData, vxPeaks,
 vyPeaks, vnIndices, POSITIVE_DIRECTION,0);
 \\The previous line needs to be moved to the end of the line before it!!!!
if( nRet < OE_NOERROR )
{
printf("Peak find error code: %d\n", nRet);
return;
}


vxPeaks.SetSize(nDataSize);
vyPeaks.SetSize(nDataSize);
vnIndices.SetSize(nDataSize);
int nIndCol, nXCol, nYCol;
```

```
nIndCol = wks2.AddCol("Indices");
nXCol = wks2.AddCol("X Coordinate");
nYCol = wks2.AddCol("Y Coordinate");
wks2.Columns(nIndCol).SetType(OKDATAOBJ_DESIGNATION_X);
wks2.Columns(nXCol).SetType(OKDATAOBJ_DESIGNATION_X);
wks2.Columns(nYCol).SetType(OKDATAOBJ_DESIGNATION_Y);
DataRange drOut;
drOut.Add("X", wks2, 0, nIndCol, -1, nIndCol);
drOut.Add("Y", wks2, 0, nXCol, -1, nXCol);
drOut.Add("Z", wks2, 0, nYCol, -1, nYCol);
drOut.SetData(&vyPeaks, &vxPeaks, &vnIndices);
XYRange plotRange;
plotRange.Add("X", wks2, 0, nXCol, -1, nXCol);
plotRange.Add("Y", wks2, 0, nYCol, -1, nYCol);
gl.AddPlot(plotRange, IDM_PLOT_SCATTER);

DataPlot dp1 = gl.DataPlots(1);
dp1.SetColor(2,TRUE);

Dataset dd (wks2,6);
int Size1 = dd.GetSize();
if( Size1 > 1 )
{
wks2.LT_execute("wsort descending:=1 bycol:=7 c1:=6 c2:=8");
}



/*End the peak-find section*/
////////////////////////////////////////////////////////////////

if (!wks1)
{
printf("Origin Sucks Ass!\nAnd Fails at Life.\n");
}
if (wks2)
{
Dataset dsa(wks2,6);
double colsize = dsa.GetSize();
wks1.SetCell(k,0,wName);//Declare the first column as the frequency point
for(int ii = 0; ii<colsize; ii++)
{
double Val = dsa[ii];
wks1.SetCell(k,ii+1.0,Val);//Cell, Column, Value
}
}
for(p=0; p<interpsize; p++)//Now Lets subtract 5 from the data.
{
SGInterp[p] -= 5.0;//Subtract five from the interpolated data.
}
```

```
Dataset yCoord (wks2,7);
int yCoordSize = yCoord.GetSize();
for(int q=0; q<yCoordSize; q++)
{
yCoord[q] -= 5.0;//Subtract five from the y-coordinate data.
}

gly.Rescale();
}

if (wks1)
{
wks1.AddCol("1000T1");
wks1.AddCol("LogF1");
wks1.AddCol("1000T2");
wks1.AddCol("LogF2");
wks1.AddCol("1000T3");
wks1.AddCol("LogF3");
wks1.AddCol("1000T4");
wks1.Columns(5).SetType(OKDATAOBJ_DESIGNATION_X);
wks1.Columns(7).SetType(OKDATAOBJ_DESIGNATION_X);
wks1.Columns(9).SetType(OKDATAOBJ_DESIGNATION_X);
wks1.Columns(11).SetType(OKDATAOBJ_DESIGNATION_X);
wks1.AddCol("LogF4");
Dataset dsFreq(wks1,0);
Dataset temp(wks1,1);
Dataset temp1(wks1,2);
Dataset temp2(wks1,3);
Dataset temp3(wks1,4);
Dataset logfreq(wks1,12);
double FreqSize = dsFreq.GetSize();
logfreq.SetSize(FreqSize);
logfreq = log10(dsFreq);

Dataset temp4(wks1,5);
Dataset LogF1(wks1,6);
Dataset temp5(wks1,7);
Dataset LogF2(wks1,8);
Dataset temp6(wks1,9);
Dataset LogF3(wks1,10);
Dataset temp7(wks1,11);
temp4.SetSize(FreqSize);
LogF1.SetSize(FreqSize);
temp5.SetSize(FreqSize);
LogF2.SetSize(FreqSize);
temp6.SetSize(FreqSize);
LogF3.SetSize(FreqSize);
temp7.SetSize(FreqSize);
temp4 = 1000.0 / temp;
LogF1 = logfreq;
temp5 = 1000.0 / temp1;
```

```
LogF2 = logfreq;
temp6 = 1000.0 / temp2;
LogF3 = logfreq;
temp7 = 1000.0 / temp3;
}

wks1.LT_execute("wsort descending:=0 bycol:=1 c1:=1 c2:=13");


Curve crv(wks1, 5, 6);
GraphPage crvgp;
crvgp.Create("Arrhenius.otp");
GraphLayer gly = crvgp.Layers();
gly.AddPlot(crv, IDM_PLOT_SCATTER);
DataPlot dp = gly.DataPlots(0);
dp.SetColor(2, TRUE);
MessageBox(GetWindow(),"Check Your Data!  This Program Sucks!","IsoHappy",
MB_OK | MB_ICONEXCLAMATION);
\\The previous line needs to be moved to the end of the line before it!!!!

printf("->Operation complete.\n");

}



/*   Begin the tan-delta isochronal section     */

void tandelta()
{
Worksheet wksa = Project.ActiveLayer();

////Get the results worksheet ready!
Worksheet wks1("Results");

if( !wks1 )
{
wks1.Create("IsoChronal.otw");
wks1.LT_execute("wks1.ncols = 5");
}


Dataset ds0  (wksa,0);//Frequency
Dataset ds1  (wksa,1);//Temperature
Dataset ds2  (wksa,2);//Constant
Dataset ds3  (wksa,3);//Loss
Dataset ds4  (wksa,4);//Tan delta
int Size = ds0.GetSize();
ds4.SetSize(Size);
ds4 = ds3 / ds2;//Calculate the tan delta column
```

```
printf("->%d datapoints in your file\n",Size);

int numfreqs = 1;
int i = 1;
//int r,n;

while (ds0[i] != ds0[0])//While the current frequency (at index i)
//is not equal to the reference frequency.
{
numfreqs++;
i++;
}

printf("->I am assuming you have %d frequencies\n for each temperature.
\n", numfreqs);
\\The previous line needs to be moved to the end of the line before it!!!!

for(int k=0; k<numfreqs; k++)
{
double wName = ds0[k];
string stri = wName;
Worksheet wks2;
wks2.Create();
Page wpg = Project.Pages();
wpg.SetLongName(""+wName+"Hz");

LT_execute("wks.nCols = 4");

wks2.Columns(0).SetName("Temperature");
wks2.Columns(1).SetName("Constant");
wks2.Columns(2).SetName("Loss");
wks2.Columns(3).SetName("Tand");

Dataset d0 (wks2,0);
Dataset d1 (wks2,1);
Dataset d2 (wks2,2);
Dataset d3 (wks2,3);

int indexer = 0;//Declare an indexer so matches aren't dumped in the same row.

for(int j = 0; j<Size; j++)//Now lets loop over the main worksheet, finding
//matching frequencies.
{
if( ds0[k] == ds0[j] )//If a match is found in the main file
//(matching frequencies), dump the match into the individual frequency worksheet.
{
wks2.SetCell(indexer,0,ds1[j]);//d0[k] = ds1[j];//Add the matched
// temperature value to the frequency worksheet
wks2.SetCell(indexer,1,ds2[j]);//d1[k] = ds2[j];//Add the matched
// dielectric constant value to the frequency worksheet
wks2.SetCell(indexer,2,ds3[j]);//d2[k] = ds3[j];//Add the matched
```

```
// dielectric loss value to the frequency worksheet
wks2.SetCell(indexer,3,ds4[j]);//d3[k] = ds4[j];//Add the matched
// tan delta value to the frequency worksheet

indexer++;
}
}

//printf("Indexed %d\n",j);

wks2.LT_execute("wsort descending:=0 bycol:=1");//Sort the worksheet by
// the temperature column in ascending order.


////////////////////////////////////////////////////////////////
/*Begin the peak-find section*/

wks2.AddCol("Xresult");
wks2.AddCol("Yresult");

wks2.LT_execute("interp1trace iy:=Col(4) method:=2 npts:=1000 oy:=(Col(5),Col(6))");

Curve crvData(wks2, 4, 5);

GraphPage gp;

gp.Create("Tandisochronal.otp");

gp.Rename("Graph"+wName);//name Graph after Worksheet

gp.SetLongName(stri);

gp.LT_execute("page.title=1");

GraphLayer gly = gp.Layers();

gly.AddPlot(crvData, IDM_PLOT_LINESYMB);

gly.Rescale();

string sCmd;

sCmd.Format("\i(f) = %f Hz",wName);

page_insert_label(gly, sCmd, "MyLabel", 20, 90);

GraphLayer gl = Project.ActiveLayer();
if (!gl)
{
return;
}
```

```
DataPlot dp = gl.DataPlots(0);
DataRange dr;
vector vxData, vyData;
if(dp.GetDataRange(dr))
{
DWORD dwPlotID;
if(dr.GetData(DRR_GET_DEPENDENT | DRR_NO_FACTORS, 0, &dwPlotID, NULL,
 &vyData, &vxData) < 0)
 \\The previous line needs to be moved to the end of the line before it!!!!
    {
       printf("get_plot_data failed GetData");
        return;
    }
}

uint nDataSize = vxData.GetSize();
int iSize = vxData.GetSize();

vector vxPeaks, vyPeaks;
vector<int> vnIndices;

vxPeaks.SetSize(nDataSize);
vyPeaks.SetSize(nDataSize);
vnIndices.SetSize(nDataSize);

int nRet = ocmath_find_peaks_1st_derivative( &nDataSize, vxData, vyData,
 vxPeaks, vyPeaks, vnIndices, POSITIVE_DIRECTION | NEGATIVE_DIRECTION,11);
 \\The previous line needs to be moved to the end of the line before it!!!!
if( nRet < OE_NOERROR )
{
printf("error code: %d\n", nRet);
return;
}
vxPeaks.SetSize(nDataSize);
vyPeaks.SetSize(nDataSize);
vnIndices.SetSize(nDataSize);
int nIndCol, nXCol, nYCol;
nIndCol = wks2.AddCol("Indices");
nXCol = wks2.AddCol("X Coordinate");
nYCol = wks2.AddCol("Y Coordinate");
wks2.Columns(nIndCol).SetType(OKDATAOBJ_DESIGNATION_X);
wks2.Columns(nXCol).SetType(OKDATAOBJ_DESIGNATION_X);
wks2.Columns(nYCol).SetType(OKDATAOBJ_DESIGNATION_Y);
DataRange drOut;
drOut.Add("X", wks2, 0, nIndCol, -1, nIndCol);
drOut.Add("Y", wks2, 0, nXCol, -1, nXCol);
drOut.Add("Z", wks2, 0, nYCol, -1, nYCol);
drOut.SetData(&vyPeaks, &vxPeaks, &vnIndices);
XYRange plotRange;
plotRange.Add("X", wks2, 0, nXCol, -1, nXCol);
```

```
plotRange.Add("Y", wks2, 0, nYCol, -1, nYCol);
gl.AddPlot(plotRange, IDM_PLOT_SCATTER);

DataPlot dp1 = gl.DataPlots(1);
dp1.SetColor(2,TRUE);

Dataset dd (wks2,7);
int Size1 = dd.GetSize();
if( Size1 > 1 )
{
wks2.LT_execute("wsort descending:=1 bycol:=8 c1:=7 c2:=9");
}



/*End the peak-find section*/
////////////////////////////////////////////////////////////

if (!wks1)
{
printf("Origin Sucks Ass!\nAnd Fails at Life.\n");
return;
}
if (wks2)
{
Dataset dsa(wks2,7);
double colsize = dsa.GetSize();
wks1.SetCell(k,0,wName);//Declare the first column as the frequency point
for(int ii = 0; ii<colsize; ii++)
{
double Val = dsa[ii];
wks1.SetCell(k,ii+1.0,Val);//Cell, Column, Value
}
}
}

printf("->Sort complete!\n->Setting up Arrhenius Data\n");

if (wks1)
{
wks1.AddCol("1000T1");
wks1.AddCol("LogF1");
wks1.AddCol("1000T2");
wks1.AddCol("LogF2");
wks1.AddCol("1000T3");
wks1.AddCol("LogF3");
wks1.AddCol("1000T4");
wks1.Columns(5).SetType(OKDATAOBJ_DESIGNATION_X);
wks1.Columns(7).SetType(OKDATAOBJ_DESIGNATION_X);
wks1.Columns(9).SetType(OKDATAOBJ_DESIGNATION_X);
wks1.Columns(11).SetType(OKDATAOBJ_DESIGNATION_X);
```

```
wks1.AddCol("LogF4");
Dataset dsFreq(wks1,0);
Dataset temp(wks1,1);
Dataset temp1(wks1,2);
Dataset temp2(wks1,3);
Dataset temp3(wks1,4);
Dataset logfreq(wks1,12);
double FreqSize = dsFreq.GetSize();
logfreq.SetSize(FreqSize);
logfreq = log10(dsFreq);

Dataset temp4(wks1,5);
Dataset LogF1(wks1,6);
Dataset temp5(wks1,7);
Dataset LogF2(wks1,8);
Dataset temp6(wks1,9);
Dataset LogF3(wks1,10);
Dataset temp7(wks1,11);
temp4.SetSize(FreqSize);
LogF1.SetSize(FreqSize);
temp5.SetSize(FreqSize);
LogF2.SetSize(FreqSize);
temp6.SetSize(FreqSize);
LogF3.SetSize(FreqSize);
temp7.SetSize(FreqSize);
temp4 = 1000.0 / temp;
LogF1 = logfreq;
temp5 = 1000.0 / temp1;
LogF2 = logfreq;
temp6 = 1000.0 / temp2;
LogF3 = logfreq;
temp7 = 1000.0 / temp3;
}

wks1.LT_execute("wsort descending:=0 bycol:=1 c1:=1 c2:=13");


Curve crv(wks1, 5, 6);
GraphPage crvgp;
crvgp.Create("Arrhenius.otp");
GraphLayer gly = crvgp.Layers();
gly.AddPlot(crv, IDM_PLOT_SCATTER);
DataPlot dp = gly.DataPlots(0);
dp.SetColor(2, TRUE);
MessageBox(GetWindow(),"Check Your Data!  This Program Sucks!","IsoHappy",
 MB_OK | MB_ICONEXCLAMATION);
 \\The previous line needs to be moved to the end of the line before it!!!!

printf("->Operation complete\n");

}
```

```
//////////////////////////////////////////////////////////////////////
//////////////////////////////////////////////////////////////////////
//////////////////////////////////////////////////////////////////////
//////////////////////////////////////////////////////////////////////
//////////////////////////////////////////////////////////////////////
//////////////////////////////////////////////////////////////////////


void lossmodulus()
{

Worksheet wks = Project.ActiveLayer();

Dataset ds0  (wks,0);
Dataset ds1  (wks,1);
Dataset ds2  (wks,2);
Dataset ds3  (wks,3);
Dataset ds4  (wks,4);
int Size = ds0.GetSize();//Set Size as the number of rows of data.
ds4.SetSize(Size);
wks.Columns(4).SetName("LossModulus");/////Rename this column from
// Tan Delta to LossModulus.

////////Begin Modulus Operation////////

ds4 = ds3/(pow(ds2,2.0) + pow(ds3,2.0));

////Lets set up the results worksheet.
Worksheet wks1("ModIsoResults");

if( !wks1 )
{
wks1.Create("IsoChronal.otw");
WorksheetPage wp = wks1.GetPage();
wks1.LT_execute("wks1.ncols = 5");
wp.Rename("ModIsoResults");
}


/////Break for the pasted section
//printf("%d datapoints in your file\n",Size);

int numfreqs = 1;
int i = 1;
//int r,n;

while (ds0[i] != ds0[0])//While the current frequency (at index i)
// is not equal to the reference frequency.
```

```
{
numfreqs++;
i++;
}

printf("->I am assuming you have %d frequencies\nfor each temperature.
\n\n", numfreqs);
\\The previous line needs to be moved to the end of the line before it!!!!

for(int k=0; k<numfreqs; k++)
{
double wName = ds0[k];
string stri = wName;
Worksheet wks2;
wks2.Create();
Page wpg = Project.Pages();
wpg.SetLongName(""+wName+" Hz");

LT_execute("wks.nCols = 3");

wks2.Columns(0).SetName("Temperature");
wks2.Columns(1).SetName("Constant");
wks2.Columns(2).SetName("Modulus’’");

Dataset d0 (wks2,0);
Dataset d1 (wks2,1);
Dataset d2 (wks2,2);

int indexer = 0;//Declare an indexer so matches aren’t dumped in the same row.

for(int j = 0; j<Size; j++)//Now lets loop over the main worksheet,
//finding matching frequencies.
{
if( ds0[k] == ds0[j] )//If a match is found in the main file
//(matching frequencies), dump the match into the individual frequency worksheet.
{
wks2.SetCell(indexer,0,ds1[j]);//Add the matched temperature value to the
// frequency worksheet
wks2.SetCell(indexer,1,ds2[j]);//Add the matched dielectric constant value
// to the frequency worksheet
wks2.SetCell(indexer,2,ds4[j]);//Add the matched SG derivative value to the
// frequency worksheet

indexer++;
}
}

//printf("Indexed %d\n",j);

wks2.LT_execute("wsort descending:=0 bycol:=1");//Sort the worksheet by the
//temperature column in ascending order.
```

```
////////////////////////////////////////////////////////////////
/*Begin the peak-find section*/

wks2.AddCol("Xresult");
wks2.AddCol("Yresult");

wks2.LT_execute("interp1trace iy:=Col(3) method:=2 npts:=1000 oy:=(Col(4),Col(5))");

Curve crvData(wks2, 3, 4);

GraphPage gp;

gp.Create("TemperatureM.otp");

gp.Rename("Graph"+wName);//name Graph after Worksheet

gp.SetLongName(stri);

gp.LT_execute("page.title=1");

GraphLayer gly = gp.Layers();

gly.AddPlot(crvData, IDM_PLOT_LINESYMB);

gly.Rescale();

string sCmd;

sCmd.Format("\i(f) = %f Hz",wName);

page_insert_label(gly, sCmd, "MyLabel", 20, 90);

GraphLayer gl = Project.ActiveLayer();
if (!gl)
{
printf("Origin can't find a graph!\n");
return;
}

DataPlot dp = gl.DataPlots(0);
DataRange dr;
vector vxData, vyData;
if(dp.GetDataRange(dr))
{
DWORD dwPlotID;
if(dr.GetData(DRR_GET_DEPENDENT | DRR_NO_FACTORS, 0, &dwPlotID, NULL,
 &vyData, &vxData) < 0)
 \\The previous line needs to be moved to the end of the line before it!!!!
    {
       printf("get_plot_data failed GetData");
```

```
        return;
    }
}

uint nDataSize = vxData.GetSize();
int iSize = vxData.GetSize();

vector vxPeaks, vyPeaks;
vector<int> vnIndices;

vxPeaks.SetSize(nDataSize);
vyPeaks.SetSize(nDataSize);
vnIndices.SetSize(nDataSize);

int nRet = ocmath_find_peaks_1st_derivative( &nDataSize, vxData, vyData, vxPeaks,
 vyPeaks, vnIndices, POSITIVE_DIRECTION | NEGATIVE_DIRECTION,11);
 \\The previous line needs to be moved to the end of the line before it!!!!
if( nRet < OE_NOERROR )
{
printf("Peak find error code: %d\n", nRet);
return;
}
vxPeaks.SetSize(nDataSize);
vyPeaks.SetSize(nDataSize);
vnIndices.SetSize(nDataSize);
int nIndCol, nXCol, nYCol;
nIndCol = wks2.AddCol("Indices");
nXCol = wks2.AddCol("X Coordinate");
nYCol = wks2.AddCol("Y Coordinate");
wks2.Columns(nIndCol).SetType(OKDATAOBJ_DESIGNATION_X);
wks2.Columns(nXCol).SetType(OKDATAOBJ_DESIGNATION_X);
wks2.Columns(nYCol).SetType(OKDATAOBJ_DESIGNATION_Y);
DataRange drOut;
drOut.Add("X", wks2, 0, nIndCol, -1, nIndCol);
drOut.Add("Y", wks2, 0, nXCol, -1, nXCol);
drOut.Add("Z", wks2, 0, nYCol, -1, nYCol);
drOut.SetData(&vyPeaks, &vxPeaks, &vnIndices);
XYRange plotRange;
plotRange.Add("X", wks2, 0, nXCol, -1, nXCol);
plotRange.Add("Y", wks2, 0, nYCol, -1, nYCol);
gl.AddPlot(plotRange, IDM_PLOT_SCATTER);

DataPlot dp1 = gl.DataPlots(1);
dp1.SetColor(2,TRUE);

Dataset dd (wks2,6);
int Size1 = dd.GetSize();
if( Size1 > 1 )
{
wks2.LT_execute("wsort descending:=1 bycol:=7 c1:=6 c2:=8");
}
```

```
/*End the peak-find section*/
////////////////////////////////////////////////////////////

if (!wks1)
{
printf("Origin Sucks Ass!\nAnd Fails at Life.\n");
}
if (wks2)
{
Dataset dsa(wks2,6);
double colsize = dsa.GetSize();
wks1.SetCell(k,0,wName);//Declare the first column as the frequency point
for(int ii = 0; ii<colsize; ii++)
{
double Val = dsa[ii];
wks1.SetCell(k,ii+1.0,Val);//Cell, Column, Value
}
}
}

if (wks1)
{
wks1.AddCol("1000T1");
wks1.AddCol("LogF1");
wks1.AddCol("1000T2");
wks1.AddCol("LogF2");
wks1.AddCol("1000T3");
wks1.AddCol("LogF3");
wks1.AddCol("1000T4");
wks1.Columns(5).SetType(OKDATAOBJ_DESIGNATION_X);
wks1.Columns(7).SetType(OKDATAOBJ_DESIGNATION_X);
wks1.Columns(9).SetType(OKDATAOBJ_DESIGNATION_X);
wks1.Columns(11).SetType(OKDATAOBJ_DESIGNATION_X);
wks1.AddCol("LogF4");
Dataset dsFreq(wks1,0);
Dataset temp(wks1,1);
Dataset temp1(wks1,2);
Dataset temp2(wks1,3);
Dataset temp3(wks1,4);
Dataset logfreq(wks1,12);
double FreqSize = dsFreq.GetSize();
logfreq.SetSize(FreqSize);
logfreq = log10(dsFreq);

Dataset temp4(wks1,5);
Dataset LogF1(wks1,6);
Dataset temp5(wks1,7);
Dataset LogF2(wks1,8);
```

```
Dataset temp6(wks1,9);
Dataset LogF3(wks1,10);
Dataset temp7(wks1,11);
temp4.SetSize(FreqSize);
LogF1.SetSize(FreqSize);
temp5.SetSize(FreqSize);
LogF2.SetSize(FreqSize);
temp6.SetSize(FreqSize);
LogF3.SetSize(FreqSize);
temp7.SetSize(FreqSize);
temp4 = 1000.0 / temp;
LogF1 = logfreq;
temp5 = 1000.0 / temp1;
LogF2 = logfreq;
temp6 = 1000.0 / temp2;
LogF3 = logfreq;
temp7 = 1000.0 / temp3;
}

wks1.LT_execute("wsort descending:=0 bycol:=1 c1:=1 c2:=13");


Curve crv(wks1, 5, 6);
GraphPage crvgp;
crvgp.Create("Arrhenius.otp");
GraphLayer gly = crvgp.Layers();
gly.AddPlot(crv, IDM_PLOT_SCATTER);
DataPlot dp = gly.DataPlots(0);
dp.SetColor(2, TRUE);
MessageBox(GetWindow(),"Check Your Data!  This Program Sucks!","IsoHappy",
MB_OK | MB_ICONEXCLAMATION);
\\The previous line needs to be moved to the end of the line before it!!!!

printf("->Operation complete.\n");

}



/*Begin the help section*/

/*Begin the help file for the isochronal program.*/
int freqhelp()
{
Note note;
note.Create();
if (note.IsValid())
{
note.Text = "*****************Isochronal Data Help File*****************\n"
"\n"
"Version 4.0\n"
```

```
"\n"
"\n"
"As of 4-06-2009, this is the newest and simplest version\n"
"of the program yet.\n"
"\n"
"\n"
"There are currently four programs contained within this\n"
"file.\n"
"\n"
"\n"
"Only a single command needs to be entered to run any of\n"
"these programs.  Type 'isochronal' into the command\n"
"window to run the main program.  You will be prompted\n"
"to choose the results file (.txt) you wish to analyze.\n"
"\n"
"A window will then pop up to ask you to choose which of\n"
"the programs you would like to run.  Click the radial\n"
"button next to the method you wish to use, then click on\n"
"the OK button.\n"
"\n"
"\n"
"When the program is finished, you should have these\n"
"windows present:\n"
" 1. 1 workbook for each frequency.\n"
" 2. 1 plot for each frequency.\n"
" 3. 1 results workbook\n"
" 4. 1 Arrhenius plot.\n"
"\n"
"\n"
"What all programs have in common:\n"
"1. They do all necessary calculations for you.  No need\n"
"   to export anything except:\n"
"   Frequency - Temperature - Constant - Loss\n"
"2. They use a single ASCII file exported from WinDETA.\n"
" a. You should export the file in Kelvin.  But the\n"
"    programs will check for you anyway.\n"
"3. They will split the single ASCII file up into a single\n"
"   workbook for every frequency.\n"
"4. They will interpolate your data (loss, tan delta, etc.)\n"
"   using a trace interpolation with 1000 points.\n"
"5. They use the first derivitive to find the peaks:\n"
"   ocmath_find_peaks_1st_derivative\n"
"6. They take the maxima and construct an Arrhenius plot.\n"
"   The Arrhenius plot only contains the first of four of\n"
"   the maxima (assuming the program found four maxima).\n"
"   If you want to plot all of the data, you can do so\n"
"   (manually) by looking at the results workbook.\n"
"\n"
"\n"
"-------> List of programs and what they do <-------\n"
"\n"
```

```
"\n"
"****************** Program 1: loss ******************\n"
"-Uses the raw dielectric loss to find maxima.\n"
"\n"
"\n"
"***************** Program 2: derivloss ***************\n"
"-Uses the derivative of the raw dielectric constant to\n"
" find maxima.\n"
"\n"
"Be careful with this one!  Your first and last two fre-\n"
"-quencies are GARBAGE!\n"
"\n"
"\n"
"***************** Program 3: tandelta *****************\n"
"-Uses tan-delta to find maxima. Useful for you EP boys\n"
" (and/or girls).\n"
"\n"
"\n"
"*************** Program 4: lossmodulus ***************\n"
"-Uses the loss modulus, calculated from the raw data to\n"
" find the relaxation times.  Note that this method can\n"
" give you the relaxation time of conductivity.  Please\n"
" also note that the relaxation times determined using\n"
" the dielectric modulus won't be the same as those\n"
" relaxation times determined with the dielectric loss,\n"
" which won't be the same as those determined from Tan-\n"
" Delta.  See Wubbenhorst 2002 JNCS for details.\n"
"\n"
"\n"
"\n"
"List of plot/workbook templates the program uses:\n"
" 1. freq - workbook\n"
" 2. IsoChronal - workbook\n"
" 3. Temperature - plot\n"
" 4. Arrhenius - plot\n"
"You can create/customize these templates to your liking.\n"
"If you don't create these templates, don't worry, Origin\n"
"will use its defalut workbook/plot.\n"
"I do recommend you create these templates.  Then you\n"
"don't have to worry about formatting errors when using\n"
"the default templates.\n"
"\n"
"\n"
"Some things I assume about your data:\n"
"1. The number of frequencies for each temperature is the\n"
"   same.\n"
"2. You use the same frequencies at each temperature.\n"
"3. You don't have any duplicate temperatures in your\n"
"   results file.\n"
"If your data violates any of these assumptions, see me\n"
"to discuss other options.\n"
```

```
"\n"
"\n"
"\n"
"As always, DON'T TRUST THE PROGRAM!  It was written by a\n"
"lousy programmer.  If you find any problems, please let me\n"
"know so I can (try to) fix them.\n"
"\n"
"\n"
"For any help with this or any other of my programs\n"
"please contact me at kmasser@gmail.com.\n"
"\n"
"**********************Kevin Masser**********************\n";
}
return 0;
}

/*End the help section*/
```

Appendix D

Origin C Code for Plotting Multiple Datasets

This appendix contains Origin C code for making plots of specified columns to a specific template. The program accepts the columns designated by the user and plots the columns from each workbook in that directory to individual plots, as well as making a 'master' plot containing all of the data on a single graph. To run the program, type 'plotdata' into the Origin 8 command window (without quotes). A window will appear prompting the user to enter the x and y column numbers, the folder containing the data, as well as a plot template. Any template can be used, but if no template is found, the program defaults to Origin's default template.

The program requires your data (workbooks) be in a folder different from the plots, and neither can be in the root folder. Shown in Figure D.1 is a screen shot of the plotting program dialog window. Note in the lower left corner the generic folder structure recommended for this program to work. For additional considerations, typing 'plotdatahelp' into the command window (without the quotes) will open a help file for this program.

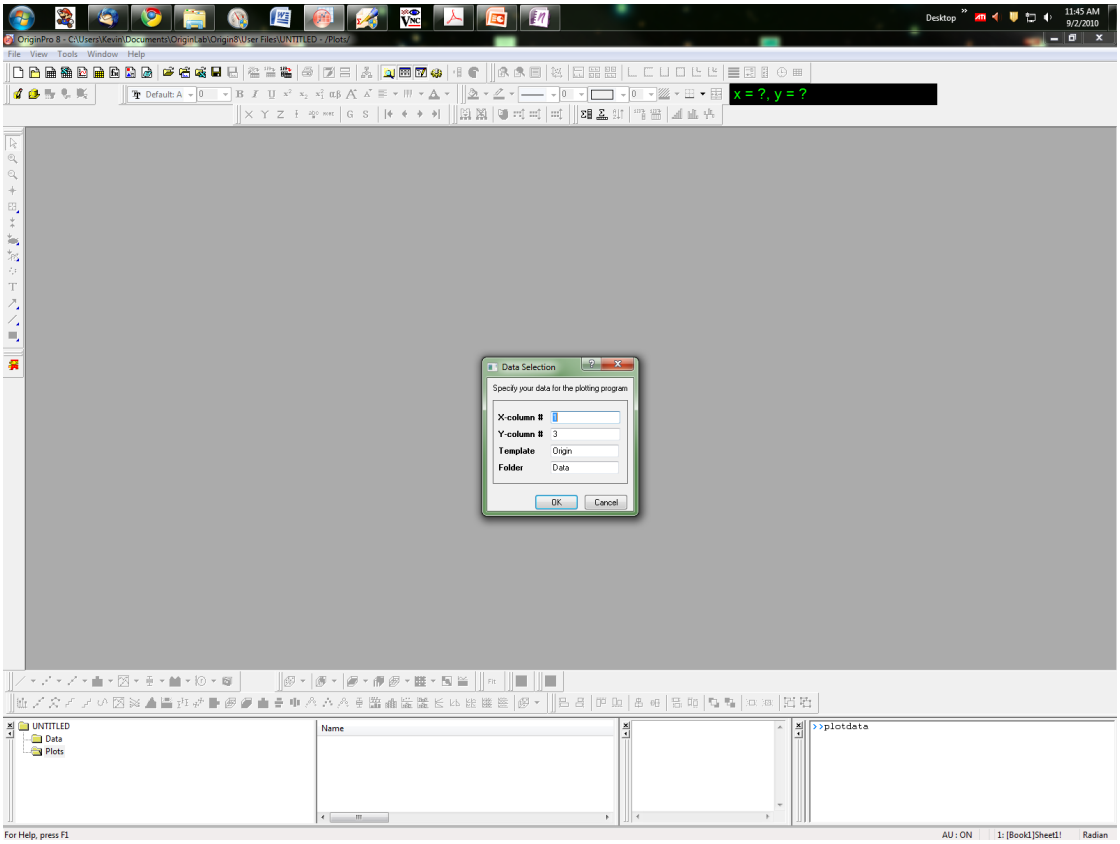

Fig. D.1: Screenshot of the plotting program.

```
/*--------------------------------------------------------------------------*
 * File Name: Master Plotter  *
 * Creation:  *
 * Purpose: OriginC Source C file *
 * Copyright (c) ABCD Corp. 2003, 2004, 2005, 2006, 2007, 2008, 2009, 2010 *
 * All Rights Reserved *
 *  *
 * Modification Log: *
 *--------------------------------------------------------------------------*/

////////////////////////////////////////////////////////////////////////////
#include <Origin.h>
#include <stdio.h>
#include <data.h>
#include <math.h>
#include <utilities.h>
#include <complex.h>
#include <wksheet.h>
#include <folder.h>
#include <Page.h>
#include <GetNbox.h>
////////////////////////////////////////////////////////////////////////////

void plotdata()
{
string str1, template, folder;

int x, y;

GETN_BOX(trTemp)
GETN_NUM(xcol,"X-column #",1)
GETN_NUM(ycol,"Y-column #",2)
GETN_STR(temp, "Template","Origin")
GETN_STR(fold,"Folder","Data")
if(GetNBox(trTemp, "Data Selection", "Specify your data for the plotting program"))
    {
        x = trTemp.xcol.dVal;
        y = trTemp.ycol.dVal;
        template = trTemp.temp.strVal;
        folder = trTemp.fold.strVal;

int ii=0;

Folder fld = Project.RootFolder;
Folder fldsub = fld.Subfolders(folder);
if(fldsub.IsValid())
{

GraphPage gpAll;

gpAll.Create(template);
```

```
gpAll.Rename("Sum");
gpAll.SetLongName("Sum Plot - x="+x+" y="+y);

foreach (PageBase pg in fldsub.Pages)

{

str1 = pg.GetName();

string str2 = pg.GetLongName();//Get the long name of each worksheet to rename
// each graph by the same long name.

Worksheet wks= str1;

DataRange dr;//Construct a datarange to handle any X-Y assignment.
dr.Add(wks, x-1, "X");
dr.Add(wks, y-1, "Y");

GraphPage gp;

gp.Create(template, CREATE_HIDDEN);

gp.Rename("Graph");//name Graph after Worksheet

gp.SetLongName(str2);

GraphLayer gly = gp.Layers();

gly.AddPlot(dr,IDM_PLOT_UNKNOWN,GAP_USE_TEMPLATE);

gly.Rescale();

gpAll.Layers(0).AddPlot(dr,IDM_PLOT_UNKNOWN,GAP_USE_TEMPLATE);

}

gpAll.Layers(0).LT_execute("legend");

gpAll.Layers(0).Rescale();
}
else
{
printf("Not Valid\nBe sure you aren't\ntrying to select your\nroot folder!\n");
return;
}
}
else
    {
     printf("Quitter!\n");
     return;
```

```
    }
}
//////////////////END PLOTTING PROGRAM//////////////////////////////

void plotdatahelp()
{
Note note;
note.Create();
if (note.IsValid())
{
note.Text = "*****************Plotting Data Help File*****************\n"
"\n"
"Version 1.0\n"
"\n"
"\n"
"To run this program, type 'plotdata' in the command window\n"
"without the quotes.\n"
"\n"
"The program will prompt you for the X and Y column numbers\n"
"as well as the folder which contains your data, and the\n"
"template you would like to use.\n"
" -Your column numbers start from 1.  There is no 0 offset\n"
"  as in Origin C.\n"
"It will then plot all of the columns you select from the\n"
"folder you specify to the template of your choice.\n"
"\n"
"\n"
"If you don't have a template, don't worry, Origin will use\n"
"its default template.\n"
"\n"
"What you need to consider:\n"
" 1. The folder you select must contain the workbooks which\n"
"    contain the data for plotting.\n"
" 2. The folder you select CAN NOT be the root folder.\n"
" 3. The folder you select shouldn't have anything besides\n"
"    workbooks, or the program may not work properly.\n"
"\n"
"\n"
"The programmer's tips for optimal performance:\n"
" 1. Create a subfolder of the root folder for just your\n"
"    data.  This makes things cleaner anyway.\n"
" 2. Create a subfolder of the root folder for the plots you\n"
"    are going to create.\n"
" 3. Create templates which are publication-ready.  This\n"
"    time spent on making good templates will make the\n"
"    presentation of your data easier.\n"
"\n"
"\n"
"The folder name and template name are not case sensitive.\n"
"\n"
"\n"
```

```
"\n"
"As always, DON'T TRUST THE PROGRAM!  It was written by a\n"
"lousy programmer.  If you find any problems, please let me\n"
"know so I can (try to) fix them.\n"
"\n"
"\n"
"For any help with this or any other of my programs\n"
"please contact me.\n"
"\n"
"************************Kevin Masser**********************\n";
}
return ;
}
```

Bibliography

[1] Coleman, M. M., Graf, J., and Painter, P. C. *Specific Interactions and the Miscibility of Polymer Blends*. Technomic Publishing Company, Lancaster, 1 edition, (1991).

[2] Coleman, M. M., Yang, X. M., Stallman, J. B., and Painter, P. C. *Macromolecular Symposia* **94**, 1 (1995).

[3] Painter, P. and Coleman, M. *Fundamentals of Polymer Science*. CRC Press, New York, (1997).

[4] Lodge, T. P., Wood, E. R., and Haley, J. C. *Journal of Polymer Science Part B-Polymer Physics* **44**(4), 756–763 (2006).

[5] Takeno, H., Koizumi, S., Hasegawa, H., and Hashimoto, T. *Macromolecules* **29**(7), 2440–2448 (1996).

[6] Takeno, H., Kobayashi, M., and Aikawa, T. *Macromolecules* **39**(6), 2183–2190 (2006).

[7] Cendoya, I., Alegria, A., Alberdi, J. M., Colmenero, J., Grimm, H., Richter, D., and Frick, B. *Macromolecules* **32**(12), 4065–4078 (1999).

[8] Roland, C. M. and Ngai, K. L. *Macromolecules* **25**(1), 363–367 (1992).

[9] Pathak, J., Colby, R., Floudas, G., and Jerome, R. *Macromolecules* (32) (1999).

[10] Wagler, T., Rinaldi, P. L., Han, C. D., and Chun, H. *Macromolecules* **33**(5), 1778–1789 (2000).

[11] Gotzen, N. A., Huth, H., Schick, C., Van Assche, G., Neus, C., and Van Mele, B. *Polymer* **51**(3), 647–654 (2010).

[12] Leroy, E., Alegria, A., and Colmenero, J. *Macromolecules* **36**(19), 7280–7288 (2003).

[13] Urakawa, O., Fuse, Y., Hori, H., Tran-Cong, Q., and Yano, O. *Polymer* **42**(2), 765–773 (2001).

[14] Lodge, T. P. and McLeish, T. C. B. *Macromolecules* **33**(14), 5278–5284 (2000).

[15] Painter, P. C. and Coleman, M. M. *Macromolecules* **42**(3), 820–829 (2009).

[16] Kim, J. K., Lee, H. H., Son, H. W., and Han, C. D. *Macromolecules* **31**(24), 8566–8578 (1998).

[17] Chung, G. C., Kornfield, J. A., and Smith, S. D. *Macromolecules* **27**(20), 5729–5741 (1994).

[18] Arendt, B. H., Krishnamoorti, R., Kornfield, J. A., and Smith, S. D. *Macromolecules* **30**(4), 1127–1137 (1997).

[19] Trask, C. A. and Roland, C. M. *Macromolecules* **22**(1), 256–261 (1989).

[20] Roovers, J. and Toporowski, P. M. *Macromolecules* **25**(13), 3454–3461 (1992).

[21] Fox, T. G. and Flory, P. J. *Journal of Applied Physics* **21**(6), 581–591 (1950).

[22] Fox, T. G. and Flory, P. J. *Journal of Polymer Science* **14**(75), 315–319 (1954).

[23] Couchman, P. R. and Karasz, F. E. *Macromolecules* **11**(1), 117–119 (1978).

[24] Kwei, T. K. *Journal of Polymer Science Part C-Polymer Letters* **22**(6), 307–313 (1984).

[25] Kwei, T. K., Pearce, E. M., Pennacchia, J. R., and Charton, M. *Macromolecules* **20**(5), 1174–1176 (1987).

[26] Painter, P. C., Graf, J., and Coleman, M. M. *Journal of Chemical Physics* **92**(10), 6166–6174 (1990).

[27] Kumar, S. K., Colby, R. H., Anastasiadis, S. H., and Fytas, G. *Journal of Chemical Physics* **105**(9), 3777 (1996).

[28] Coleman, M. M., Pehlert, G. J., Yang, X. M., Stallman, J. B., and Painter, P. C. *Polymer* **37**(21), 4753–4761 (1996).

[29] Coleman, M. M., Pehlert, G. J., and Painter, P. C. *Macromolecules* **29**(21), 6820–6831 (1996).

[30] Pehlert, G. J., Yang, X. M., Painter, P. C., and Coleman, M. M. *Polymer* **37**(21), 4763–4771 (1996).

[31] Coleman, M. M. and Painter, P. C. *Macromolecular Chemistry And Physics* **199**(7), 1307–1314 (1998).

[32] Painter, P., Zhao, H. Q., and Park, Y. *Macromolecules* **42**(1), 435–444 (2009).

[33] Zhang, S. H., Jin, X., Painter, P. C., and Runt, J. *Polymer* **45**(11), 3933–3942 (2004).

[34] Zhang, S. H., Casalini, R., Runt, J., and Roland, C. M. *Macromolecules* **36**(26), 9917–9923 (2003).

[35] Zhang, S. H., Painter, P. C., and Runt, J. *Macromolecules* **35**(22), 8478–8487 (2002).

[36] Zhang, S. H., Painter, P. C., and Runt, J. *Macromolecules* **35**(25), 9403–9413 (2002).

[37] Zhang, S. *Broadband Dielectric Study of Miscible Polymer Blends with Intermolecular Hydrogen Bonding*. PhD thesis, The Pennsylvania State University, (2003).

[38] Yang, Z. and Han, C. D. *Macromolecules* **41**(6), 2104–2118 (2008).

[39] Viswanathan, S. and Dadmun, M. D. *Macromolecules* **35**(13), 5049–5060 (2002).

[40] He, Y., Zhu, B., and Inoue, Y. *Progress in Polymer Science* **29**(10), 1021 (2004).

[41] Zhang, S. H. and Runt, J. *Journal of Physical Chemistry B* **108**(20), 6295–6302 (2004).

[42] Zhang, S. H., Jin, X., Painter, P. C., and Runt, J. *Macromolecules* **35**(9), 3636–3646 (2002).

[43] Zhang, S. H., Painter, P. C., and Runt, J. *Macromolecules* **37**(7), 2636–2642 (2004).

[44] Zhang, S. H., Jin, X., Painter, P. C., and Runt, J. *Macromolecules* **36**(19), 7179–7188 (2003).

[45] Atorngitjawat, P., Klein, R. J., McDermott, A. G., Masser, K. A., Painter, P. C., and Runt, J. *Polymer* **50**(11), 2424–2435 (2009).

[46] Coleman, M. M. and Painter, P. C. *Progress in Polymer Science* **20**(1), 1–59 (1995).

[47] Pehlert, G. J., Painter, P. C., and Coleman, M. M. *Macromolecules* **31**(23), 8423–8424 (1998).

[48] Yang, X. M., Painter, P. C., Coleman, M. M., Pearce, E. M., and Kwei, T. K. *Macromolecules* **25**(8), 2156–2165 (1992).

[49] Luo, D. X., Pearce, E. M., and Kwei, T. K. *Macromolecules* **26**(23), 6220–6225 (1993).

[50] Jiang, M., Chen, W. J., and Yu, T. Y. *Polymer* **32**(6), 984–989 (1991).

[51] Chen, C. T. and Morawetz, H. *Macromolecules* **22**(1), 159–164 (1989).

[52] Boyd, R. H., Liu, F., Runt, J., and Fitzgerald, J. J. *Dielectric spectroscopy of polymeric materials : fundamentals and applications*. American Chemical Society, Washington DC, (1997).

[53] Kremer, F. and Schonhals, A. *Broadband Dielectric Spectroscopy*. Springer-Verlag, New York, 1 edition, (2003).

[54] Masser, K. A. and Runt, J. *Macromolecular Symposia* **279**(1), 221–227 (2009).

[55] Masser, K. A. and Runt, J. *Macromolecules* **43**(15), 6414–6421 (2010).

[56] Masser, K. A., Patil, H. P., Hedden, R. C., and Runt, J. *Journal of Non-Crystalline Solids* **356**(11-17), 578–581 (2010).

[57] Lu, Z. J., Manias, E., Macdonald, D. D., and Lanagan, M. *Journal of Physical Chemistry A* **113**(44), 12207–12214 (2009).

[58] Lu, Z. J., Lanagan, M., Manias, E., and Macdonald, D. D. *Journal of Physical Chemistry B* **113**(41), 13551–13559 (2009).

[59] Baker-Jarvis, J., Vanzura, E. J., and Kissick, W. A. *Ieee Transactions on Microwave Theory and Techniques* **38**(8), 1096–1103 (1990).

[60] Riande, E. and Diaz-Calleja, R. *Electrical Properties of Polymers*. Marcel Dekker, New York, 1 edition, (2004).

[61] Onsager, L. *Journal Of The American Chemical Society* **58**, 1486–1493 (1936).

[62] Kirkwood, J. G. *Journal of Chemical Physics* **7**(10), 911–919 (1939).

[63] Stockmayer, W. H. *Pure and Applied Chemistry* **15**(3-4), 539–554 (1967).

[64] Watanabe, H. *Macromolecular Rapid Communications* **22**(3), 127–175 (2001).

[65] Williams, G. *Macromolecular Symposia* **286**(1), 1–19 (2009).

[66] Watanabe, H. *Progress in Polymer Science* **24**(9), 1253–1403 (1999).

[67] Adachi, K., Imanishi, Y., and Kotaka, T. *Journal Of The Chemical Society-Faraday Transactions I* **85**, 1065–1074 (1989).

[68] Adachi, K. and Kotaka, T. *Progress in Polymer Science* **18**(3), 585 (1993).

[69] Ngai, K. L., Plazek, D. J., and Roland, C. M. *Macromolecules* (2008).

[70] McCrumb, N., Read, B., and Williams, G. *Anelastic and Dielectric Effects in Polymeric Solids*. Dover Publications, New York, (1967).

[71] Beiner, M., Kahle, S., Abens, S., Hempel, E., Horing, S., Meissner, M., and Donth, E. *Macromolecules* **34**(17), 5927 (2001).

[72] Bergman, R., Alvarez, F., Alegria, A., and Colmenero, J. *Journal of Chemical Physics* **109**(17), 7546 (1998).

[73] Gaborieau, M., Graf, R., Kahle, S., Pakula, T., and Spiess, H. W. *Macromolecules* **40**(17), 6249–6256 (2007).

[74] Garwe, F., Schonhals, A., Lockwenz, H., Beiner, M., Schroter, K., and Donth, E. *Macromolecules* **29**(1), 247 (1996).

[75] Hempel, E., Beiner, M., Renner, T., and Donth, E. *Acta Polymerica* **47**(11-12), 525 (1996).

[76] Casalini, R. and Roland, C. M. *Journal Of Chemical Physics* **119**(7), 4052–4059 (2003).

[77] Cerveny, S., Colmenero, J., and Alegria, A. *Macromolecules* **38**(16), 7056–7063 (2005).

[78] Fragiadakis, D. and Runt, J. *Macromolecules* **43**(2), 1028–1034 (2010).

[79] Madbouly, S. A., Mansour, A. A., and Abdou, N. Y. *European Polymer Journal* **43**(5), 1892–1904 (2007).

[80] Ngai, K. L. and Roland, C. M. *Polymer* **43**(2), 567–573 (2002).

[81] Ellison, W. J., Lamkaouchi, K., and Moreau, J. M. *Journal of Molecular Liquids* **68**(2-3), 171–279 (1996).

[82] Jenkins, S., Hodgetts, T. E., Clarke, R. N., and Preece, A. W. *Measurement Science And Technology* **1**(8), 691–702 (1990).

[83] Tsonos, C., Apekis, L., and Pissis, P. *Journal of Materials Science* **35**(23), 5957–5965 (2000).

[84] Sjoestroem, J., Swenson, J., Bergman, R., and Kittaka, S. *Journal of Chemical Physics* **128**(15), 9 (2008).

[85] Paddison, S. J., Bender, G., Kreuer, K. D., Nicoloso, N., and Zawodzinski, T. A. *Journal of New Materials for Electrochemical Systems* **3**(4), 291–300 (2000).

[86] Paddison, S. J., Reagor, D. W., and Zawodzinski, T. A. 91–97. Elsevier Science Sa, (1998).

[87] Hickner, M. A., Fujimoto, C. H., and Cornelius, C. J. *Polymer* **47**(11), 4238–4244 (2006).

[88] Cerveny, S., Alegria, A., and Colmenero, J. *Physical Review E* **77**(3), 0318031–0318035 (2008).

[89] Kilic, M. S., Bazant, M. Z., and Ajdari, A. *Physical Review E* **75**(2), 16 (2007).

[90] Angell, C. A. *Science* **267**(5206), 1924–1935 (1995).

[91] Sato, T., Chiba, A., and Nozaki, R. In *EMLG Meeting on Physical Chemistry of Liquids - Molecules, Macromolecules, Biomolecule*, 327–339 (Elsevier Science Bv, Regensburg, Germany, 2000).

[92] Cerveny, S., Colmenero, J., and Alegria, A. 49–52. Edp Sciences S A, (2007).

[93] Cerveny, S., Colmenero, J., and Alegria, A. 4523–4527. Elsevier Science Bv, (2007).

[94] Capaccioli, S., Ngai, K. L., and Shinyashiki, N. *Journal of Physical Chemistry B* **111**(28), 8197–8209 (2007).

[95] Gomez, D., Alegria, A., Arbe, K., and Colmenero, J. *Macromolecules* **34**(3), 503–513 (2001).

[96] Smith, G. D., Liu, F. G., Devereaux, R. W., and Boyd, R. H. *Macromolecules* **25**(2), 703–708 (1992).

[97] Banhegyi, G. *Colloid And Polymer Science* **264**(12), 1030–1050 (1986).

[98] Macdonald, J. R. *Physical Review* **92**(1), 4 (1953).

[99] Coelho, R. 1136–1139. Elsevier Science Bv, (1991).

[100] Wübbenhorst, M. and van Turnhout, J. *Journal of Non-Crystalline Solids* **305**(1-3), 40–49 (2002).

[101] Klein, R. J., Zhang, S. H., Dou, S., Jones, B. H., Colby, R. H., and Runt, J. *Journal of Chemical Physics* **124**(14), 8 (2006).

[102] Klein, R. J. *Dielectric Properties of Conductive Polymers*. PhD thesis, (2007).

[103] Fragiadakis, D., Dou, S. C., Colby, R. H., and Runt, J. *Macromolecules* **41**(15), 5723–5728 (2008).

[104] Fragiadakis, D., Dou, S., Colby, R. H., and Runt, J. *Journal of Chemical Physics* **130**(6), 0649071–06490711 (2009).

[105] Macdonald, J. R. *Journal of Chemical Physics* **22**(8), 1317–1322 (1954).

[106] Macdonald, J. R. and Brachman, M. K. *Journal of Chemical Physics* **22**(8), 1314–1316 (1954).

[107] Macdonald, J. R. *Journal of Chemical Physics* **22**(11), 1857–1866 (1954).

[108] Macdonald, J. R. *Transactions of the Faraday Society* **66**(568), 943–958 (1970).

[109] Macdonald, J. R. *Journal of Chemical Physics* **61**(10), 20 (1974).

[110] Gunning, J., Chan, D. Y. C., and White, L. R. *Journal of Colloid and Interface Science* **170**(2), 522–537 (1995).

[111] Scott, M., Paul, R., and Kaler, K. *Journal of Colloid and Interface Science* **230**(2), 377–387 (2000).

[112] Scott, M., Paul, R., and Kaler, K. *Journal of Colloid and Interface Science* **230**(2), 388–395 (2000).

[113] Hollingsworth, A. D. and Saville, D. A. *Journal of Colloid and Interface Science* **257**(1), 65–76 (2003).

[114] Kenkel, S. W. and Macdonald, J. R. *Journal of Chemical Physics* **81**(7), 3215–3221 (1984).

[115] Sangoro, J. R., Serghei, A., Naumov, S., Galvosas, P., Karger, J., Wespe, C., Bordusa, F., and Kremer, F. *Physical Review E* **77**(5), 4 (2008).

[116] Martin, B. and Kliem, H. *Journal of Non-Crystalline Solids* **356**(11-17), 701–704 (2010).

[117] Martin, B. and Kliem, H. *Journal of Applied Physics* **107**(7), 3 (2010).

[118] Adamson, A. W. *Physical Chemistry of Surfaces*. John Wiley and Sons, 5 edition, (1990).

[119] Zhou, H., Preston, M. A., Tilton, R. D., and White, L. R. *Journal of Colloid and Interface Science* **292**(1), 277–289 (2005).

[120] Bazant, M. Z., Thornton, K., and Ajdari, A. *Physical Review E* **70**(2), 24 (2004).

[121] Sangoro, J., Iacob, C., Serghei, A., Naumov, S., Galvosas, P., Karger, J., Wespe, C., Bordusa, F., Stoppa, A., Hunger, J., Buchner, R., and Kremer, F. *Journal of Chemical Physics* **128**(21), 5 (2008).

[122] Sangoro, J., R., Turky, G., Abdel Rehim, M., Iacob, C., Naumov, S., Ghoneim, A., Karger, J., and Kremer, F. *Macromolecules* (2009).

[123] Sangoro, J. R., Iacob, C., Serghei, A., Friedrich, C., and Kremer, F. *Physical Chemistry Chemical Physics* **11**(6), 913–916 (2009).

[124] Tuncer, E., Serdyuk, Y. V., and Gubanski, S. M. *Ieee Transactions On Dielectrics And Electrical Insulation* **9**(5), 809–828 (2002).

[125] Cole, K. S. and Cole, R. H. *Journal of Chemical Physics* **9**(4), 341–351 (1941).

[126] Davidson, D. W. and Cole, R. H. *Journal of Chemical Physics* **18**(10), 1417–1417 (1950).

[127] Davidson, D. W. and Cole, R. H. *Journal of Chemical Physics* **19**(12), 1484–1490 (1951).

[128] Havriliak, S. and Negami, S. *Journal Of Polymer Science Part C-Polymer Symposium* (14), 99–117 (1966).

[129] Havriliak, S. and Negami, S. *Polymer* **8**(4), 161–210 (1967).

[130] Havriliak, S. and Negami, S. *Rohm and Haas Research Laboratories* (1969).

[131] Angell, C. A. *Polymer* **38**(26), 6261–6266 (1997).

[132] Brachman, M. K. and Macdonald, J. R. *Physica* **20**(12), 1266–1270 (1954).

[133] Steeman, P. A. M. and vanTurnhout, J. *Colloid And Polymer Science* **275**(2), 106–115 (1997).

[134] Wübbenhorst, M., vanKoten, E. M., Jansen, J. C., Mijs, W., and vanTurnhout, J. *Macromolecular Rapid Communications* **18**(2), 139–147 (1997).

[135] Wübbenhorst, M., van Turnhout, J., Folmer, B. J. B., Sijbesma, R. P., and Meijer, E. W. *Ieee Transactions on Dielectrics and Electrical Insulation* **8**(3), 365–372 (2001).

[136] Wübbenhorst, M., de Rooij, A. L., van Turnhout, J., Tacx, J., and Mathot, V. *Colloid And Polymer Science* **279**(6), 525–531 (2001).

[137] Gorry, P. A. *Analytical Chemistry* **62**(6), 570–573 (1990).

[138] Müller, M., Stadler, R., Kremer, F., and Williams, G. *Macromolecules* **28**(20), 6942–6949 (1995).

[139] Müller, M., Kremer, F., Stadler, R., Fischer, E. W., and Seidel, U. *Colloid and Polymer Science* **273**(1), 38–46 (1995).

[140] Müller, M., Seidel, U., and Stadler, R. *Polymer* **36**(16), 3143–3150 (1995).

[141] Müller, M., Dardin, A., Seidel, U., Balsamo, V., Ivan, B., Spiess, H. W., and Stadler, R. *Macromolecules* **29**(7), 2577–2583 (1996).

[142] Sato, T., Tsujii, Y., Kita, Y., Fukuda, T., and Miyamoto, T. *Macromolecules* **24**(16), 4691–4697 (1991).

[143] Zentel, R., Strobl, G. R., and Ringsdorf, H. *Macromolecules* **18**(5), 960–965 (1985).

[144] Gouda, F., Lagerwall, S. T., Skarp, K., Stebler, B., Kremer, F., and Vallerien, S. U. *Liquid Crystals* **17**(3), 367–379 (1994).

[145] Kresse, H. *Advances in Liquid Crystals* **6**, 109–172 (1983).

[146] Atorngitjawat, P. and Runt, J. *Macromolecules* **40**(4), 991–996 (2007).

[147] Asami, K. *Progress in Polymer Science* **27**(8), 1617–1659 (2002).

[148] Drago, R. S. and Epley, T. D. *Journal of the American Chemical Society* **91**(11), 2883–2890 (1969).

[149] Drago, R. S., Obryan, N., and Vogel, G. C. *Journal of the American Chemical Society* **92**(13), 3924–3929 (1970).

[150] Serman, C. J., Xu, Y., Painter, P. C., and Coleman, M. M. *Polymer* **32**(3), 516–522 (1991).

[151] Zhang, S. H. and Runt, J. *Journal of Polymer Science Part B-Polymer Physics* **42**(18), 3405–3415 (2004).

[152] Colmenero, J. and Arbe, A. *Soft Matter* **3**(12), 1474–1485 (2007).

[153] Lee, J. Y., Painter, P. C., and Coleman, M. M. *Applied Spectroscopy* **40**(7), 991–994 (1986).

[154] Zhang, S. H., Jin, X., Painter, P. C., and Runt, J. *Macromolecules* **36**(15), 5710–5718 (2003).

[155] Ngai, K. L., Rendell, R. W., and Yee, A. F. *Macromolecules* **21**(12), 3396–3401 (1988).

[156] Ngai, K. L., Rendell, R. W., Yee, A. F., and Plazek, D. J. *Macromolecules* **24**(1), 61–67 (1991).

[157] Adam, G. and Gibbs, J. H. *Journal of Chemical Physics* **43**(1), 139–146 (1965).

[158] Saiter, A., Saiter, J. M., and Grenet, J. *European Polymer Journal* **42**(1), 213–219 (2006).

[159] McKenna, G. B. *Journal of Non-Crystalline Solids* **355**(10-12), 663–671 (2009).

[160] Alves, N. M., Ribelles, J. L. G., Tejedor, J. A. G., and Mano, J. F. *Macromolecules* **37**(10), 3735–3744 (2004).

[161] Kalakkunnath, S., Kalika, D. S., Lin, H. Q., and Freeman, B. D. *Macromolecules* **38**(23), 9679–9687 (2005).

[162] Casalini, R. and Roland, C. M. *Journal of Polymer Science Part B-Polymer Physics* **48**, 582–587 (2010).

[163] Stukalin, E. B., Douglas, J. F., and Freed, K. F. *Journal of Chemical Physics* **131**(11), 1149051–11490511 (2009).

[164] Stukalin, E. B., Douglas, J. F., and Freed, K. F. *Journal of Chemical Physics* **132**(8), 0845041–08450411 (2010).

[165] Leibler, L., Rubinstein, M., and Colby, R. H. *Macromolecules* **24**(16), 4701–4707 (1991).

[166] Douglas, E. P., Waddon, A. J., and Macknight, W. J. *Macromolecules* **27**(15), 4344–4352 (1994).

[167] Atorngitjawat, P., Klein, R. J., and Runt, J. *Macromolecules* **39**(5), 1815–1820 (2006).

[168] Robertson, C. G. and Roland, C. M. *Journal of Polymer Science Part B-Polymer Physics* **42**(13), 2604–2611 (2004).

[169] Painter, P. C., Veytsman, B., Kumar, S., Shenoy, S., Graf, J. F., Xu, Y., and Coleman, M. M. *Macromolecules* **30**(4), 932–942 (1997).

[170] Choperena, A. and Painter, P. *Macromolecules* **42**(16), 6159–6165 (2009).

[171] Gaikwad, A. N., Choperena, A., Painter, P. C., and Lodge, T. P. *Macromolecules* **43**(10), 4814–4821 (2010).

[172] Cerveny, S., Alegria, A., and Colmenero, J. *Journal of Chemical Physics* **128**(4), 0449011 – 0449017 (2008).

[173] Kim, S., Mundra, M. K., Roth, C. B., and Torkelson, J. M. *Macromolecules* **43**(11), 5158–5161 (2010).

[174] Tyagi, M., Alegria, A., and Colmenero, J. *Physical Review E* **75**(6), 0618051–0618059 (2007).

[175] Tyagi, M., Arbe, A., Alvarez, F., Colmenero, J., and Gonzalez, M. A. *Journal of Chemical Physics* **129**(22), 2249031–22490314 (2008).

[176] Stadler, R. and Freitas, L. D. *Macromolecules* **22**(2), 714–719 (1989).

[177] Mukhopadhyay, R., Alegria, A., Colmenero, J., and Frick, B. *Journal of Non-Crystalline Solids* **235**, 233–236 (1998).

[178] Leland, M., Wu, Z. Q., Chhajer, M., Ho, R. M., Cheng, S. Z. D., Keller, A., and Kricheldorf, H. R. *Macromolecules* **30**(18), 5249–5254 (1997).

[179] Tokita, M., Osada, K., and Watanabe, J. *Liquid Crystals* **23**(3), 453–456 (1997).

[180] Patil, H. P., Liao, J., and Hedden, R. C. *Macromolecules* **40**(17), 6206–6216 (2007).

[181] Ishige, R., Osada, K., Tagawa, H., Niwano, H., Tokita, M., and Watanabe, J. *Macromolecules* **41**(20), 7566–7570 (2008).

[182] Tsuwi, J., Hartmann, L., Kremer, F., Pospiech, D., Jehnichen, D., and Haussler, L. *Polymer* **47**(20), 7189–7197 (2006).

[183] Kremer, F., Vallerien, S. U., Zentel, R., and Kapitza, H. *Macromolecules* **22**(10), 4040–4045 (1989).

[184] Mano, J. F., Alves, N. M., Duenas, J. M. M., and Ribelles, J. L. G. *Polymer* **40**(23), 6545–6556 (1999).

[185] Hellermark, C., Gedde, U. W., Hult, A., Boeffel, C., Boyd, R. H., and Liu, F. *Macromolecules* **31**(14), 4531–4536 (1998).

[186] Mierzwa, M., Floudas, G., Neidhofer, M., Graf, R., Spiess, H. W., Meyer, W. H., and Wegner, G. *Journal Of Chemical Physics* **117**(13), 6289–6299 (2002).

[187] Mano, J. F. and Ribelles, J. L. G. *Macromolecules* **36**(8), 2816–2824 (2003).

[188] Garcia-Bernabe, A., Calleja, R. D., Sanchis, M. J., del Campo, A., Bello, A., and Pérez, E. *Polymer* **45**(5), 1533–1543 (2004).

[189] del Campo, A., Ezquerra, T. A., Wilbert, G., Passmann, M., and Zentel, R. *Macromolecular Chemistry And Physics* **203**(14), 2089–2094 (2002).

[190] Ezquerra, T. A., Martinez-Gomez, A., Alvarez, C., Alonso, E., Sanz, A., Garcia-Gutierrez, M. C., Bello, A., Perez, E., Funari, S. S., and Dommach, M. *Journal Of Non-Crystalline Solids* **351**(33-36), 2768–2772 (2005).

[191] Furukawa, T., Uchinokura, O., Takahashi, Y., Tokita, M., Osada, K., and Watanabe, J. *Polymer Journal* **32**(2), 122–126 (2000).

[192] Ferry, J. D. *Viscoelastic Properties of Polymers*. Wiley and Sons, (1980).

[193] Damman, S. B., Buijs, J., and Vanturnhout, J. *Polymer* **35**(11), 2364–2371 (1994).

[194] Adachi, H., Adachi, K., Ishida, Y., and Kotaka, T. *Journal Of Polymer Science Part B-Polymer Physics* **17**(5), 851–857 (1979).

[195] Gedde, U. W., Liu, F., Hult, A., Gustafsson, A., Jonsson, H., and Boyd, R. H. *Polymer* **32**(7), 1219–1222 (1991).

[196] Blundell, D. J. and Buckingham, K. A. *Polymer* **26**(11), 1623–1627 (1985).

[197] Gedde, U. W., Buerger, D., and Boyd, R. H. *Macromolecules* **20**(5), 988–992 (1987).

[198] Alhajmohammed, M. H., Davies, G. R., Jawad, S. A., and Ward, I. M. *Journal of Polymer Science Part B-Polymer Physics* **26**(8), 1751–1760 (1988).

[199] Coburn, J. C. and Boyd, R. H. *Macromolecules* **19**(8), 2238–2245 (1986).

[200] Nimmagadda, R. D. and McRae, C. *Tetrahedron Letters* **47**(32), 5755–5758 (2006).

[201] Wind, M., Graf, R., Heuer, A., and Spiess, H. W. *Physical Review Letters* **91**(15), 4 (2003).

[202] Beiner, M. *Macromolecular Rapid Communications* **22**(12), 869–895 (2001).

[203] Painter, P., Park, Y., and Coleman, M. *Journal of Applied Polymer Science* **70**(7), 1273–1281 (1998).

Vita

Kevin Allen Masser

Kevin Masser was born in the small farming town of Klingerstown, PA on April 6, 1983 to Rickey and Amy Masser. After graduating from Line Mountain high school, he enrolled at Penn State University. During his two year stint as a history major, a basic materials science class convinced him that polymer physics was the way to go. Three years after switching majors, he graduated from Penn State with a B.S. in Materials Science and Engineering in the Polymers option. While completing his undergraduate degree, he was given the opportunity to do research in the Ralph Colby group under the guidance of his senior student, Brian Erwin. During this time, he was exposed to broadband dielectric relaxation spectroscopy, and decided to pursue his doctorate with Professor James Runt, studying a very broad range of polymeric materials, and on occasion, working on his dissertation.